



Microbial Oxidation of Methane in Aquatic Systems Illuminated by Functional Metagenomics

Freshwater and marine environments are hotspots of methane cycling. Vast amounts of methane, a potent greenhouse gas, are produced predominantly in the sediments of these environments but very little eventually escapes to the atmosphere due to the activity of methane-oxidizing microorganisms. These microorganisms are pivotal in regulating methane emissions from the oceans and freshwater systems and their study therefore transcends scientific curiosity and is of global relevance to society as a whole. Despite their importance, the knowledge about these microorganisms is restricted to cultured isolates and little is known about the physiology of environmentally-relevant uncultured species. Using culture-independent functional metagenomics in combination with physiological experiments, this thesis aims to improve our understanding of the individual metabolic potential and activity that underlie the ecophysiology and environmental relevance of several uncultured methane-oxidizing microorganisms.

Autor: Jon S. Graf
Universität Bremen
Max Planck Institut für Marine Mikrobiologie

Erstgutachter: Prof. Dr. Marcel M.M. Kuypers
Universität Bremen
Max Planck Institut für Marine Mikrobiologie

Zweitgutachter: Prof. Dr. Dr. h. c. Michael Wagner
Department für Mikrobiologie und Ökosystemforschung, Universität Wien

Datum des Promotionskolloquiums: 18. Januar 2018

Diese Arbeit wurde in der Zeit vom September 2012 bis Oktober 2017 im Rahmen des Programms 'The International Max Planck Research School of Marine Microbiology' (MarMic) angefertigt. Die Ergebnisse dieser Arbeit wurden am Max Planck Institut für Marine Mikrobiologie (Biogeochemie) erarbeitet.



Cover image: Epifluorescence microscopy image of cells involved in sulfate-dependent anaerobic oxidation of methane after hybridization with specific rRNA-targeted oligonucleotide probes.

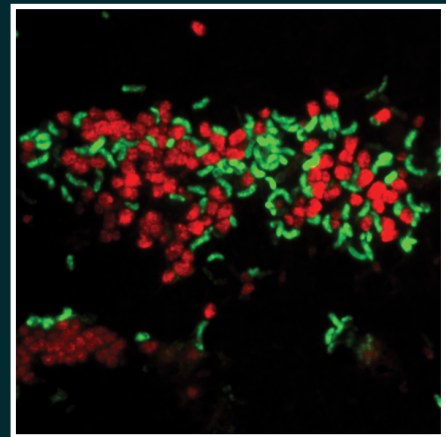
Jon S. Graf

Microbial Oxidation of Methane in Aquatic Systems Illuminated by Functional Metagenomics

Jon S. Graf

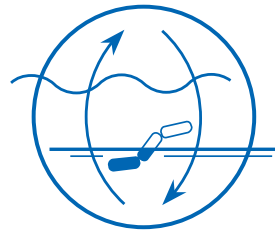
Dissertation zur Erlangung des Grades eines Doktors der Naturwissenschaften - Dr. rer. nat. -
im Fachbereich Geowissenschaften der Universität Bremen

Microbial Oxidation of Methane in Aquatic Systems
Illuminated by Functional Metagenomics



Bremen, Oktober 2017

Microbial Oxidation of Methane in Aquatic Systems Illuminated by Functional Metagenomics



Dissertation

zur Erlangung des Grades eines Doktors der Naturwissenschaften

- Dr. rer. nat. -

im Fachbereich Geowissenschaften der



Jon S. Graf

Bremen, Oktober 2017

Diese Arbeit wurde in der Zeit vom September 2012 bis Oktober 2017 im Rahmen des Programms 'The International Max Planck Research School of Marine Microbiology' (MarMic) angefertigt. Die Ergebnisse dieser Arbeit wurden am Max Planck Institut für Marine Mikrobiologie (Biogeochemie) erarbeitet.

Autor: **Jon S. Graf**

Universität Bremen

Max Planck Institut für Marine Mikrobiologie

Erstgutachter: **Prof. Dr. Marcel M.M. Kuypers**

Universität Bremen

Max Planck Institut für Marine Mikrobiologie

Zweitgutachter: **Prof. Dr. Dr. h .c. Michael Wagner**

Department für Mikrobiologie und Ökosystemforschung, Universität Wien

Datum des Promotionskolloquiums: 18. Januar 2018

Summary

Freshwater and marine environments are hotspots of methane cycling. Vast amounts of methane, a potent greenhouse gas, are produced predominantly in the sediments of these environments but very little eventually escapes to the atmosphere due to the activity of methane-oxidizing microorganisms. These microorganisms are pivotal in regulating methane emissions from the oceans and freshwater systems and their study therefore transcends scientific curiosity and is of global relevance to society as a whole. Despite their importance, the knowledge about these microorganisms is restricted to cultured isolates and little is known about the physiology of environmentally-relevant uncultured species. The aim of this study was to use culture-independent functional metagenomics in combination with other physiological experiments to study the individual metabolic potential and activity that underlie the ecophysiology of several uncultured methane-oxidizing microorganisms.

The first study (Chapter 2) shows that uncultivated gamma-proteobacteria related to *Crenothrix* are major methane consumers in two stratified Swiss lakes (Lake Zug and Rotsee). Although *Crenothrix* bacteria have been infamous for infestation of drinking water supplies for more than a century, little was known about their role in methane cycling in the environment. This study provides first insights into the metabolic potential and activity of *Crenothrix* and demonstrates their methane-dependent growth under aerobic as well as under oxygen-deficient and denitrifying conditions. Reconstruction of *Crenothrix* genomes allowed us to clarify the phylogenetic assignment of their methane monooxygenase, an important classification marker for methanotrophs, and revealed the metabolic potential for nitrate respiration to nitric or even nitrous oxide. Overall these results suggest that *Crenothrix* can act as relevant biological sink for methane in stratified lakes.

Chapter 3 focuses on methanotrophs of the candidate phylum NC10 in Lake Zug. These bacteria form a relevant link between the methane and nitrogen cycle but generally constitute only a minor part of the methanotrophic communities. We show that NC10 bacteria, which couple methane oxidation to a unique O₂-producing denitrification pathway, dominated the microbial community in the anoxic hypolimnion of Lake Zug, comprising almost a third of the total bacterial population. This is the hitherto highest reported abundance from any environment. We describe the

physiology and the habitat of this new species of the genus "*Candidatus Methyloirabilis*". The reconstructed genome of "*Ca. Methyloirabilis limnetica*" confirmed its methane-oxidizing, denitrifying potential and revealed features, such as formation of gas vesicles, previously not described for this genus. We could show that "*Ca. M. limnetica*" was transcriptionally highly active *in situ* but the full biogeochemical impact of NC10 bacteria has yet to be quantified.

In Chapters 4 and 5, the physiology and metabolic potential of an archaeal-bacterial consortium involved in the sulfate-dependent anaerobic oxidation of methane (S-AOM) was investigated using a highly active S-AOM enrichment culture. In contrast to freshwater environments, this strictly anaerobic process is the dominant methane sink in marine systems and controls the flux of methane to the atmosphere.

In Chapter 4 unravels the individual metabolic potential and activity of ANME-2c archaea and SEEP-SRB1 bacteria using functional metagenomics in order to elucidate the division of labor and interactions between these intertwined microorganisms. The reconstructed genomes in conjunction with transcriptomic and proteomic data were used to gather support for current hypotheses concerning the physiology of the two microorganisms. We confirmed that ANME-2c encode, transcribe and express a complete reverse methanogenesis pathway for methane oxidation and propose several transcribed candidate genes, in particular two sulfite reductases, which might be involved in a previously proposed archaeal dissimilatory sulfate reduction pathway. Moreover we highlight the possibility of flavin-based electron bifurcation by soluble heterodisulfide reductase as an important but overlooked aspect in the electron transport chain of ANME. We confirm that SEEP-SRB1 express a complete canonical sulfate reduction pathway, which arguably could also be involved in sulfur disproportionation, and we also investigate the genomic potential for electron transfer between ANME-2c and SEEP-SRB1.

Finally, Chapter 5 investigates a potential involvement of an S-AOM-associated archaeal-bacterial consortium in the cycling of inorganic phosphate. We demonstrate that the S-AOM microorganisms appear to utilize phosphate beyond assimilatory uptake and observed an enigmatic shuffling of phosphate between soluble and particulate fractions that was only active when methane was oxidized. These laboratory results highlight an intriguing yet unresolved involvement of phosphate in S-AOM that remains to be verified *in situ*.

Zusammenfassung

Süsswassersysteme und Ozeane sind durch intensive Methanzyklen geprägt. Obwohl grosse Mengen an Methan in den Sedimenten produziert werden, entweicht jedoch nur sehr wenig von diesem potenten Treibhausgas in die Atmosphäre. Hauptverantwortlich dafür sind Methan-oxidierende Mikroorganismen, welche eine entscheidende Rolle in der Regulierung von Methanemissionen spielen. Die Studie dieser Mikroorganismen erstreckt sich somit über die wissenschaftliche Neugier hinaus und ist für die Gesellschaft von grosser Bedeutung. Trotz ihrer Wichtigkeit ist das Wissen über diese Mikroorganismen auf kultivierte Isolate beschränkt und es ist wenig über die Physiologie von unkultivierten aber umweltrelevanten Spezies bekannt. Ziel dieser Studie war es, das individuelle Stoffwechselfpotential und die Aktivität dieser unkultivierten Mikroorganismen mittels kulturunabhängiger, funktioneller Metagenomik in Kombination mit physiologischen Experimenten zu untersuchen.

In der ersten Studie (Kapitel 2) wird gezeigt, dass unkultivierte *Crenothrix*-Bakterien, welche den Gamma-Proteobakterien angehören, zu den wichtigsten Methan-Konsumenten in zwei geschichteten Schweizer Seen (Zug und Rotsee) zählen. Obwohl *Crenothrix*-Bakterien seit mehr als einem Jahrhundert für den Befall von Trinkwasserversorgungssystemen bekannt sind, ist ihre Rolle im ökologischen Methanzyklus weitestgehend nicht verstanden. Diese Studie liefert auch erste Einblicke in das metabolische Potenzial und die Aktivität von *Crenothrix* und hebt ihr methanabhängiges Wachstum unter aeroben sowie unter sauerstoffarmen und denitrifizierenden Bedingungen hervor. Die Rekonstruktion von *Crenothrix*-Genomen ermöglichte es erstmals, die phylogenetische Zuordnung der Methanmonooxygenase, einem wichtigen phylogenetischen Marker für methanotrophe Bakterien, aufzuklären und zeigte das metabolische Potenzial für Nitratatmung zu Stickstoffmonoxid oder Distickstoffmonoxid auf. Insgesamt deuten diese Ergebnisse darauf hin, dass *Crenothrix*-Bakterien als wichtige biologische Senke für Methan in geschichteten Seen fungieren.

In Kapitel 3 wurden Bakterien des Kandidaten-Phylum NC10 im Zugersee untersucht. Diese Bakterien sind aufgrund ihrer Fähigkeit, Methan- und Stickstoffzyklen zu verknüpfen, von Bedeutung, jedoch bilden NC10-Bakterien in der Regel nur einen kleinen Teil der methanotrophen Gemeinschaft. Wir zeigen, dass NC10-Bakterien, welche Methan-Oxidation mit einem einzigartigen O₂-produzierenden Denitrifikations-Stoffwechselweg verbinden, die mikrobielle Gemeinschaft im anoxischen Hypolimnion des Zugersees dominierten und fast ein Drittel der gesamten Bakterienpopulation umfassten. Dies ist die bislang höchste Abundanz von NC10-Bakterien, die je in der Umwelt beschrieben wurde und erlaubte die erste Charakterisierung der Physiologie und dem Habitat dieser neuen Spezies der Gattung "*Candidatus Methyloirabilis*". Das

rekonstruierte Genom von "*Ca. Methyloirabilis limnetica*" bestätigte das Potential zur Methanoxidation und Denitrifikation und zeigte für diese Gattung neuartige Merkmale, wie zum Beispiel Gasvesikelgene, welche wahrscheinlich eine Adaption an das planktonische Habitat darstellen. Obwohl die hohe *in situ* Aktivität von "*Ca. M. limnetica*" transkriptionell nachgewiesen werden konnte, muss die biogeochemische Bedeutung der NC10-Bakterien erst noch quantifiziert werden.

In den Kapiteln 4 und 5 wurde das physiologische und metabolische Potential eines Archaeen-Bakterien-Konsortiums in einer hochaktiven Anreicherungskultur untersucht, welches an der sulfatabhängigen anaeroben Oxidation von Methan (S-AOM) beteiligt ist. Im Gegensatz zu Süßwassersystemen ist dieser streng anaerobe Prozess die dominierende Methan-Senke in marinen Systemen und kontrolliert den Fluss von Methan in die Atmosphäre.

In Kapitel 4 entschlüsseln wir das individuelle metabolische Potential und die Aktivität von ANME-2c-Archaeen und SEEP-SRB1-Bakterien mit funktionellen metagenomischen Methoden, um die metabolische Arbeitsteilung und die Wechselwirkung zwischen diesen Mikroorganismen zu untersuchen. Die rekonstruierten Genome und transkriptomischen sowie proteomischen Daten wurden verwendet, um aktuelle Hypothesen über die Physiologie der beiden Mikroorganismen zu bestätigen. Unsere Untersuchungen zeigten, dass ANME-2c einen vollständigen Reverse-Methanogenese-Stoffwechselweg zur Methanoxidation exprimierten. Zudem wurden mehrere transkribierte Kandidatengene identifiziert, insbesondere zwei Sulfid-Reduktasen, die an dem zuvor vorgeschlagenen archaealen, dissimilatorischen Stoffwechselweg zur Sulfatreduktion beteiligt sein könnten. Darüber hinaus stellen wir die Möglichkeit einer Flavin-basierten Elektronen-Bifurkation durch lösliche Heterodisulfid-Reduktase als wichtiger und zuvor übersehener Aspekt in der Elektronentransportkette von ANME heraus. Wir zeigen, dass SEEP-SRB1-Bakterien einen vollständigen Stoffwechselweg zur Sulfatreduktion exprimieren, der auch an Schwefel-Disproportionierung beteiligt sein könnte. Darüber hinaus wurde das genomische Potential für den Elektronentransfer zwischen ANME-2c und SEEP-SRB1 untersucht.

Schließlich wurde in Kapitel 5 eine mögliche Beteiligung eines S-AOM-assoziierten Konsortiums am Zyklus von anorganischem Phosphat betrachtet. Die S-AOM-Mikroorganismen scheinen Phosphat jenseits des assimilatorischen Bedarfs zu nutzen, da eine rätselhafte Umschichtung von Phosphat zwischen löslicher und partikulärer Phase beobachtet wurde. Diese Umschichtungen waren nur aktiv, wenn Methan oxidiert wurde. Diese Laborergebnisse zeigen eine faszinierende, aber noch ungelöste Beteiligung von Phosphat am S-AOM-Prozess, die aber *in situ* noch verifiziert werden muss.

Contents

Summary	i
Zusammenfassung	iii
Chapter 1	1
General Introduction	1
Aims and Outline	21
Chapter 2	37
<i>Crenothrix</i> are major methane consumers in stratified lakes	
Chapter 3	57
Bloom of a denitrifying methanotroph, " <i>Candidatus Methylomirabilis limnetica</i> ", in a deep stratified lake	
Chapter 4	93
Physiology of microorganisms mediating sulfate-dependent anaerobic oxidation of methane illuminated by functional metagenomics	
Chapter 5	145
Cycling of phosphate associated with microorganisms involved in the sulfate-dependent anaerobic oxidation of methane	
Chapter 6	167
Conclusions and Outlook	
Acknowledgements	182
Appendix A	184
Contributions to other studies	

Chapter 1

Introduction

"[...] life is driven by nothing else but electrons, by the energy given off by these electrons while cascading down from the high level to which they have been boosted up by photons."

– Albert Szent-Györgyi

Anthropogenic greenhouse gases such as carbon dioxide (CO₂), methane (CH₄) and nitrous oxide (N₂O) are recognized to be the main drivers of global warming observed since the beginning of the industrial Era (Ciais et al, 2014). The Intergovernmental Panel on Climate Change (IPCC) 5th Assessment Report predicts a grim future: without additional mitigation efforts, such as substantial reduction in anthropogenic greenhouse gas emission, "warming by the end of the 21st century will lead to high to very high risk of severe, widespread and irreversible impacts globally" (Pachauri et al, 2014). Methane, a very potent greenhouse gas, is present in earth's atmosphere in trace amounts (<2 parts per million). Albeit its low atmospheric concentration, methane is the second most impactful anthropogenic greenhouse gas and atmospheric methane concentrations have steadily increased since the mid-20th century (Pachauri et al, 2014). Emission and consumption of methane are tightly linked to the activity of microorganisms. They are not only the main producers but also consumers of methane in the environment. By studying these microorganisms we are able to better understand the methane cycle and the factors controlling it – a prerequisite to mitigate methane emissions in the future.

1 The aquatic methane cycle – sources and sinks

It is estimated that around 70% of the global methane production (~550 Tg CH₄ year⁻¹ (Kirschke et al, 2013)) is produced by methanogenic microorganisms (Conrad, 2009), which makes them the largest source of methane globally. Non-biological sources of methane (i.e. thermogenic or pyrogenic origin) constitute around 30% of the global methane production (Ciais et al, 2014; Neef et al, 2010).

Biologically, methane is formed under anaerobic conditions from organic matter (OM) by a consortium of fermentative primary degraders and methanogenic archaea.

Among other anaerobic environments, aquatic sediments are hotspots of methanogenesis as they provide an oxygen-free environment continuously supplied with OM. Primary producers fix carbon into OM by harnessing the sun's energy near the surface. As the OM sinks through the water column it is degraded by heterotrophic microorganisms and some of it reaches the bottom where it enters the sediment. In the sediment, oxygen is quickly depleted by microbial respiration and mineralization of the OM continues under anoxic conditions with alternative electron acceptors (i.e. nitrate or sulfate). Additionally, OM is degraded by fermentative primary degraders to simple molecules (e.g. acetate, CO₂, H₂) in deeper layers of the sediment. Here, methane is finally produced by methanogenic archaea that feed off the fermentation products. Important environments acting as methane sources generally receive high fluxes of organic matter (e.g. wetlands, swamps or sediments), but environments heavily controlled by human activities such as rice paddies, ruminant animals, landfills or anaerobic digestion plants are also major sources of methane (Conrad, 2009).

Methane that reaches the atmosphere is relatively short-lived and undergoes photochemical oxidation by OH radicals, which accounts for >80% of all atmospheric sinks (Ciais et al, 2014; Conrad, 2009). However, more than half of the globally produced methane never reaches the atmosphere. It is consumed close to the source by microorganisms which are the single most important process stopping methane from reaching the atmosphere (Reeburgh, 2003). Consumption before emission is especially pronounced in marine environments; oceans contribute relatively little to the global methane budget despite significant gross methane production (Reeburgh, 2007).

In marine sediments, the vast majority of methane is readily oxidized under anaerobic conditions by the microbially-mediated process of anaerobic oxidation of methane (AOM) with sulfate as electron acceptor (S-AOM, (Hinrichs & Boetius, 2002; Reeburgh, 2007)). Quantitatively, sulfate-dependent AOM is the main sink of methane produced in the ocean and is responsible for removing an equivalent of 7 – 25% of the globally produced methane (Knittel & Boetius, 2009). Methane that escapes the sediment (mainly at cold seeps or hydrothermal vents) is oxidized by aerobic methanotrophs which further reduce the amount of methane that eventually reaches the atmosphere (Boetius & Wenzhöfer, 2013; Valentine, 2011).

In contrast to marine environments, microbially-mediated aerobic oxidation of methane is the primary route of methane removal (30 – 99% of produced methane) in most freshwater systems (Bastviken et al, 2008). Anaerobic oxidation of methane also plays a significant role in selected lakes (Crowe et al, 2011; Schubert et al, 2011), but its contribution to total methane oxidation in freshwater systems is currently poorly constrained (Borrel et al, 2011).

2 Microbial methane oxidation

Methane oxidation is performed by specialized microorganisms, so-called methanotrophs, which make a living off redox processes involving the oxidation of methane. Methanotrophs are ubiquitous in many oxic and anoxic environments where methane is present, ranging from subseafloor sediments to acidic hotsprings or hypersaline soda lakes. Methanotrophs can be broadly classified into two groups: aerobic methanotrophs that rely on oxygen for methane oxidation and anaerobic methanotrophs that use a range of alternative electron acceptors (e.g. sulfate or nitrate) to oxidize methane.

2.1 Aerobic methane oxidation

Major habitats of aerobic methanotrophs are freshwater systems (i.e. lakes, rivers or wetlands). In these environments, the highest oxidation rates and abundance of aerobic methanotrophs can generally be found at interfaces of anoxic and oxic zones such as the sediment surface or at the oxycline in stratified lakes (Hanson & Hanson, 1996).

In marine ecosystems, aerobic methanotrophs are abundant at the surface sediments characterized by high methane fluxes – such as methane seeps, gas hydrates or hydrothermal vent areas – but have also been detected in open ocean waters (Bowman, 2014). The habitat of aerobic methanotrophs also extends to extreme environments such as alkaline or acidic ecosystems and hot springs (Bodrossy et al, 1997; Pol et al, 2007; Sorokin et al, 2000). Most methanotrophic strains can grow over a range of oxygen concentrations, including microaerophilic conditions, and can readily survive under anoxic conditions for prolonged durations (Roslev & King, 1995).

2.1.1 Aerobic Methanotrophs

A common feature shared by aerobic methane-oxidizing microorganisms described to date is that they rely on molecular oxygen for methane oxidation and that they belong to the domain *Bacteria*. They are a subgroup of methylotrophs and specialize in the utilization of methane (and sometimes methanol) for anabolism and catabolism.

Historically, aerobic methane-oxidizing bacteria (MOB) have been classified into type I and type II methanotrophs based on cellular morphology, ultrastructure, phylogeny and biochemical traits (Hanson & Hanson, 1996; Whittenbury & Dalton, 1981). However, it has become clear in recent years that this broad classification scheme could not accommodate newly discovered MOB without introducing various exceptions. The scheme is still used to describe gamma (type I)- and alphaproteobacterial (type II) MOB but has been mostly replaced by taxonomic classification based on 16S ribosomal RNA (rRNA) sequence (Knief, 2015; Op den Camp et al, 2009). Most known MOB belong to *Alpha*- and *Gammaproteobacteria*, more specifically alpha-proteobacterial families *Methylocystaceae* and *Beijerinckiaceae* as well as gamma-proteobacterial families *Methylococcaceae* and *Methylothermaceae* (Bowman, 2014; Hirayama et al, 2014). Recently, MOB have also been discovered in the phylum *Verrucomicrobia* (Dunfield et al, 2007; Islam et al, 2008; Pol et al, 2007).

Most methanotrophs exhibit coccoid or rod-like morphology – a peculiar exception are uncultivated filamentous microorganisms which belong to genera *Crenothrix* and *Clonothrix* (Cohn, 1870; Roze, 1896). Despite being known to infest and block drinking water systems for decades, it was only recently that their ability to perform methane oxidation was only recently discovered (Stoecker et al, 2006; Vigliotta et al, 2007). Both genera form long sheathed filaments and apparently feature distinct complex life cycles involving propagation through septation and release of individual coccoid cells (Bowman, 2014; Völker et al, 1977). Besides their morphology and methane-oxidizing capacity, little is known about the ecology and physiology of these uncultivated methanotrophs.

2.1.2 Methane oxidation, C1 metabolism and respiratory chain

Aerobic methanotrophs employ a specialized enzyme machinery to oxidize methane gradually to methanol, formaldehyde, formate and finally to CO₂ (Figure 1). The first step of this pathway, the oxidation of methane to methanol, is catalyzed by two separate methane monooxygenases (MMO) that are hallmark enzymes of aerobic methanotrophy and are present in all aerobic MOB described so far (Hanson & Hanson, 1996; Trotsenko & Murrell, 2008). Two distinct forms of MMO have been described: soluble MMO (sMMO) and particulate MMO (pMMO) (Anthony, 1986; Hakemian & Rosenzweig, 2007). The particulate, membrane-bound form is found in nearly all MOB (except genus *Methylocella*) while the cytoplasmic, soluble form is only found in a subset of MOB (Bowman, 2014; Dumont & Murrell, 2005). Particulate MMO are related to ammonia monooxygenases (AMO) which oxidize ammonia as their primary substrate but are also capable of oxidizing methane (Holmes et al, 1995; Hyman et al, 1988). Intriguingly, the filamentous gammaproteobacterial MOB *Crenothrix polyspora* has been reported to possess an 'unusual' pMMO closely related to AMO (Stoecker et al, 2006). However, these findings have recently been questioned. Studies suggested that the 'unusual' *Crenothrix* pMMO was likely misassigned and represented a phylogenetically divergent AMO of ammonia-oxidizing *Nitrospira* bacteria instead (Daims et al, 2015; van Kessel et al, 2015).

Methanol from methane oxidation by MMOs is further oxidized to formaldehyde by methanol dehydrogenase (MDH). Two MDH homologs have been described for MOB: calcium-dependent MxaF-type MDHs (Anthony, 2004) and lanthanide-dependent XoxF MDHs (Keltjens et al, 2014). Traditionally, MxaF-type MDHs were assumed to be the major functional MDHs in MOB. Though, XoxF homologs are encoded by many MOB and are likely the predominant MDHs in the environment. (Chistoserdova, 2016; Pol et al, 2014). The product of methanol oxidation, formaldehyde, is oxidized to formate via tetrahydromethanopterin (H₄MPT)- or tetrahydrofolate (H₄F)-linked C1 transfer pathway (Chistoserdova et al, 2009). Finally, formate is converted to CO₂ by formate dehydrogenases, which conclude the aerobic methane oxidation pathway (Hanson & Hanson, 1996).

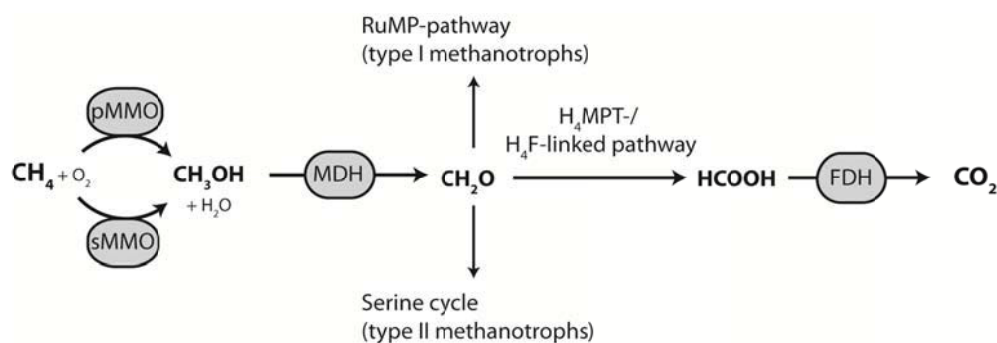


Figure 1. Enzymatic pathways of aerobic methane oxidation and carbon assimilation of proteobacterial methanotrophs (adapted from Hanson and Hanson, 1996). Initial oxidation of methane to methanol is carried out by particulate or soluble methane monooxygenase (pMMO , sMMO) followed by methanol oxidation to formaldehyde by methanol dehydrogenase (MDH). Further oxidation of formaldehyde is mediated by enzymes of the tetrahydromethanopterin (H_4MPT) or tetrahydrofolate (H_4F)-linked C1 transfer pathway to formate, which is oxidized to the final product, CO_2 , by formate dehydrogenase (FDH). Carbon for biomass is classically derived from formaldehyde via Ribulose monophosphate (RuMP) pathway in type I methanotrophs or Serine cycle in type II methanotrophs.

Most MOB derive carbon for biomass formation from methane oxidation (Figure 1). Gammaproteobacterial (type I) MOB use formaldehyde, which is transiently formed during methane oxidation, as the sole carbon source for assimilation via the ribulose monophosphate (RuMP) cycle (Anthony, 1982; Chistoserdova, 2011). Alphaproteobacterial type II MOB use the serine cycle for carbon assimilation that combines carbon from CO_2 and formaldehyde for biomass formation (Anthony, 1982; Chistoserdova, 2011). A third, purely autotrophic carbon fixation pathway (Calvin–Benson–Bassham cycle; CBB cycle) is used by verrucomicrobial methanotrophs (Op den Camp et al, 2009).

Aerobic MOB couple methane oxidation to the reduction of molecular oxygen. The electron donor for methane oxidation to methanol, which is an energy-dependent reaction, is thought to be either NADH (sMMO) or a membrane-integral quinol (pMMO) (DiSpirito et al, 2004). Periplasmic methanol oxidation by MDH is coupled to c-type cytochromes while cytosolic oxidation of formate and formaldehyde generates NADH . Subsequently, reducing equivalents from NADH are transferred to periplasmic cytochrome c via membrane-bound enzymes of the respiratory chain (NADH dehydrogenase, cytochrome bc_1 complex). Finally, cytochrome c serves as electron donor for terminal cytochrome c oxidases that reduce O_2 .

Methane oxidation via MMO by aerobic MOB directly relies directly on molecular oxygen (Murrell et al, 2000), which is either provided externally or produced internally

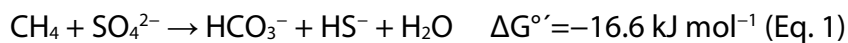
by NC10 bacteria via NO dismutation (Ettwig et al, 2012). However, aerobic MOB can be abundant and active in oxygen-deficient environments (e.g. (Oswald et al, 2016; Tavormina et al, 2013)). Genomic studies have revealed that many gamma-proteobacterial “aerobic” methanotrophs encode partial denitrification pathways (often terminating N_2O) potentially enabling survival under oxygen-limited conditions (Kalyuzhnaya et al, 2015; Kits et al, 2015a; Stein & Klotz, 2011). Furthermore, it has been shown that the gamma-proteobacterial methanotroph *Methylomonas denitrificans* is capable of coupling denitrification to methane oxidation under hypoxic conditions (Kits et al, 2015b). “Aerobic” MOB might be able to utilize both oxygen and nitrogen oxides as terminal electron acceptors (Chen & Strous, 2013), which could allow these microorganisms to conserve O_2 (for methane oxidation by MMO) under oxygen-deficient conditions. However, the physiology and activity of these denitrifying “aerobic” MOB is still poorly characterized but might be important in environmental methane and nitrogen cycling.

3 Anaerobic oxidation of methane

Anaerobic oxidation of methane (AOM) is a microbially-mediated process that couples methane oxidation to the reduction of electron acceptors other than oxygen. Known electron acceptors for anaerobic oxidation of methane include nitrate, nitrite, metal ions (i.e. iron or manganese) and sulfate.

3.1 Sulfate-dependent anaerobic oxidation of methane

First indications for sulfate-dependent AOM arose from geochemical studies of marine sediments that showed a concurrent decrease of sulfate and methane in anoxic, distinct sediment layers, so-called sulfate-methane transition zone (SMTZ) (Barnes & Goldberg, 1976; Martens & Berner, 1974; Reeburgh, 1976). Subsequent studies indicated that the methane oxidation and sulfate reduction in sediments was stoichiometrically coupled (Eq. 1) (Iversen & Jørgensen, 1985).



Based on radiotracer and inhibition experiments it was suggested that S-AOM could be mediated by methanogenic archaea and sulfate-reducing bacteria despite the low Gibbs free energy change of the reaction (Alperin & Reeburgh, 1985; Hoehler et al, 1994; Zehnder & Brock, 1979). Indirect evidence for the involvement of anaerobic methanotrophic archaea (ANME) came from archaeal lipid biomarkers that were imprinted with the isotopic ^{13}C signature of methane and 16S rRNA gene sequences of a novel archaeal group related to methanogens (Hinrichs et al, 1999). Using fluorescence *in situ* hybridization (FISH), tightly packed consortia of ANME and SRB could be visualized (Boetius et al, 2000) and were subsequently discovered to be highly abundant in various methane-rich anoxic sediments and other environments such as the Black Sea (Michaelis et al, 2002), mud volcanoes (Lösekann et al, 2007) as well as cold and hot seepage sites (Holler et al, 2011; Omoregie et al, 2009).

In marine sediments, the most widespread niche of S-AOM is the sulfate-methane transition zone (SMTZ) that is typically located from one to several meters below the sediment surface (Jørgensen & Kasten, 2006). The products of S-AOM, bicarbonate and hydrogen sulfide, can reach high concentrations within and around

the SMTZ leading to the formation of authigenic mineral phases (i.e. Mg- and Ca-carbonates) and alter redox chemistry of the sediment (Moore et al, 2004). For example, particulate Fe(III) oxo-hydroxides readily undergo reductive dissolution together with hydrogen sulfide within the SMTZ and release inorganic phosphate which was adsorbed to Fe(III) oxo-hydroxides. This mechanism can lead to increased porewater concentrations of soluble Fe(II) and phosphate in the SMTZ and likely controls authigenesis of phosphate minerals such as vivianite present in and below the SMTZ of anoxic basins and deep-sea fans (Jilbert & Slomp, 2013; März et al, 2008).

3.1.1 Microorganisms involved in S-AOM

The microorganisms that mediate S-AOM are related to anaerobic methanotrophic archaea (ANME) and associated *Deltaproteobacteria*, which often form tightly clustered aggregates (Figure 2). ANME are strict anaerobes and are phylogenetically related to methanogenic archaea of the orders *Methanosarcinales* and *Methanomicrobiales*. Based on 16S rRNA sequence analysis, anaerobic methanotrophic archaea (ANME) are phylogenetically subdivided into three main polyphyletic groups (ANME-1, ANME-2 and ANME-3). These groups are separated by considerably large phylogenetic distances which suggest that they belong to different families or even orders (Knittel & Boetius, 2009). The ANME-1 group is distantly related to *Methanomicrobiales* while ANME-2 and ANME-3 represent lineages within *Methanosarcinales* (Hinrichs et al, 1999; Knittel et al, 2005; Niemann et al, 2006). The co-occurring bacterial partners are related to delta-proteobacterial *Desulfococcus/Desulfosarcina* cluster (DSS) or *Desulfobulbus* (DBB). ANME-1 and ANME-2 groups are frequently associated with SEEP-SRB1 and SEEP-SRB2 subgroups of the DSS cluster whereas ANME-3 are often found together with *Desulfobulbus* (DBB) (Kleindienst et al, 2012; Knittel et al, 2003; Knittel et al, 2005; Niemann et al, 2006). Thermophilic members of ANME-1 associate with bacteria of the delta-proteobacterial HotSeep-1 cluster which form a separate group unrelated to DSS or DBB (Holler et al, 2011; Krukenberg et al, 2016). Additionally, ANME-1 are also consistently found as single cells or as monospecific aggregates which are apparently not associated with a bacterial partner (Knittel et al, 2005; Orphan et al, 2002).

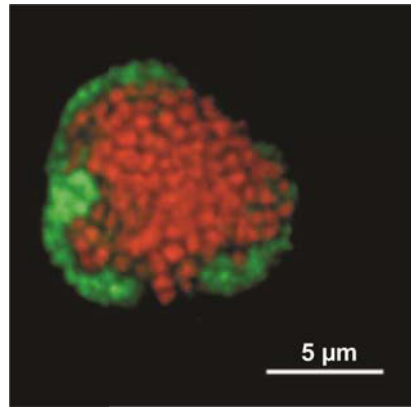


Figure 2. Confocal laser scanning micrograph of an S-AOM consortium visualized by fluorescence *in situ* hybridization (from Boetius et al., 2000). DSS bacteria, targeted by probe Δ S5658, are shown in green. ANME archaea are shown in red (labeled by EelMS932 probe)

3.1.2 Mechanisms underlying the S-AOM process

The co-occurrence of ANME with bacterial partner suggests that S-AOM is achieved by the combined metabolic activity of the partners. Microbial syntrophy, an interaction for the common good, is indeed a widespread phenomenon in nature, especially in anoxic environments (Morris et al, 2013; Stams et al, 2006). Several fundamentally different syntrophic and non-syntrophic S-AOM models have been proposed and extensively tested – yet, an unequivocal mechanism for S-AOM is still missing.

A common denominator shared between all S-AOM models is that ANME are responsible for methane oxidation. Two syntrophic S-AOM models have been proposed that assume bacterial sulfate reduction: methane-derived organic intermediates or reducing equivalents produced by ANME serve as substrate for the bacterial partner (Figure 3a); or indirect or direct electron transfer via redox active carriers or nanowires (Figure 3b). Alternatively, two non-syntrophic interaction models assume dissimilatory sulfate reduction by ANME: zero-valent sulfur compounds produced by sulfate-reducing ANME serve as intermediates, which are disproportionated by the bacterial partner to sulfide and sulfate (Milucka et al, 2012) (Figure 4a); or ANME perform complete sulfate reduction and excrete reduced metabolic by-products that are scavenged by the sulfate-reducing bacterial microorganism (Thauer & Shima, 2008; Widdel et al, 2007) (Figure 4b).

S-AOM models that predict sulfate reduction by the bacterial partner inherently must have a mechanism that couple the two redox processes. Acetate, formate,

hydrogen and methanol are classic intermediates that are exchanged in syntrophic partnerships and their role was also investigated in S-AOM. Addition of these intermediate would lead to a stimulation of the SRB partner as well as inhibition of S-AOM activity – however, sulfate reduction rates under S-AOM conditions were on par (or lower) upon the addition of acetate, formate, hydrogen or methanol (Nauhaus et al, 2002; Nauhaus et al, 2005); likewise, no repression of S-AOM activity was observed (Meulepas et al, 2010).

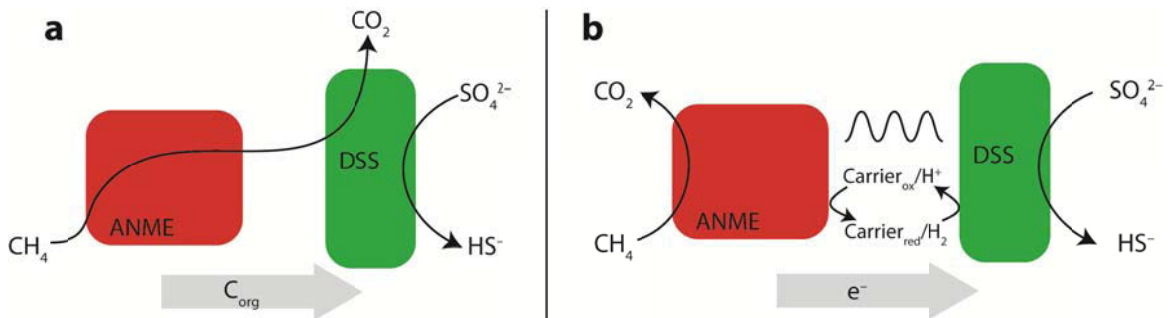


Figure 3. Schematic illustration of syntrophic S-AOM hypotheses that assume sulfate reduction by the bacterial partner. (a) Methane-derived carbon is transferred from ANME to DSS that oxidize the organic carbon intermediates coupled to sulfate reduction. (b) Electrons from methane oxidation are transferred to sulfate-reducing DSS either directly or via redox-active carriers.

Consistent with these results, exchange of carbon intermediates between the partners was not supported by ¹³C isotopic labeling studies showing autotrophic growth of S-AOM-associated SRB (Kellermann et al, 2012a; Wegener et al, 2008). More recently, the bacterial partner of a thermophilic S-AOM consortium, consisting of ANME-1 and HotSeep-1 bacteria, has been shown to be capable of hydrogen oxidation; however, it was suggested that hydrogen was not provided by ANME-1 as an intermediate (Krukenberg et al, 2016; Wegener et al, 2015). Two other potential intermediates, carbon monoxide and methanethiol, were tested but appeared to be not involved in S-AOM (Meulepas et al, 2010; Moran et al, 2008; Nauhaus et al, 2002; Nauhaus et al, 2005).

Besides methane-derived intermediates, electron transfer mediated via electron carriers, direct cell-cell contacts or conductive structures have been investigated as coupling mechanism in S-AOM. Several electron carrier systems such as the humic acid, anthraquinone-2,6-disulfonate (AQDS) or phenazines were tested but no decoupling of methane oxidation by ANME could be observed (Nauhaus et al, 2005). These findings were recently challenged by a study which demonstrated that methane oxidation by

ANME-2 could be decoupled from sulfate reduction upon the addition of humic acid, AQDS and iron(III) complexes (Scheller et al, 2016).

Type IV pili, extracellular cytochromes *c* of the bacterial partner and S-layer containing multi-heme cytochromes *c* of ANME were also hypothesized to be involved in direct interspecies electron transfer (DIET) (McGlynn et al, 2015; Wegener et al, 2015). However, physical cell-cell contacts necessary for DIET (Reguera et al, 2005; Stams et al, 2006) were not observed in some cases (e.g. microbial AOM mats, monospecific ANME aggregates or single, free-living cells) (Durisch-Kaiser et al, 2005; Orphan et al, 2002; Treude et al, 2007) suggesting alternative mechanism(s) mediating S-AOM.

A fundamentally different S-AOM mechanism has been proposed by Milucka and colleagues (2012), which attributes sulfate reduction to ANME archaea (Milucka et al, 2012). In this model, ANME-2 archaea couple methane oxidation to sulfate reduction, producing zero-valent sulfur (or sulfide) that was shown to accumulate intracellularly. Zero-valent sulfur could exit the archaea and subsequently react extracellularly with sulfide, forming polysulfides, which could be disproportionated to sulfate and sulfide by the DSS. Accordingly, S-AOM might not be an obligate syntrophic process, which also could explain the occurrence of active single ANME-2 cells found *in vitro* (House et al, 2011) and in marine environments (Orphan et al, 2002; Treude et al, 2007). While this model has been corroborated using ANME-2/DSS consortia, the underlying biochemical pathway of archaeal sulfate reduction and bacterial polysulfide disproportionation remain largely unresolved.

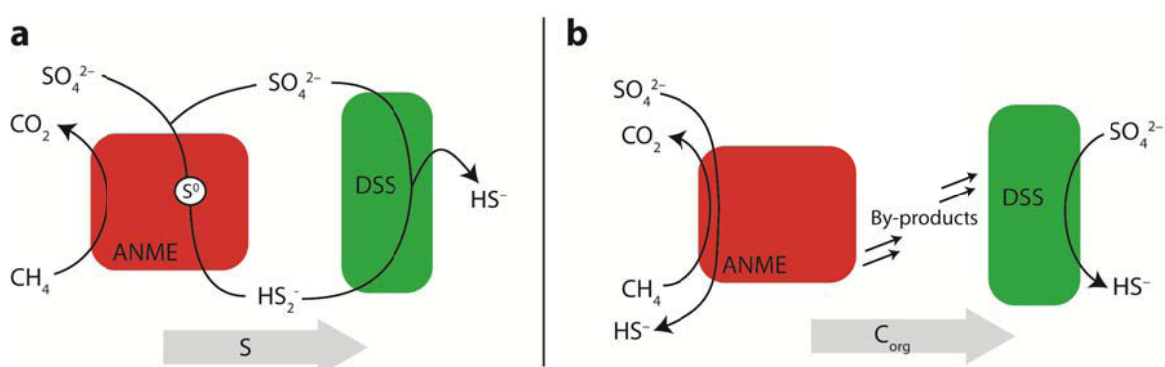


Figure 4. Schematic illustration of AOM hypotheses that include sulfate reduction by ANME. (a) ANME perform methane oxidation coupled to sulfate reduction. Polysulfides (likely disulfide) are disproportionated by DSS bacteria to sulfate and sulfide. (b) ANME oxidize methane and perform complete sulfate reduction while excreting organic by-products that are substrates for DSS that perform sulfate reduction.

In the same vein, a commensalistic relationship has been proposed that suggests methane oxidation and sulfate reduction by ANME archaea. But the sulfate-reducing partner would feed off of unknown carbon intermediates or products excreted by ANME instead of zero-valent sulfur (Thauer & Shima, 2008; Widdel et al, 2007). Thus far, experimental evidence for this model is mostly circumstantial (i.e. reports of monospecific archaeal aggregates) and is not supported by ^{13}C isotopic labeling studies (Kellermann et al, 2012a; Wegener et al, 2008).

3.1.3 Physiology of S-AOM-associated microorganisms

S-AOM-associated microorganisms are often considered to be living at the thermodynamic limit of life which is estimated to be -15 kJ mol^{-1} (Caldwell et al, 2008). Indeed, the Gibbs free energy change, which apparently has to be shared by two separate microorganisms, is estimated to yield only -22 to $-35 \text{ kJ (mol CH}_4\text{)}^{-1}$ under *in situ* conditions ($-16.6 \text{ kJ mol}^{-1}$ under standard conditions) (Caldwell et al, 2008). Due to the low energy yield, the growth of AOM consortia is extremely slow with estimated doubling times of 2 to 6 months (Holler et al, 2011; Milucka et al, 2012; Nauhaus et al, 2007). Owing to the slow growth, enrichment of AOM consortia take years (and have been ongoing since more than a decade) and so far no axenic culture of an S-AOM consortium has been obtained. Physiological studies of S-AOM are also hindered by the fact that, with the exception of the bacterial TAOM partner "*Ca. Desulfofervidus auxilii*", no S-AOM microbe could be successfully separated.

3.1.3.1 Methane oxidation and carbon metabolism

Labeling studies using ^{14}C methane with methanogenic archaea suggested that the enzymatic pathway of methanogenesis in principle is reversible, albeit only marginally (Harder, 1997; Moran et al, 2005; Zehnder & Brock, 1979). Consequently it was proposed that ANME oxidize methane by reverse methanogenesis and indeed, genes encoding for most or all enzymes of the methanogenesis pathway are present and expressed in all methane-oxidizing ANME species investigated thus far (Arshad et al, 2015; Hallam et al, 2004; Haroon et al, 2013; Meyerdierks et al, 2010; Wang et al, 2014). Much knowledge of this pathway and its reversibility has been drawn from previous extensive biochemical studies of methanogenesis (Thauer, 1998; Thauer, 2011).

Reverse methanogenesis is a multistep enzymatic pathway during which methane is completely oxidized to CO₂ (Figure 5). The first step in this process is catalyzed by methyl-coenzyme M reductase (Mcr) – a hallmark enzyme of anaerobic methanotrophs, similar to MMO of aerobic methanotrophs. In S-AOM-active microbial mats from the Black Sea, Mcr accounted for up to 7% of total extractable protein (Krüger et al, 2003). Methane is activated by Mcr and bound as methyl group to coenzyme M (CoM-SH) forming methyl-S-CoM; this reaction is coupled to the reduction of the disulfide of coenzyme M and coenzyme B (CoB-SS-CoM). The methyl group of methyl-S-CoM is subsequently transferred to tetrahydromethanopterin (H₄MPT) by the membrane-bound methyl-H₄MPT:CoM methyltransferase (Mtr). CoM-SH produced during this step is oxidized with CoB-SH by heterodisulfide reductase (Hdr) forming CoB-SS-CoM, which again can be used by Mcr. Methyl-H₄MPT is subsequently oxidized gradually to methylene-, methenyl-, and formyl-H₄MPT by enzymes methylene-H₄MPT reductase (Mer), methylene-H₄MPT dehydrogenase (Mtd) and methenyl-H₄MPT cyclohydrolase (Mch), respectively. Following the transfer of the formyl group from H₄MPT to methanofuran (MFR) by formyl-MFR: H₄MPT formyltransferase (Ftr), CO₂ is released in the last step of reverse methanogenesis from formyl-MFR by the formyl-MFR dehydrogenase (Fmd). Reducing equivalents derived from the oxidation of methane during reverse methanogenesis (equivalent to 8 e⁻) are transferred to three different electron carriers (coenzyme F420, CoM-SH/CoB-SH and ferredoxin; Figure 5). With the exception of ANME-1 (Meyerdierks et al, 2010), which apparently lacks a Mer homolog, genomes of all ANME members sequenced to date encode the full reverse methanogenesis pathway.

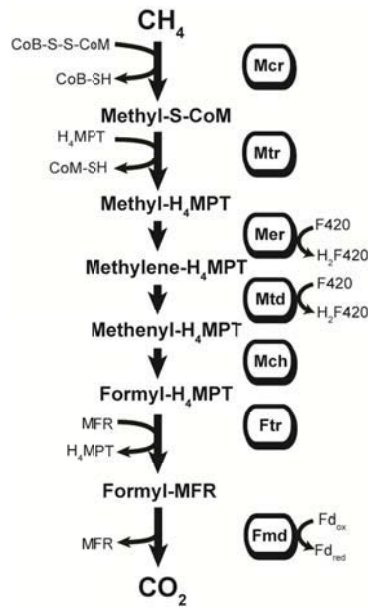


Figure 5. Schematic illustration of the archaeal reverse methanogenesis pathway of ANME. Methane is gradually oxidized to CO_2 by the seven core enzymes (black boxes) of the reverse methanogenesis pathway. Reducing equivalents exit the pathway through the electron carriers coenzyme F420, CoB-SH/CoM-SH and ferredoxin (Fd). Abbreviations of enzymes and cofactors are listed in text.

It appears that ANME-1 do not assimilate methane (only CO_2) while other members of cold seep-related ANME have been reported to incorporate methane and CO_2 in a 1:1 ratio (Kellermann et al, 2012b; Wegener et al, 2008). In any case, genomic studies indicate that all members of ANME use the Wood-Ljungdahl pathway for carbon assimilation (Arshad et al, 2015; Haroon et al, 2013; Meyerdierks et al, 2010; Wang et al, 2014). The bacterial partners of S-AOM are also autotrophs as they apparently derive all of their carbon from CO_2 likely via the Wood-Ljungdahl pathway (Wegener et al, 2016; Wegener et al, 2008). HotSeep-1 bacteria, which are phylogenetically unrelated to DSS, apparently utilize the reductive tricarboxylic citric acid cycle for carbon fixation (Krukenberg et al, 2016).

3.1.3.2 Sulfur metabolism

Sulfate reduction plays a central role in S-AOM depending on the proposed mechanism, it is either attributed to ANME or the bacterial partner. Classically, sulfate reduction is thought to be performed by the bacterial partner via a dissimilatory sulfate reduction (SR) pathway (Figure 6).

In the first step of this pathway, sulfate is activated together with ATP by sulfate adenylyltransferase (Sat) forming adenosine 5'-phosphosulfate (APS), which is

subsequently reduced to sulfite by APS reductase (AprAB). Recent evidence has shown that reduction of sulfite to sulfide is a two-step process (Santos et al, 2015). First, sulfite is reduced and bound as trisulfide to the small sulfur carrier protein, DsrC, by dissimilatory sulfite reductase (DsrAB). In the second step, sulfide is released from the DsrC trisulfide by reduction by the DsrMKJOP complex. Electrons for the cytosolic sulfate reduction are mainly derived from the membrane-bound quinone pool via membrane-bound and/or cytoplasmic enzyme complexes (i.e. DsrMKJOP or QmoABC) (Grein et al, 2013; Pereira et al, 2011).

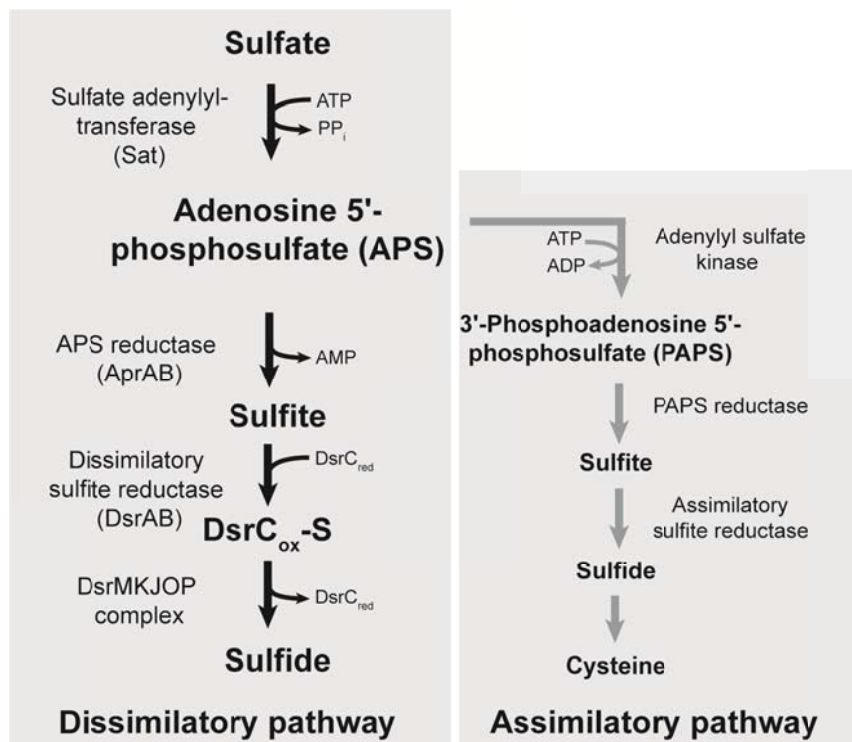


Figure 6. Schematic illustration of the prokaryotic dissimilatory and assimilatory sulfate reduction pathway (adapted from Grein et al, 2013). Sulfate reduction can either serve assimilatory or dissimilatory function. The purpose of the assimilatory pathway is to produce small quantities of sulfide from sulfate. Sulfide is converted to cysteine which serves as universal sulfur donor for various sulfur-containing biological molecules. If available, exogenous sulfide can also be used for assimilatory purposes. The dissimilatory sulfate reduction pathway uses sulfate as electron acceptor for respiration; hence, electrons are supplied by dedicated membrane-bound respiratory chain complexes, which is not the case for the assimilatory pathway.

Enzymes of the dissimilatory SR pathway are abundant in S-AOM-active microbial mats from the Black Sea (up to 2% of total soluble protein) and immunolabeling studies have shown these enzymes are exclusively found in DSS bacteria (Basen et al, 2011; Milucka et al, 2013). Another S-AOM hypothesis suggests that DSS bacteria perform sulfur disproportionation rather than sulfate reduction

(Milucka et al, 2012). Disproportionation of intermediate oxidation state sulfur compounds (i.e. elemental sulfur, polysulfides, sulfite or thiosulfate) is performed by members of *Desulfocapsa*, *Desulfobulbus*, *Desulfovibrio* and *Desulfofustis* that belong to *Deltaproteobacteria* (Finster, 2008). It has been shown for *Desulfocapsa sulfexigens* that disproportionation of intermediate sulfur compounds is apparently mediated by the same enzymes that mediate the canonical SR pathway (Finster et al, 2013; Frederiksen & Finster, 2003). Apr and Sat are thought to operate in reverse and produce sulfate by reverse electron flow to Dsr that reduces sulfite to sulfide. Hence it is equally plausible that the SR enzymes detected in DSS cells are involved in sulfur disproportionation as opposed to sulfate reduction (Milucka et al, 2012). Yet, little is known how the various intermediate oxidation state sulfur compounds are disproportionated by enzymes of the SR pathway but it has been shown that sulfite plays a crucial intermediate (Frederiksen & Finster, 2003). Molybdopterin oxidoreductases and rhodanese-related sulfurtransferases have also been suggested as potential candidates for disproportionation of thiosulfate and elemental sulfur (Finster et al, 2013).

There is currently no evidence that ANME possess enzymes or genes of the canonical dissimilatory SR pathway (Milucka et al, 2013; Wang et al, 2014). Archaeal sulfate reduction so far has only been observed in few genera of sulfate-reducing thermophilic archaea that use the canonical SR pathway which was likely obtained from an ancient bacterial donor (Klein et al, 2001; Klenk et al, 1997). However, a nearly complete gene set encoding for assimilatory sulfate reduction has been identified in an ANME-1 draft genome (Meyerdierks et al, 2010). A dissimilatory role of this pathway cannot be excluded, especially since ANME likely rely on sulfide as sulfur source. Additionally, genes encoding for a F_{420} -dependent sulfite reductase (Fsr) were identified on a metagenomic contig assigned to ANME (Hallam et al, 2004). Fsr is found in many genomes of methanogens where it was shown to be involved in sulfite detoxification and sulfur assimilation from sulfite (Johnson & Mukhopadhyay, 2005; Johnson & Mukhopadhyay, 2008). Moreover, Meyerdierks and colleagues (2005, 2010) identified several expressed, non-canonical heterodisulfide reductase (Hdr) gene clusters missing CoM-SH/CoB-SH-interacting subunits with potential relevance to sulfate reduction in ANME.

3.1.3.3 C-type cytochromes

Cytochromes *c* are heme-containing electron transfer proteins and important enzymes involved in microbial sulfur and nitrogen transformations (de Almeida et al, 2011; Lovley, 2017; Simon et al, 2011). Large outer-membrane cytochromes *c* in particular have been shown to be involved in extracellular electron transfer by *Geobacter sulfurreducens* (reviewed in (Lovley, 2012)). Among archaea, genes encoding cytochromes *c* are especially abundant in genomes of metal-reducing species, such as *Ferroglobus placidus* or “*Ca. Methanoperedens nitroreducens*”, but other ANME archaea also appear to harbor a large diversity of multi-heme cytochromes *c* (Kletzin et al, 2015; McGlynn et al, 2015).

The pinkish color of microbial mats from the Black Sea (Figure 7) has been attributed to cytochromes, presumably of ANME-1 archaea (Michaelis et al, 2002; Pimenov et al, 1997). McGlynn and colleagues (2015) suggested that large multi-heme cytochromes (MHC; sometimes with fused S-layer domains) encoded by ANME-2 genomes might be involved in short-range extracellular electron transfer. It is also conceivable that MHCs increase the metabolic flexibility of ANME by coupling methane oxidation to electron acceptors other than sulfate, such as iron or manganese (Beal et al, 2009; Ettwig et al, 2016). Furthermore, genomic and transcriptomic studies of the bacterial TAOM partner, HotSeep-1, have provided evidence that bacterial extracellular multiheme cytochromes *c* (possibly in combination with type IV pili) could also be involved in direct electron transfer between HotSeep-1 to ANME-1.

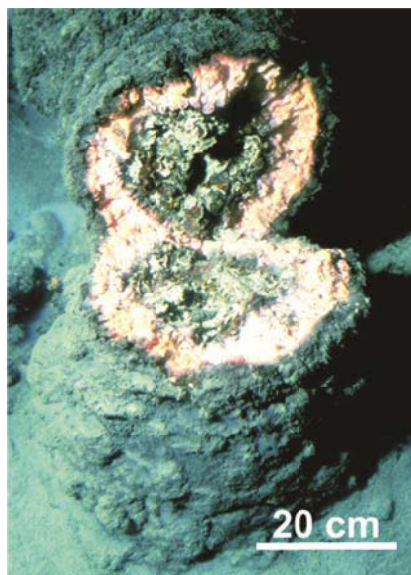


Figure 7. Fractured chimney-like microbial AOM mat from a Black Sea microbial reef (from (Michaelis et al, 2002)). The inner part of the structure consists of porous carbonate populated by a thick microbial mat. The mat is grey-black on the outside; the interior is pinkish in color.

3.2 Anaerobic oxidation of methane coupled to denitrification

Anaerobic methane oxidation coupled to denitrification is carried out by two metabolically distinct groups of microorganisms: "*Ca. Methyloirabilis oxyfera*" of the NC10 candidate phylum and "*Ca. Methanoperedens nitroreducens*" of the ANME group.

Nitrite-dependent AOM is carried out by bacteria of the candidate phylum NC10 (Raghoebarsing et al, 2006). The main habitat of NC10 bacteria appears to be anoxic freshwater systems (Deutzmann & Schink, 2011; He et al, 2016; Kojima et al, 2012) although NC10 have also been identified in marine oxygen minimum zones (Padilla et al, 2016). The first described member of NC10, "*Ca. Methyloirabilis oxyfera*", has been shown to utilize a typical aerobic methane oxidation pathway for methane oxidation that includes the oxygen-dependent MMO enzyme (Ettwig et al, 2010a). In contrast most MOB, NC10 bacteria related to "*Ca. Methyloirabilis oxyfera*" are autotrophs. They do not derive biomass carbon from methane and fix CO₂ via the autotrophic Calvin–Benson–Bassham cycle (Ettwig et al, 2010a). "*Ca. M. oxyfera*" has been shown to couple methane oxidation to nitrite reduction (to N₂ gas) via a unique O₂-producing denitrification pathway. It is believed that molecular oxygen is formed by NO dismutation to N₂ and O₂, which is apparently catalyzed by an unusual membrane-bound nitric oxide reductase that is speculated to work as NO dismutase (Ettwig et al, 2010b; Ettwig et al, 2012). Intracellular oxygen production via denitrification is believed to be the defining feature of NC10 that allows these bacteria to perform methane oxidation by pMMO under anaerobic conditions.

Nitrate-dependent AOM is carried out by the archaeon "*Ca. Methanoperedens nitroreducens*" (sometimes referred to as ANME-2d), which belongs to the lineage of ANME-2 that also harbors S-AOM-associated ANME groups (Haroon et al, 2013). "*Ca. M. nitroreducens*" is similar to S-AOM-associated ANME as it also utilized the reverse methanogenesis pathway for methane oxidation. However, "*Ca. M. nitroreducens*" performs AOM coupled to nitrate reduction (to nitrite) by itself as it possesses a nitrate reductase (Arshad et al, 2015; Haroon et al, 2013). Moreover, it has been recently shown that "*Ca. M. nitroreducens*" is also capable of metal ion-dependent AOM (i.e. Fe³⁺, Mn⁴⁺) (Ettwig et al, 2016).

In addition to these microorganisms, denitrification by aerobic MOB is an emerging topic in methanotroph research and has been introduced in the respective section that covers aerobic methanotrophs. Methane oxidation by MMO in these microorganisms apparently still relies on exogenous molecular oxygen, which makes them distinctly different from NC10 and "*Ca. Methanoperedens nitroreducens*".

Aims and Outline

The importance of methane-oxidizing microorganisms in limiting emissions of methane, a potent greenhouse gas, from aquatic environments cannot be overstated. One could even argue that it is hard to imagine how different Earth's climate and ecosystems would be without these methane-devouring microorganisms. Despite their importance, relatively little is known about their individual physiology since many methane-oxidizing microorganisms are not available for study in pure culture. The aim of this thesis was to gain a better understanding of the physiology and ecology of several groups of methane-oxidizing microorganisms found in freshwater and marine systems. Throughout this thesis, genome-centric functional metagenomics was the main tool used to study these microorganisms, which allowed us to infer and in some cases unravel their physiology in the absence of pure cultures. Furthermore, we combined this approach with a variety of other analytical and experimental techniques to learn more about their habitat and ecophysiology. The results and data generated during this thesis will also serve as foundation for future research to expand and build upon. This will allow us to better understand and predict the role methane-oxidizing microorganisms play in a changing environment increasingly affected by human activity.

In Chapters 2 and 3 of this thesis, we investigate the methanotrophic community in two Swiss stratified lakes (Lake Zug and Rotsee). These eutrophied lakes are seasonally or permanently stratified and harbor a diverse community of proteobacterial aerobic methanotrophs (Oswald et al, 2016). The role of *Crenothrix* bacteria in the methane cycle in these freshwater lakes is explored in Chapter 2. These filamentous bacteria have been known as contaminants of drinking water supplies for more than a century; however, their ecological relevance has remained unclear. Using stable-isotope labeling incubations in combination with bulk and single-cell imaging mass spectrometry as well as metagenomics, we highlight several aspects pertaining to their physiology and their role in the environment. In Chapter 3, we returned to Lake Zug in a different year to investigate the methanotrophic community and discovered highly abundant methane-oxidizing bacteria of the candidate phylum NC10. These methanotrophic bacteria, which were not detected in previous years ((Oswald et al,

2016), Chapter 2), have been described as widespread but rare members of the methanotrophic bacterial community in lakes. We highlight their metabolic and functional activity using metagenomics and metatranscriptomic techniques and suggest a niche for NC10 in the lacustrine methane and nitrogen cycle.

In contrast to freshwater environments, sulfate-dependent anaerobic oxidation of methane (S-AOM) is the predominant process in marine environments that controls the flux of methane from sediments. This microbial process is mediated by a consortium of methanotrophic archaea and associated bacteria. Despite several decades of research, the individual physiology and relationship between these two different microorganisms has only been partially elucidated. In Chapter 4, we describe a genome-centric functional metagenomics approach to obtain the genomic blueprint of S-AOM-associated microorganisms from an enrichment culture. By using gene transcription profiles and detection of enzymes by metaproteomics, we reconstructed important metabolic pathways of both microorganisms that underlie their functional activity. Based on this, we evaluated different hypotheses regarding the physiology and interaction of microorganisms involved in S-AOM.

Previous research has suggested that S-AOM-associated microorganisms not only play a role in sedimentary biogeochemical cycles of carbon and sulfur, but that their influence might also extend to the cycles of phosphorus and iron. In Chapter 5, we trace the fate of inorganic phosphate in a highly active AOM enrichment culture incubated with radiolabeled, inorganic phosphate (^{33}P -phosphate). Additionally, we used scanning transmission electron microscopy coupled to energy dispersive x-ray analysis (STEM-EDX) to visualize and analyze electron-dense particles within AOM-associated bacteria and use the combined results to speculate on the underlying mechanism that might cause the observed cycling of inorganic phosphate.

References

- Alperin MJ, Reeburgh WS (1985) Inhibition experiments on anaerobic methane oxidation. *Applied and environmental microbiology* **50**: 940-945
- Anthony C (1982) *Biochemistry of methylotrophs*: Academic Press.
- Anthony C (1986) Bacterial oxidation of methane and methanol. *Advances in microbial physiology* **27**: 113-210
- Anthony C (2004) The quinoprotein dehydrogenases for methanol and glucose. *Archives of biochemistry and biophysics* **428**: 2-9
- Arshad A, Speth DR, de Graaf RM, den Camp HJO, Jetten MS, Welte CU (2015) A metagenomics-based metabolic model of nitrate-dependent anaerobic oxidation of methane by Methanoperedens-like archaea. *Frontiers in microbiology* **6**
- Barnes R, Goldberg E (1976) Methane production and consumption in anoxic marine sediments. *Geology* **4**: 297-300
- Basen M, Krüger M, Milucka J, Kuever J, Kahnt J, Grundmann O, Meyerdierks A, Widdel F, Shima S (2011) Bacterial enzymes for dissimilatory sulfate reduction in a marine microbial mat (Black Sea) mediating anaerobic oxidation of methane. *Environmental microbiology* **13**: 1370-1379
- Bastviken D, Cole JJ, Pace ML, Van de Bogert MC (2008) Fates of methane from different lake habitats: connecting whole-lake budgets and CH₄ emissions. *Journal of Geophysical Research: Biogeosciences* **113**
- Beal EJ, House CH, Orphan VJ (2009) Manganese- and iron-dependent marine methane oxidation. *Science* **325**: 184-187
- Bodrossy L, Holmes EM, Holmes AJ, Kovács KL, Murrell JC (1997) Analysis of 16S rRNA and methane monooxygenase gene sequences reveals a novel group of thermotolerant and thermophilic methanotrophs, *Methylocaldum* gen. nov. *Archives of Microbiology* **168**: 493-503
- Boetius A, Ravensschlag K, Schubert CJ, Rickert D, Widdel F, Gieseke A, Amann R, Jørgensen BB, Witte U, Pfannkuche O (2000) A marine microbial consortium apparently mediating anaerobic oxidation of methane. *Nature* **407**: 623-626
- Boetius A, Wenzhöfer F (2013) Seafloor oxygen consumption fuelled by methane from cold seeps. *Nature Geoscience* **6**: 725-734
- Borrel G, Jézéquel D, Biderre-Petit C, Morel-Desrosiers N, Morel J-P, Peyret P, Fonty G, Lehours A-C (2011) Production and consumption of methane in freshwater lake ecosystems. *Research in microbiology* **162**: 832-847

Bowman JP (2014) The family Methylococcaceae. In *The Prokaryotes*, pp 411-440. Springer

Caldwell SL, Laidler JR, Brewer EA, Eberly JO, Sandborgh SC, Colwell FS (2008) Anaerobic oxidation of methane: mechanisms, bioenergetics, and the ecology of associated microorganisms. *Environmental science & technology* **42**: 6791-6799

Chen J, Strous M (2013) Denitrification and aerobic respiration, hybrid electron transport chains and co-evolution. *Biochimica et Biophysica Acta (BBA)-Bioenergetics* **1827**: 136-144

Chistoserdova L (2011) Modularity of methylotrophy, revisited. *Environmental microbiology* **13**: 2603-2622

Chistoserdova L (2016) Lanthanides: New life metals? *World Journal of Microbiology and Biotechnology* **32**: 1-7

Chistoserdova L, Kalyuzhnaya MG, Lidstrom ME (2009) The expanding world of methylotrophic metabolism. *Annual review of microbiology* **63**: 477

Ciais P, Sabine C, Bala G, Bopp L, Brovkin V, Canadell J, Chhabra A, DeFries R, Galloway J, Heimann M (2014) Carbon and other biogeochemical cycles. In *Climate Change 2013: The Physical Science Basis. Contribution of Working Group I to the Fifth Assessment Report of the Intergovernmental Panel on Climate Change*, pp 465-570. Cambridge University Press

Cohn F (1870) Über den Brunnenfaden (*Crenothrix polyspora*) mit Bemerkungen über die mikroskopische Analyse des Brunnenwassers. *Beiträge zur Biologie der Pflanzen* **1**: 108-131

Conrad R (2009) The global methane cycle: recent advances in understanding the microbial processes involved. *Environmental Microbiology Reports* **1**: 285-292

Crowe S, Katsev S, Leslie K, Sturm A, Magen C, Nomosatryo S, Pack M, Kessler J, Reeburgh W, Roberts J (2011) The methane cycle in ferruginous Lake Matano. *Geobiology* **9**: 61-78

Daims H, Lebedeva EV, Pjevac P, Han P, Herbold C, Albertsen M, Jehmlich N, Palatinszky M, Vierheilig J, Bulaev A (2015) Complete nitrification by *Nitrospira* bacteria. *Nature* **528**: 504-509

de Almeida NM, Maalcke WJ, Keltjens JT, Jetten MS, Kartal B. (2011) Proteins and protein complexes involved in the biochemical reactions of anaerobic ammonium-oxidizing bacteria. Portland Press Limited.

Deutzmann JS, Schink B (2011) Anaerobic oxidation of methane in sediments of Lake Constance, an oligotrophic freshwater lake. *Applied and environmental microbiology* **77**: 4429-4436

DiSpirito AA, Kunz RC, Choi D-W, Zahn JA, Zannoni D (2004) Respiration in methanotrophs. *Respiration in archaea and bacteria* **16**: 149-168

Dumont MG, Murrell JC (2005) Community-Level Analysis: Key Genes of Aerobic Methane Oxidation. *Methods in enzymology* **397**: 413-427

Dunfield PF, Yuryev A, Senin P, Smirnova AV, Stott MB, Hou S, Ly B, Saw JH, Zhou Z, Ren Y (2007) Methane oxidation by an extremely acidophilic bacterium of the phylum Verrucomicrobia. *Nature* **450**: 879-882

Durisch-Kaiser E, Klauer L, Wehrli B, Schubert C (2005) Evidence of intense archaeal and bacterial methanotrophic activity in the Black Sea water column. *Applied and environmental microbiology* **71**: 8099-8106

Ettwig KF, Butler MK, Le Paslier D, Pelletier E, Mangenot S, Kuypers MM, Schreiber F, Dutilh BE, Zedelius J, De Beer D (2010a) Nitrite-driven anaerobic methane oxidation by oxygenic bacteria. *Nature* **464**: 543-548

Ettwig KF, Butler MK, Le Paslier D, Pelletier E, Mangenot S, Kuypers MMM, Schreiber F, Dutilh BE, Zedelius J, de Beer D, Gloerich J, Wessels HJCT, van Alen T, Luesken F, Wu ML, van de Pas-Schoonen KT, Op den Camp HJM, Janssen-Megens EM, Francoijs K-J, Stunnenberg H, Weissenbach J, Jetten MSM, Strous M (2010b) Nitrite-driven anaerobic methane oxidation by oxygenic bacteria. *Nature* **464**: 543-548

Ettwig KF, Speth DR, Reimann J, Wu ML, Jetten MS, Keltjens JT (2012) Bacterial oxygen production in the dark. *Frontiers in microbiology* **3**: 273

Ettwig KF, Zhu B, Speth D, Keltjens JT, Jetten MS, Kartal B (2016) Archaea catalyze iron-dependent anaerobic oxidation of methane. *Proceedings of the National Academy of Sciences* **113**: 12792-12796

Finster K (2008) Microbiological disproportionation of inorganic sulfur compounds. *Journal of Sulfur Chemistry* **29**: 281-292

Finster KW, Kjeldsen KU, Kube M, Reinhardt R, Mussmann M, Amann R, Schreiber L (2013) Complete genome sequence of *Desulfocapsa sulfexigens*, a marine deltaproteobacterium specialized in disproportionating inorganic sulfur compounds. *Standards in genomic sciences* **8**: 58

Frederiksen T-M, Finster K (2003) Sulfite-oxido-reductase is involved in the oxidation of sulfite in *Desulfocapsa sulfoexigens* during disproportionation of thiosulfate and elemental sulfur. *Biodegradation* **14**: 189-198

Grein F, Ramos AR, Venceslau SS, Pereira IA (2013) Unifying concepts in anaerobic respiration: insights from dissimilatory sulfur metabolism. *Biochimica et Biophysica Acta (BBA)-Bioenergetics* **1827**: 145-160

Hakemian AS, Rosenzweig AC (2007) The biochemistry of methane oxidation. *Annu Rev Biochem* **76**: 223-241

Hallam SJ, Putnam N, Preston CM, Detter JC, Rokhsar D, Richardson PM, DeLong EF (2004) Reverse methanogenesis: testing the hypothesis with environmental genomics. *Science* **305**: 1457-1462

Hanson RS, Hanson TE (1996) Methanotrophic bacteria. *Microbiological reviews* **60**: 439-471

Harder J (1997) Anaerobic methane oxidation by bacteria employing ¹⁴C-methane uncontaminated with ¹⁴C-carbon monoxide. *Marine geology* **137**: 13-23

Haroon MF, Hu S, Shi Y, Imelfort M, Keller J, Hugenholtz P, Yuan Z, Tyson GW (2013) Anaerobic oxidation of methane coupled to nitrate reduction in a novel archaeal lineage. *Nature* **500**: 567-570

He Z, Cai C, Wang J, Xu X, Zheng P, Jetten MS, Hu B (2016) A novel denitrifying methanotroph of the NC10 phylum and its microcolony. *Scientific reports* **6**: 32241

Hinrichs K-U, Boetius A (2002) The anaerobic oxidation of methane: new insights in microbial ecology and biogeochemistry. In *Ocean margin systems*, pp 457-477. Springer

Hinrichs K-U, Hayes JM, Sylva SP, Brewer PG, DeLong EF (1999) Methane-consuming archaeobacteria in marine sediments. *Nature* **398**: 802-805

Hirayama H, Abe M, Miyazaki M, Nunoura T, Furushima Y, Yamamoto H, Takai K (2014) *Methylomarinovum caldicuralii* gen. nov., sp. nov., a moderately thermophilic methanotroph isolated from a shallow submarine hydrothermal system, and proposal of the family Methylothermaceae fam. nov. *International journal of systematic and evolutionary microbiology* **64**: 989-999

Hoehler TM, Alperin MJ, Albert DB, Martens CS (1994) Field and laboratory studies of methane oxidation in an anoxic marine sediment: Evidence for a methanogen-sulfate reducer consortium. *Global Biogeochemical Cycles* **8**: 451-463

Holler T, Widdel F, Knittel K, Amann R, Kellermann MY, Hinrichs K-U, Teske A, Boetius A, Wegener G (2011) Thermophilic anaerobic oxidation of methane by marine microbial consortia. *The ISME journal* **5**: 1946-1956

Holmes AJ, Costello A, Lidstrom ME, Murrell JC (1995) Evidence that particulate methane monooxygenase and ammonia monooxygenase may be evolutionarily related. *FEMS microbiology letters* **132**: 203-208

- House CH, Beal EJ, Orphan VJ (2011) The apparent involvement of ANMEs in mineral dependent methane oxidation, as an analog for possible Martian Methanotrophy. *Life* **1**: 19-33
- Hyman MR, Murton IB, Arp DJ (1988) Interaction of ammonia monooxygenase from *Nitrosomonas europaea* with alkanes, alkenes, and alkynes. *Applied and environmental microbiology* **54**: 3187-3190
- Islam T, Jensen S, Reigstad LJ, Larsen Ø, Birkeland N-K (2008) Methane oxidation at 55 C and pH 2 by a thermoacidophilic bacterium belonging to the Verrucomicrobia phylum. *Proceedings of the National Academy of Sciences* **105**: 300-304
- Iversen N, Jørgensen B (1985) Anaerobic methane oxidation rates at the sulfate-methane transition in marine sediments from Kattegat and Skagerrak (Denmark). *Limnol Oceanogr* **30**: 944-955
- Jilbert T, Slomp CP (2013) Iron and manganese shuttles control the formation of authigenic phosphorus minerals in the euxinic basins of the Baltic Sea. *Geochimica et Cosmochimica Acta* **107**: 155-169
- Johnson EF, Mukhopadhyay B (2005) A new type of sulfite reductase, a novel coenzyme F420-dependent enzyme, from the methanarchaeon *Methanocaldococcus jannaschii*. *Journal of Biological Chemistry* **280**: 38776-38786
- Johnson EF, Mukhopadhyay B (2008) A novel coenzyme F420 dependent sulfite reductase and a small sulfite reductase in methanogenic archaea. In *Microbial Sulfur Metabolism*, pp 202-216. Springer
- Jørgensen BB, Kasten S (2006) Sulfur cycling and methane oxidation. In *Marine geochemistry*, pp 271-309. Springer
- Kalyuzhnaya MG, Lamb AE, McTaggart TL, Oshkin IY, Shapiro N, Woyke T, Chistoserdova L (2015) Draft genome sequences of gammaproteobacterial methanotrophs isolated from Lake Washington sediment. *Genome announcements* **3**: e00103-00115
- Kellermann MY, Wegener G, Elvert M, Yoshinaga MY, Lin Y-S, Holler T, Mollar XP, Knittel K, Hinrichs K-U (2012a) Autotrophy as a predominant mode of carbon fixation in anaerobic methane-oxidizing microbial communities. *Proceedings of the National Academy of Sciences* **109**: 19321-19326
- Kellermann MY, Wegener G, Elvert M, Yoshinaga MY, Lin Y-S, Holler T, Mollar XP, Knittel K, Hinrichs K-U (2012b) Autotrophy as a predominant mode of carbon fixation in anaerobic methane-oxidizing microbial communities. *Proceedings of the National Academy of Sciences*
- Keltjens JT, Pol A, Reimann J, den Camp HJO (2014) PQQ-dependent methanol dehydrogenases: rare-earth elements make a difference. *Applied microbiology and biotechnology* **98**: 6163-6183

Kirschke S, Bousquet P, Ciais P, Saunois M, Canadell JG, Dlugokencky EJ, Bergamaschi P, Bergmann D, Blake DR, Bruhwiler L (2013) Three decades of global methane sources and sinks. *Nature Geoscience* **6**: 813-823

Kits KD, Campbell DJ, Rosana AR, Stein LY (2015a) Diverse electron sources support denitrification under hypoxia in the obligate methanotroph *Methylomicrobium album* strain BG8. *Frontiers in microbiology* **6**

Kits KD, Klotz MG, Stein LY (2015b) Methane oxidation coupled to nitrate reduction under hypoxia by the Gammaproteobacterium *Methylomonas denitrificans*, sp. nov. type strain FJG1. *Environmental microbiology* **17**: 3219-3232

Klein M, Friedrich M, Roger AJ, Hugenholtz P, Fishbain S, Abicht H, Blackall LL, Stahl DA, Wagner M (2001) Multiple lateral transfers of dissimilatory sulfite reductase genes between major lineages of sulfate-reducing prokaryotes. *Journal of Bacteriology* **183**: 6028-6035

Kleindienst S, Ramette A, Amann R, Knittel K (2012) Distribution and in situ abundance of sulfate-reducing bacteria in diverse marine hydrocarbon seep sediments. *Environmental microbiology* **14**: 2689-2710

Klenk H-P, Clayton RA, Tomb J-F, White O, Nelson KE, Ketchum KA, Dodson RJ, Gwinn M, Hickey EK, Peterson JD (1997) The complete genome sequence of the hyperthermophilic, sulphate-reducing archaeon *Archaeoglobus fulgidus*. *Nature* **390**: 364-370

Kletzin A, Heimerl T, Flechsler J, van Niftrik L, Rachel R, Klingl A (2015) Cytochromes c in Archaea: distribution, maturation, cell architecture, and the special case of *Ignicoccus hospitalis*. *Frontiers in microbiology* **6**: 439

Knief C (2015) Diversity and habitat preferences of cultivated and uncultivated aerobic methanotrophic bacteria evaluated based on *pmoA* as molecular marker. *Frontiers in microbiology* **6**

Knittel K, Boetius A (2009) Anaerobic oxidation of methane: progress with an unknown process. *Annual review of microbiology* **63**: 311-334

Knittel K, Boetius A, Lemke A, Eilers H, Lochte K, Pfannkuche O, Linke P, Amann R (2003) Activity, distribution, and diversity of sulfate reducers and other bacteria in sediments above gas hydrate (Cascadia Margin, Oregon). *Geomicrobiology Journal* **20**: 269-294

Knittel K, Lösekann T, Boetius A, Kort R, Amann R (2005) Diversity and distribution of methanotrophic archaea at cold seeps. *Applied and environmental microbiology* **71**: 467-479

Kojima H, Tsutsumi M, Ishikawa K, Iwata T, Mußmann M, Fukui M (2012) Distribution of putative denitrifying methane oxidizing bacteria in sediment of a freshwater lake, Lake Biwa. *Systematic and Applied Microbiology* **35**: 233-238

Krüger M, Meyerdierks A, Glöckner FO, Amann R, Widdel F, Kube M, Reinhardt R, Kahnt J, Böcher R, Thauer RK (2003) A conspicuous nickel protein in microbial mats that oxidize methane anaerobically. *Nature* **426**: 878-881

Krukenberg V, Harding K, Richter M, Glöckner FO, Gruber-Vodicka HR, Adam B, Berg JS, Knittel K, Tegetmeyer HE, Boetius A (2016) *Candidatus Desulfofervidus auxilii*, a hydrogenotrophic sulfate-reducing bacterium involved in the thermophilic anaerobic oxidation of methane. *Environmental microbiology*

Lösekann T, Knittel K, Nadalig T, Fuchs B, Niemann H, Boetius A, Amann R (2007) Diversity and abundance of aerobic and anaerobic methane oxidizers at the Haakon Mosby Mud Volcano, Barents Sea. *Applied and environmental microbiology* **73**: 3348-3362

Lovley DR (2012) Electromicrobiology. *Annual review of microbiology* **66**: 391-409

Lovley DR (2017) Syntrophy Goes Electric: Direct Interspecies Electron Transfer. *Annual review of microbiology*

Martens CS, Berner RA (1974) Methane production in the interstitial waters of sulfate-depleted marine sediments. *Science* **185**: 1167-1169

März C, Hoffmann J, Bleil U, De Lange G, Kasten S (2008) Diagenetic changes of magnetic and geochemical signals by anaerobic methane oxidation in sediments of the Zambezi deep-sea fan (SW Indian Ocean). *Marine geology* **255**: 118-130

McGlynn SE, Chadwick GL, Kempes CP, Orphan VJ (2015) Single cell activity reveals direct electron transfer in methanotrophic consortia. *Nature* **526**: 531-535

Meulepas RJ, Jagersma CG, Khadem AF, Stams AJ, Lens PN (2010) Effect of methanogenic substrates on anaerobic oxidation of methane and sulfate reduction by an anaerobic methanotrophic enrichment. *Applied microbiology and biotechnology* **87**: 1499-1506

Meyerdierks A, Kube M, Kostadinov I, Teeling H, Glöckner FO, Reinhardt R, Amann R (2010) Metagenome and mRNA expression analyses of anaerobic methanotrophic archaea of the ANME-1 group. *Environmental microbiology* **12**: 422-439

Michaelis W, Seifert R, Nauhaus K, Treude T, Thiel V, Blumenberg M, Knittel K, Gieseke A, Peterknecht K, Pape T (2002) Microbial reefs in the Black Sea fueled by anaerobic oxidation of methane. *Science* **297**: 1013-1015

Milucka J, Ferdelman TG, Polerecky L, Franzke D, Wegener G, Schmid M, Lieberwirth I, Wagner M, Widdel F, Kuypers MM (2012) Zero-valent sulphur is a key intermediate in marine methane oxidation. *Nature*

Milucka J, Widdel F, Shima S (2013) Immunological detection of enzymes for sulfate reduction in anaerobic methane-oxidizing consortia. *Environmental microbiology* **15**: 1561-1571

Moore TS, Murray R, Kurtz A, Schrag D (2004) Anaerobic methane oxidation and the formation of dolomite. *Earth and Planetary Science Letters* **229**: 141-154

Moran JJ, Beal EJ, Vrentas JM, Orphan VJ, Freeman KH, House CH (2008) Methyl sulfides as intermediates in the anaerobic oxidation of methane. *Environmental microbiology* **10**: 162-173

Moran JJ, House CH, Freeman KH, Ferry JG (2005) Trace methane oxidation studied in several Euryarchaeota under diverse conditions. *Archaea* **1**: 303-309

Morris BE, Henneberger R, Huber H, Moissl-Eichinger C (2013) Microbial syntrophy: interaction for the common good. *FEMS microbiology reviews* **37**: 384-406

Murrell JC, Gilbert B, McDonald IR (2000) Molecular biology and regulation of methane monooxygenase. *Archives of Microbiology* **173**: 325-332

Nauhaus K, Albrecht M, Elvert M, Boetius A, Widdel F (2007) In vitro cell growth of marine archaeal-bacterial consortia during anaerobic oxidation of methane with sulfate. *Environmental microbiology* **9**: 187-196

Nauhaus K, Boetius A, Krüger M, Widdel F (2002) In vitro demonstration of anaerobic oxidation of methane coupled to sulphate reduction in sediment from a marine gas hydrate area. *Environmental microbiology* **4**: 296-305

Nauhaus K, Treude T, Boetius A, Krüger M (2005) Environmental regulation of the anaerobic oxidation of methane: a comparison of ANME-I and ANME-II communities. *Environmental microbiology* **7**: 98-106

Neef L, van Weele M, van Velthoven P (2010) Optimal estimation of the present-day global methane budget. *Global Biogeochemical Cycles* **24**

Niemann H, Lösekann T, De Beer D, Elvert M, Nadalig T, Knittel K, Amann R, Sauter EJ, Schlüter M, Klages M (2006) Novel microbial communities of the Haakon Mosby mud volcano and their role as a methane sink. *Nature* **443**: 854-858

Omereglio EO, Niemann H, Mastalerz V, De Lange GJ, Stadnitskaia A, Mascle J, Foucher J-P, Boetius A (2009) Microbial methane oxidation and sulfate reduction at cold seeps of the deep Eastern Mediterranean Sea. *Marine geology* **261**: 114-127

Op den Camp HJ, Islam T, Stott MB, Harhangi HR, Hynes A, Schouten S, Jetten MS, Birkeland NK, Pol A, Dunfield PF (2009) Environmental, genomic and taxonomic perspectives on methanotrophic Verrucomicrobia. *Environmental Microbiology Reports* **1**: 293-306

Orphan VJ, House CH, Hinrichs K-U, McKeegan KD, DeLong EF (2002) Multiple archaeal groups mediate methane oxidation in anoxic cold seep sediments. *Proceedings of the National Academy of Sciences* **99**: 7663-7668

Oswald K, Milucka J, Brand A, Hach P, Littmann S, Wehrli B, Kuypers MM, Schubert CJ (2016) Aerobic gammaproteobacterial methanotrophs mitigate methane emissions from oxic and anoxic lake waters. *Limnology and Oceanography* **61**

Pachauri RK, Allen MR, Barros V, Broome J, Cramer W, Christ R, Church J, Clarke L, Dahe Q, Dasgupta P (2014) *Climate change 2014: synthesis Report. Contribution of working groups I, II and III to the fifth assessment report of the intergovernmental panel on climate change*: IPCC.

Padilla CC, Bristow LA, Sarode N, Garcia-Robledo E, Ramírez EG, Benson CR, Bourbonnais A, Altabet MA, Girguis PR, Thamdrup B (2016) NC10 bacteria in marine oxygen minimum zones. *The ISME journal* **10**: 2067-2071

Pereira I, Ramos A, Grein F, Marques M, da Silva S, Venceslau S. (2011) A comparative genomic analysis of energy metabolism in sulfate reducing bacteria and archaea. *Front. Microbiol.* **2**: 69.

Pimenov N, Rusanov I, Poglazova M, Mityushina L, Sorokin DY, Khmelenina V, Trotsenko YA (1997) Bacterial mats on coral-like structures at methane seeps in the Black Sea. *MICROBIOLOGY-AIBS-C/C OF MIKROBIOLOGIJA* **66**: 354-360

Pol A, Barends TR, Dietl A, Khadem AF, Eygensteyn J, Jetten MS, Op den Camp HJ (2014) Rare earth metals are essential for methanotrophic life in volcanic mudpots. *Environmental microbiology* **16**: 255-264

Pol A, Heijmans K, Harhangi HR, Tedesco D, Jetten MS, Den Camp HJO (2007) Methanotrophy below pH 1 by a new Verrucomicrobia species. *Nature* **450**: 874-878

Raghoebarsing AA, Pol A, Van de Pas-Schoonen KT, Smolders AJ, Ettwig KF, Rijpstra WIC, Schouten S, Damsté JSS, den Camp HJO, Jetten MS (2006) A microbial consortium couples anaerobic methane oxidation to denitrification. *Nature* **440**: 918-921

Reeburgh WS (1976) Methane consumption in Cariaco Trench waters and sediments. *Earth and Planetary Science Letters* **28**: 337-344

Reeburgh WS (2003) Global methane biogeochemistry. *Treatise on geochemistry* **4**: 347

Reeburgh WS (2007) Oceanic methane biogeochemistry. *Chemical reviews* **107**: 486-513

Reguera G, McCarthy KD, Mehta T, Nicoll JS, Tuominen MT, Lovley DR (2005) Extracellular electron transfer via microbial nanowires. *Nature* **435**: 1098-1101

Roslev P, King GM (1995) Aerobic and anaerobic starvation metabolism in methanotrophic bacteria. *Applied and environmental microbiology* **61**: 1563-1570

Roze E (1896) *Le Clonothrix: un nouveau type générique de Cyanophycées*: Mersch.

Santos AA, Venceslau SS, Grein F, Leavitt WD, Dahl C, Johnston DT, Pereira IA (2015) A protein trisulfide couples dissimilatory sulfate reduction to energy conservation. *Science* **350**: 1541-1545

Scheller S, Yu H, Chadwick GL, McGlynn SE, Orphan VJ (2016) Artificial electron acceptors decouple archaeal methane oxidation from sulfate reduction. *Science* **351**: 703-707

Schubert CJ, Vazquez F, Lösekann-Behrens T, Knittel K, Tonolla M, Boetius A (2011) Evidence for anaerobic oxidation of methane in sediments of a freshwater system (Lago di Cadagno). *FEMS Microbiology Ecology* **76**: 26-38

Simon J, Kern M, Hermann B, Einsle O, Butt JN. (2011) Physiological function and catalytic versatility of bacterial multihaem cytochromes c involved in nitrogen and sulfur cycling. Portland Press Limited.

Sorokin DY, Jones BE, Kuenen JG (2000) An obligate methylotrophic, methane-oxidizing *Methylomicrobium* species from a highly alkaline environment. *Extremophiles* **4**: 145-155

Stams AJ, De Bok FA, Plugge CM, Eekert V, Miriam H, Dolfing J, Schraa G (2006) Exocellular electron transfer in anaerobic microbial communities. *Environmental microbiology* **8**: 371-382

Stein LY, Klotz MG. (2011) Nitrifying and denitrifying pathways of methanotrophic bacteria. Portland Press Limited.

Stoecker K, Bendinger B, Schöning B, Nielsen PH, Nielsen JL, Baranyi C, Toenshoff ER, Daims H, Wagner M (2006) Cohn's *Crenothrix* is a filamentous methane oxidizer with an unusual methane monooxygenase. *Proceedings of the National Academy of Sciences of the United States of America* **103**: 2363-2367

Tavormina PL, Ussler W, Steele JA, Cannon SA, Klotz MG, Orphan VJ (2013) Abundance and distribution of diverse membrane-bound monooxygenase (Cu-MMO) genes within the Costa Rica oxygen minimum zone. *Environmental Microbiology Reports* **5**: 414-423

Thauer RK (1998) Biochemistry of methanogenesis: a tribute to Marjory Stephenson: 1998 Marjory Stephenson Prize Lecture. *Microbiology* **144**: 2377-2406

- Thauer RK (2011) Anaerobic oxidation of methane with sulfate: on the reversibility of the reactions that are catalyzed by enzymes also involved in methanogenesis from CO₂. *Current opinion in microbiology* **14**: 292-299
- Thauer RK, Shima S (2008) Methane as fuel for anaerobic microorganisms. *Annals of the New York Academy of Sciences* **1125**: 158-170
- Treude T, Orphan V, Knittel K, Gieseke A, House CH, Boetius A (2007) Consumption of methane and CO₂ by methanotrophic microbial mats from gas seeps of the anoxic Black Sea. *Applied and environmental microbiology* **73**: 2271-2283
- Trotsenko YA, Murrell JC (2008) Metabolic Aspects of Aerobic Obligate Methanotrophy. *Advances in applied microbiology* **63**: 183-229
- Valentine DL (2011) Emerging topics in marine methane biogeochemistry. *Annual review of marine science* **3**: 147-171
- van Kessel MA, Speth DR, Albertsen M, Nielsen PH, den Camp HJO, Kartal B, Jetten MS, Lückler S (2015) Complete nitrification by a single microorganism. *Nature* **528**: 555-559
- Vigliotta G, Nutricati E, Carata E, Tredici SM, De Stefano M, Pontieri P, Massardo DR, Prati MV, De Bellis L, Alifano P (2007) *Clonothrix fusca* Roze 1896, a filamentous, sheathed, methanotrophic γ -proteobacterium. *Applied and environmental microbiology* **73**: 3556-3565
- Völker H, Schweisfurth R, Hirsch P (1977) Morphology and ultrastructure of *Crenothrix polyspora* Cohn. *Journal of Bacteriology* **131**: 306-313
- Wang F-P, Zhang Y, Chen Y, He Y, Qi J, Hinrichs K-U, Zhang X-X, Xiao X, Boon N (2014) Methanotrophic archaea possessing diverging methane-oxidizing and electron-transporting pathways. *The ISME journal* **8**: 1069-1078
- Wegener G, Krukenberg V, Riedel D, Tegetmeyer HE, Boetius A (2015) Intercellular wiring enables electron transfer between methanotrophic archaea and bacteria. *Nature* **526**: 587-590
- Wegener G, Krukenberg V, Ruff SE, Kellermann MY, Knittel K (2016) Metabolic capabilities of microorganisms involved in and associated with the anaerobic oxidation of methane. *Frontiers in microbiology* **7**
- Wegener G, Niemann H, Elvert M, Hinrichs KU, Boetius A (2008) Assimilation of methane and inorganic carbon by microbial communities mediating the anaerobic oxidation of methane. *Environmental microbiology* **10**: 2287-2298
- Whittenbury R, Dalton H (1981) The methylotrophic bacteria. In *The prokaryotes*, pp 894-902. Springer

Widdel F, Musat F, Knittel K, Galushko A (2007) *Anaerobic degradation of hydrocarbons with sulphate as electron acceptor*: Cambridge, UK: Cambridge University Press.

Zehnder A, Brock T (1979) Methane formation and methane oxidation by methanogenic bacteria. *Journal of Bacteriology* **137**: 420-432

Manuscript Chapters 2 - 5

- 2 *Crenothrix* in lakes
- 3 Bloom of NC10 in Lake Zug
- 4 Physiology of S-AOM
- 5 P cycling associated with S-AOM

Chapter 2

***Crenothrix* are major methane consumers in stratified lakes**

Kirsten Oswald^{1,2,*}, Jon S. Graf^{3,*}, Sten Littmann³, Daniela Tienken³, Andreas Brand^{1,2}, Bernhard Wehrli^{1,2}, Mads Albertsen⁴, Holger Daims⁵, Michael Wagner⁵, Marcel M.M. Kuypers³, Carsten J. Schubert¹ & Jana Milucka^{3,5}

¹Department of Surface Waters–Research and Management, Eawag, Swiss Federal Institute of Aquatic Science and Technology, Kastanienbaum, Switzerland; ²Institute of Biogeochemistry and Pollutant Dynamics, ETH Zurich, Swiss Federal Institute of Technology, Zurich, Switzerland; ³Department of Biogeochemistry, Max Planck Institute for Marine Microbiology, Bremen, Germany; ⁴Department of Chemistry and Bioscience, Center for Microbial Communities, Aalborg University, Aalborg, Denmark; ⁵Division of Microbial Ecology, Department of Microbiology and Ecosystem Science, Research Network Chemistry meets Microbiology, University of Vienna, Vienna, Austria

* These authors contributed equally to this work

⁵ Corresponding author: Jana Milucka (jmilucka@mpi-bremen.de)

Published in *The ISME Journal*

doi: 10.1038/ismej.2017.77

Author contributions

J. M., M. M. M. K. and C. J. S. designed research, K. O. and A. B. performed field measurements, incubation experiments and sampling, J. S. G. performed metagenomic analyses on lake water samples and phylogenetic analyses, H. D., M. W. and M. A. performed metagenomic analysis on the sand filter *Crenothrix* sample, S. L., D. T. performed FISH and nanoSIMS measurements, B. W., M. M. M. K. and C. J. S. contributed material and analysis tools, K. O., J. S. G. and J. M. wrote the paper with input from all co-authors

ORIGINAL ARTICLE

Crenothrix are major methane consumers in stratified lakes

Kirsten Oswald^{1,2,6}, Jon S Graf^{3,6}, Sten Littmann³, Daniela Tienken³, Andreas Brand^{1,2}, Bernhard Wehrli^{1,2}, Mads Albertsen⁴, Holger Daims⁵, Michael Wagner⁵, Marcel MM Kuypers³, Carsten J Schubert¹ and Jana Milucka³

¹Department of Surface Waters—Research and Management, Eawag, Swiss Federal Institute of Aquatic Science and Technology, Kastanienbaum, Switzerland; ²Institute of Biogeochemistry and Pollutant Dynamics, ETH Zurich, Department of Environmental Systems Science, Swiss Federal Institute of Technology, Zurich, Switzerland; ³Department of Biogeochemistry, Max Planck Institute for Marine Microbiology, Bremen, Germany; ⁴Department of Chemistry and Bioscience, Center for Microbial Communities, Aalborg University, Aalborg, Denmark and ⁵Division of Microbial Ecology, Department of Microbiology and Ecosystem Science, Research Network Chemistry meets Microbiology, University of Vienna, Vienna, Austria

Methane-oxidizing bacteria represent a major biological sink for methane and are thus Earth's natural protection against this potent greenhouse gas. Here we show that in two stratified freshwater lakes a substantial part of upward-diffusing methane was oxidized by filamentous gamma-proteobacteria related to *Crenothrix polyspora*. These filamentous bacteria have been known as contaminants of drinking water supplies since 1870, but their role in the environmental methane removal has remained unclear. While oxidizing methane, these organisms were assigned an 'unusual' methane mono-oxygenase (MMO), which was only distantly related to 'classical' MMO of gamma-proteobacterial methanotrophs. We now correct this assignment and show that *Crenothrix* encode a typical gamma-proteobacterial PmoA. Stable isotope labeling in combination with single-cell imaging mass spectrometry revealed methane-dependent growth of the lacustrine *Crenothrix* with oxygen as well as under oxygen-deficient conditions. *Crenothrix* genomes encoded pathways for the respiration of oxygen as well as for the reduction of nitrate to N₂O. The observed abundance and planktonic growth of *Crenothrix* suggest that these methanotrophs can act as a relevant biological sink for methane in stratified lakes and should be considered in the context of environmental removal of methane.

The ISME Journal (2017) 11, 2124–2140; doi:10.1038/ismej.2017.77; published online 6 June 2017

Introduction

Freshwater lakes represent large natural sources of methane and contribute more to methane emissions than the oceans despite their comparably smaller area (Bastviken *et al.*, 2004). Highest rates of methane removal are usually measured at the oxyclines, either in the water column or in the sediment. Lake Rotsee and Lake Zug in Central Switzerland are typical examples of temperate lake systems with methane fluxes across the oxycline of 13 ± 3 mmol and 10 ± 3 mmol m⁻² d⁻¹, respectively (Oswald *et al.*, 2015, 2016). Both lakes are stratified, with methane-rich hypolimnia, but whereas the shallow Lake Rotsee overturns annually, the deep Lake Zug remains stratified throughout the year.

In both lakes, the vast majority of the upward-diffusing methane is removed at the base of the oxycline at *in situ* oxygen concentrations in the low micromolar range (Oswald *et al.*, 2015, 2016). Methane oxidation at the oxycline was shown to be coupled to the reduction of residual or *in situ*-produced oxygen, but there were also indications for methane-oxidizing activity under oxygen-deficient conditions (Oswald *et al.*, 2015, 2016).

Abundant gamma-proteobacterial methane-oxidizing bacteria (gamma-MOB) were shown to be involved in methane removal in both lakes (Oswald *et al.*, 2015, 2016). Gamma-MOB are considered aerobes requiring oxygen for methane activation, even though some cultured representatives can perform methane oxidation under denitrifying conditions (Kits *et al.*, 2015a,b). Environmentally relevant representatives of gamma-MOB in lakes and other freshwater habitats belong to the 'classical' genera of *Methylobacter*, *Methylomonas*, *Methylosarcina* and *Methylomicrobium* (Boschker *et al.*, 1998; Bodelier *et al.*, 2013; Oshkin *et al.*, 2015), and all possess particulate methane monoxygenase

Correspondence: J Milucka, Department of Biogeochemistry, Max Planck Institute for Marine Microbiology, Celsiusstrasse 1, Bremen 28359, Germany.

E-mail: jmilucka@mpi-bremen.de

⁶These two authors contributed equally to this work.

Received 4 November 2016; revised 13 April 2017; accepted 21 April 2017; published online 6 June 2017

(pMMO) as the key methane-oxidizing enzyme (Bowman, 2005). In Lake Rotsee and Lake Zug, unicellular gamma-MOB represented a stable community at the oxycline. The bacteria showed rapid growth on methane as evidenced by the increase in cell abundances and the uptake of ^{13}C -methane into their biomass (Oswald *et al.*, 2015, 2016).

In these studies, gamma-MOB were identified by fluorescence *in situ* hybridization using the 16S rRNA-targeted oligonucleotide probes Mgamma84+705. Interestingly however, these probes do not bind to members of a potentially important subgroup of gamma-proteobacterial MOB, the putative family *Crenothrichaceae*. Contrary to 'classical' MOB, these gamma-MOB are multicellular and filamentous. So far, only two of these bacteria have been documented in literature, *Crenothrix polyspora* and *Clonothrix fusca*, and both were retrieved from groundwater (Stoecker *et al.*, 2006; Vigliotta *et al.*, 2007). Sporadically, environmental occurrence of *Crenothrix* is reported in literature based on retrieved 16S rRNA or *pmoA* sequences (Dörr *et al.*, 2010; Drewniak *et al.*, 2012), but its role in methane cycling has remained unclear.

The metabolism of *Crenothrix* has been a matter of debate since its first description as 'Brunnenfaden' ('a well thread'; Cohn, 1870). Initially, *Crenothrix/Clonothrix* filaments were considered to belong to the 'iron bacteria' due to the presence of metal particles in their sheaths (Roze, 1896; Jackson, 1902; Molisch, 1910). This belief was challenged by studies that failed to observe iron encrustation in *Crenothrix/Clonothrix* filaments (Kolk, 1938; Wolfe, 1960), and the later discovery of membrane invaginations has prompted suggestions for a methanotrophic lifestyle (Völker *et al.*, 1977). Eventually, the capacity to oxidize methane was experimentally confirmed on filaments retrieved from man-made habitats (Stoecker *et al.*, 2006; Vigliotta *et al.*, 2007). Interestingly, *C. polyspora* was reported to possess an 'unusual' pMMO, which was only distantly related to 'classical' MMO of gamma-proteobacterial methanotrophs (Stoecker *et al.*, 2006), and has now been recognized to cluster together with the ammonium monooxygenases of completely nitrifying 'comammox' bacteria (Daims *et al.*, 2015; van Kessel *et al.*, 2015).

Here we investigated the occurrence and involvement of these filamentous bacteria in methane oxidation at and below the oxyclines of Lake Rotsee and Lake Zug. We performed stable isotope labeling experiments followed by single-cell imaging to explore the role of these microorganisms in environmental methane cycling, and metagenomic analyses to investigate their metabolic potential with respect to aerobic and anaerobic respiration. For comparison, we also performed metagenomic analysis of a sample from Wolfenbüttel waterworks sand filter reportedly containing high proportions of *C. polyspora*.

Materials and methods

Geochemical profiling in Lake Rotsee

Profiling was done in October 2014 at the deepest point (16 m depth, 47°04.259'N, 8°18.989'E). A multi-parameter probe was used to measure photosynthetically active radiation (PAR; LI-193 Spherical Underwater Quantum Sensor, LI-COR, Lincoln, NE, USA) along with conductivity, turbidity, depth (pressure), temperature and pH (XRX 620, RBR, Ottawa, ON, Canada). Dissolved oxygen was simultaneously monitored online with normal and trace micro-optodes (types PSt1 and TOS7, Presens, Regensburg, Germany) with detection limits of 125 and 20 nM, respectively, and a response time of 7 s (Kirf *et al.*, 2014).

Water samples for dissolved methane analysis were retrieved from distinct depths with a Niskin bottle. Serum bottles (120 ml) were filled completely without bubbles or headspace through a gas-tight outlet tubing allowing water to overflow. Solid copper chloride [Cu(I)Cl] was immediately added in excess to the water samples and the bottles were crimped. Before analysis, a 30 ml headspace was set with N_2 and after overnight equilibration methane concentrations were measured in the headspace with a gas chromatograph (GC; Agilent 6890 N, Agilent Technologies, Santa Clara, CA, USA) equipped with a Carboxen 1010 column (30 m \times 0.53 mm, Supelco, Bellefonte, PA, USA) and a flame ionization detector. Methane concentrations in the water phase were back-calculated according to (Wiesenburg and Guinasso, 1979). Stable carbon isotopes of methane were determined in the same headspace by isotope ratio mass spectrometry with a trace gas instrument (T/GAS PRE CON, Micromass UK Ltd., Wilmslow, UK) coupled to a mass spectrometer (GV Instruments, Manchester, UK; Isoprime, Stockport, UK). Isotopic ratios are given in δ -notation relative to the Vienna Pee Dee Belemnite reference standard.

Oxygen, PAR, methane concentration and methane isotope profiles for the sampling campaign in October 2014 are shown in Supplementary Figure 1. Geochemical profiles from other Lake Rotsee campaigns are reported in Oswald *et al.* (2015).

Lake Rotsee methane oxidation rates

Methane oxidation rates were measured in incubations set up in October 2014, with water from the 7 m depth (oxycline), and from 8 m depth (with no detectable oxygen). Water was collected with a Niskin bottle and filled into sterile 1 l Schott bottles without a headspace, closed with butyl stoppers and kept cold and dark until further handling. In the laboratory, 120 ml was distributed into 160 ml serum bottles in an anoxic (N_2 -containing) glove box (Iner Tec, Grenchen, Switzerland), closed with butyl stoppers and crimped. Each incubation was supplemented with ^{13}C -labeled methane (99 at%, Campro Scientific, Berlin, Germany) and ^{12}C -methane to

reach 2 bar overpressure, resulting in $\sim 1.8 \text{ mmol l}^{-1}$ CH_4 in the water phase and 50 at% ^{13}C labeling percentage. For comparison, *in situ* methane concentrations at 7 and 8 m depth were ca. 15 and $35 \mu\text{mol l}^{-1}$ (Supplementary Figure 1). Duplicate bottles were incubated at 6°C under dark and light conditions along with a control (sterile filtered lake water). Methane oxidation was monitored during an incubation period of 7 days as production of $^{13}\text{CO}_2$. Anoxically withdrawn water samples (2 ml) were transferred into 6 ml Exetainers (Labco, Lampeter, UK), fixed with 200 μl zinc chloride (50% w/v) and acidified with concentrated H_3PO_4 (100 μl). Isotopic ratios of CO_2 were determined in the headspace with a preparation system (MultiFlow, Isoprime) coupled to an isotope ratio mass spectrometry (Micromass, Isoprime). Subsequently, methane oxidation rates were calculated as described previously (Oswald *et al.*, 2015). These rates are shown in Supplementary Figure 1. As these incubations were unamended (apart from methane addition), aerobic methane oxidation in these incubations was presumably sustained solely by oxygenic photosynthesis (Milucka *et al.*, 2015; Oswald *et al.*, 2015). At selected time points, sub-samples were also taken for catalyzed reporter deposition fluorescence *in situ* hybridization (CARD-FISH) analysis. These data are shown in Supplementary Figure 3. Nanometer-scale secondary ion mass spectrometry (NanoSIMS) and metagenome analyses reported for Lake Rotsee (shown in Figure 1 and Supplementary Figure 2) were performed on samples collected on a previous sampling campaign in August 2013 (rates and other data from this campaign are reported in Oswald *et al.* (2015)).

Lake Zug nitrate addition experiment

The sampling campaign was carried out in October 2013. Water samples from the anoxic 160 m depth were collected with a Niskin bottle, filled into sterile Schott bottles, closed with a stopper and stored as described above. The water was distributed into sterile 160 ml serum bottles (a 120 ml) in an N_2 glove box (Mecaplex, Grenchen, Switzerland) as described in detail in Oswald *et al.* (2016). ^{13}C -labeled methane (99 at%, Campro Scientific) was supplied at a $\sim 20\%$ labeling percentage. A 2 bar methane overpressure was set using ^{12}C -methane. One set of duplicate bottles received no further addition and served as a control and one set of duplicate bottles was amended with $^{15}\text{NO}_3^-$ (from a sterile anoxic 100 mmol l^{-1} stock solution) to a final concentration of $50 \mu\text{mol l}^{-1}$. Bottles were incubated in the dark under *in situ* temperatures ($\sim 5^\circ\text{C}$) for 16 days. At regular intervals, bottles were subsampled for $^{13}\text{CO}_2$ measurements in order to determine methane oxidation rates. For this, anoxically withdrawn water samples (2 ml) were transferred into 6 ml Exetainers, fixed with zinc chloride and acidified with concentrated H_3PO_4 . Isotopic ratios of CO_2 were determined in the headspace using a Finnigan Gas-Bench II attached to an isotope ratio mass spectrometer

(IRMS; Finnigan Delta Plus, Thermo Fisher Scientific, Waltham, MA, USA). Subsequently, methane oxidation rates were calculated as described previously (Oswald *et al.*, 2015). At selected time points, sub-samples were also taken for CARD-FISH and nanoSIMS analyses. An early time point ($T = 2$ d) was analyzed by nanoSIMS to obtain data for the calculation of methane uptake rates reported in Table 1. FISH and nanoSIMS images from Lake Zug nitrate incubation (Figure 1; Supplementary Figure 6) originate from the last time point of the incubation ($T = 16$ d). The sample for metagenome analysis (sample Z3) was also taken at this time point. Additionally, an *in situ* water sample from 160 m was also used for metagenome analysis (sample Z1). During this sampling campaign, no incubations with added oxygen were performed.

O_2 -supplemented incubations referred to in this manuscript were only performed during a sampling campaign in June 2014 and are described in detail in Oswald *et al.* (2016), where also the corresponding geochemical profiles and methane oxidation rates from relevant depths and incubations are reported. Briefly, O_2 -supplemented incubations were set up as described above, with the difference that instead of nitrate, sterile air was injected to the incubations to reach final O_2 concentrations of ca. $80 \mu\text{mol l}^{-1}$ ('low O_2 ') and ca. $200 \mu\text{mol l}^{-1}$ ('high O_2 '), respectively. Incubations were subsampled at regular intervals for methane oxidation rates, CARD-FISH and nanoSIMS analyses. The CARD-FISH and nanoSIMS analyses shown in Figure 1 were performed on samples taken from 160 m incubation after $T = 2$ d. The sample for metagenome analysis was taken at the last time point of the 'low O_2 ' 160 m incubation ($T = 11$ d).

Catalyzed reporter deposition fluorescence *in situ* hybridization

Formaldehyde- (2% (v/v) final concentration) fixed water samples were incubated for 30 min at room temperature before being filtered onto polycarbonate GTTP filters (0.2 μm pore size; Merck Millipore, Darmstadt, Germany). For nanoSIMS analysis, samples were filtered onto Au or Au/Pd-coated GTTP filters (0.2 μm pore size). Permeabilization with lysozyme, peroxidase inactivation, hybridization with specific oligonucleotide probes labeled with horseradish peroxidase in combination with tyramide signal amplification (Oregon Green 488) and DAPI counter staining was performed as described previously (Pernthaler *et al.*, 2002). An overview of probes used (Biomers, Ulm, Germany) is included in Supplementary Table 2. For cell counts and biovolume determinations, one filter was analyzed for each sample. Hybridized filaments (using probe Mgamma669) were enumerated in randomly selected fields of view with a confocal laser scanning microscope (SP5 DMI 6000, Leica, Wetzlar, Germany). For biovolume calculations, length and width of > 15 filaments in > 10 fields of view were then measured directly in confocal micrographs using LAS AF Lite software (Leica). Values for the cell counts

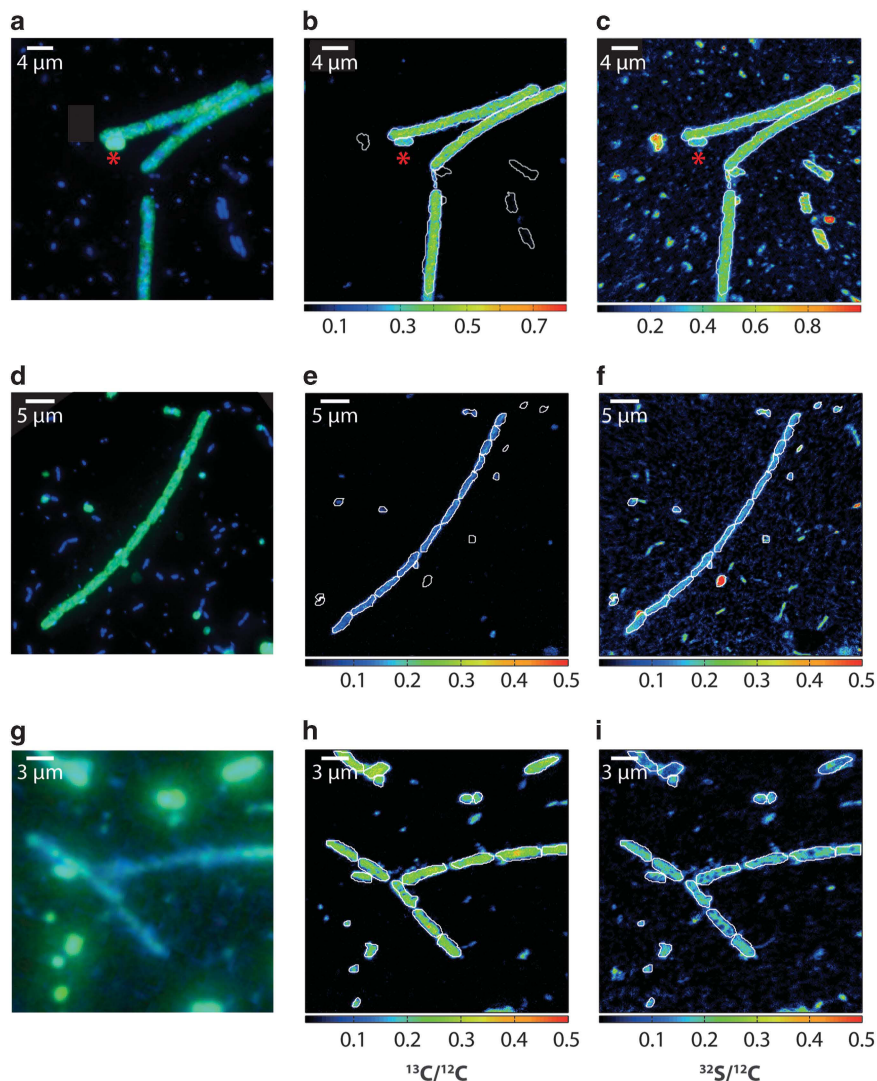


Figure 1 Methane-dependent growth of *Crenothrix* in Lake Rotsee and Lake Zug. (a) *Crenothrix* in the Lake Rotsee oxic incubation visualized by CARD-FISH (green; counterstained by DAPI in blue) with a specific probe Creno445 (Stoecker *et al.*, 2006). A small coccoid cell targeted by the probe (marked by the asterisk) might represent a gonidial cell, which *Crenothrix* is reportedly capable of producing (Völker *et al.*, 1977). (b) The corresponding $^{13}\text{C}/^{12}\text{C}$ nanoSIMS image shows homogeneous ^{13}C enrichment throughout the cell filament. The small coccoid cell is also significantly enriched, albeit less. (c) The corresponding $^{32}\text{S}/^{12}\text{C}$ nanoSIMS image showing distribution of organic material on the filter. (d) Putative *Crenothrix* filaments in the Lake Zug oxic incubation visualized by DAPI (blue) and CARD-FISH (green) with probe Mgamma669. (e) Corresponding $^{13}\text{C}/^{12}\text{C}$ and (f) $^{32}\text{S}/^{12}\text{C}$ nanoSIMS images. Note the fragmented nature of the *Crenothrix* filaments and the attached small (unidentified) bacteria. (g) Putative *Crenothrix* filaments in the Lake Zug anoxic incubation visualized by DAPI (blue) and CARD-FISH (green) with probe Mgamma669. (h) Corresponding $^{13}\text{C}/^{12}\text{C}$ and (i) $^{32}\text{S}/^{12}\text{C}$ nanoSIMS images.

and methane uptake rates of unicellular gamma-MOB cells were taken from Oswald *et al.* (2015) and Oswald *et al.* (2016).

Nanometer-scale secondary ion mass spectrometry

Areas of interest containing positive CARD-FISH hybridization signals were marked with a laser micro-dissection microscope (DM 6000, Leica Microsystems, Mannheim, Germany). Laser-marked areas were analyzed by nanoSIMS (NanoSIMS 50 l, Cameca, Paris, France) at the MPI Bremen as described previously. For Lake Rotsee (light incubation, 9 m depth), 12 and 26 filaments were analyzed in five fields of view after 2 and 7 days of incubation,

respectively. For the Lake Zug low and high O_2 addition experiments, 19 and 13 filaments were measured in 9 and 7 fields of view, respectively, after 2 days of incubation. For the Lake Zug nitrate addition incubation, 6 filaments were measured in 5 fields of view after 2 days of incubation and 7 filaments were measured in 5 fields of view after 16 days of incubation. Obtained secondary ion images were drift corrected, accumulated and processed with Look@NanoSIMS (Polerecky *et al.*, 2012).

Biovolume and carbon assimilation rates

The biovolume of individual *Crenothrix* filaments was calculated from their measured length and width

Table 1 Overview of methane carbon uptake rates by *Crenothrix* and unicellular gamma-MOB in Lake Rotsee and Lake Zug

	¹³ C at % ^a (n)	Avg biovolume (CARD-FISH-based) ^b (µm ³ ; n)	Methane-C uptake per cell ^c (fmol cell ⁻¹ d ⁻¹)	Cell count ^d (cell ml ⁻¹)	Total population biovolume ^e (µm ³ ml ⁻¹)	Methane-C uptake per population ^f (µmol l ⁻¹ d ⁻¹)
<i>Lake Rotsee (oxic)</i>						
<i>Crenothrix</i> (Mgamma669)	NA	85 ± 8.3 (59)	147.7 ± 26.3 ^g	1.2E+04	1.0E+06	1.73 ^h
<i>Crenothrix</i> (Creno445)	22.00 ± 4.8 (17)	73.7 ± 8.4 (51)	128.0 ± 22.8	9.2E+03	6.8E+05	1.18
Other gamma-MOB ^h	28.77 ± 4.1	4.2	10.6 ± 0.9	2.6E+04	1.1E+05	0.27
<i>Lake Zug (oxic)</i>						
<i>Crenothrix</i> (Mgamma669; low O ₂)	9.26 ± 1.7 (19)	32.5 ± 5.5 (20)	38.1 ± 6.9	1.1E+03	3.5E+04	0.041
<i>Crenothrix</i> (Mgamma669; high O ₂)	8.68 ± 1.9 (10) ⁱ	32.5 ± 5.5 (20)	35.3 ± 7.8	1.1E+03	3.5E+04	0.038
Other gamma-MOB (low O ₂) ^j	10.39 ± 3.1	4.2	5.7 ± 1.2	6.8E+04	2.9E+05	0.39
Other gamma-MOB (high O ₂) ^j	12.13 ± 3.75	4.2	6.9 ± 1.6	6.8E+04	2.9E+05	0.47
<i>Lake Zug (anoxic)</i>						
<i>Crenothrix</i> (Mgamma669)	13.27 ± 4.9 (6)	49.7 ± 20.3 (15)	74.2 ± 26.6 (6)	0.4E+03	2.0E+04	0.03
Other gamma-MOB	NA	NA	NA	NA	NA	NA

Abbreviations: CARD-FISH, catalyzed reporter deposition fluorescence *in situ* hybridization; MOB, methane-oxidizing bacteria; n, number of analyzed cells, NA, not analyzed.

^aCalculated as an average (± s.d.) of the ¹³C/¹²C ratios of individual regions of interest (i.e., cells) determined by nanoSIMS.

^bCalculated from CARD-FISH data as an average biovolume (± s.d.) using Mgamma669 or Creno445 probe (*Crenothrix*) and Mgamma84+705 probes (other gamma-MOB).

^cCalculated as follows: data from column a were converted into ¹³C excess in fmol per cell (of a given average biovolume; cell_{avg}) using the avg cell biovolume reported in column b and a conversion factor of 6.4 fmol C µm⁻³ (Musat *et al.*, 2008). The numbers were corrected for labeling percentage and incubation time.

^dCounted from the same filters from which avg biovolumes (column b) were obtained. As the boundaries between individual cells within the filament were often not recognizable, only hybridized filaments were counted. Cell counts refer to cell abundances at the start of each incubation and thus do not account for increase of cell abundances during the incubation period.

^eCalculated as follows: data from column b were upscaled using data in column d.

^fCalculated as follows: data from column c were upscaled using data from column d.

^gAssuming the same ¹³C enrichment as determined with the probe Creno445 on the same sample.

^hAccording to Oswald *et al.*, 2015.

ⁱIn this sample, three analyzed filaments had ¹³C/¹²C < 0.015 and were not included in the analysis.

^jAccording to Oswald *et al.*, 2016.

Calculations are based on incubations from Lake Rotsee (oxic, 2013) and Lake Zug (oxic and anoxic, 2013, 2014; see Supplementary Table 4 for sample details).

by assuming a cylindrical shape. The length and the width of filaments were determined from the CARD-FISH images that were used for cell counting. Due to the varying length of filaments, an average biovolume of *Crenothrix* was calculated and is reported in Table 1. The 'average biovolume determined from CARD FISH' was calculated as an average of biovolumes of individual filaments hybridized with a *Crenothrix*-targeting probe (Mgamma669 or Creno445) at the start of the respective incubation and is reported with the s.d. 'Total' *Crenothrix* biovolume reported in Table 1 and Supplementary Figure 4 was obtained by multiplying the average filament biovolume by the number of filaments per ml of water. For comparison, the biovolume of unicellular gamma-MOB cells was calculated from total cell counts and by assuming an average spherical cellular diameter of 2 μm .

Cellular ^{13}C at % were calculated from $^{13}\text{C}/^{12}\text{C}$ values of individual ROIs (regions of interest). Regions of interests were drawn to outline single *Crenothrix* cells (for example, Figures 1h and i), whole filaments (Figures 1e and f) or parts of filaments (Figures 1b and c). Both the background (cell-free polycarbonate filter in the same field of view) and the ^{13}C enrichment of all cells in every field of view was evaluated and compared for all measurements. Rates of methane carbon uptake ($\text{fmol C cell}_{\text{avg}}^{-1} \text{d}^{-1}$) of *Crenothrix* and unicellular gamma-MOB were calculated from the ^{13}C excess of the measured cells using a conversion factor of 6.4 $\text{fmol C } \mu\text{m}^{-3}$ reported in Musat *et al.* (2008). These uptake rates were corrected for the labeling percentage and the incubation time. The methane uptake rates were calculated only for filamentous cells, which were stained with the Creno445 or Mgamma669 probe. Hybridized single cells (such as in Figures 1a–c) were not considered in the calculation.

DNA extraction, 16S rRNA gene amplicon sequencing and analysis

Two *in situ* water samples from Lake Rotsee were used for 16S rRNA gene amplicon sequencing. One was collected from the oxycline (9 m depth) during a campaign in August 2013 and the other from anoxic water (8 m depth) during a campaign in October 2014 (Supplementary Table 4). Volumes of ca. 250 ml were filtered onto polycarbonate Nuclepore Track-Etched Membrane filters (0.2 μm pore size; Whatman, Maidstone, UK). Filters were stored at -80°C until DNA was extracted with the UltraClean Soil DNA Isolation Kit (MoBio Laboratories, Carlsbad, CA, USA). Extraction procedure was performed according to manufacturer's instructions with the following adjustment: vortexing with the Bead Solution was reduced to 30 s with subsequent incubation on ice (30 s), and this cycle was repeated four times.

The V3–V4 regions of the 16S rRNA gene were targeted with primer pair 341 F (5'-CCTACGGGNGCWGCAG-3') and 805 R (5'-GACTACCGGGTATC

TAATC-3'). The forward primers contained unique identifier sequences at the 5'-end for each sample to allow for multiplex sequencing. Ten separate PCR reactions (25 μl volume) were set up for each sample including both forward and reverse primers (500 nM each), deoxyribose nucleotide triphosphates (dNTPs; 800 μM), 1 \times Taq reaction buffer, Taq DNA polymerase (0.25 U) and DNA extracts of the respective samples (0.5–1 μl). The reactions proceeded as follows: initial denaturation (3 min at 95°C), 25 cycles of denaturation (30 s at 95°C), annealing (30 s at 54°C) and elongation (90 s at 72°C); and final elongation (10 min at 72°C). Parallel reactions were combined and purified with the QIAquick PCR Purification Kit (Qiagen, Hilden, Germany) following manufacturer's instructions, with a final elution in 1 \times TE buffer (30 μl ; 10 mM Tris-HCl (pH 8.0)+1 mM EDTA). The DNA was further purified with a gel using SYBR Green I Nucleic Acid Gel Stain (Invitrogen, Carlsbad, CA, USA) followed by gel extraction with QIAquick Gel Extraction Kit (Qiagen) according to the manufacturer's protocol. Extract concentrations were measured fluorometrically using the Qubit dsDNA HS Assay Kit and the Qubit 2.0 Fluorometer (Invitrogen). Illumina sequencing was performed on the amplicons at the Max Planck-Genome Centre (Cologne, Germany).

16S rRNA gene amplicon paired-end reads were trimmed (right end only, trim quality threshold = 10) and merged (20 bases minimum overlap) using BBmap software version 35.43 (sourceforge.net/projects/bbmap). Reads were then separated by barcode and trimmed (minimum length = 300, maximum homopolymer length = 8, maximum number of ambiguous bases = 0, minimum average quality score allowed over 50 bp window = 20) using mothur v.1.36.1 (Schloss *et al.*, 2009). The separated reads were processed using SILVAngs and standard parameters (Quast *et al.*, 2013).

Lake metagenome sequencing and assembly

Two *in situ* water samples (Lake Rotsee, 9 m depth, August 2013 (sample R1) and Lake Zug, 160 m depth, October 2013 (sample Z1)) and four end time points of incubations (Lake Rotsee, O_2 -supplemented (sample R2), Lake Rotsee, light (sample R3), Lake Zug, low O_2 -supplemented (sample Z2), Lake Zug, anoxic, nitrate-supplemented (sample Z3); see Supplementary Tables 3 and 4 for additional sample information) were analyzed by Illumina sequencing. The following water volumes were filtered onto polycarbonate Nucleopore Tracked-Etched membrane filters (0.2 μm pore size; Whatman) and stored at -80°C : 250 ml for *in situ* samples (R1 and Z1), 50 ml for Lake Rotsee incubations (R2 and R3) and 40 ml for Lake Zug incubations (Z2 and Z3). DNA was extracted from cut-up filters using the PowerSoil DNA isolation kit according to manufacturer's instructions (MoBio Laboratories). DNA from lake Zug was fragmented by sonication (MiSeq: 600–700 bp; HiSeq2500: 300 bp) using a Covaris S2 sonicator (Covaris, Woburn, MA, USA). The library was prepared using Ovation

Ultra Low Library Systems V1 (for MiSeq) or V2 (for HiSeq2500) kits (NuGEN Technologies, San Carlos, CA, USA) and paired-end sequencing (2×300 or 2×150 bp) was performed using the Illumina MiSeq (2×300 bp) or HiSeq2500 (2×150 bp) platform (Illumina Inc., San Diego, CA, USA). DNA from Lake Rotsee was fragmented by sonication (350 bp) using a Covaris S2 sonicator (Covaris), the library was prepared using NEBNext Ultra DNA Library Prep Kit for Illumina (New England Biolabs, Ipswich, MA, USA) and paired-end sequencing (2×150 or 2×100 bp) was performed using the Illumina HiSeq2500 or 3000 platform (Illumina Inc.). Both MiSeq and HiSeq sequencing was performed by the Max Planck-Genome-centre, Cologne, Germany (<http://mpgc.mpipz.mpg.de/home/>; Supplementary Table 3).

Sequences were quality checked using FastQC (Andrews, 2010) and trimming, as well as adapter removal was done using Trimmomatic 0.32 and parameters MINLEN:20 ILLUMINAACLIPT:TruSeq3-PE.fa:2:30:10 LEADING:3 TRAILING:3 SLIDING-WINDOW:4:15 MINLEN:50 (Bolger *et al.*, 2014). Metagenome assembly of sequences from the Lake Zug incubation (anoxic, nitrate-supplemented (Z3; Supplementary Tables 3, 4)) was performed using SPAdes 3.5.0 (Bankevich *et al.*, 2012) with mismatch corrector enabled and default parameters.

Sand filter *Crenothrix* metagenome sequencing and assembly

Samples containing high proportions of *C. polyspora* filaments were taken from the backwash water of rapid sand filters of the Wolfenbüttel waterworks (Germany), which treats a mixture of oxic and anoxic groundwater. During sampling, *Crenothrix* filaments were retained from 600 to 850 liters of backwash water by either sedimentation or filtration through a fine-mesh sieve (200 or 400 μm). One sample was collected in 2004 (on 21 June; sample C) and was incubated with $500 \mu\text{mol l}^{-1}$ ammonium for 212 h. The second sample was collected in 2005 (10 October, sample B) and was incubated at different methane concentrations for 24 h. It should also be noted that earlier we deposited one additional partial and unpublished *Crenothrix* genome from a sand filter sample from the Wolfenbüttel waterworks at IMG (genome ID 3300005627). We did not analyze that older genome sequence in the course of the present study, because it originated from the same site but had been sequenced less deeply than the two sand filter *Crenothrix* genomes described here.

After the incubations, samples B and C were frozen at -20°C and DNA was extracted in 2016 using a phenol chloroform protocol (Zhou *et al.*, 1996) including two bead-beating steps. Paired-end sample libraries were prepared using Illumina Nextera DNA Library Preparation Kit (Illumina Inc.) and sequenced at Aalborg University (Denmark) using an Illumina MiSeq with MiSeq Reagent Kit v3 (2×301 bp; Supplementary Table 3). Paired-end

reads were imported to CLC Genomics Workbench v. 8.0 (CLCBio, Aarhus, Denmark) and trimmed using a minimum phred score of 20, a minimum length of 50 bp, allowing no ambiguous nucleotides and trimming off Illumina sequencing adaptors if found. All trimmed paired-end metagenome reads were assembled using CLC's *de novo* assembly algorithm, using a kmer of 63 and a minimum scaffold length of 1 kbp.

Metagenome binning, reassembly and annotation

Binning of contigs of the Lake Zug metagenomic assembly (sample Z3, Supplementary Table 3) was performed by exploiting differential contig coverage from three sequenced metagenomic data sets: Z1 (Lake Zug, *in situ*), Z2 (Lake Zug, O_2 -supplemented incubation) and Z3 (Lake Zug, anoxic, nitrate-supplemented incubation) as described previously (Albertsen *et al.*, 2013) and implemented in the mmgenome R package (<http://madsalbertsen.github.io/mmgenome/>; Karst *et al.*, 2016). Only contigs longer than 500 bp were used and the average coverage of each contig was computed directly using BBmap 35.43 (<http://sourceforge.net/projects/bbmap/>) with default parameters. Prodigal 2.60 (Hyatt *et al.*, 2010) in metagenomic mode (-p meta) and standard parameters was used to predict open reading frames, which were translated to amino-acid sequences and subsequently searched for using HMMER 3.1b (Eddy *et al.*, 2013) against a set of 107 hidden markov models of essential single-copy genes (Dupont *et al.*, 2012) using default settings and trusted cutoff (-cut_tc) enabled. Protein sequences coding for essential single copy genes were searched against NCBI non-redundant database (retrieved in August 2015) using BLASTP (Camacho *et al.*, 2009) and an e-value cutoff of 10^{-6} . The taxonomy (class level) of each essential single-copy gene was assigned using MEGAN5 (Huson *et al.*, 2011; with the previously generated BLASTP xml file as input) and the mmgenome script 'hmm.majority.vote.pl'. Bowtie2 (Langmead and Salzberg, 2012) with standard settings was used to map reads to contigs and the number of paired-end connections between separate contigs was calculated from the SAM file using the mmgenome script 'network.pl'.

Differential coverage of contigs between the two sand filter *Crenothrix* metagenomes (Supplementary Figure 8) and between the Lake Zug metagenomes (Supplementary Figure 7), as well as paired-end connections between separate contigs were used to extract genomic bins from the metagenome using the mmgenome R package (<http://madsalbertsen.github.io/mmgenome/>; Karst *et al.*, 2016). Reads used for the initial assembly were mapped to the binned contigs using BBmap of the BBmap package 35.43 (<http://sourceforge.net/projects/bbmap/>) using stringent settings (approximate minimum identity = 0.98) or CLC (sand filter *Crenothrix*). Mapped reads were reassembled (only for the lacustrine *Crenothrix*) using SPAdes 3.5.0 (Bankevich *et al.*, 2012) with mismatch corrector enabled and default parameters.

Quality of the reassembled bins was assessed using CheckM 1.05 running the lineage-specific workflow (Parks *et al.*, 2015). Annotation of the *Crenothrix* D3 draft genome was performed using RAST (Aziz *et al.*, 2008). CDS prediction and automated pre-annotation of the two Wolfenbüttel sand filter *Crenothrix* genome sequence bins were performed using the PROKKA pipeline (Seemann, 2014) with an in-house extended protein reference database. The annotation of key metabolic pathways was manually refined.

The Whole Genome Shotgun project of lacustrine *Crenothrix* sp. D3 has been deposited at DDBJ/ENA/GenBank under the accession MBQZ00000000. The version described in this paper is version MBQZ01000000. Reads (Lake Zug and Lake Rotsee) have been deposited at the Sequence Read Archive under BioProject PRJNA325574. The two sand filter *Crenothrix* metagenomic assemblies are available in the European Nucleotide Archive (ENA) under the study accession number PRJEB19189.

Phylogenetic analyses

Full-length amino-acid sequences of bacterial PmoA and AmoA protein sequences were retrieved from the Integrated Microbial Genomes database (IMG-ER; Markowitz *et al.*, 2009) using Pfam family PF02461. Previously published protein sequences of 'unusual' PmoA of *C. polyspora* (accession ABC59822–ABC59827; Stoecker *et al.*, 2006), partial PmoA of *C. fusca* (accession ABL64049; Vigliotta *et al.*, 2007) AmoA sequences belonging to Candidatus *Nitrospira nitrosa*, (accession CUS31358; van Kessel *et al.*, 2015) as well as Candidatus *Nitrospira inopinata* (accession CUQ66826; Daims *et al.*, 2015) were added to the reference set. After removing duplicate sequences, protein sequences were aligned using Clustal Omega 1.2.0 (Sievers *et al.*, 2011) and default parameters. A phylogenetic tree (135 taxa) was calculated using RAxML 8.2.6 (Stamatakis, 2014) and parameters: -f a -k -x 48020621 -p 6809427 -N 100 -T 8 -m PROTGAMMAWAG.

Partial *Crenothrix* 16S rRNA gene sequences were retrieved from the *Crenothrix* draft genomes using RNAmmer 1.2 (Lagesen *et al.*, 2007), aligned using the SILVA incremental aligner (SINA) 1.2.11 (Pruesse *et al.*, 2012) and imported to the SILVA SSU NR99_123 database (Quast *et al.*, 2013) using ARB 6.1 (Ludwig *et al.*, 2004). Phylogenetic trees of the 16S rRNA gene sequences were calculated using RAxML 7.7.2 integrated in ARB with the GAMMA model of rate heterogeneity and the GTR substitution model with 100 bootstraps.

Results and discussion

Crenothrix in Lake Rotsee and Lake Zug

To investigate the potential occurrence of filamentous *Crenothrix* bacteria in two stratified lakes and their involvement in the lacustrine methane cycle,

we first recorded geochemical evidence for methane oxidation *in situ*. Concentration profiles recorded in Lake Rotsee and Lake Zug over the course of 3 years suggested a zone of methane consumption that persistently coincided with the oxycline (profiles from Lake Rotsee 2013 are shown in Oswald *et al.* (2015), from 2014 in Supplementary Figure 1; profiles from Lake Zug 2012, 2013 and 2014 are shown in Oswald *et al.*, 2016). Concurrently, incubations with $^{13}\text{CH}_4$ confirmed high rates of methane oxidation at the oxycline (Oswald *et al.*, 2015, 2016; Supplementary Figure 1). These incubations were set up under both oxic and anoxic conditions. In Lake Rotsee, oxic incubation conditions were obtained either by addition of air or solely by incubation of anoxic water in the light. In the latter case, aerobic methane oxidation was presumably sustained by oxygenic photosynthesis (Milucka *et al.*, 2015; Oswald *et al.*, 2015). In Lake Zug, oxic incubations were solely supplemented with air and incubated in the dark. These different incubation set ups reflected the different nature of the two lakes, Lake Rotsee has a shallow, sun-lit oxycline, whereas the oxycline of Lake Zug is very deep and dark. Additionally, anoxic Lake Zug incubations supplemented with nitrate were also set up as Lake Zug had the appropriate environment to test for methane-dependent denitrification (Supplementary Table 4).

We then analyzed the microbial community at the Lake Rotsee oxycline by 16S rRNA gene amplicon sequencing in 2 consecutive years (2013 and 2014; Supplementary Figure 2). Along with gamma-proteobacterial *Methylococcaceae* (*Methylobacter*, *Methylocaldum*, *Methylomonas* and *Methyloglobulus* species), CAB2E06 (an uncultured *Methylococcales* clone; Wang *et al.*, 2012; Quaiser *et al.*, 2014), and the marine methylotrophic group, also sequences belonging to *Crenothrix* were retrieved. On the basis of the number of recovered sequences, *Crenothrix*-related organisms were 2–5-fold less abundant than *Methylococcaceae* and comprised 0.06–0.1% of the total bacterial sequences *in situ*. However, it is possible that the true abundance of *Crenothrix in situ* was higher than what the 16S rRNA gene abundances suggest, as, for example, DNA extraction biases might strongly select against these thickly sheathed microorganisms.

We could additionally confirm the presence of *Crenothrix* in both lakes by CARD-FISH with two oligonucleotide probes reported to target *Crenothrix*, Mgamma669 and Creno445 (Eller *et al.*, 2001; Stoecker *et al.*, 2006). The more specific oligonucleotide probe Creno445 bound only sporadically, when the hybridization stringency was strongly reduced (Supplementary Figure 3). On the other hand, the Mgamma669 probe hybridized most of the conspicuous filaments in all analyzed samples from both lakes (*in situ* water as well as incubations, Figure 1; Supplementary Figure 3) even though some filaments did not hybridize even with this more general

probe (for example, Supplementary Figures 3a, b). With both probes, we observed two hybridized cell morphotypes—filaments and single round cells (Figure 1; Supplementary Figure 3). Both morphotypes have been observed for *Crenothrix* spp. previously and it has been proposed that the smaller round cells represent reproductive cells that bud from the ends of vegetative cell filaments (Cohn, 1870; Völker *et al.*, 1977). However, given the compromised specificity of the Creno445 probe at low stringency and the broad specificity of the Mgamma669 probe, it is also possible that the hybridized single cells represented other gamma-MOB, reportedly targeted by the Mgamma669 probe (for example, *Methylobacter* or *Methylomonas*; Eller *et al.*, 2001). Therefore, the here-reported *Crenothrix* cell counts and biovolumes are solely based on counts of Creno445- or Mgamma669-hybridized filaments and thus represent conservative estimates. Overall, in all analyzed incubations from both lakes total *Crenothrix* biovolumes increased over time (Supplementary Figure 4b). This confirms that *Crenothrix* was growing under both oxic and anoxic conditions.

Whereas unicellular gamma-MOB had consistently cell sizes of ca. 2 μm , the individual cells in *Crenothrix*-like filaments reached an average length of ca. 5 μm (Figure 1; Supplementary Figures 3a and 5a). The average length and width of Lake Rotsee *Crenothrix* filaments was ca. 45 and ca. 1.5 μm , respectively, with individual filaments reaching >100 μm length (Supplementary Figure 3). Filaments were often intertwined and bunched together, as observed previously (Cohn, 1870; Völker *et al.*, 1977). In Lake Rotsee, the biovolume of *Crenothrix* was about eight-fold higher than that of unicellular gamma-MOB at depths corresponding to the highest observed methane oxidation rates (in 2012 and 2013; Supplementary Figure 4a). Only in 2014 unicellular gamma-MOB biomass contribution was higher than that of *Crenothrix* (Supplementary Figure 4). We speculate that these differences might be connected to the complex life cycle of *Crenothrix* (Supplementary Discussion). In Lake Zug, the filaments were shorter but more consistent in terms of length, reaching an average length and width of ca. 28 and 1.4 μm (in 2013) and ca. 20 and ca. 1.4 μm (in 2014), respectively.

Methanotrophic growth of *Crenothrix*

To confirm that the observed cell growth (that is, increase in cell numbers and biovolume over time; Supplementary Figure 4b) was methane-derived, samples from the $^{13}\text{CH}_4$ -supplemented incubations were further analyzed by nanoSIMS. Filamentous bacteria hybridized with the Mgamma669 probe consistently constituted the highest ^{13}C -enriched population in all three investigated incubations (Lake Rotsee oxic, Lake Zug oxic and Lake Zug anoxic; Figure 1; Supplementary Figure 5). The ^{13}C

enrichment confirmed that $^{13}\text{CH}_4$ was assimilated into cell biomass, such as is common for gamma-proteobacterial methanotrophs (Trotsenko and Murrell, 2008). In some of the images, fragmentation of filaments into single vegetative cells was apparent, even though the uptake of ^{13}C appeared homogeneously spread throughout the whole filament. In both lakes, *Crenothrix* filaments appeared to be colonized by other non-identified bacteria, which did not show comparably strong enrichment in ^{13}C and might thus represent heterotrophic epibionts (Figure 1). In contrast, the single round cells (hybridized with Mgamma669 probe) were similarly enriched in ^{13}C as the *Crenothrix* filaments (Figures 1a–c), supporting the speculation that these cells belong to methanotrophic bacteria and might potentially represent reproductive *Crenothrix* cells.

In the Lake Rotsee oxic incubation, the uptake of methane-derived carbon by *Crenothrix* filaments was comparable to that of 'classical' unicellular gamma-MOB (^{13}C enrichment of 22 ± 4.8 at % and 29 ± 4.1 at %, respectively; Table 1; Figure 1; Supplementary Figure 2). However, due to its larger biovolume *Crenothrix* assimilated ca. 4–6-fold more methane than the 'classical' gamma-MOB in the same incubation (1.73 or 1.18 μmol methane $\text{l}^{-1} \text{d}^{-1}$ and 0.27 μmol methane $\text{l}^{-1} \text{d}^{-1}$, respectively; Table 1). These numbers are based on average filament biovolumes and cell counts determined by CARD-FISH at the beginning of the incubation and do not take into account any increase in cell numbers over time, as the incubation conditions might have differently affected the growth of the different MOB. However, even if we take into account the increase of cell numbers over time, overall contribution of *Crenothrix* to methane uptake in Lake Rotsee was still higher than that of the unicellular gamma-MOB, even though the difference was not so pronounced (ca. 1.4 higher based on T_{end} cell counts).

Crenothrix filaments in Lake Zug oxic incubations were also active and assimilated methane at rates of ca. 0.04 μmol methane $\text{l}^{-1} \text{d}^{-1}$ (Table 1; Figures 1d–f). This is much lower than the overall contribution of *Crenothrix* in Lake Rotsee, which is largely due to their lower abundance (1.1E+03 cells per ml) and smaller average biovolume (ca. 30 μm^3).

Additionally, *Crenothrix* was also active in our anoxic denitrifying incubations where not enough oxygen was present to account for measured methane oxidation rates (2.7 μmol $\text{l}^{-1} \text{d}^{-1}$ $^{13}\text{CO}_2$ produced in $^{15}\text{NO}_3$ -supplemented incubation, a ca. 10-fold increase compared to control incubation without any added electron acceptor (0.234 μmol $\text{l}^{-1} \text{d}^{-1}$ $^{13}\text{CO}_2$ produced)). The methane-dependent growth under oxygen-deficient conditions was evidenced as cell biomass enrichment in both ^{13}C (from $^{13}\text{C}\text{-CH}_4$; Figures 1g–i) and ^{15}N (from ^{15}N -nitrate; Supplementary Figure 6), even though the methane uptake rates were somewhat lower (0.03 μmol

methane $l^{-1} d^{-1}$) than those in incubations supplemented with oxygen (Table 1).

Metagenomic analyses of Lake Rotsee and Lake Zug

Due to the strong dominance of eukaryotic sequences in Lake Rotsee, we were not able to assemble a genomic bin of *Crenothrix* from any of the sequenced samples (Supplementary Table 1a).

On the other hand, in the Lake Zug metagenomes eukaryotic sequences were almost completely absent and the relative abundance of *Crenothrix*-related sequences was considerably higher (Supplementary Table 1a). Therefore, a metagenome from a Lake Zug anoxic incubation (sample Z3, Supplementary Table 4) was used for the assembly of a *Crenothrix* genome.

The *Crenothrix* D3 draft genome was binned by exploiting the differential coverage of contigs in metagenomes obtained from the *in situ* metagenome of Lake Zug and two different incubations (an oxygen-supplemented and an anoxic, nitrate-supplemented; Supplementary Figure 7a; see also Materials and Methods section and Supplementary Table 4 for sample details). We retrieved several bins representing gamma-MOB from the Lake Zug assembly (data not shown). The metagenomic sequences within these two bins were also present in our Lake Rotsee metagenomes, as indicated by their respective coverage (Supplementary Figure 7b). 16S rRNA gene retrieved from one of these bins putatively belonged to a *Methylobacter* (Figure 2a). The other bin contained a partial 16S rRNA gene (909 bp) that clustered closely with *C. polyspora* (Figure 2a), even though the level of similarity (95% identity) suggests that the Lake Zug *Crenothrix* is a different species. Most closely related environmental sequences were retrieved from groundwater and habitats highlighted primarily for iron richness (Bruun *et al.*, 2010), yet apparently containing methane (Kojima *et al.*, 2009; Kato *et al.*, 2013).

Retrieval of the *Crenothrix* D3 16S rRNA gene sequence from the Lake Zug metagenome allowed us to also investigate the reasons behind the poor performance of the Creno445 probe. The comparison of the probe binding region on the 16S rRNA gene sequence revealed that the Creno445 FISH probe (length: 18 nt) had five mismatches with the partial 16S rRNA gene from our metagenomic *Crenothrix* D3 bin (Supplementary Table 2). Interestingly, out of 47 16S rRNA gene sequences in the SILVA database (NR99, release 123) that were assigned to *Crenothrix*/*Crenothrichaceae*, only seven sequences (including four *C. polyspora* sequences published by Stoecker *et al.* (2006)) contained less than five mismatches. Thus it seems that while the Creno445 probe is very specific to *C. polyspora*, it might not be suitable for environmental detection of other *Crenothrix* strains and species. In comparison, the lacustrine *Crenothrix* 16S rRNA gene had only a single mismatch with the Mgamma669 probe, which explains the

comparably better performance of this (not *Crenothrix*-specific) probe on our samples.

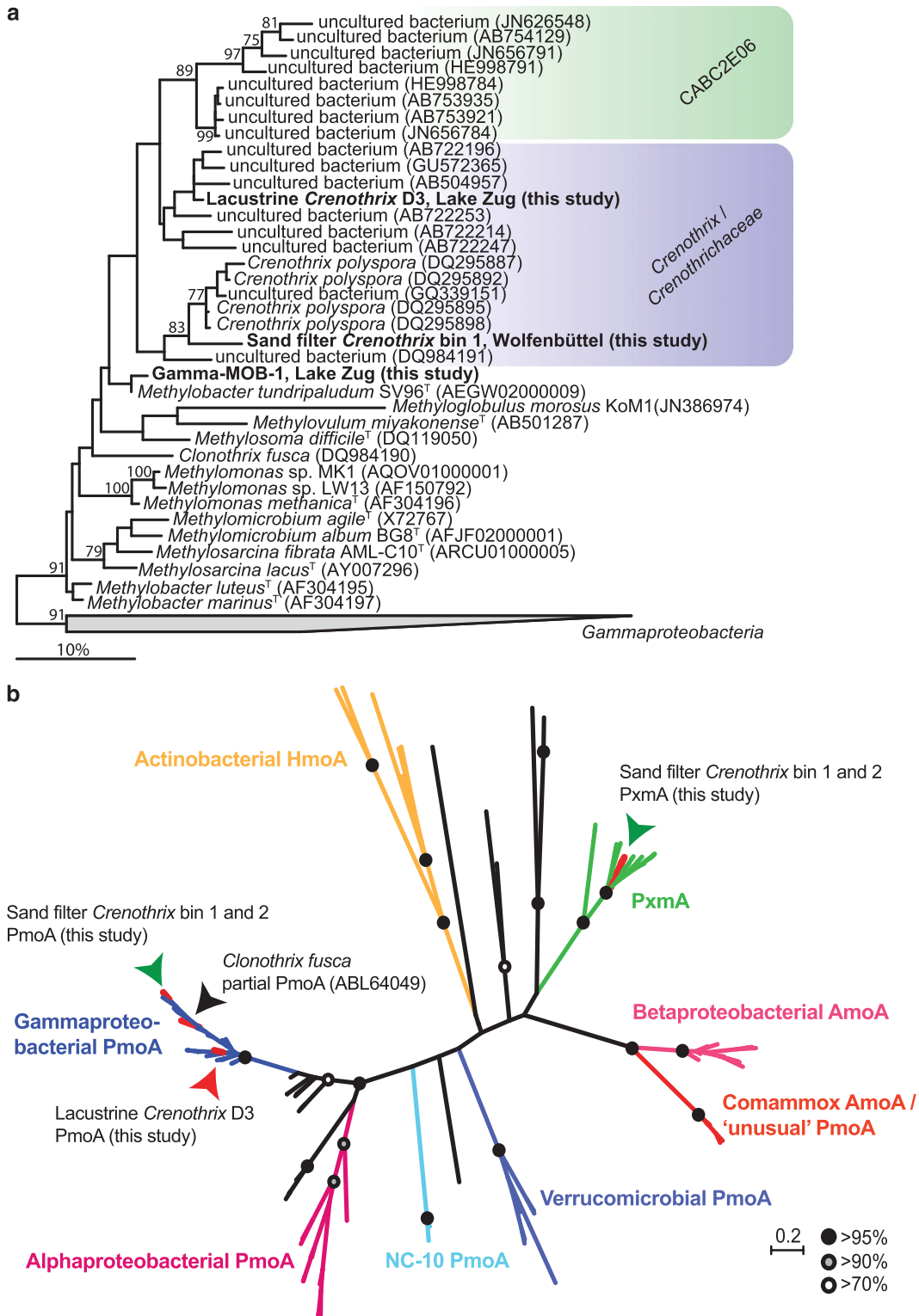
Interestingly, the clade CAB2E06, which forms an apparent sister group to *Crenothrix* based on the 16S rRNA tree (Figure 2a), had an identical number of mismatches to both probes. As the 16S rRNA gene sequences assigned to this group were retrieved from both Lake Rotsee (Supplementary Figure 2) and Lake Zug (data not shown), it is feasible that the CAB2E06 bacteria in these samples were also hybridized by the Mgamma669 probe. Additionally, if the CAB2E06 bacteria were filamentous, they may have been included in the here-reported cell and biovolume counts.

Genome-inferred C1 metabolism of lacustrine *Crenothrix* D3

In the *Crenothrix* D3 draft genome from Lake Zug (Supplementary Table 1b), we searched for pMMO genes. We found all genes encoding for pMMO, which were organized in the arrangement *pmoCAB*, such as is common for gamma-proteobacterial type I MOB (Trotsenko and Murrell, 2008). The phylogenetic analysis of the PmoA amino-acid sequence showed that the sequence fell within the PmoA group of other known gamma-MOB, including the PmoA sequence of the other described filamentous methane oxidizer, *C. fusca* (Figure 2b). However, the presence of conventional gamma-proteobacterial *pmoA* in the lacustrine *Crenothrix* strain was inconsistent with the findings of 'unusual' *pmoA* previously reported for *C. polyspora* based on PCR and quantitative PCR (Stoecker *et al.*, 2006). Our *Crenothrix* D3 draft genome did not contain any 'unusual' *pmoA*; in fact, no 'unusual' *pmoA* or *amoA* has been retrieved in any of the other gamma-MOB-assigned bins either.

We thus decided to address this discrepancy by obtaining metagenomic data from the original samples used in the Stoecker *et al.* (2006) study. Two samples obtained in 2004 from the rapid sand filters of the Wolfenbüttel waterworks (Germany) were analyzed and, after differential coverage binning, genomic information of two *Crenothrix* strains was obtained (Supplementary Figure 8). A partial 16S rRNA sequence retrieved from one sand filter *Crenothrix* bin (bin 1; 817 bp) was 98% identical to the *C. polyspora* 16S rRNA sequence. As the sample reportedly contained high proportions of *C. polyspora*, it is feasible that (at least one of) the sand filter *Crenothrix* was in fact *C. polyspora*. However, throughout this manuscript we refer to these organisms as sand filter *Crenothrix*, without a species name. The sand filter and the lacustrine *Crenothrix* likely represented different species as indicated by the average sequence identities of their shared genes (Supplementary Discussion).

Both genomes of the sand filter *Crenothrix* species contained a *pmoCAB* operon (gene similarities



between both bins 96–99%) and a *pxmABC* operon (gene similarities between both bins 93–99%). PmoA encoded by the genes from the *pmoCAB* operon clustered together with other gamma-proteobacterial PmoA sequences (Figure 2b) and the affiliation of the *pxmABC* operon with the sequence-divergent *pxm* cluster was confirmed by a phylogenetic analysis of

pxmA (Tavormina *et al.*, 2011; Figure 2b). PxmA has been suggested to play a role in methane oxidation under hypoxic and denitrifying conditions by *Methylomonas denitrificans* and *Methylomicrobium album* (Kits *et al.*, 2015a, b). It thus appears that *Crenothrix* might be another denitrifying methanotroph containing both *pmoCAB* and *pxmABC*

Figure 2 Phylogenetic tree of *Crenothrix* 16S rRNA gene and PmoA amino-acid sequences retrieved from Lake Zug and sand filters of the Wolfenbüttel waterworks. (a) Phylogenetic tree of partial 16S rRNA gene sequence retrieved from the lacustrine *Crenothrix* (909 bp) and from one sand filter *Crenothrix* (817 bp, bin 1) draft genomes. Note that the 16S rRNA gene sequence of Lake Zug ‘lacustrine’ *Crenothrix* (but not of the sand filter *Crenothrix*) is monophyletic with clade CAB32E06. The tree was calculated with the RAxML maximum likelihood program implemented in the ARB package without constraining the alignment by a filter or weighting mask. Bootstrap values >70 (out of 100 resamplings) are shown in front of each node. The taxonomic affiliations indicated by the colored boxes are based on the SILVA SSU reference database (release 123; (Pruesse *et al.*, 2007)). Fourteen type strains spread among gamma-proteobacteria were used as an outgroup. Nucleotide accession numbers are listed in brackets. The bar shows an estimated nucleotide sequence divergence of 10%. (b) Maximum likelihood phylogenetic tree of bacterial PmoA/AmoA amino-acid sequences (135 taxa) showing affiliation of PmoA sequences recovered from the Lake Zug *Crenothrix* bin (red arrow) as well as of the two sand filter *Crenothrix* genome bins (green arrows). All three *Crenothrix* PmoA sequences clustered within the ‘classical’ gamma-proteobacterial PmoA branch. Bootstrap support of total 100 bootstraps are shown in black (>95%), gray (>90%) and white (>70%) circles. Scale bar indicates substitutions per site.

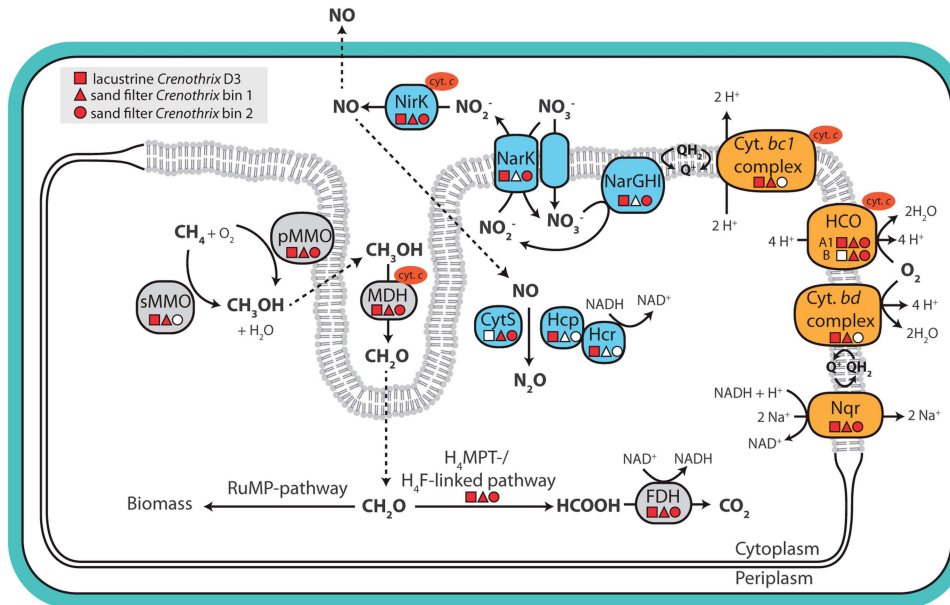


Figure 3 Genome-inferred metabolic potential of *Crenothrix* for respiration and methane oxidation. Predicted metabolic potential of the lacustrine *Crenothrix* as well as of the two sand filter *Crenothrix* species with respect to its CH_4 and N metabolism inferred from the three draft genomes. Indicated are the methane oxidation pathway (gray boxes), the aerobic respiratory chain (orange boxes) and the pathway for nitrate respiration (blue boxes). Genes that were found in the respective *Crenothrix* genomes (square: lacustrine *Crenothrix* D3; triangle: sand filter *Crenothrix* bin 1; circle: sand filter *Crenothrix* bin 2) are depicted in red, not found in white. Cyt. *bc1* complex, cytochrome *bc1* complex; Cyt. *bd* complex, cytochrome *bd* complex (*cydABCD*); *cyt c*, cytochrome *c*; CytS, cytochrome *c*-beta; FDH, formate dehydrogenase; H_4F , tetrahydrofolate; H_4MPT , tetrahydromethanopterin; HCO, heme copper oxygen reductase (*COXI-III*); Hcp, hybrid cluster protein; Hcr, NADH-dependent Hcp reductase; MDH, methanol dehydrogenase (*xoxF*); Nar, nitrate reductase (*narGH*); NarK, nitrate/nitrite antiporter (*narK*); NirS, copper-containing nitrite reductase (*nirS*); Nqr, sodium-translocating NADH:quinone oxidoreductase; pMMO, particulate methane monooxygenase (*pmoCAB*); Q, ubiquinone; RuMP, ribulose monophosphate; sMMO, soluble methane monooxygenase (*smmoXYBZDC*).

operons. Importantly, no ‘unusual’ *pmoA* could be detected in the sand filter *Crenothrix* bins. However, the ‘unusual’ *pmoA* sequence previously assigned to *C. polyspora* was detected in a different bin, clearly belonging to the completely nitrifying *Nitrospira*, apparently co-occurring with *C. polyspora* in the sample (Daims *et al.*, 2015; van Kessel *et al.*, 2015; Pinto *et al.*, 2016). This finding is discussed in more detail in the Supplementary Discussion. It is interesting to note that whereas all three *Crenothrix* PmoA sequences fell within the ‘classical’ gamma-proteobacterial PmoA branch, the lacustrine *Crenothrix* PmoA clustered separate from the sand filter *Crenothrix* bins 1 and 2 and *C. fusca* (Figure 2b). Comparison of the 16S rRNA gene and PmoA amino-

acid trees suggested that the PmoA of the lacustrine *Crenothrix* might have been obtained laterally from another gamma-proteobacterial methanotroph. This is supported by the fact that transposase genes were located immediately up- and downstream of the lacustrine *Crenothrix* *pmoCAB* operon on the respective contig (data not shown).

In addition to the gene cluster encoding for pMMO, we also retrieved a full gene cluster for soluble methane monooxygenase (sMMO; *smmoX-YBZDC*) in the lacustrine *Crenothrix* and in one sand filter *Crenothrix* bin. This enzyme is relatively rare in gamma-proteobacterial methanotrophs (Murrell, 2010) and was not found in *C. polyspora* previously (Stoecker *et al.*, 2006), presumably due to the

mismatches between the applied PCR primers and the respective target regions in the *mmoX* gene. We cannot conclusively prove involvement of sMMO in methane oxidation by *Crenothrix*; however, as the substrate range of sMMO seems much broader than that of pMMO (Dalton, 2005; Semrau *et al.*, 2011), it is feasible that *Crenothrix* might have the capacity to utilize other C-compounds as suggested previously (Stoecker *et al.*, 2006). This could explain the reported occurrence of *Crenothrix* in, for example, natural bitumen deposits (Saidi-Mehrabad *et al.*, 2013). All three retrieved genomes (two sand filter *Crenothrix* genomes as well as the lacustrine *Crenothrix* D3 genome) further contained all necessary genes for complete oxidation of methane to CO₂ (Supplementary Discussion; Figure 3).

Like many other type I methanotrophs (Chistoserdova and Lidstrom, 2013), *Crenothrix* might use the RuMP pathway for C1 assimilation from formaldehyde, as genes for all necessary enzymes were found in all three draft genomes (Figure 3). On the other hand, the serine cycle apparently missed genes encoding for hydroxypyruvate reductase and malate thiokinase. *Crenothrix* had the genomic potential for mixed acid fermentation to succinate and potentially acetate (gene encoding for phosphate acetyltransferase was missing in lacustrine *Crenothrix* D3 genome and one sand filter *Crenothrix*, but was putatively present in the other sand filter *Crenothrix* bin) and hydrogen production (via NAD-reducing hydrogenase, *hox-FUYH*; only present in the lacustrine *Crenothrix*). Pyruvate, which serves as the starting point for fermentation, could be generated from formaldehyde via enzymes of the RuMP and pyrophosphate-mediated glycolytic pathway that was encoded in all three *Crenothrix* genomes. Mixed acid fermentation and H₂ production via these pathways has been shown to be a major route of methane-derived carbon respiration in methanotrophs growing under oxygen limitation (Kalyuzhnaya *et al.*, 2013).

Aerobic and anaerobic respiration by Crenothrix

In agreement with the demonstrated cell growth and activity in our oxic incubations, all three *Crenothrix* genomes encoded a multitude of aerobic respiratory chain complexes, such as a sodium-pumping NADH:ubiquinone oxidoreductase (Na⁺-NQR), the M and L subunits of the NADH:quinone oxidoreductase, the *bc1* complex, an A1-type heme copper cytochrome *c* oxidase, a type B heme copper cytochrome *c* oxidase (only the sand filter *Crenothrix*) and a cytochrome *bd* oxidase that might potentially act as a high-affinity terminal oxidase (Figure 3).

Additionally, the draft genome of the lacustrine *Crenothrix* D3 as well as one of the sand filter *Crenothrix* strains also contained a partial pathway for the respiration of nitrate. We retrieved genes encoding for a membrane-bound respiratory nitrate reductase (*narGHI*), a nitrite/nitrate antiporter (*narK*) as

well as a periplasmic multi-copper nitrite reductase (*nirK*). Genes encoding for nitric oxide (NO) and nitrous oxide (N₂O) reductases (*norBC* and q-type *nor*, and *nosZ*, respectively) were not found in any of the three bins. Yet, interestingly, all three *Crenothrix* genomes encoded proteins for alternative pathways of NO detoxification to N₂O. In the genome of *Crenothrix* D3, a gene cluster containing *hcp* and *hcr* genes was found. The *hcp* gene encodes for a unique hybrid cluster protein (Hcp), which has recently been shown to act as a high-affinity NO reductase in *Escherichia coli*, producing N₂O as the end product (Wang *et al.*, 2016). The Hcp sequence retrieved from the *Crenothrix* D3 genome contained the six highly conserved residues involved in 4Fe-2S-2O cluster coordination (Aragao *et al.*, 2008) as well as a glutamic acid residue (E492 of *E. coli* Hcp) essential for NO reductase activity (Wang *et al.*, 2016). Overall, the *Crenothrix* D3 Hcp shared 49% amino-acid identity with the NO-reducing Hcp of *E. coli*. The *hcr* gene, located immediately downstream from *hcp*, encodes for the Hcr protein and acts as a NADH-dependent Hcp reductase (van den Berg *et al.*, 2000), while simultaneously protecting Hcp from nitrosylation by its substrate, NO (Wang *et al.*, 2016). The *hcp/hcr* genes in *Crenothrix* D3 genome were preceded by *norR*, a transcriptional regulator of three different enzymes (NO reductase, flavorubredoxin and flavohaemoglobin) that all utilize NO as a substrate (Rodionov *et al.*, 2005). We thus speculate that, despite being routinely annotated as a hydroxylamine reductase, the Hcp/Hcr system in *Crenothrix* could in fact act as a NO reductase and substitute Nor-type NO reductases under denitrifying conditions. In the two sand filter *Crenothrix* genome bins no homologs of Hcp were found. However, both bins (but not the lacustrine *Crenothrix* genome bin) contained a homolog of cytochrome *c'*-beta, a member of the cytochrome P460 family found in, for example, gamma-proteobacterial methane oxidizers (Zahn *et al.*, 1996; Campbell *et al.*, 2011) and gamma- and beta-proteobacterial ammonia oxidizers (Bergmann and Hooper, 2003; Klotz *et al.*, 2006). Cytochrome *c'*-beta can reduce NO to N₂O (Elmore *et al.*, 2007). Interestingly, in one of the bins this gene (*cytS*) was located directly downstream of the *haoA* and *haoB* genes encoding for hydroxylamine dehydrogenase. As both the Hcp and the cytochrome *c'*-beta are predicted to be cytoplasmic proteins and NO is produced in the periplasm (by NirK), it is feasible that their activities are not coupled and (some) NO might escape out of the cell (Figure 3).

The experimentally demonstrated and genome analysis-supported metabolic potential for methane-dependent growth under nitrate-reducing conditions cannot serve as a final proof of nitrate reduction by *Crenothrix* in Lake Zug. However, it is interesting to speculate that such metabolic versatility might expand the habitat of these facultative anaerobic bacteria, potentially enabling them to survive periods of oxygen starvation by switching to using nitrate as an electron acceptor for methane

oxidation. Denitrification is an emerging feature of gamma-MOB, which has been supported by genomics and was also experimentally demonstrated (Hoefman *et al.*, 2014; Kalyuzhnaya *et al.*, 2015; Skennerton *et al.*, 2015; Kits *et al.*, 2015a, 2015b). It has been proposed that respiration of nitrate might enable aerobic gamma-MOB to colonize anoxic waters (Chistoserdova, 2015; Knief, 2015). In Lake Rotsee and Lake Zug, *Crenothrix* was indeed found in the anoxic waters below the oxycline in at least 2 consecutive years. Its abundance in anoxic lake waters suggests that it might successfully compete with more obligate anaerobic methane oxidizers, such as archaeal methanotrophs (Haroon *et al.*, 2013) or ‘*Candidatus* Methyloirabilis oxyfera’ (Ettwig *et al.*, 2010).

Conclusions

Members of the genus *Crenothrix* are rare methane oxidizers, which are not available in pure or enrichment cultures and will not be readily picked up in environmental samples by the currently available specific FISH probe (Creno445). The ambiguity surrounding their *pmoA* has further complicated the *in situ* detection using molecular methods. In the past, this has hampered our understanding of these peculiar organisms and possibly led us to underestimate their role in the biogeochemical nutrient and element cycles.

In our study, we could unambiguously demonstrate a key role for these organisms in the mitigation of methane emissions from two stratified lakes. In Lake Rotsee, *Crenothrix* even contributed more to methane uptake than the ‘classical’ unicellular gamma-MOB. In up to 3 consecutive years *Crenothrix* was recurrently found throughout the stratification period of Lake Rotsee and Lake Zug, and thus appears to be a stable part of the indigenous microbial community. Our data are also the first to demonstrate that *Crenothrix* is capable of growing as a planktonic species in the lake water column. Given the capacity of *Crenothrix* to rapidly grow up into large biomass, its participation in methane cycling also in other relevant habitats should be considered.

Conflict of Interest

The authors declare no conflict of interest.

Acknowledgements

We would like to thank Christian Dinkel, Carole Guggenheim and Jasmine Berg for support during field campaigns and Bernd Bendinger for providing the sand filter *Crenothrix* samples. We thank Philipp Hach, Hannah Marchant, Bernhard Fuchs, Gaute Lavik, Michaela Steinberger and Petra Pjevac for technical support, Craig Herbold for ANI and AAI analyses, Laura Bristow for critical reading of the manuscript, and Boran Kartal for his input regarding the Hcp. This study was supported by the

Max-Planck Society, the ETH, the Eawag and the Swiss National Science Foundation (SNF grant no. 135299, 153091 & 128707). MW was supported by an ERC Advanced Grant (NITRICARE, 294343).

Author contributions

JM, MMMK and CJS designed research, KO and AB performed field measurements, incubation experiments and sampling, JSG performed metagenomic analyses on lake water samples and phylogenetic analyses; HD, MW and MA performed metagenomic analysis on the sand filter *Crenothrix* sample; SL and DT performed FISH and nanoSIMS measurements, BW, MMMK and CJS contributed material and analysis tools; KO, JSG and JM wrote the paper with input from all co-authors.

References

- Albertsen M, Hugenholtz P, Skarshewski A, Nielsen KL, Tyson GW, Nielsen PH. (2013). Genome sequences of rare, uncultured bacteria obtained by differential coverage binning of multiple metagenomes. *Nat Biotechnol* **31**: 533–538.
- Andrews S. (2010). FastQC: A quality control tool for high throughput sequence data. Available at: <http://www.bioinformatics.babraham.ac.uk/projects/fastqc>.
- Aragao D, Mitchell EP, Frazao CF, Carrondo MA, Lindley PF. (2008). Structural and functional relationships in the hybrid cluster protein family: structure of the anaerobically purified hybrid cluster protein from *Desulfovibrio vulgaris* at 1.35 Å resolution. *Acta Crystallogr D* **64**: 665–674.
- Aziz RK, Bartels D, Best AA, DeJongh M, Disz T, Edwards RA *et al.* (2008). The RAST Server: rapid annotations using subsystems technology. *BMC Genomics* **9**: 75.
- Bankevich A, Nurk S, Antipov D, Gurevich AA, Dvorkin M, Kulikov AS *et al.* (2012). SPAdes: a new genome assembly algorithm and its applications to single-cell sequencing. *J Comp Biol* **19**: 455–477.
- Bastviken D, Cole J, Pace M, Tranvik L. (2004). Methane emissions from lakes: dependence of lake characteristics, two regional assessments, and a global estimate. *Global Biogeochem Cyc* **18**: 1–12.
- Bergmann DJ, Hooper AB. (2003). Cytochrome P460 of *Nitrosomonas europaea*. *Eur J Biochem* **270**: 1935–1941.
- Bodelier PLE, Meima-Franke M, Hordijk CA, Steenbergh AK, Hefting MM, Bodrossy L *et al.* (2013). Microbial minorities modulate methane consumption through niche partitioning. *ISME J* **7**: 2214–2228.
- Bolger AM, Lohse M, Usadel B. (2014). Trimmomatic: a flexible trimmer for Illumina sequence data. *Bioinformatics* **30**: 2114–2120.
- Boschker HTS, Nold SC, Wellsbury P, Bos D, de Graaf W, Pel R *et al.* (1998). Direct linking of microbial populations to specific biogeochemical processes by C-13-labelling of biomarkers. *Nature* **392**: 801–805.

- Bowman JP. (2005). Order VII. *Methylococcales* ord. nov. In: Garrity G, Brenner DJ, Krieg NR, Staley JR (eds). *Bergey's Manual of Systematic Bacteriology*, 2nd edn. Springer: New York, USA, pp 248–270.
- Bruun AM, Finster K, Gunnlaugsson HP, Nornberg P, Friedrich MW. (2010). A comprehensive investigation on iron cycling in a freshwater seep including microscopy, cultivation and molecular community analysis. *Geomicrobiol J* **27**: 15–34.
- Camacho C, Coulouris G, Avagyan V, Ma N, Papadopoulos J, Bealer K *et al.* (2009). BLAST+: architecture and applications. *BMC Bioinformatics* **10**: 1.
- Campbell MA, Nyerges G, Kozlowski JA, Poret-Peterson AT, Stein LY, Klotz MG. (2011). Model of the molecular basis for hydroxylamine oxidation and nitrous oxide production in methanotrophic bacteria. *Fems Microbiol Lett* **322**: 82.
- Chistoserdova L, Lidstrom ME. (2013). Aerobic methylo-trophic prokaryotes. In: Rosenberg E, DeLong EF, Thompson F, Lory S, Stackebrandt E (eds), *The Prokaryotes* 4th edn Springer: Berlin, Heidelberg, pp 267–285.
- Chistoserdova L. (2015). Methylo-trophs in natural habitats: current insights through metagenomics. *Appl Microbiol Biot* **99**: 5763–5779.
- Cohn F. (1870). Über den Brunnenfaden (*Crenothrix polyspora*) mit Bemerkungen über die mikroskopische Analyse des Brunnenwassers. *Beitr Biol Pflanzen* **1**: 108–131.
- Daims H, Lebedeva EV, Pjevac P, Han P, Herbold C, Albertsen M *et al.* (2015). Complete nitrification by *Nitrospira* bacteria. *Nature* **528**: 504–509.
- Dalton H. (2005). The Leeuwenhoek Lecture 2000 - the natural and unnatural history of methane-oxidizing bacteria. *Philos Trans R Soc Lond B Biol Sci* **360**: 1207–1222.
- Dörr N, Glaser B, Kolb S. (2010). Methanotrophic communities in Brazilian ferralsols from naturally forested, afforested, and agricultural sites. *Appl Environ Microb* **76**: 1307–1310.
- Drewniak L, Maryan N, Lewandowski W, Kaczanowski S, Sklodowska A. (2012). The contribution of microbial mats to the arsenic geochemistry of an ancient gold mine. *Environ Pollut* **162**: 190–201.
- Dupont CL, Rusch DB, Yooseph S, Lombardo M-J, Richter RA, Valas R *et al.* (2012). Genomic insights to SAR86, an abundant and uncultivated marine bacterial lineage. *ISME J* **6**: 1186–1199.
- Eddy SR, Wheeler TJ. HMMER development team. (2013). HMMER 3.1b1 (May 2013). Available at: <http://hmmer.org>.
- Eller G, Stubner S, Frenzel P. (2001). Group-specific 16S rRNA targeted probes for the detection of type I and type II methanotrophs by fluorescence in situ hybridisation. *Fems Microbiol Lett* **198**: 91–97.
- Elmore BO, Bergmann DJ, Klotz MG, Hooper AB. (2007). Cytochromes P460 and c'-beta: a new family of high-spin cytochromes *c*. *FEBS Lett* **581**: 911–916.
- Ettwig KF, Butler MK, Le Paslier D, Pelletier E, Mangenot S, Kuypers MMM *et al.* (2010). Nitrite-driven anaerobic methane oxidation by oxygenic bacteria. *Nature* **464**: 543–548.
- Haroon MF, Hu SH, Shi Y, Imelfort M, Keller J, Hugenholtz P *et al.* (2013). Anaerobic oxidation of methane coupled to nitrate reduction in a novel archaeal lineage. *Nature* **500**: 567–570.
- Hoefman S, van der Ha D, Boon N, Vandamme P, De Vos P, Heylen K. (2014). Niche differentiation in nitrogen metabolism among methanotrophs within an operational taxonomic unit. *BMC Microbiol* **14**: 83.
- Huson DH, Mitra S, Ruscheweyh H-J, Weber N, Schuster SC. (2011). Integrative analysis of environmental sequences using MEGAN4. *Genome Res* **21**: 1552–1560.
- Hyatt D, Chen G-L, LoCascio PF, Land ML, Larimer FW, Hauser LJ. (2010). Prodigal: prokaryotic gene recognition and translation initiation site identification. *BMC Bioinformatics* **11**: 1.
- Jackson DD. (1902). A new species of *Crenothrix* (*C. manganifera*). *Trans Am Microsc Soc* **23**: 31–39.
- Kalyuzhnaya MG, Yang S, Rozova ON, Smalley NE, Clubb J, Lamb A *et al.* (2013). Highly efficient methane biocatalysis revealed in a methanotrophic bacterium. *Nat Commun* **4**: 2785.
- Kalyuzhnaya MG, Lamb AE, McTaggart TL, Oshkin IY, Shapiro N, Woyke T *et al.* (2015). Draft genome sequences of gammaproteobacterial methanotrophs isolated from Lake Washington sediment. *Genome Announc* **3**: e00103–15.
- Karst SM, Kirkegaard RH, Albertsen M. (2016). mmgenome: a toolbox for reproducible genome extraction from metagenomes. *bioRxiv*: 059121.
- Kato S, Chan C, Itoh T, Ohkuma M. (2013). Functional gene analysis of freshwater iron-rich flocs at circumneutral pH and isolation of a stalk-forming microaerophilic iron-oxidizing bacterium. *Appl Environ Microb* **79**: 5283–5290.
- Kirf MK, Dinkel C, Schubert CJ, Wehrli B. (2014). Submicromolar oxygen profiles at the oxic–anoxic boundary of temperate lakes. *Aquat Geochem* **20**: 39–57.
- Kits KD, Campbell DJ, Rosana AR, Stein LY. (2015a). Diverse electron sources support denitrification under hypoxia in the obligate methanotroph *Methylomicrobium album* strain BG8. *Front Microbiol* **6**: 1072.
- Kits KD, Klotz MG, Stein LY. (2015b). Methane oxidation coupled to nitrate reduction under hypoxia by the Gammaproteobacterium *Methylomonas denitrificans*, sp nov type strain FJG1. *Environ Microbiol* **17**: 3219–3232.
- Klotz MG, Arp DJ, Chain PSG, El-Sheikh AF, Hauser LJ, Hommes NG *et al.* (2006). Complete genome sequence of the marine, chemolithoautotrophic, ammonia-oxidizing bacterium *Nitrosococcus oceani* ATCC 19707. *Appl Environ Microb* **72**: 6299–6315.
- Knief C. (2015). Diversity and habitat preferences of cultivated and uncultivated aerobic methanotrophic bacteria evaluated based on pmoA as molecular marker. *Front Microbiol* **6**: 1346.
- Kojima H, Fukuhara H, Fukui M. (2009). Community structure of microorganisms associated with reddish-brown iron-rich snow. *Syst Appl Microbiol* **32**: 429–437.
- Kolk LA. (1938). A comparison of the filamentous iron organisms, *Clonothrix fusca* Roze and *Crenothrix polyspora* Cohn. *Am J Bot* **25**: 11–17.
- Lagesen K, Hallin P, Rødland E, Stærfeldt H, Rognes T, Ussery D. (2007). RNAMmer: consistent annotation of rRNA genes in genomic sequences. *Nucleic Acids Res* **35**: 3100–3108.
- Langmead B, Salzberg SL. (2012). Fast gapped-read alignment with Bowtie 2. *Nat Methods* **9**: 357–359.

- Ludwig W, Strunk O, Westram R, Richter L, Meier H, Buchner A *et al.* (2004). ARB: a software environment for sequence data. *Nucleic Acids Res* **32**: 1363–1371.
- Markowitz VM, Mavromatis K, Ivanova NN, Chen I-MA, Chu K, Kyrpides NC. (2009). IMG ER: a system for microbial genome annotation expert review and curation. *Bioinformatics* **25**: 2271–2278.
- Milucka J, Kirf M, Lu L, Krupke A, Lam P, Littmann S *et al.* (2015). Methane oxidation coupled to oxygenic photosynthesis in anoxic waters. *ISME J* **9**: 1991–2002.
- Molisch H. (1910). Die Eisenbakterien: Gustav Fischer, Jena. Available at: <http://library.wur.nl/WebQuery/clc/speccol/181818>.
- Murrell JC. (2010). The aerobic methane oxidizing bacteria (methanotrophs). In: Timmis KN (ed). Handbook of Hydrocarbon and Lipid Microbiology. Springer Berlin Heidelberg: Berlin, Heidelberg, Germany, pp 1953–1966.
- Musat N, Halm H, Winterholler B, Hoppe P, Peduzzi S, Hillion F *et al.* (2008). A single-cell view on the ecophysiology of anaerobic phototrophic bacteria. *Proc Natl Acad Sci USA* **105**: 17861–17866.
- Oshkin IY, Beck DAC, Lamb AE, Tchesnokova V, Benuska G, McTaggart TL *et al.* (2015). Methane-fed microbial microcosms show differential community dynamics and pinpoint taxa involved in communal response. *ISME J* **9**: 1119–1129.
- Oswald K, Milucka J, Brand A, Littmann S, Wehrli B, Kuypers MMM *et al.* (2015). Light-dependent aerobic methane oxidation reduces methane emissions from seasonally stratified lakes. *PLoS ONE* **10**: e0132574.
- Oswald K, Milucka J, Brand A, Hach P, Littmann S, Wehrli B *et al.* (2016). Aerobic gammaproteobacterial methanotrophs mitigate methane emissions from oxic and anoxic lake waters. *Limnol Oceanogr* **61**: S101–S118.
- Parks DH, Imelfort M, Skennerton CT, Hugenholtz P, Tyson GW. (2015). CheckM: assessing the quality of microbial genomes recovered from isolates, single cells, and metagenomes. *Genome Res* **25**: 1043–1055.
- Pernthaler A, Pernthaler J, Amann R. (2002). Fluorescence *in situ* hybridization and catalyzed reporter deposition for the identification of marine bacteria. *Appl Environ Microb* **68**: 3094–3101.
- Pinto AJ, Marcus DN, Ijaz UZ, Bautista-de los Santos QM, Dick GJ, Raskin L. (2016). Metagenomic evidence for the presence of comammox *Nitrospira*-like bacteria in a drinking water system. *mSphere* **1**: pii: e00054-15.
- Polerecky L, Adam B, Milucka J, Musat N, Vagner T, Kuypers MMM. (2012). Look@NanoSIMS - a tool for the analysis of nanoSIMS data in environmental microbiology. *Environ Microbiol* **14**: 1009–1023.
- Pruesse E, Quast C, Knittel K, Fuchs BM, Ludwig WG, Peplies J *et al.* (2007). SILVA: a comprehensive online resource for quality checked and aligned ribosomal RNA sequence data compatible with ARB. *Nucleic Acids Res* **35**: 7188–7196.
- Pruesse E, Peplies J, Glöckner FO. (2012). SINA: accurate high-throughput multiple sequence alignment of ribosomal RNA genes. *Bioinformatics* **28**: 1823–1829.
- Quaiser A, Bodi X, Dufresne A, Naquin D, Francez AJ, Dheilly A *et al.* (2014). Unraveling the stratification of an iron-oxidizing microbial mat by metatranscriptomics. *PLoS ONE* **9**: e102561.
- Quast C, Pruesse E, Yilmaz P, Gerken J, Schweer T, Yarza P *et al.* (2013). The SILVA ribosomal RNA gene database project: improved data processing and web-based tools. *Nucleic Acids Res* **41**: D590–D596.
- Rodionov DA, Dubchak IL, Arkin AP, Alm EJ, Gelfand MS. (2005). Dissimilatory metabolism of nitrogen oxides in bacteria: comparative reconstruction of transcriptional networks. *PLoS Comput Biol* **1**: e55.
- Roze E. (1896). Le *Clonothrix*, un nouveau type generique de Cyanophycees. *J Bot* **10**: 325–330.
- Saidi-Mehrabad A, He Z, Tamas I, Sharp CE, Brady AL, Rochman FF *et al.* (2013). Methanotrophic bacteria in oilsands tailings ponds of northern Alberta. *ISME J* **7**: 908–921.
- Schloss PD, Westcott SL, Ryabin T, Hall JR, Hartmann M, Hollister EB *et al.* (2009). Introducing mothur: open-source, platform-independent, community-supported software for describing and comparing microbial communities. *Appl Environ Microbiol* **75**: 7537–7541.
- Seemann T. (2014). Prokka: rapid prokaryotic genome annotation. *Bioinformatics* **30**: 2068–2069.
- Semrau JD, DiSpirito AA, Vuilleumier S. (2011). Facultative methanotrophy: false leads, true results, and suggestions for future research. *Fems Microbiol Lett* **323**: 1–12.
- Sievers F, Wilm A, Dineen D, Gibson TJ, Karplus K, Li W *et al.* (2011). Fast, scalable generation of high-quality protein multiple sequence alignments using Clustal Omega. *Mol Syst Biol* **7**: 539.
- Skenneron CT, Ward LM, Michel A, Metcalfe K, Valiente C, Mullin S *et al.* (2015). Genomic reconstruction of an uncultured hydrothermal vent gammaproteobacterial methanotroph (family Methylothermaceae) indicates multiple adaptations to oxygen limitation. *Front Microbiol* **6**: 1425.
- Stamatakis A. (2014). RAxML version 8: a tool for phylogenetic analysis and post-analysis of large phylogenies. *Bioinformatics* **30**: 1312–1313.
- Stoecker K, Bendinger B, Schoning B, Nielsen PH, Nielsen JL, Baranyi C *et al.* (2006). Cohn's *Crenothrix* is a filamentous methane oxidizer with an unusual methane monooxygenase. *Proc Natl Acad Sci USA* **103**: 2363–2367.
- Tavormina PL, Orphan VJ, Kalyuzhnaya MG, Jetten MSM, Klotz MG. (2011). A novel family of functional operons encoding methane/ammonia monooxygenase-related proteins in gammaproteobacterial methanotrophs. *Environ Microbiol Rep* **3**: 91–100.
- Trotsenko YA, Murrell JC. (2008). Metabolic aspects of aerobic obligate methanotrophy. *Adv Appl Microbiol* **63**: 183–229.
- van den Berg WAM, Hagen WR, van Dongen WMAM. (2000). The hybrid-cluster protein ('prismane protein') from *Escherichia coli*. *Eur J Biochem* **267**: 666–676.
- van Kessel MAHJ, Speth DR, Albertsen M, Nielsen PH, Op den Camp HJM, Kartal B *et al.* (2015). Complete nitrification by a single microorganism. *Nature* **528**: 555–559.
- Vigliotta G, Nutricati E, Carata E, Tredici SM, De Stefano M, Pontieri P *et al.* (2007). *Clonothrix fusca* Roze 1896, a filamentous, sheathed, methanotrophic gamma-proteobacterium. *Appl Environ Microbiol* **73**: 3556–3565.
- Völker H, Schweisfurth R, Hirsch P. (1977). Morphology and ultrastructure of *Crenothrix polyspora* Cohn. *J Bacteriol* **131**: 306–313.
- Wang J, Vine CE, Balasiny BK, Rizk J, Bradley CL, Tinajero-Trejo M *et al.* (2016). The roles of the hybrid cluster protein, Hcp and its reductase, Hcr, in high

- affinity nitric oxide reduction that protects anaerobic cultures of *Escherichia coli* against nitrosative stress. *Mol Microbiol* **100**: 877–892.
- Wang JJ, Krause S, Muyzer G, Meima-Franke M, Laanbroek HJ, Bodelier PLE. (2012). Spatial patterns of iron- and methane-oxidizing bacterial communities in an irregularly flooded, riparian wetland. *Front Microbiol* **3**: 64.
- Wiesenburg DA, Guinasso NL Jr. (1979). Equilibrium solubilities of methane, carbon monoxide, and hydrogen in water and sea water. *Journal of Chemical and Engineering Data* **24**: 356–360.
- Wolfe RS. (1960). Observations and studies of *Crenothrix polyspora*. *J Am Water Works Assoc* **52**: 915–918.
- Zahn JA, Arciero DM, Hooper AB, Dispirito AA. (1996). Cytochrome *c*' of *Methylococcus capsulatus* bath. *Eur J Biochem* **240**: 684–691.

Zhou JZ, Bruns MA, Tiedje JM. (1996). DNA recovery from soils of diverse composition. *Appl Environ Microb* **62**: 316–322.



This work is licensed under a Creative Commons Attribution 4.0 International License. The images or other third party material in this article are included in the article's Creative Commons license, unless indicated otherwise in the credit line; if the material is not included under the Creative Commons license, users will need to obtain permission from the license holder to reproduce the material. To view a copy of this license, visit <http://creativecommons.org/licenses/by/4.0/>

© The Author(s) 2017

Supplementary Information accompanies this paper on *The ISME Journal* website (<http://www.nature.com/ismej>)

Supplementary Information File

Supplementary Discussion

Life cycle of Crenothrix and lake turnover

In Lake Rotsee, the proportion of small gonidial to large filamentous cells varied between sampling years. In 2012 and 2013 we observed many long intact filaments (Supplementary Figure 3), whereas in 2014 we only detected short *Crenothrix* fragments and gonidial cells seemed to be more numerous. In 2012 and 2013 our sampling was conducted in August, when stratification was stable and methane fluxes had probably reached their maximum ($13 \pm 3 \text{ mmol m}^{-2} \text{ d}^{-1}$; (Oswald et al, 2015) whereas in 2014 the sampling campaign was conducted in late October and though the lake still showed stable stratification below 7 m depth, the methane fluxes were somewhat lower ($8 \pm 2 \text{ mmol m}^{-2} \text{ d}^{-1}$; Supplementary Figure 1). It is possible that filaments may have propagated just before the lake overturn which increased the ratio of comparably small gonidial cells to long vegetative cells. These changes in their life cycle could explain the comparably lower *Crenothrix* biovolume contribution in 2014.

Average nucleotide and amino acid identities of lacustrine and sand filter Crenothrix

The average nucleotide identities (ANI; (Richter & Rosselló-Móra, 2009) between *Crenothrix* strain D3 and the two sand filter *Crenothrix* genomes were 72.9 - 73% and 80.5 % between the latter two genomes, respectively. These values are far below proposed species delineation boundaries of 95 - 97% (Goris et al, 2007; Varghese et al, 2015). The average amino acid identity (AAI, (Konstantinidis & Tiedje, 2005) between *Crenothrix* strain D3 and the two sand filter *Crenothrix* species is 66.1 – 66.4 % and the AAI between the two latter genomes is 77.4%. These AAI values are above the proposed genus delineation boundary of 60% (Luo et al, 2014) suggesting that all three *Crenothrix* species indeed belong to the same genus. It should be noted that also other members of the *Methylococcaceae* (such as *Methyloglobulus morosus*; (Deutzmann et al, 2014) have AAI values with the three *Crenothrix* genomes that suggest affiliation to the same genus (data not shown), and therefore the taxonomy of this order might need to be revised.

Extended genome description of sand filter Crenothrix species and the lacustrine Crenothrix D3

Downstream oxidation of methanol

All *Crenothrix* genomes contained a *XoxF* homolog encoding for the large subunit of the pyrroloquinoline quinone- and cerium-dependent methanol dehydrogenase (MDH), an enzyme catalyzing downstream oxidation of methanol to formaldehyde or formate. Interestingly, *mx*a genes encoding for the calcium-dependent MDH and its accessory proteins were not found in the lacustrine *Crenothrix* D3 draft genome and sand filter *Crenothrix* bin 2 but were found in sand filter *Crenothrix* bin 1. Absence of *mx*a-type MDHs in genomes containing *xoxF*-type MDHs have so far been described for several methylotrophs (Chistoserdova, 2011; Giovannoni et al, 2008; Kalyuzhnaya et al, 2009; Wilson et al, 2008) as well as verrucomicrobial methanotrophs (Khadem et al, 2012; Op den Camp et al, 2009; Pol et al, 2014). Genes encoding for enzymes catalyzing a four-step C1 interconversion of formaldehyde to formate via the methenyl-tetrahydromethanopterin pathway (*fae*, *mtdB*, *mch*, *fhc*) were all present, in both the lacustrine and the sand filter *Crenothrix* genomes. The alternative tetrahydrofolate (H₄F)-linked pathway was missing F₀D, the bifunctional enzyme acting as methylene-H₄F dehydrogenase and methenyl-H₄F cyclohydrolase. However, in the case of *Crenothrix*, this enzyme might be substituted by Fch and Mtd, such as has been shown for other methylotrophs (Chistoserdova, 2011). These genes (*fch*, *mtdB*, and several *mtd* homologues) were found in the *Crenothrix* genomes. In the last step, formate can further be oxidized to CO₂ by a NAD-dependent formate dehydrogenase, which was encoded in all three *Crenothrix* draft genomes.

Carbohydrate metabolism (only annotated for the lacustrine Crenothrix)

All genes encoding for core enzymes involved in the pentose phosphate pathway, tricarboxylic acid cycle, Entner-Doudoroff pathway as well as Embden-Meyerhof-Parnas pathway were present in the lacustrine *Crenothrix* D3 draft genome.

Nitrogen assimilation (only annotated for the lacustrine Crenothrix)

Genes encoding for assimilatory nitrate and NAD(P)H-dependent nitrite reductase were retrieved from the lacustrine *Crenothrix* D3 draft genome. Downstream

assimilation of ammonium can proceed via the GS/GOGAT-pathway by glutamine synthetase and glutamate synthase which genes are both present in the genome.

Nitrogen fixation

Lacustrine *Crenothrix* might also have the potential to fix dinitrogen gas since the genome contains key genes encoding for nitrogenase as well as a suite of its accessory proteins (i.e. *nifKDHWENX*). Nitrogenase genes were absent from both sand filter *Crenothrix* draft genomes, with the exception of *nifK* in bin 1.

Discussion of the canonical gamma-proteobacterial and 'unusual' *pmoA* sequence in the sand filter *Crenothrix*

Stoecker *et al.* (2006) have retrieved 'unusual' *pmoA* from a sample strongly dominated by filaments that were identified by morphology as *C. polyspora*. *C. polyspora* abundance was observed by FISH using a *Crenothrix*-specific probe as well as Bacteria- and Archaea- and Eukarya-specific FISH probes and was independently confirmed by qPCR using two general and two *C. polyspora*-specific 16S rRNA gene targeting primer sets [Figure 3 of the Stoecker *et al.* (2006) paper]. By using additional qPCR assays for the 'unusual' *pmoA* (two assays) and canonical gamma-proteobacterial *pmoA* (two assays) a much higher abundance of the 'unusual' than the canonical *pmoA* was observed and thus it was concluded that *C. polyspora* very likely encodes the 'unusual' *pmoA* gene. This conclusion was further supported by the fact that transcription of the 'unusual' *pmoA* was strongly induced by methane addition [Figure 7 in the Stoecker *et al.* (2006) paper]. Surprisingly, we and others recently demonstrated that completely nitrifying *Nitrospira* species (comammox) encode *amoA* genes that are highly similar to the 'unusual' *pmoA* genes assigned to *C. polyspora* (Daims *et al.*, 2015; Palomo *et al.*, 2016; Pinto *et al.*, 2016; van Kessel *et al.*, 2015).

To address this issue, we obtained frozen material from the sample used in the Stoecker *et al.* 2006 paper (this sample material had been used for unpublished incubation experiments before freezing) and reconstructed two draft *C. polyspora* genomes by metagenomic sequencing. Interestingly, these genomes had ANI values that demonstrated that they represent two different *Crenothrix* species to which we thus refer to as sand filter *Crenothrix* species in this manuscript. In both genome bins the

canonical gamma-proteobacterial methane monooxygenase (in addition to another gamma-proteobacterial *pmoABC* operon; see main text) was encoded, while the 'unusual' *pmoA* could not be detected. However, the 'unusual' *pmoA* previously assigned to *C. polyspora* was detected in the metagenome from this sample in one of the two comammox *Nitrospira* bins (see Supplementary Figure 8; the other comammox *Nitrospira* bin contains another 'unusual' *amoA*). We thus conclude from these data that in the sample used by Stoecker *et al.* 2006 comammox *Nitrospira* thrived, which encode the 'unusual' *pmoA* (and use it as *amoA*), and that the two *C. polyspora* strains encode the canonical gamma-proteobacterial *pmoA* [which was also retrieved in the Stoecker *et al.* (2006) study but assigned to another gamma-MOB in the sample, *Methylomicrobium album*]. We do not have a conclusive explanation for the qPCR data shown in Figure 3 in the Stoecker *et al.* (2006). The strongly increased transcription of the 'unusual' *pmoA* gene after addition of methane to the *C. polyspora*-dominated sample as described by Stoecker *et al.* could either be explained by the existence of a low abundant methane-oxidizing *Crenothrix* strain possessing this gene (as speculated below) or by methane-induced secretion of metabolites by *C. polyspora* that stimulated the comammox *Nitrospira* in the sample. In the Stoecker *et al.* (2006) study DNA for the qPCR assays was extracted using the FastDNA kit (QBiogene, Irvine, CA) while the much harsher phenol chloroform bead beating protocol was used in our metagenome analysis of the same sample. One could thus speculate that the FastDNA kit did not lyse the dominant populations of *Crenothrix* strains (with canonical gamma-proteobacterial *pmoA*) and only DNA from a low abundant *Crenothrix* strain (not binned in the metagenome) was obtained, whose canonical *pmoA* has been replaced by the comammox *amoA*. The existence of comammox *Nitrospira* that are very closely related to purely nitrite-oxidizing *Nitrospira* strains, which do not possess the 'unusual' *pmoA/amoA* gene, indicate lateral gene transfer events of the genes necessary for ammonia oxidation, and suggest a complex evolutionary history of these genes (Daims *et al.*, 2015).

Supplementary Tables

Supplementary Table 1a. Average coverage of the lacustrine *Crenothrix* D3 draft genome in all metagenomic data sets of Lake Zug and Lake Rotsee (see Supplementary Table 3 for additional information on the metagenomic data sets)

	Lake Zug (metagenomic data sets Z1-3)		Lake Rotsee (metagenomic data sets R1-3)			
	<i>in situ</i> (Z1)	O ₂ -supplemented (Z2)	nitrate-supplemented (Z3)	<i>in situ</i> (R1)	dark, O ₂ -supplemented (R2)	light (R3)
Lacustrine <i>Crenothrix</i> D3	2.2	16.8	23.1	0.01	0.3	0.13

Supplementary Table 1b. Summary statistics of sand filter *Crenothrix* and lacustrine *Crenothrix* D3 draft genomes. N50 is a length weighted median of contig length and is defined as the shortest contig length needed to cover 50% of the metagenomic bin. Completeness, contamination and strain heterogeneity were assessed by CheckM (Parks et al, 2015) using 290 lineage-specific marker sets of Gamma-proteobacteria.

Metagenomic bin	Length (Mb)	GC content	No. of contigs (N50)	Completeness / Contamination / Strain heterogeneity (%)
Lacustrine <i>Crenothrix</i> D3	3.63	42.2%	103 (89.8 Kb)	98.4 / 1.8 / 0.0
Sand filter <i>Crenothrix</i> bin 1	3.97	44.2%	180 (51.2 Kb)	98.3/1.4/0.0
Sand filter <i>Crenothrix</i> bin 2	3.57	44.7%	467 (11.7 Kb)	92.1/3.6/57.1

Supplementary Table 2. Overview of used oligonucleotide probes. Listed are target groups, 5'-3' sequence, % [v/v] formamide in the hybridization buffer and respective references.

Probe	Target group	Probe sequence (5'-3')	% Formamide	Mismatch (nt)*	Reference
Creno445	<i>Crenothrix polyspora</i>	GCT TGC CTT TTT CCT CCC	0-35 [§]	5	(Stoecker et al, 2006)
EUB338 I-III	most bacteria	GCT GCC TCC CGT AGG AGT GCA GCC ACC CGT AGG TGT GCT GCC ACC CGT AGG TGT	35	0 (EUB338 I) 3 (EUB338 II) 2 (EUB338 III)	(Daims et al, 1999)
Mgamma84	type-I methanotrophs	CCA CTC GTC AGC GCC CGA	20	2	(Eller et al, 2001)
Mgamma705		CTG GTG TTC CTT CAG ATC		1	
Mgamma669	<i>Crenothrix</i> , <i>Methylobacter</i> , <i>Methylomonas</i>	GCT ACA CCT GAA ATT CCA CTC	20	1	(Eller et al, 2001)

*Mismatch of the retrieved lacustrine *Crenothrix* D3 16S rRNA gene sequence with the respective probe (number of nucleotides)[§]For Creno445 probe various formamide concentrations were used

Supplementary Table 3. Summary of raw metagenomic sequences obtained from Wolfenbüttel waterworks sand filters, Lake Zug and Lake Rotsee (*in situ* and *in vitro* incubations). See Supplementary Table 4 for additional information on the origin of sequenced samples.

Metagenome sample [identifier]	Sequencing technology	No. of paired-end reads	Total sequenced (Gb)	Sample origin and date
Lake Zug, <i>in situ</i> [Z1]	MiSeq, 2x300bp	7,401,029	4.4	Lake Zug water column (160 m), <i>in situ</i> , October 2013
Lake Zug, oxic incubation [Z2]	HiSeq2500, 2x100bp	44,545,098	8.9	Lake Zug, water column (160 m), O ₂ -supplemented dark incubation (t=11 d), June 2014
Lake Zug, anoxic incubation [Z3]	MiSeq, 2x300bp	8,766,855	5.3	Lake Zug, water column (160 m), nitrate-supplemented dark incubation (t=16 d), October 2013
Lake Rotsee, <i>in situ</i> [R1]	HiSeq2500, 2x100bp	45,352,147	9.1	Lake Rotsee, water column (9 m), <i>in situ</i> , August 2013
Lake Rotsee, oxic (O ₂ -supplemented) incubation [R2]	HiSeq3000, 2x150bp	81,632,757	24.5	Lake Rotsee, water column (9 m), O ₂ -supplemented dark incubation (t=11 d), August 2013
Lake Rotsee, oxic (light) incubation [R3]	HiSeq2500, 2x100bp	43,258,628	8.7	Lake Rotsee, water column (9 m), light incubation (t=11 d), August 2013
Wolfenbüttel sand filter <i>Crenothrix</i> , sample B	MiSeq, 2x301 bp	1,841,331	1.1	Wolfenbüttel waterworks, sand filter, October 2005
Wolfenbüttel sand filter <i>Crenothrix</i> , sample C	MiSeq, 2x301 bp	2,406,567	1.4	Wolfenbüttel waterworks, sand filter, June 2004

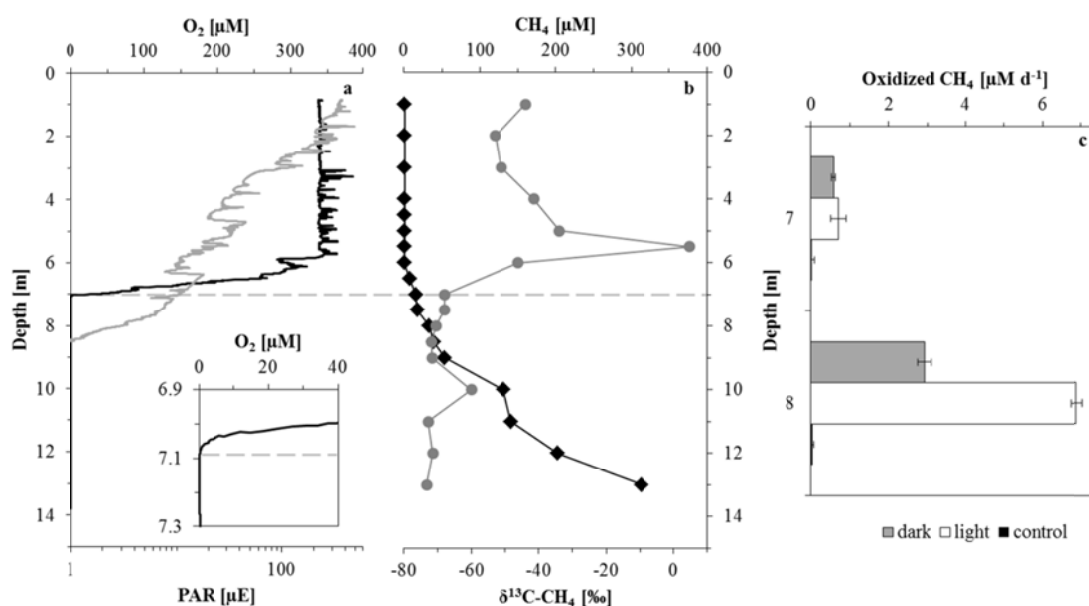
Supplementary Table 4. Overview of samples from Lake Rotsee, Lake Zug and Wolfenbüttel waterworks (rapid sand filters) analyzed and shown in this study. Indicated are sample treatment, performed analyses and relevant figures. For detailed description of incubation experiments see Materials and Methods section in this manuscript and Oswald *et al.*, 2015, 2016, respectively. Additional information on the metagenomic datasets R1-3, Z1-3, and B and C can be found Supplementary Table 3.

relevant samples*	detailed description	methane oxidation rates	FISH, cell counts, biovolumes			16S rRNA amplicon sequencing		metagenome sequencing
			nanoSIMS	nanoSIMS	nanoSIMS	16S rRNA amplicon sequencing	metagenome sequencing	
Lake Rotsee 2013	water sample from the oxycline, sampled in August							
<i>in situ</i>	9 m	(Oswald et al, 2015)	this study (SupplFig 3, 4)	this study (SupplFig 2)	this study (SupplFig 2)	sample R1		
oxic (light)	T=2d (FISH, nanoSIMS); T _{end} =11d (metagenome)	(Oswald et al, 2015)	this study (Fig 1; SupplFig 3, 4, 5)	this study (Fig 1; SupplFig 2)		sample R3		
oxic (O ₂ -supplemented)	T _{end} =11d	(Oswald et al, 2015)				sample R2 (SupplFig 7)		
Lake Rotsee 2014	water sample from the oxycline, sampled in October							
<i>in situ</i>	7 m	this study (SupplFig1)	this study (SupplFig 4)					
	8 m	this study (SupplFig1)	this study (SupplFig 3)		this study (SupplFig 2)			
Lake Zug 2013	water sample from an anoxic depth, sampled in October							
<i>in situ</i>	160 m		this study (SupplFig 4)			sample Z1 (SupplFig 7)		
anoxic (NO ₃ ⁻ supplemented)	50 µmol l ⁻¹ ¹⁵ NO ₃ ⁻ ; T _{end} =16 d (FISH, nanoSIMS, metagenome)		this study (Fig 1, SupplFig 4)	this study (Fig 1, SupplFig 6)		sample Z3 (SupplFig 7)		
Lake Zug 2014	water sample from an anoxic depth, sampled in June							
<i>in situ</i>	160 m	(Oswald et al,	this study					

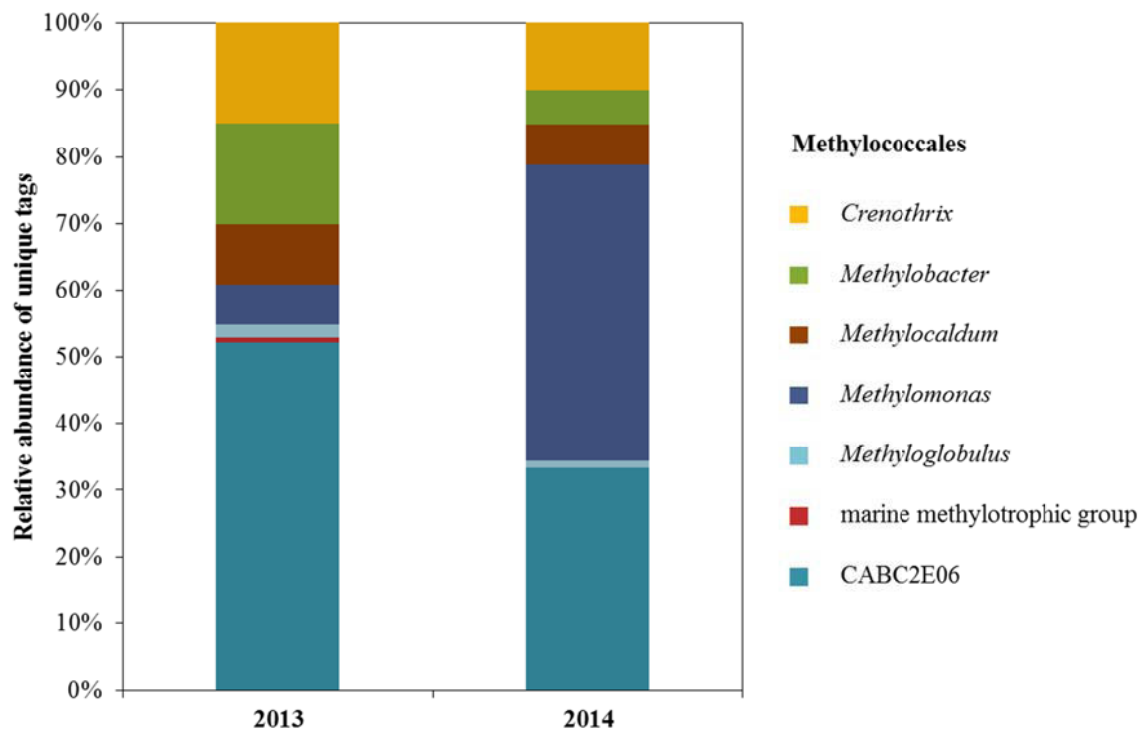
oxic (O ₂ -supplemented; low O ₂)	80 µmol l ⁻¹ O ₂ ; T=2 d (FISH, nanoSIMS); T _{end} =11 d (metagenome)	2016)	(SupplFig 4)	this study (Fig1)		sample Z2 (SupplFig 7)
oxic (O ₂ -supplemented; high O ₂)	200 µmol l ⁻¹ O ₂ ; T=2 d (FISH, nanoSIMS); T _{end} =11 d (metagenome)	(Oswald et al, 2016) (Oswald et al, 2016)	this study (Fig1, Suppl Fig 4) this study (Fig1, Suppl Fig 4)	this study (Fig1)		
Wolfenbüttel waterworks Sample C (21.6.2004)	Sieved backwash water of rapid sand filters. Sample was incubated for 190 to 240 h at 4 to 40°C with 3 µmol/l dissolved methane and subsequently stored at -20°C until DNA extraction.					Sample C (SupplFig 8)
Wolfenbüttel waterworks Sample B (18.10.2005)	Sieved backwash water of rapid sand filters. Sample was incubated for 24h at 20°C with 0.15 to 125 µmol/l dissolved methane and subsequently stored at -20°C until DNA extraction.					Sample B (SupplFig 8)

*all in vitro incubations were supplemented with methane in excess

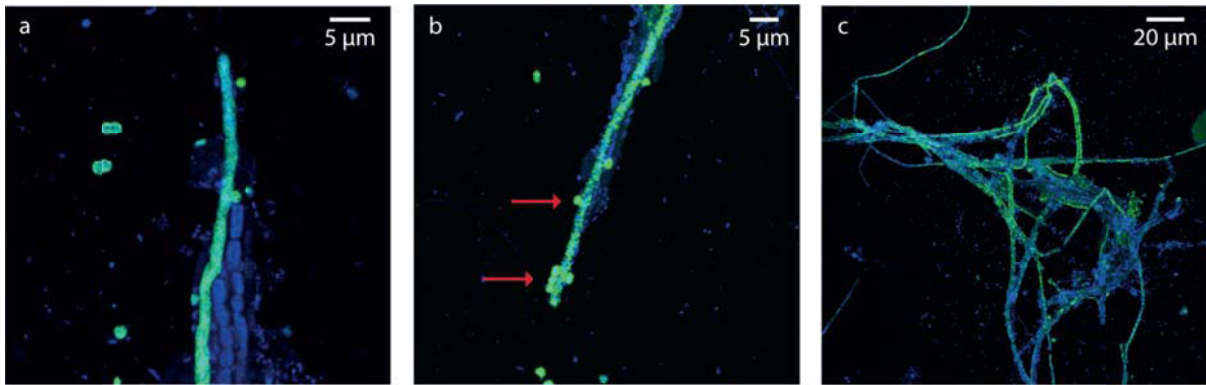
Supplementary Figures



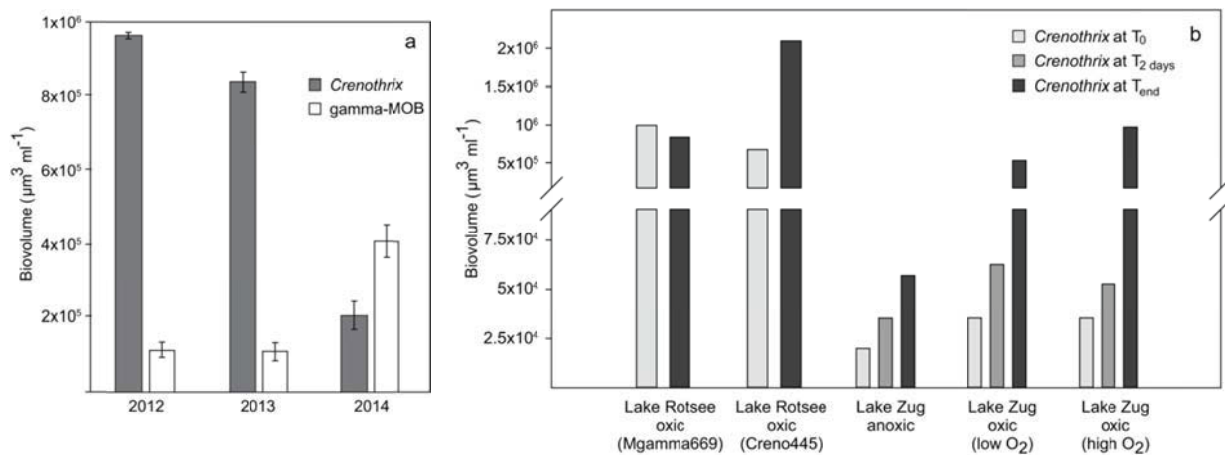
Supplementary Figure 1. Hydrochemical conditions and methane oxidation rates in Lake Rotsee in October 2014. a, Depth profiles of oxygen (black line) and photosynthetically active radiation (PAR) (grey line). The inset shows the exact location of the oxycline at 7.1 m measured with the trace oxygen optode. Note the logarithmic scale for PAR and that light penetrated below the oxycline (dashed line). b, Methane concentrations (black diamonds) and corresponding stable carbon isotopes of methane (grey circles). The isotopic signature of methane became substantially heavier at and above the oxycline, indicative of biological methane oxidation. The sharp peak in the methane isotopic ratio profile at ca. 5.5 m depth is indicative of a local source supplying methane at this depth (by *in situ* production or by lateral transport from littoral sediments). c, methane oxidation rates under dark and light conditions with water from the oxycline (7 m) and the anoxic waters below (8 m). No methane oxidation was detected in a sterile-filtered control.



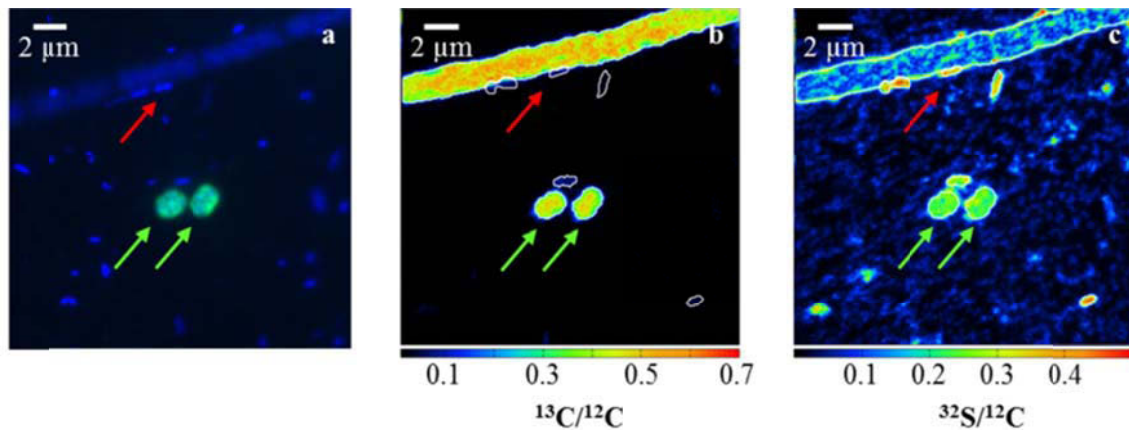
Supplementary Figure 2. Taxonomic assignment of 16S rRNA amplicon sequences recovered from the Lake Rotsee oxycline in August 2013 and October 2014 assigned to the Methylococcales order (Bowman, 2005). In this order, unicellular *Methylococcaceae*, CABC2E06 and *Crenothrix* 16S rRNA sequences comprised 31%, 52% and 15% (2013) and 56%, 33% and 10% (2014), respectively. Retrieved *Crenothrix* 16S rRNA sequences (n=66 and n= 270 for 2013 and 2014, respectively) comprised between 0.06-0.1% of all retrieved 16S rRNA bacterial sequences.



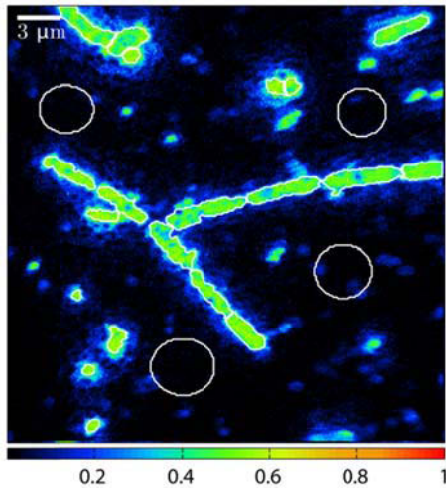
Supplementary Figure 3. *Crenothrix* in Lake Rotsee. DAPI (blue) and CARD-FISH (green) signals of *Crenothrix a*, *in situ* samples from 8 m depth in 2014 (probe Mgamma669); b, filaments at the beginning of the incubation experiment with water from 9 m depth in 2013 (probe Creno445). Red arrows indicate possible gonidial cells. c, Filaments after 11 days of oxic incubation under light conditions (probe Creno445; 2013).



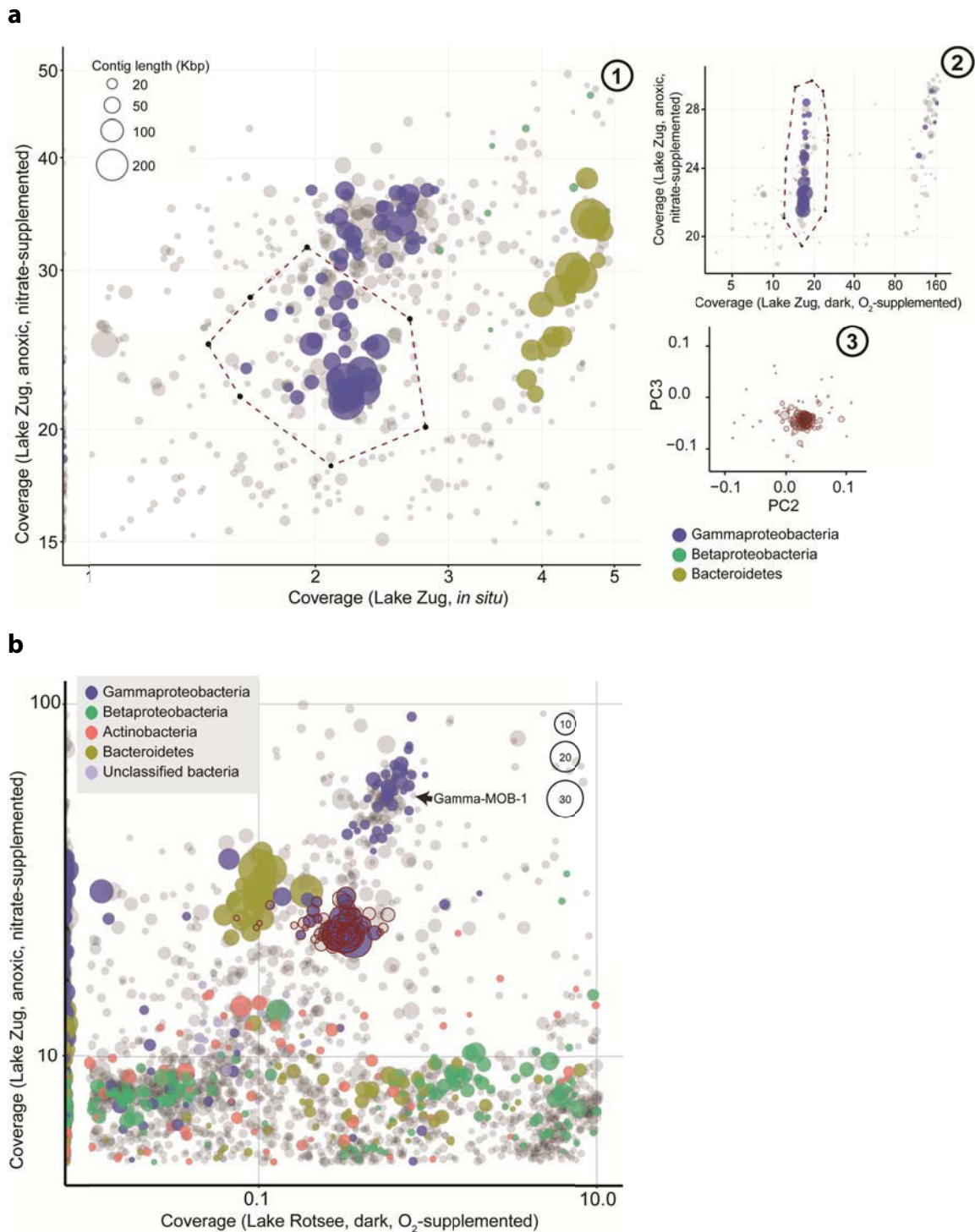
Supplementary Figure 4. Overview of *Crenothrix* biovolume *in situ* and in incubations. a, biovolume of *Crenothrix* filaments and unicellular gamma-MOB at and below the oxycline of Lake Rotsee. *Crenothrix* biovolume refers to an average biovolume determined for Mgamma669 and Creno445-hybridized filaments and gamma-MOB refers to an average biovolume determined for cells targeted by the Mgamma84+705 probes. Biovolume was calculated in depths that displayed the highest methane oxidation rates. In 2012 and 2014 this was below the oxycline (at 7 m depth) and in 2013 directly at the oxycline (at 9 m depth). Error bars represent a cumulative standard error of the mean between measured filaments and counted fields of view (n=20). b, increase of *Crenothrix* filament biovolumes in oxic and anoxic incubation from Lake Rotsee and Lake Zug over time. *Crenothrix* in Lake Rotsee were detected using either Mgamma669 or Creno445 probe, *Crenothrix* in Lake Zug was detected using only Mgamma669 probe. Biovolume was determined for incubations from the oxycline [9 m depth in Lake Rotsee (2013) and 160 m in Lake Zug (2013, 2014)]. T_{end} refers to 11 days for Lake Rotsee incubation, 16 days for Lake Zug anoxic incubation and 11 days for Lake Zug oxic incubations.



Supplementary Figure 5. Methane-dependent growth of *Crenothrix* in Lake Rotsee. a, DAPI (blue) and CARD-FISH (green) fluorescent signals of gamma-MOB (green arrows, probes Mgamma84+705) and an unhybridized filamentous bacterium (red arrow) from Lake Rotsee oxic incubation. b, The corresponding $^{13}\text{C}/^{12}\text{C}$ nanoSIMS image shows uptake of $^{13}\text{CH}_4$ by the coccoid gamma MOB as well the filamentous bacterium. Note that the ^{13}C enrichment in the filamentous organism is comparable to that of the coccoid gamma-MOB. c, The corresponding $^{32}\text{S}/^{12}\text{C}$ nanoSIMS images show distribution of organic material in the analyzed fields of view. The higher S/C ratio of the unicellular gamma-MOB compared to *Crenothrix* cells might be due to a presence of the carbon-rich polysaccharide sheath surrounding the filaments.

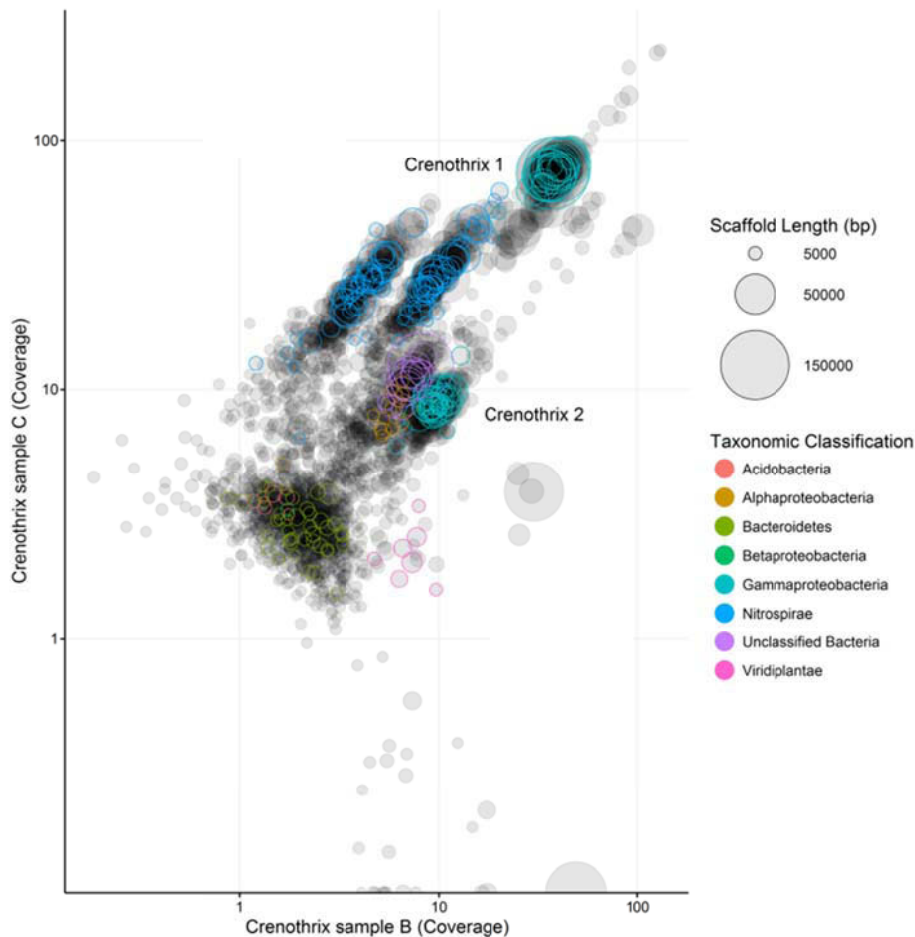


Supplementary Figure 6. A $^{12}\text{C}^{15}\text{N}/^{12}\text{C}^{14}\text{N}$ nanoSIMS image corresponding to the field of view displayed in Figure 1g-i. Due to the long incubation time (16 days) it is not possible to conclude that the ^{15}N in the cell biomass was taken up in the form of $^{15}\text{NO}_3^-$ which was added into the incubation. Therefore, the cellular ^{15}N uptake is only used as an indicator for growth under incubation conditions.



Supplementary Figure 7. Differential coverage overview of the different bins retrieved from Lake Zug and their classification based on marker genes and 16S rRNA genes. a, Lacustrine *Crenothrix* D3 bin (outlined by dotted line) was extracted from metagenomic contigs of the Lake Zug assembly (metagenome data set Z3: Lake Zug, anoxic, nitrate-supplemented incubation) by exploiting differential coverage binning. Each contig is represented by a circle and the circles size reflects contig length (in Kbp). Colored circles show taxonomic assignment of essential single copy genes present on the contig. A preliminary bin was obtained by differential coverage of the Lake Zug *in situ* sample (data set: Z1) and the Lake Zug anoxic, nitrate-supplemented incubation (data set: Z3; plot 1). This bin was further refined by differential coverage of the Lake Zug anoxic, nitrate-supplemented incubation (data set: Z1)

and Lake Zug dark, O₂-supplemented (data set: Z2, plot 2). Tetranucleotide frequencies of the final *Crenothrix* D3 bin are shown in plot 3. b, Differential coverage plot of the same Lake Zug assembly. Contigs are plotted with their respective average coverage of two sequenced samples: Lake Zug, anoxic, nitrate-supplemented incubation (data set: Z3; y-axis) as well as Lake Rotsee, dark, O₂-supplemented incubation (data set: R2; x-axis). Lacustrine *Crenothrix* D3 bin (dark red circles) as well as another gamma-proteobacterial bin (Gamma-MOB-1) is shown.



Supplementary Figure 8: Differential coverage plot for the *C. polyspora* metagenomes.

Differential coverage plot of the Wolfenbüttel waterworks sand filter (sieved *Crenothrix* biomass) assembly. Contigs are plotted with their respective average coverage of two sequenced samples: sample B, collected in 2005 and incubated at different methane concentrations for 24 hours (x-axis) as well as sample C, collected in 2004 and incubated with 500 $\mu\text{mol l}^{-1}$ ammonium for 212 hours (y-axis). Each contig is represented by a circle and the circles size reflects contig length (in Kbp). Colored circles show taxonomic assignment of essential single copy genes present on the contig. Clusters of similarly colored circles represent potential genome bins. The two *Crenothrix* bins (light blue), two comammox *Nitrospira* bins (dark blue), and bins representing various other organisms (other colors) are shown.

Supplementary References

Bowman JP (2005) Order VII. *Methylococcales* ord. nov. In *Bergey's manual of systematic bacteriology, 2nd ed.*, Garrity G, Brenner DJ, Krieg NR, Staley JR (eds), Vol. 2, pp 248-270. New York, NY: Springer

Chistoserdova L (2011) Modularity of methylotrophy, revisited. *Environmental microbiology* **13**: 2603-2622

Daims H, Bruhl A, Amann R, Schleifer KH, Wagner M (1999) The domain-specific probe EUB338 is insufficient for the detection of all Bacteria: Development and evaluation of a more comprehensive probe set. *Systematic and Applied Microbiology* **22**: 434-444

Daims H, Lebedeva EV, Pjevac P, Han P, Herbold C, Albertsen M, Jehmlich N, Palatinszky M, Vierheilig J, Bulaev A (2015) Complete nitrification by *Nitrospira* bacteria. *Nature* **528**: 504-509

Deutzmann JS, Hoppert M, Schink B (2014) Characterization and phylogeny of a novel methanotroph, *Methyloglobulus morosus* gen. nov., spec. nov. *Systematic and Applied Microbiology* **37**: 165-169

Eller G, Stubner S, Frenzel P (2001) Group-specific 16S rRNA targeted probes for the detection of type I and type II methanotrophs by fluorescence in situ hybridisation. *Fems Microbiology Letters* **198**: 91-97

Giovannoni SJ, Hayakawa DH, Tripp HJ, Stingl U, Givan SA, Cho JC, Oh HM, Kitner JB, Vergin KL, Rappé MS (2008) The small genome of an abundant coastal ocean methylotroph. *Environmental Microbiology* **10**: 1771-1782

Goris J, Konstantinidis KT, Klappenbach JA, Coenye T, Vandamme P, Tiedje JM (2007) DNA-DNA hybridization values and their relationship to whole-genome sequence similarities. *International Journal of Systematic and Evolutionary Microbiology* **57**: 81-91

Kalyuzhnaya MG, Martens-Habbena W, Wang T, Hackett M, Stolyar SM, Stahl DA, Lidstrom ME, Chistoserdova L (2009) Methylophilaceae link methanol oxidation to denitrification in freshwater lake sediment as suggested by stable isotope probing and pure culture analysis. *Environmental Microbiology Reports* **1**: 385-392

Khadem AF, Wieczorek AS, Pol A, Vuilleumier S, Harhangi HR, Dunfield PF, Kalyuzhnaya MG, Murrell JC, Francoijs K-J, Stunnenberg HG (2012) Draft genome sequence of the volcano-inhabiting thermoacidophilic methanotroph *Methylacidiphilum fumariolicum* strain SolV. *Journal of Bacteriology* **194**: 3729-3730

Konstantinidis KT, Tiedje JM (2005) Towards a genome-Based taxonomy for prokaryotes. *Journal of Bacteriology* **187**: 6258-6264

- Luo C, Rodriguez-R LM, Konstantinidis KT (2014) MyTaxa: an advanced taxonomic classifier for genomic and metagenomic sequences. *Nucleic Acids Research*
- Op den Camp HJ, Islam T, Stott MB, Harhangi HR, Hynes A, Schouten S, Jetten MS, Birkeland NK, Pol A, Dunfield PF (2009) Environmental, genomic and taxonomic perspectives on methanotrophic Verrucomicrobia. *Environmental Microbiology Reports* **1**: 293-306
- Oswald K, Milucka J, Brand A, Hach P, Littmann S, Wehrli B, Kuypers MM, Schubert CJ (2016) Aerobic gammaproteobacterial methanotrophs mitigate methane emissions from oxic and anoxic lake waters. *Limnology and Oceanography* **61**
- Oswald K, Milucka J, Brand A, Littmann S, Wehrli B, Kuypers MMM, Schubert CJ (2015) Light-dependent aerobic methane oxidation reduces methane emissions from seasonally stratified lakes. *Plos One* **10**
- Palomo A, Jane Fowler S, Gulay A, Rasmussen S, Sicheritz-Ponten T, Smets BF (2016) Metagenomic analysis of rapid gravity sand filter microbial communities suggests novel physiology of *Nitrospira* spp. *The ISME journal*
- Parks DH, Imelfort M, Skennerton CT, Hugenholtz P, Tyson GW (2015) CheckM: assessing the quality of microbial genomes recovered from isolates, single cells, and metagenomes. *Genome research* **25**: 1043-1055
- Pinto AJ, Marcus DN, Ijaz UZ, Bautista-de Iose Santos QM, Dick GJ, Raskin L (2016) Metagenomic evidence for the presence of comammox *Nitrospira*-like bacteria in a drinking water system. *mSphere* **1**: e00054-00015
- Pol A, Barends TR, Dietl A, Khadem AF, Eygensteyn J, Jetten MS, Op den Camp HJ (2014) Rare earth metals are essential for methanotrophic life in volcanic mudpots. *Environmental microbiology* **16**: 255-264
- Richter M, Rosselló-Móra R (2009) Shifting the genomic gold standard for the prokaryotic species definition. *Proceedings of the National Academy of Sciences* **106**: 19126-19131
- Stoecker K, Bendinger B, Schoning B, Nielsen PH, Nielsen JL, Baranyi C, Toenshoff ER, Daims H, Wagner M (2006) Cohn's *Crenothrix* is a filamentous methane oxidizer with an unusual methane monooxygenase. *Proceedings of the National Academy of Sciences of the United States of America* **103**: 2363-2367
- van Kessel MA, Speth DR, Albertsen M, Nielsen PH, den Camp HJO, Kartal B, Jetten MS, Lücker S (2015) Complete nitrification by a single microorganism. *Nature* **528**: 555-559
- Varghese NJ, Mukherjee S, Ivanova N, Konstantinidis KT, Mavrommatis K, Kyrpides NC, Pati A (2015) Microbial species delineation using whole genome sequences. *Nucleic Acids Research*

Wilson SM, Gleisten MP, Donohue TJ (2008) Identification of proteins involved in formaldehyde metabolism by *Rhodobacter sphaeroides*. *Microbiology* **154**: 296-305

Chapter 3

Bloom of a denitrifying methanotroph, “*Candidatus Methylomirabilis limnetica*”, in a deep stratified lake

Jon S. Graf^{1,§}, Hannah K. Marchant¹, Daniela Tienken¹, Philipp F. Hach¹, Andreas Brand², Carsten J. Schubert², Marcel M. M. Kuypers¹, Jana Milucka¹

¹Max-Planck-Institute for Marine Microbiology, Bremen, Germany; ²Eawag, Swiss Federal Institute of Aquatic Science and Technology, Kastanienbaum, Switzerland

[§] Corresponding author: Jon Graf (jgraf@mpi-bremen.de)

In preparation for *Environmental Microbiology*

Author contributions

J.S.G, J.M., H.K.M. and M.M.M. K. designed research, J.S.G., J.M., H.K.M., P.F.H., D.T. and A.B. performed field measurements and sampling, J.S.G. reconstructed the genome and performed metagenomic and metatranscriptomic data analyses, D.T. performed CARD-FISH, M.M.M.K. and C.J.S. contributed material and analysis tools, J.S.G. and J.M. wrote the manuscript with contributions from all co-authors.

Summary

Methanotrophic bacteria represent an important biological filter regulating methane emissions into the atmosphere. Planktonic methanotrophic communities in freshwater lakes are typically dominated by aerobic gamma-proteobacteria, with some contribution from alpha-proteobacterial methanotrophs, and the NC10 bacteria. These uncultured methanotrophs, related to "*Candidatus Methyloirabilis oxyfera*", oxidize methane using a unique pathway of denitrification, which produces N_2 and O_2 from nitric oxide (NO). Here we describe a new species, "*Ca. Methyloirabilis limnetica*", which dominated the planktonic methanotrophic community in the anoxic depths of the stratified Lake Zug, comprising 27 % of the total bacterial population. Gene transcripts assigned to "*Ca. M. limnetica*" constituted approximately one third of all metatranscriptomic sequences retrieved *in situ*. The reconstructed genome encoded a complete pathway for methane oxidation, and an incomplete denitrification pathway, including two non-canonical NO reductases that presumably function as O_2 -producing NO dismutases. In contrast to "*Ca. M. oxyfera*", the genome of "*Ca. M. limnetica*" appeared to lack some key metabolic genes, such as membrane-bound nitrate reductase, hydroxylamine oxidoreductase, the cytochrome *bc*₁-complex and two heme-copper oxidases. We speculate that "*Ca. M. limnetica*" temporarily bloomed in the lake during non-steady-state conditions suggesting a niche for NC10 in the lacustrine methane and nitrogen cycle.

Introduction

Temperate lakes are environments with intense methane cycling. Methane, a potent greenhouse gas, is abundantly produced in lake sediments from buried organic matter. Due to the comparably low sulfate concentrations, sulfate-dependent anaerobic methane oxidation often fails to completely consume the upward methane flux, in contrast to marine sediments. Therefore, large amounts of methane tend to enter the bottom waters of lakes. Lakes with oxic water columns, in which aerobic methane oxidation is constrained to a thin layer at the sediment surface, significantly contribute to atmospheric methane emissions (Bastviken et al, 2004). In contrast, in lakes that develop hypoxic and anoxic bottom waters, methane is often completely consumed at the lake oxycline by aerobic methane oxidation.

Aerobic methane-oxidizing bacteria have long been recognized to play an important role in the regulation of methane emissions to the atmosphere (Reeburgh, 2003). Major taxa of gamma-MOB in lakes and other aquatic habitats include *Methylomonas*, *Methylobacter*, *Methylosoma* and *Methylosarcina* (Bowman, 2014). It has emerged recently that some of these organisms also possess the capacity to thrive in apparently anoxic waters and sediments, where their activity and growth can be sustained by oxygen production and transport (Blees et al, 2014; Milucka et al, 2015; Oswald et al, 2016a), fermentation (Kalyuzhnaya et al, 2013) or denitrification (Kits et al, 2015a; Kits et al, 2015b; Oswald et al, 2017; Padilla et al, 2017). Interestingly, dedicated anaerobic methane oxidizers belonging or related to the ANME archaea (Ettwig et al, 2016; Haroon et al, 2013; Knittel & Boetius, 2009) seem to be constrained to lake sediments (Schubert et al, 2011; Weber et al, 2017) and play a comparably minor role in methane removal even in fully anoxic water columns.

A group of methanotrophs, whose role in the environmental methane cycle is yet to be fully assessed, are the bacteria of the NC10 phylum (Raghoebarsing et al, 2006). These organisms oxidize methane using nitrite as an electron acceptor. The first described representative of this clade, "*Candidatus Methylomirabilis oxyfera*" has been proposed to have a unique capacity to disproportionate nitrogen oxide(s) intracellularly and produce molecular oxygen, which is used for methane oxidation (Ettwig et al, 2010b; Ettwig et al, 2012). This unique pathway allows NC10 to thrive in hypoxic habitats, despite the obligate need for oxygen to activate and oxidize methane (He et al,

2016; López-Archilla et al, 2007; Padilla et al, 2016; Raghoebarsing et al, 2006; Shen et al, 2016; Zhu et al, 2012). Recent studies have demonstrated that NC10-related methanotrophs are present in the anoxic water column of a freshwater reservoir and sediments of deep freshwater lakes (i.e. Lake Constance (Deutzmann & Schink, 2011; Deutzmann et al, 2014) and Lake Biwa (Kojima et al, 2012)), and they were proposed to significantly contribute to methane removal in these lakes. However, direct activity of NC10 *in situ* has not been demonstrated to date. Despite the increasing number of environmental reports, "*Ca. M. oxyfera*" rarely appears to dominate bacterial, or specifically methanotrophic, communities, particularly in planktonic habitats.

So far, bacteria of the NC10 phylum have not been found in Lake Zug (Oswald et al, 2016a) or the other well-studied temperate lakes of Switzerland. Here, we report an incidental finding of a "*Ca. M. oxyfera*"-related bacterium that dominated the bacterial community in the deep anoxic methane-rich hypolimnion. We report a morphological and genomic description of this new putative species "*Candidatus Methylomirabilis limnetica*", infer its *in situ* activity from metatranscriptomics, and describe the biogeochemical conditions during the sampling period that presumably led to the bloom of this bacterium.

Results and Discussion

Biogeochemistry of Lake Zug

Lake Zug is a deep eutrophic freshwater lake located in Central Switzerland. The lake is permanently stratified and has reportedly not turned over since 1950 (Müller, 1993). During the sampling campaign in September 2016, several interesting features in the chemical profiles were noted (Figure 1a,b).

The oxycline was located at about 106 m depth, well above the usual depth (140 - 150 m) that was measured in 2012, 2013 and 2014 (Oswald et al, 2016b). No oxygen was detected with the trace optode (TOS7, Presens, Regensburg, Germany; detection limit approximately 20 nmol l⁻¹) below this depth on two consecutive sampling days. Methane concentrations at the given depths were ca. 2-fold higher than the years before and methane was depleted ca. 10 m below and not at the oxycline. During the current sampling campaign in 2016, the flux of oxygen and methane across their respective zones of consumption was 7.8 and 2.2 mmol m⁻² d⁻¹, respectively, and thus

lower than the years before. Concentration profiles of NO_x (nitrate + nitrite) was concave, decreasing from ca. $22 \mu\text{mol l}^{-1}$ at the oxycline to a minimum of ca. $6 \mu\text{mol l}^{-1}$ at 150 m depth and then increased again to a maximum of ca. $45 \mu\text{mol l}^{-1}$ at 180 m depth, as opposed to decreasing towards the sediment (Oswald et al, 2016b). Ammonium concentrations in the bottom waters were ca. 3-fold higher than in previous years and ammonium was consumed at ca. 115 m, the same depth where methane disappeared. The flux of ammonium into this zone was $1.8 \text{ mmol m}^{-2} \text{ d}^{-1}$. Both methane and ammonium indicated an additional zone of consumption between 150 and 160 m. The flux of CH_4 and NH_4 in the deeper depths was 2.6 and $4.9 \text{ mmol m}^{-2} \text{ d}^{-1}$, respectively.

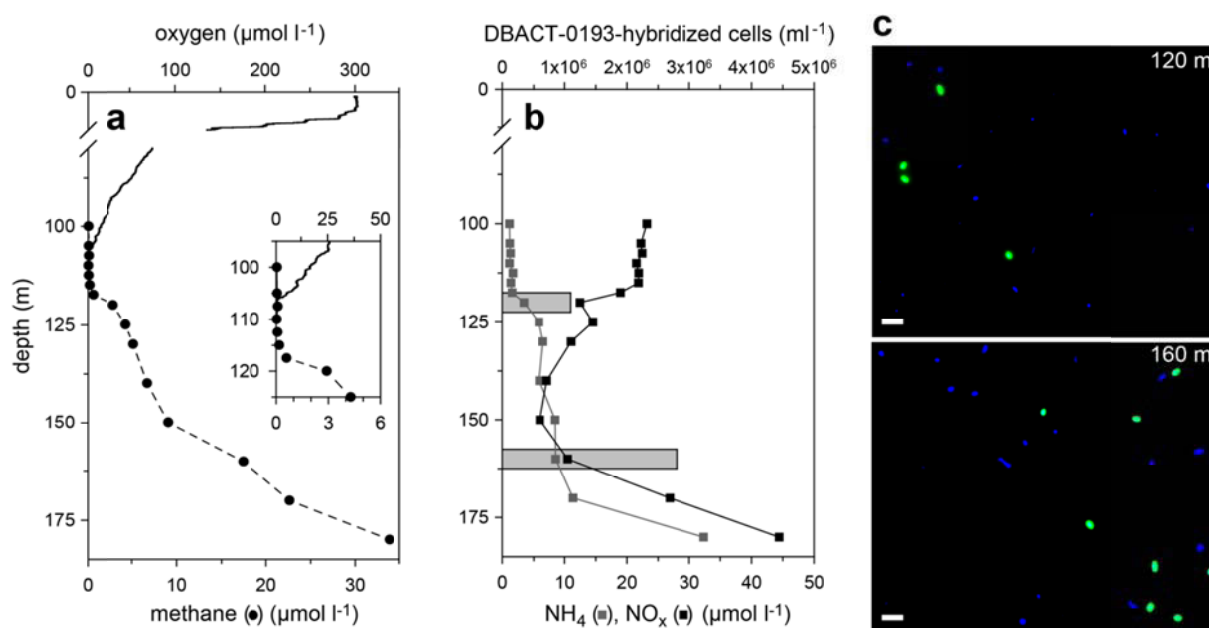


Figure 1. Physico-chemical parameters and abundance of NC10 bacteria in Lake Zug in September 2016. (a) Depth concentration profiles of oxygen and methane throughout the water column (100–180 m). The inset shows oxygen and methane concentration profiles near the oxycline. (b) Concentration profiles of NO_x (nitrate+nitrite) and ammonium. The grey bars at 120 m and 160 m show absolute cell counts of NC10 bacteria identified by CARD-FISH (probe DBACT-0193). (c) Fluorescent image of water from 120 m and 160 m showing NC10 bacteria (in green; counterstained with DAPI in blue) after CARD-FISH using a specific oligonucleotide probe DBACT-0193 (Supplementary Table S1; (Raghoebarsing et al, 2006)). Scale bar represents 2.5 μm .

In the Lake Zug region, temperatures in late summer of 2016 were well above average, it is thus possible that higher rates of primary productivity resulted in an upward shift of the oxycline and presumably higher deposition rates of organic matter into the hypolimnion. This might have resulted in increased fluxes of methane and ammonium out of the sediment. The most parsimonious explanation for the obviously non-steady state NO_x profile is that vertical mixing or hyperpycnal flow resulted in a one-off event of oxygen intrusion into the bottom waters which in turn led to the

oxidation of ammonium and production of nitrogen oxides. This event most likely occurred before our sampling campaign.

NC10 bacteria were abundant in the profundal anoxic waters of Lake Zug

In the previous years, a large portion of upwards-diffusing methane was shown to be oxidized near the oxycline by abundant gamma-proteobacterial methane-oxidizing bacteria (Oswald et al, 2016a). Additionally, it was shown that filamentous gamma-proteobacterial *Crenothrix* bacteria were major methane consumers in Lake Zug (Oswald et al, 2017).

To obtain a quantitative overview of the methane-oxidizing community in Lake Zug in 2016, we first classified and quantified 16S rRNA gene sequences in the unassembled metagenomic sequences from all three depths; near the oxycline (110 m), below it (120 m) and in middle of the anoxic hypolimnion (160 m; Figure 1a). For all three depths, a metagenome (Illumina HiSeq2500 2×250 bp; Supplementary Table S2) and a metatranscriptome (Illumina HiSeq3000 1×150 bp; Supplementary Table S2) was generated.

Methylococcales were stable members of the microbial community at all three investigated depths. Up to 10% of all 16S rRNA gene sequences were classified as *Methylococcales*; the majority of these belonged to genera *Methylobacter*, *Crenothrix*, *Methylomicrobium* and the CAB2E06 clade. Sequences classified as verrucomicrobial methanotrophs (mainly “*Ca. Methylacidiphilum* sp.”) were also detected, albeit at low abundance (0.1–0.3%). However, this assignment might require verification as these verrucomicrobial methanotrophs are known to thrive under conditions not found in Lake Zug (i.e. pH 1-5 and temperature above 50°C; (Op den Camp et al, 2009)). Known alphaproteobacterial methanotrophs (e.g. *Methylocystaceae* and *Beijerinckiaceae*) were not detected. This is consistent with the methanotrophic community analyzed in this lake previously by CARD-FISH (Oswald et al, 2017; Oswald et al, 2016a).

Interestingly, we found conspicuously high abundances of 16S rRNA gene sequences putatively assigned to the NC10 phylum in the metagenomic sequences from 120 m and 160 m depth. In these metagenomes, NC10-related sequences constituted approximately 10% and 19% of all classified metagenomic 16S rRNA gene sequences, respectively, and thus were two-fold more abundant than the ‘classical’

gamma-proteobacterial methanotrophs. At 110 m depth, which was nearest to the oxycline, only 0.7% of all classified 16S rRNA gene sequences were assigned to NC10.

The high abundance of NC10 bacteria was confirmed by catalyzed reporter deposition fluorescence *in situ* hybridization (CARD-FISH; Fig 1c). Water samples obtained from 120 m and 160 m were stained with an oligonucleotide CARD-FISH probe specific for NC10 bacteria (DBACT-0193; Figure 1c) and contained 1.1 and 2.8×10^6 cells ml^{-1} , accounting for 10.0% (120 m) and 26.8% (160 m) of all DAPI-stained cells. This probe has 1 nucleotide mismatch to the 16S rRNA gene sequence belonging to NC10 retrieved from Lake Zug (Supplementary Table S1). A similarly high proportion of cells was hybridized with the DBACT-1027 probe (0 mismatches), whereas no hybridized cells were found with the DBACT-447 probe (5 mismatches; data not shown).

These results showed that in September 2016 planktonic NC10 bacteria were the dominant methanotrophic microorganisms in the profundal, anoxic waters of Lake Zug. To our knowledge, this is the highest relative abundance of NC10 that has been so far reported from any environment. The highest previous report was from the Feitsui reservoir where up to 16 % of all cells were identified as NC10 using CARD-FISH (DBACT-1027 probe; (Kojima et al, 2014)). Interestingly, apart from being eutrophic, Lake Zug and Feitsui reservoir share few similarities. Whereas Lake Zug is a deep and permanently stratified temperate lake, Feitsui reservoir is a comparably shallow (mean depth of 40 m) and monomictic subtropical reservoir. It is thus not immediately obvious which habitat might favor the growth of NC10 to such high abundances. It is possible that during the non-steady-state conditions during the sampling campaign in September 2016 a unique combination of factors contributed to the observed bloom of NC10 bacteria, possibly including microoxic conditions and/or high organic matter content.

Genome reconstruction and phylogenetic assignment of “*Ca. M. limnetica*”

The high abundance of NC10 bacteria in the sample enabled us to assemble a putative NC10 genomic bin. The binning process was based on guanine-cytosine content as well as average contig coverage of the 160 m metagenome and a putative NC10 genomic bin was obtained from a co-assembly of all three depths. The contigs within this bin had the highest average coverage in the metagenomes from 120 m and 160 m (average contig coverage 451-fold and 851-fold) but only comparatively low coverage (30-fold) in the 110 m metagenome. The average contig coverage of the

metagenomic bin matched well with the abundance of NC10 bacteria previously estimated in our 16S rRNA read survey and CARD-FISH analysis. Summary statistics of the genomic bin (after targeted re-assembly) and comparison to the closed genome of “*Ca. M. oxyfera*” is shown in Table 1. Analysis by CheckM (Parks et al, 2015) suggested that the genomic bin was of high quality with similar estimates of completeness (96.2%) and contamination (1.7%) as the closed genome of “*Ca. M. oxyfera*” (accession FP565575.1, Table 1).

Table 1. Overview of genome statistics for “*Ca. M. limnetica*” and comparison to “*Ca. M. oxyfera*”. The complete genome of “*Ca. M. oxyfera*” was retrieved from GenBank (accession number FP565575.1). Coding sequences, rRNAs and tRNAs were predicted using Prodigal (Hyatt et al, 2010), Aragorn (Laslett & Canback, 2004) and RNAmmer (Lagesen et al, 2007) implemented in the Prokka annotation pipeline (Seemann, 2014b). Genome quality metrics were computed using CheckM (Parks et al, 2015) running the lineage specific workflow.

	“ <i>Ca. M. limnetica</i> ”	“ <i>Ca. M. oxyfera</i> ”
Contigs	40	1
Genome size (bases)	2,554,766	2,752,854
GC content (%)	58.4	58.6
Coding sequences	2530	2707
rRNAs / tRNAs	16S-23S-5S / 52	16S-23S-5S / 48
Completeness / Contamination /	96.2 / 1.7 / 0.0	96.3 / 2.6 / 0.0
Strain heterogeneity (%)	(marker sets: 117)	(marker sets: 117)

Next we used the assembled full-length 16S rRNA gene sequence (1549 bp) retrieved from the NC10 genomic bin for taxonomic classification. Comparative analysis of the 16S rRNA gene sequence showed 95.1% identity to “*Ca. M. sinica*” (He et al, 2016) and 96.3% identity to “*Ca. M. oxyfera*” (Ettwig et al, 2010a; Raghoebarsing et al, 2006). These values are higher than the threshold for genus definition (95%) but are below the species cutoff value (98.6%; (Konstantinidis et al, 2017; Yarza et al, 2014)). A whole genome analysis further showed that the pairwise average nucleotide identity (ANI) between our retrieved NC10 genome and the genome of “*Ca. M. oxyfera*” was 81.8%. This is well below the accepted ANI species boundary (95–96%; (Goris et al, 2007; Richter & Rosselló-Móra, 2009)). Taken together these data suggest that the NC10 population present in Lake Zug likely represented a new species within the genus “*Ca. Methylomirabilis*”, which we here name “*Ca. Methylomirabilis limnetica*”.

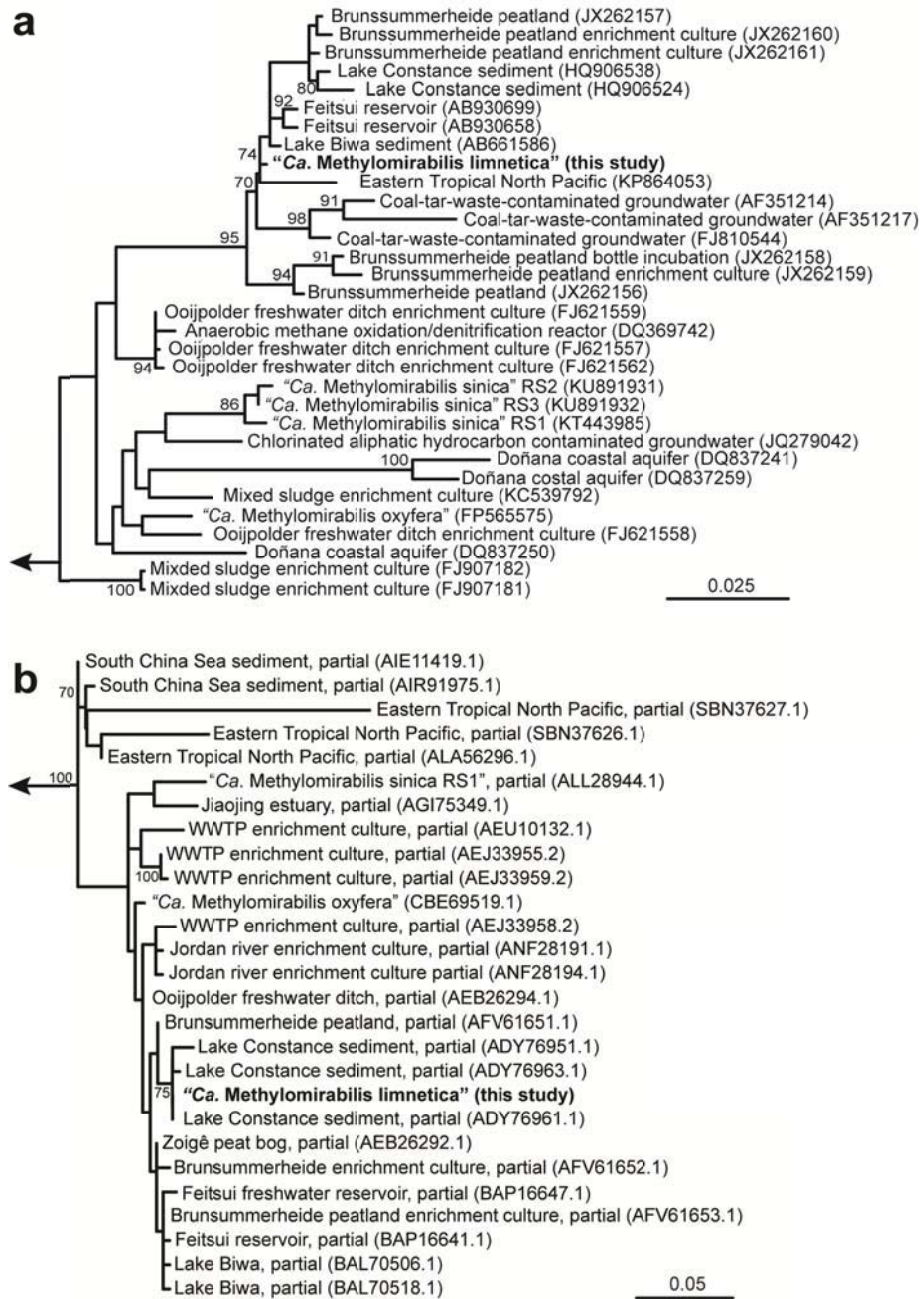


Figure 2. Phylogenetic trees of "*Ca. M. limnetica*" full-length 16S rRNA gene (a) and PmoA amino-acid sequence (b). (a) Maximum likelihood phylogenetic tree of 16S rRNA gene sequence without constraining the alignment by a weighting mask or filter. Bootstrap values > 70% (out of 1000 resamplings) are shown in front of respective nodes. Three sequences of *Nitrospiraceae* were chosen as outgroup [*Leptospirillum ferriphilum* (AF356829), *Leptospirillum ferrooxidans* (X86776), *Nitrospira moscoviensis* (X82558)]. Scale bar indicates substitutions per site. (b) Maximum likelihood phylogenetic tree of PmoA amino-acid sequence of "*Ca. M. limnetica*". Bootstrap support (> 70%) of total 500 resamplings are shown. Four PmoA/AmoA amino-acid sequences belonging to *Proteobacteria* and *Verrucomicrobia* served as outgroup (accession numbers BAE86885.1, AAG60667.1, CCJ08278.1, CCG92750.1). Scale bar indicates substitutions per site.

Phylogenetic analysis of the 16S rRNA gene sequences showed that the sequence “*Ca. M. limnetica*” clustered within a subgroup of NC10 (Figure 2a). The sequences within this subgroup were nearly identical (>99% sequence identity) and likely represented the same species. Interestingly, the sequences were retrieved from geographically distant freshwater lakes (Lake Constance (Germany) and Lake Biwa (Japan), a freshwater reservoir (Feitsui, Taiwan) (Deutzmann & Schink, 2011; Kojima et al, 2014; Kojima et al, 2012) and a minerotrophic peatland (Brunssummerheide, The Netherlands (Zhu et al, 2012)). Both currently described species of the genus “*Ca. Methylophilus*”, “*Ca. M. oxyfera*” and “*Ca. M. sinica*”, clustered in a different, more divergent branch of the 16S rRNA gene tree (Figure 2a).

Phylogenetic analysis of the “*Ca. M. limnetica*” PmoA (Figure 2b) showed that the sequence clustered together with partial PmoA sequences assigned to NC10 which were retrieved from Lake Constance (Deutzmann & Schink, 2011). The Lake Constance sequences were almost identical to the PmoA sequence of “*Ca. M. limnetica*” (98.2–99.3%; 61–69% coverage). Partial PmoA sequences retrieved from Brunssummerheide (Zhu et al, 2012), Lake Biwa (Kojima et al, 2012) and Feitsui reservoir (Kojima et al, 2014) formed a separate but closely related sister clade (approximately 96–97% identity). A third, more distantly related polyphyletic cluster mainly constituted PmoA sequences retrieved from a waste water treatment plant (Lieshout) (Luesken et al, 2011), a river sediment (Bhattacharjee et al, 2016) as well as “*Ca. M. oxyfera*” and “*Ca. M. sinica*”. The sequences in this cluster were more distantly related to “*Ca. M. limnetica*” PmoA sequence (91–96% identity).

Genome-inferred central C1 and energy metabolism

The high-quality genome of “*Ca. M. limnetica*” allowed for a reconstruction of pathways involved in carbon and energy metabolism (Figure 3). “*Ca. M. limnetica*” encoded the pathway for complete aerobic oxidation of methane (Table 3), including particulate methane monooxygenase (pMMO; *pmoCAB*) and one Xox-type methanol dehydrogenase (MDH; *xoxFJG*). Genes encoding for soluble methane monooxygenase (sMMO) and MxaF-type methanol dehydrogenase, which was found in “*Ca. M. oxyfera*” previously (Ettwig et al., 2010?), were not encoded in “*Ca. M. limnetica*” genome. Downstream conversion of formaldehyde to formate could either proceed via tetrahydromethanopterin (H₄MPT)-dependent or tetrahydrofolate (H₄F)-dependent C₁

transfer pathway. Formate dehydrogenase (*fdhA*), catalyzing the oxidation of formate to CO_2 , was likewise encoded in the genome of “*Ca. M. limnetica*”.

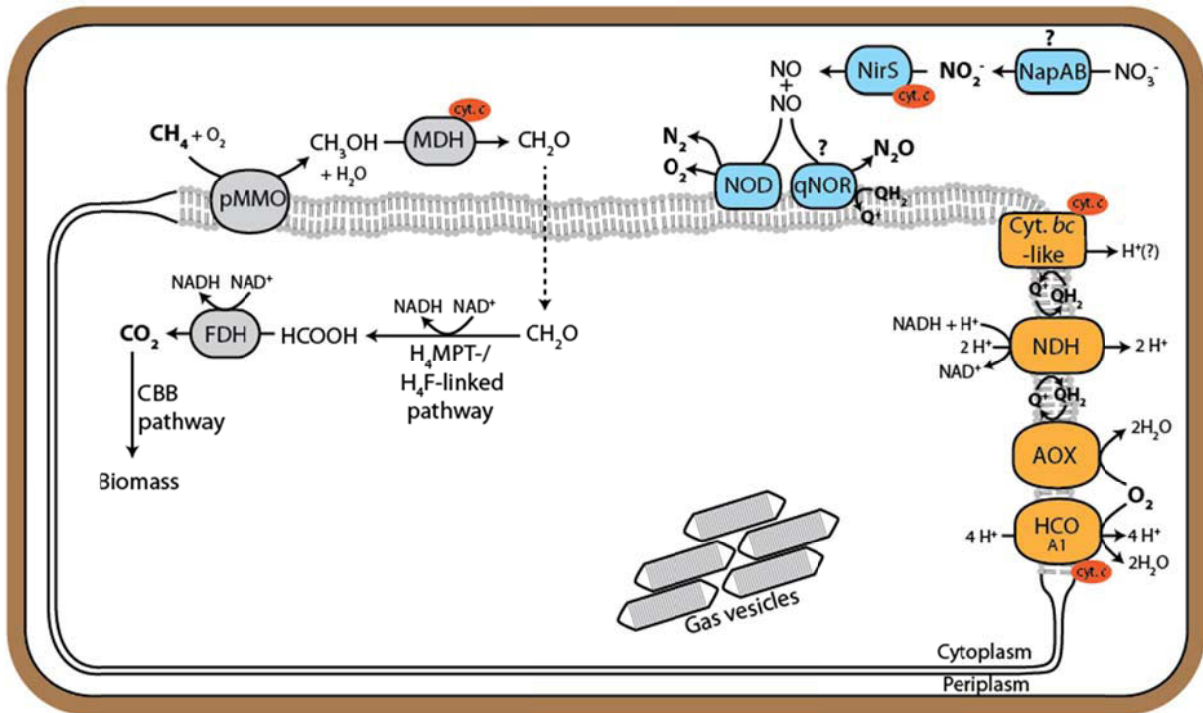


Figure 3. Genome-inferred metabolic potential of “*Ca. M. limnetica*”. Predicted metabolic potential of “*Ca. M. limnetica*” with respect to carbon, nitrogen and respiratory pathways are shown. Indicated are the pathways for methane oxidation (grey), denitrification (blue) and (aerobic) respiratory chain (orange). Abbreviations: pMMO, particulate methane monooxygenase; MDH, methanol dehydrogenase; FDH, formate dehydrogenase; CBB, Calvin-Benson-Bassham cycle; NapAB, periplasmic nitrate reductase; NirS, cytochrome *cd*, nitrite reductase; qNOR, quinol-dependent nitric oxide reductase; NOD, NO dismutase; *cyt. bc*-like, cytochrome *bc*-like complex; NDH, NADH dehydrogenase; AOX, alternative oxidase; HCO, heme-copper oxidase.

“*Ca. M. limnetica*” appears to derive its biomass carbon solely from carbon dioxide and not from methane, which has also been reported for “*Ca. M. oxyfera*” (Rasigraf et al, 2014). The genome encoded a complete Calvin-Benson-Bassham (CBB) cycle for autotrophic carbon fixation including ribulose-1,5-bisphosphate carboxylase/oxygenase (RubisCO; *cbbLS*) and phosphoribulokinase (*prk*), which are exclusive to the CBB cycle (Hügler & Sievert, 2010). Both the serine and ribulose monophosphate (RuMP) pathways of “*Ca. M. limnetica*”, which allow for methane-derived carbon assimilation, were incomplete. The RuMP pathway was missing both key genes hexulosephosphate synthase (*hps*) and hexulosephosphate isomerase (*hpi*). The serine pathway was missing hydroxypyruvate reductase (*hpr*), glycerate 2-kinase (*gck*), malate thiokinase (*mtk*) and malyl-coenzyme A lyase (*mcl*).

Respiratory complexes of “*Ca. M. limnetica*”

It has been proposed that NC10 bacteria, specifically “*Ca. M. oxyfera*”, produce O₂ from nitrogen oxides by a unique intra-aerobic denitrification pathway involving a nitrite reductase and a putative NO dismutase (Ettwig et al, 2010a; Ettwig et al, 2012; Wu et al, 2011b). The genome of “*Ca. M. limnetica*” also encoded for a partial denitrification pathway (Figure 3; Table 2a) including periplasmic nitrate reductase (*napAB*), cd₁-type nitrite reductase (*nirS*) and three genes encoding for quinone-interacting nitric oxide reductase (qNOR; *norB*). Membrane-bound nitrate reductase (*narGHI*) and nitrous oxide reductase (*nosZ*) were not found in the “*Ca. M. limnetica*” genome. The amino-acid sequences of two nitric oxide reductases of “*Ca. M. limnetica*” (encoded by tandem genes MEZU 00035-26) featured nearly all modified residues of the quinol-binding and catalytic site that have been identified in two divergent qNORs of “*Ca. M. oxyfera*” and marine NC10 bacteria (Figure 4, (Ettwig et al, 2012; Padilla et al, 2016)). These qNOR enzymes have been speculated to function as NO dismutase (NOD) that disproportionates two molecules of NO into N₂ and O₂ thus allowing NC10 bacteria to oxidize methane using pMMO in the absence of exogenous O₂ (Ettwig et al, 2010a; Ettwig et al, 2012). Like “*Ca. M. oxyfera*”, “*Ca. M. limnetica*” also encoded for a third, most likely genuine NO-reducing qNOR that contained the same conserved residues of canonical qNORs of “*Ca. M. oxyfera*” and other microorganisms (Figure 4).

In addition to nitrogen oxides, “*Ca. M. limnetica*” also has the genomic potential to use O₂ as terminal electron acceptor. We identified genes encoding for two types of terminal oxidases (Table 2b); a heme copper oxidase (A1-type HCO; (Pereira et al, 2001)) and an alternative oxidase (AOX) that belongs to the di-iron carboxylate group of proteins (Berthold & Stenmark, 2003). Although NC10 bacteria grow anaerobically, it has been speculated that O₂ from NO dismutation could be respired by these terminal oxidases (Wu et al, 2011a). The genome of “*Ca. M. oxyfera*” also encoded for two additional heme-copper terminal oxidases (*bo*- and *ba*₃-type; labeled HCO 2 and 3 (Wu et al, 2011a)) which were however not found in the genome of “*Ca. M. limnetica*”. Alignment of Lake Zug metagenomic reads (160 m) to the genome of “*Ca. M. oxyfera*” further confirmed that these HCOs were encoded in genomic regions not present in our metagenomic dataset (Supplementary Figure 2).

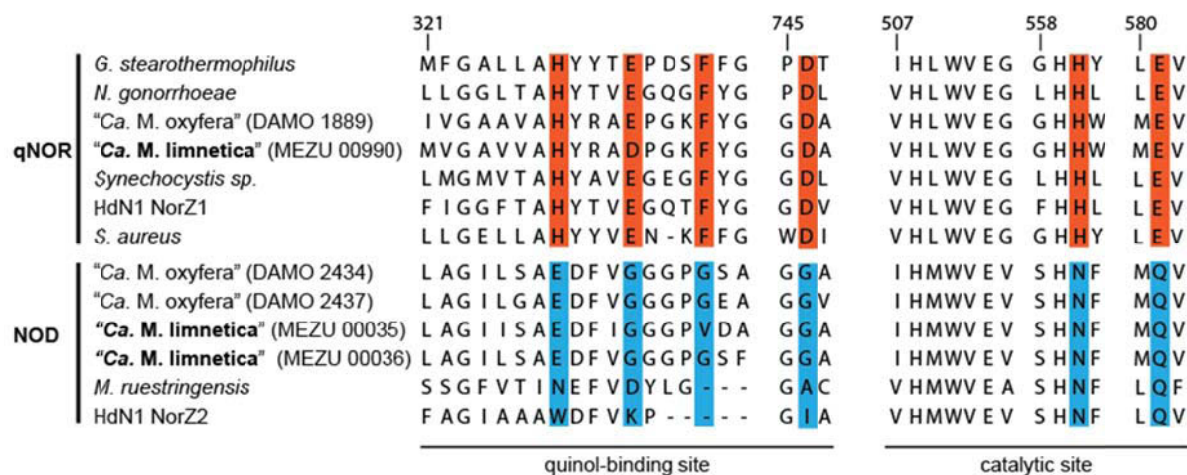


Figure 4. Multiple alignment of nitric oxide reductase (qNOR) and putative nitric oxide dismutase (NOD). Quinol-binding site and catalytic site are shown for qNOR (red) and NOD (blue) following the previous alignment by (Ettwig et al, 2012); the numbering is according to the residue number of *G. stearothermophilus*. Accession numbers: *Geobacillus stearothermophilus* 3AYF_A, *Neisseria gonorrhoeae* ZP_04723508.1, *Synechocystis* sp. PCC 6803 BAA18795.1, gamma proteobacterium HdN1 NorZ1 (CBL45628.1) NorZ2 (YP_003809511.1), *Staphylococcus aureus* EGL94648.1, *Muricauda ruestringensis* G2PJH6.

Intriguingly, the cytochrome bc_1 complex, a key component of the respiratory electron transfer present in "*Ca. M. oxyfera*" (Ettwig et al, 2010b; Wu et al, 2011a), was not found in the genome of "*Ca. M. limnetica*". Instead we identified genes encoding for two cytochrome bc -like complexes, homologs of which were also encoded in the genome of "*Ca. M. oxyfera*" (Table 2). Both cytochrome bc -like complexes featured tandem genes encoding for a cytochrome b and a Rieske iron-sulfur protein in addition to multi-heme cytochromes c (Supplementary Figure 3). The cytochromes b were either encoded as single, long gene (MEZU_00164) or as two separate, shorter genes (MEZU_00213-14) that appeared to constitute two different, evolutionary-related subfamilies of cytochromes b (Dibrova et al, 2013; Dibrova et al, 2017). Since "*Ca. M. limnetica*" did not encode for a canonical cytochrome bc_1 complex, we suggest that either one or both cytochrome bc -like complexes, which were well transcribed (Table 2), act as a quinol:cytochrome c oxidoreductase.

In addition to the cytochrome bc_1 complex several other key metabolic genes encoding for nitrogen metabolism and the respiratory chain of "*Ca. M. oxyfera*" appeared to be absent from the genome of "*Ca. M. limnetica*" (Table 4). These were genes encoding for membrane-bound nitrate reductase (Nar), two heme copper oxidases (previously assigned HCO2 and HCO3 (Wu et al, 2011a)), MxaF-type as well as one additional XoxF-type methanol dehydrogenase, and hydroxylamine

oxidoreductase (Hao). The absence of *hao* genes from the “*Ca. M. limnetica*” genome is intriguing as Hao has been suggested to play a role in the detoxification of hydroxylamine in methanotrophs (Campbell et al, 2011; Nyerges & Stein, 2009). Hydroxylamine is formed via the co-metabolism of ammonium by methane monooxygenase – a process that is likely also relevant in Lake Zug as methane and ammonium were present in almost equimolar concentrations *in situ* (Figure 1a,1b). Other genes encoding for enzymes known to be involved in hydroxylamine detoxification, such as cytochrome P460 (*cytL*) (Bergmann et al, 1998), were also absent from the “*Ca. M. limnetica*” genome thus raising the question of how “*Ca. M. limnetica*” disposes of this toxic intermediate. To confirm that these genes were indeed absent from the genome of “*Ca. M. limnetica*” we searched the whole metagenomic assembly for genes encoding the aforementioned enzymes but could not identify highly covered contigs encoding for close homologs. Additionally, by mapping the sequences of the 160 m metagenome to the genome of “*Ca. M. oxyfera*” we saw that whereas genomic regions with gene homologs shared between both species were well covered (per-base coverage > 100), the average coverage was close to zero for all genomic regions containing aforementioned genes exclusive to “*Ca. M. oxyfera*” (Supplementary Figure 2).

***In situ* gene expression of “*Ca. M. limnetica*”**

To investigate whether “*Ca. M. limnetica*” was transcriptionally active *in situ*, we aligned the metatranscriptomic reads obtained from 110 m, 120 m and 160 m depth to the “*Ca. M. limnetica*” genome. We found that nearly one third of all non-rRNA metatranscriptomic sequences from 120 m and 160 m (28.4% and 32%, respectively) aligned to the genome of “*Ca. M. limnetica*”. The overall alignment rate of the metatranscriptome from 110 m (2.8%) was much lower, in line with the much lower abundance of “*Ca. M. limnetica*” at this depth.

A comparison of the 100 most transcribed genes of “*Ca. M. limnetica*” showed a clear difference between metatranscriptomes originating from near the oxycline (110 m) and from below (120 m & 160 m). We found that 94 out of the top 100 transcribed genes were shared between the two deeper metatranscriptomes from 120 m and 160 m depth. This was not the case for the 110 m metatranscriptome where only about half of the top 100 transcribed genes were shared with the metatranscriptomes from 120 m

and 160 m. We found several genes encoding for toxin-antitoxin systems and proteases exclusively transcribed among the top 100 genes by "*Ca. M. limnetica*" at 110 m. Toxin-antitoxin systems appear to have an important role in bacterial stress physiology and growth control (Blower et al, 2011; Buts et al, 2005; Hayes & Low, 2009). Hence, the increased transcription of these genes might reflect a response of "*Ca. M. limnetica*" to hypoxic conditions close to the oxycline.

Transcription of functional genes involved in methane oxidation and denitrification was in accord with the proposed anaerobic, methanotrophic and denitrifying lifestyle of NC10 bacteria. Among the 100 most transcribed genes of "*Ca. M. limnetica*" shared in all three metatranscriptomes were the genes encoding for methane oxidation and denitrification (Table 3); in particular genes encoding for particulate methane monooxygenase, nitrite reductase and one gene copy of the putative NO dismutase (MEZU 0035; Table 2a). At 120 m and 160 m, transcription of the second gene copy (MEZU 0036) was three orders of magnitude lower (Table 2). Interestingly, at 110 m both putative NO reductase genes were highly transcribed (Table 2a). This observation is in line with the suggestion of Luesken et al (2012) who proposed that "*Ca. M. oxyfera*" might only transcribe both copies of NO reductase when exposed to oxygen. Transcription of the "canonical" qNOR was detected at all depths, implying that "*Ca. M. limnetica*" might also reduce NO to N₂O *in situ*. However, the transcription levels of the 'canonical' qNOR were significantly lower than those of the predominantly transcribed putative NOD (84 to 146-fold). "*Ca. M. limnetica*" also encoded a periplasmic nitrate reductase (NapAB) but its transcription was much lower than that of e.g. the nitrite reductase (NirS; Table 2). It thus remains unclear, whether *M. limnetica* can use nitrate as an electron acceptor *in situ*. "*Ca. M. oxyfera*", which also possesses NapAB, was incapable of using nitrate as electron acceptor (Ettwig et al, 2010a).

Table 2. *In situ* transcription of selected functional respiratory genes of “*Ca. M. limnetica*”.

Listed are functional genes encoding for dissimilatory nitrogen metabolism and respiratory complexes of “*Ca. M. limnetica*” and their respective transcription. Transcription was quantified as RPKM (reads per 1 kb gene length and per million mapped transcripts) in metatranscriptomes obtained from 110 m, 120 m and 160 m depth. Gene homologs of “*Ca. M. oxyfera*” have been identified using amino-acid sequences BLASTP; only the top hit (by *e*-value or % sequence identity) is shown (alignment coverage >94%; except NapA 83%).

Protein	Gene	Locus tag	Homolog in “ <i>Ca. M. oxyfera</i> ”	Transcription (RPKM)		
				110 m	120 m	160 m
Periplasmic nitrate reductase	napA	MEZU_02571	DAMO_2411	435	6,096	6,668
	napB	MEZU_02570	DAMO_2410	746	8,539	9,888
Nitrite reductase	nirS	MEZU_02574	DAMO_2415	7485	231,857	267,063
Nitric oxide reductase	norZ1	MEZU_00990	DAMO_1889	478	3,560	3,748
	norZ2	MEZU_00036	DAMO_2434	12,188	1,215	1,472
	norZ3	MEZU_00035	DAMO_2437	40,540	468,670	549,730
Cytochrome c oxidase, A1-type	coxIII	MEZU_00432	DAMO_1162	116	3,901	3,804
	coxIII	MEZU_00433	DAMO_1164	109	2,927	3,027
	coxI	MEZU_00434	DAMO_1165	113	1,912	2,135
	coxII	MEZU_00435	DAMO_1166	159	2,247	2,332
Alternative oxidase	aox	MEZU_01093	DAMO_2910	62	1,694	1,653
Cytochrome <i>bc</i> -like complex	qcrA	MEZU_00163	DAMO_0820	229	6,660	7,053
	qcrB	MEZU_00164	DAMO_0821	217	5,212	5,884
	-	MEZU_00165	DAMO_0822	191	4,840	5,400
Cytochrome <i>bc</i> -like complex	qcrA	MEZU_00213	DAMO_1672	431	4,460	4,270
	qcrB	MEZU_00214	DAMO_1671	402	4,461	4,949
	-	MEZU_00215	DAMO_1670	237	2,739	2,934
	-	MEZU_00216	DAMO_1669	311	4,786	5,246

Table 3. *In situ* transcription of functional genes of “*Ca. M. limnetica*” involved in methane oxidation. Listed are functional genes encoding for the complete methane oxidation pathway in “*Ca. M. limnetica*” and their respective transcription. Transcription was quantified as RPKM (reads per 1 kb gene length and per million mapped transcripts) in metatranscriptomes obtained from 110 m, 120 m and 160 m depth. Gene homologs of “*Ca. M. oxyfera*” were identified using amino-acid sequences BLASTP; only the top hit (by *e*-value or % sequence identity) is shown (alignment coverage >93%).

Protein	Gene	Locus tag	Homolog in “ <i>Ca. M. oxyfera</i> ”	Transcription (RPKM)		
				110 m	120 m	160 m
Particulate methane monooxygenase	pmoC	MEZU_00022	DAMO_2451	20,096	294,363	345,326
	pmoA	MEZU_00023	DAMO_2450	11,744	245,506	291,305
	pmoB	MEZU_00024	DAMO_2448	11,669	237,046	273,803
Methanol dehydrogenase	xoxG	MEZU_01075	DAMO_0138	736	17,397	17,994
	xoxJ	MEZU_01076	DAMO_0136	777	20,638	22,392
	xoxF	MEZU_01077	DAMO_0134	4,206	97,097	110,208
Formaldehyde activating enzyme	fae	MEZU_01323	DAMO_0454	4,534	123,653	122,288
Methylene H ₄ MPT dehydrogenase	mtd	MEZU_01324	DAMO_0455	1,298	39,926	43,705
Formyltransferase/hydrolase complex	fhcB	MEZU_01326	DAMO_0457	776	23,016	25,528
	fhcA	MEZU_01327	DAMO_0458	567	15,587	16,861
	fhcD	MEZU_01328	DAMO_0459	580	18,222	19,083
	fhcC	MEZU_01329	DAMO_0460	777	22,242	23,125
Bifunctional methylene H ₄ F dehydrogenase / methenyl H ₄ MPT cyclohydrolase	folD	MEZU_00798	DAMO_1852	322	5,799	5,560
Formyl H ₄ F deformylase	purU	MEZU_02250	DAMO_2586	69	855	1,076
Formate dehydrogenase	fdhA	MEZU_00184	DAMO_0853	130	2,869	3,429

Table 4. Overview of genes encoding for enzymes involved in nitrogen oxide and oxygen respiration of “*Ca. M. limnetica*” and “*Ca. M. oxyfera*”. The nomenclature of heme-copper oxidase 1-3 of “*Ca. M. oxyfera*” is listed according to (Wu et al, 2011a).

	Nar	Nap	NirS	qNor	Nos	Hao	HCO1 (<i>cox</i>)	HCO2 (<i>cyo</i>)	HCO3 (<i>cba</i>)	AOX	cytochrome <i>bc₁</i> complex
“ <i>Ca. M. limnetica</i> ”	-	+	+	+	-	-	+	-	-	+	(-)
“ <i>Ca. M. oxyfera</i> ”	+	+	+	+	-	+	+	+	+	+	+

Besides genes involved in methane oxidation and dissimilatory nitrogen metabolism, many genes encoding for proteins involved in transcription and translation (i.e. RNA polymerase, translation initiation factor) as well as numerous ribosomal proteins were among the highest transcribed genes at all depths. Furthermore, we identified a well transcribed gene cluster encoding for several gas vesicle-related

proteins including the main structural gas vesicle protein (GvpA) and associated proteins (GvpL/F, GvpN and GvpK). In fact, *gvpA* was among the highest transcribed genes at all depths (~500,000 RPKM at 120 and 160 m). The presence and expression of genes encoding for gas vesicles suggests that "*Ca. M. limnetica*" might be capable of adjusting or maintaining its position in the water column. Interestingly, "*Ca. M. oxyfera*", which was isolated from freshwater sediment, appears not to encode homologs of these Gvp-associated proteins.

The large proportion of highly transcribed genes in all three *in situ* transcriptomes suggests that at the time of sampling the "*Ca. M. limnetica*" population was still transcriptionally active, even though it is not clear whether this activity was accompanied by methane oxidation.

Experimental Procedures

Geochemical profiling and sample collection

Sampling was carried out in September 2016 at a single station located in the deep, southern lake basin of Lake Zug (~200 m water depth; 47°06'00.8" N, 8°29'35.0" E). A multi-parameter probe was used to measure conductivity, turbidity, depth (pressure), temperature and pH (XRX 620, RBR, Ottawa, ON, Canada). Dissolved oxygen was monitored online with normal and trace micro-optodes (types PSt1 and TOS7, Presens, Regensburg, Germany) with detection limits of 125 and 20 nM, respectively, and a response time of 7 s (Kirf et al, 2014). Water samples for measurements of methane and nitrous oxide concentrations were retrieved from distinct depths with a syringe sampler. Water from individual 50 ml syringes was filled through a gas-tight rubber tubing into serum bottles (120 ml), allowing water to overflow. Solid copper chloride (CuCl_2) was immediately added in excess to the water samples and the bottles were closed with a butyl rubber stopper (head-space free) and crimped. Before analysis, a 30ml headspace was set with N_2 and after overnight equilibration methane and nitrous oxide concentrations were measured in the headspace with a gas chromatograph (GC; Agilent 6890 N, Agilent Technologies, Santa Clara, CA, USA) equipped with a Carboxen 1010 column (30m \times 0.53 mm, Supelco, Bellefonte, PA, USA) and a flame ionization detector. Methane concentrations in the water phase were back-calculated according to (Wiesenburg & Guinasso Jr, 1979).

Concomitantly with dissolved gases, water samples for ammonium and NO_x measurements were collected from the same depths using the same syringe sampler. 40 ml of water was directly injected into a 50-ml Falcon tube containing 10 ml of OPA reagent for fluorometric ammonium quantification according to (Holmes et al, 1999). For NO_x quantification, 1.5 ml of water was added to an eppendorf cup prefilled with 15 μl HgCl_2 and combined nitrate and nitrite concentration was determined by commercial chemiluminescence NO_x analyzer after reduction to NO with acidic Vanadium (II) chloride (Braman & Hendrix, 1989). After reduction to NO, nitrite was determined with acidic potassium iodide and nitrate was then calculated as the difference between NO_x and nitrite.

From each depth, 3 ml of water were sampled into a 15 ml Falcon tube containing formaldehyde for subsequent FISH analyses.

Water for DNA/RNA analyses were collected with a Niskin bottle from 110m, 120m and 160m water depth. For each depth, 2 x 1 L water was immediately filtered onboard (0.2 µm GTTP filter; Merck Millipore, Darmstadt, Germany); filters for DNA extraction were air dried and filters for RNA extraction were immediately immersed in RNAlater preservation solution (Life Technologies, Carlsbad, CA, USA). DNA and RNA filters were stored at – 20°C until further processing.

Diffusive flux calculation

Diffusive fluxes (J) of O_2 , NH_4 and CH_4 across the hypolimnion–epilimnion interface were calculated assuming steady state by using the maximum concentration change (δC) over a specific depth range (δx ; that is, m) applying Fick's first law:

$$J = -D \frac{\delta C}{\delta x}$$

A turbulent diffusion coefficient (that is, Eddy diffusivity D) of $2.7 \times 10^{-5} \text{ m}^2 \text{ s}^{-1}$ was used. Diffusive fluxes were calculated over depth intervals where gradients of the respective solutes were highest. For O_2 , the depth interval was 60 and 106 m. For CH_4 and NH_4 , the depth interval was 120 and 117.5 m. CH_4 and NH_4 flux in deeper depths was calculated over a depth interval of 150 and 180 m and 170 and 180 m, respectively.

Catalyzed reporter deposition-fluorescence in situ hybridization (CARD-FISH)

Water samples (3 ml) were fixed with formaldehyde (final concentration 2% [w/v]) for 1.5 h at room temperature before being filtered onto polycarbonate GTTP filters (0.2 µm pore size, effective filter diameter = 20 mm; Merck Millipore, Darmstadt, Germany). Permeabilization with lysozyme, peroxidase inactivation, hybridization with specific oligonucleotide probes labeled with horseradish peroxidase (for details see Supplementary Table S1; Biomers, Ulm, Germany), tyramide reporter deposition (Oregon Green 488) and 4',6-diamidino-2-phenylindole (DAPI) counter staining was performed according to (Pernthaler et al, 2002). Filters were embedded in a mix of Citifluor/Vectashield (4:1) and mounted onto glass slides. Cell counting was performed with Nikon Eclipse Ci microscope (Axioskop 2, Zeiss, Germany) in randomly selected fields of view until ~1000 DAPI-stained cells were counted.

Nucleic acid extraction and metagenome and metatranscriptome sequencing

DNA was extracted from cut-up filters using Powersoil DNA isolation kit. For RNA extraction, filters were briefly rinsed with nuclease-free water and RNA was extracted from cut-up filters using PowerWater RNA isolation kit (including removal of genomic DNA by DNase I digestion). Both nucleic acid extraction kits (MoBio Laboratories, Carlsbad, CA, USA) were used according to manufacturer's instructions. DNA and RNA were quantified using the Qubit dsDNA HS or RNA HS Assay kits and the Qubit 2.0 Fluorometer (Invitrogen, Carlsbad, CA, USA).

For metagenomic sequencing, DNA was fragmented by sonication (500 nt) using a Covaris S2 sonicator (Covaris, Woburn, MA, USA) and library preparation was done according to manufacturer's instructions using NEBNext Ultra II DNA Library Prep Kit for Illumina (New England Biolabs, Ipswich, MA, USA). Paired-end sequencing (2×250 bp) was performed using the Illumina HiSeq2500 platform (Illumina Inc., San Diego, CA, USA) in rapid mode with SBS chemistry v2. For metatranscriptomic sequencing, total RNA was first concentrated using the RNA Clean & Concentrator kit (Zymo Research Corp., Irvine, CA, USA) according to manufacturer's instructions. Depletion of rRNAs was done with the Ribo-Zero rRNA Removal Kit (Bacteria) for Illumina (Epicentre, Madison, WI, USA) with a protocol adaptation for low input amounts. cDNA library preparation was done with the NEBNext Ultra Directional RNA Library Prep Kit for Illumina (New England Biolabs) according to protocol and sequencing (1×150 bp) was performed using the Illumina HiSeq3000 platform (Illumina Inc.) with SBS chemistry. Library preparation and sequencing was performed by the Max Planck-Genome-centre Cologne, Germany (<http://mpgc.mpipz.mpg.de/home/>). Detailed information for each metagenomic and metatranscriptomic dataset can be found in Supplementary Table S2.

Metagenomic assembly, binning and genome analysis

Paired-end Illumina reads were trimmed using Trimmomatic 0.32 (Bolger et al, 2014) and parameters MINLEN:20 ILLUMINACLIP: TruSeq3-PE.fa:2:30:10 LEADING:3 TRAILING:3 SLIDINGWINDOW:4:15 MINLEN:50. Trimmed Illumina reads from all three metagenomes were co-assembled using metaSPAdes assembler 3.9.1 (Nurk et al, 2016) and k-mer lengths of 21,33,55,77,99,127. Illumina reads of each metagenome were

mapped to the assembled contigs using BBmap 35.43 (Bushnell, 2016) with approximate minimum identity of 95% (minid=0.95) and default parameters. Open reading frames were predicted using Prodigal 2.60 (Hyatt et al, 2010) running in metagenomic mode (-p meta) and standard parameters. Translated amino-acid sequences were subsequently searched for using HMMER3 (<http://hmmer.org/>) against a set of 107 hidden markov models of essential single-copy genes (Dupont et al, 2012) using trusted cutoff values (-cut_tc) and default settings. Protein sequences coding for essential single copy genes were searched against NCBI non-redundant database (retrieved August 2015) using DIAMOND 0.8.34 blastp (Buchfink et al, 2015) and an *e*-value cutoff of 10^{-6} . The taxonomy (class level) of each essential single-copy gene was assigned using MEGAN5 and the mmgenome script 'hmm.majority.vote.pl' (<http://madsalbertsen.github.io/mmgenome/>). Binning of "*Ca. M. limnetica*" contigs from the co-assembly was based on differential contig coverage in metagenomes from 160 m and 120 m (Supplementary Figure 1) and was performed using the mmgenome R package (<http://madsalbertsen.github.io/mmgenome/>; (Karst et al, 2016)). Trimmed Illumina reads of the 160 m metagenome were mapped to the binned contigs using BBmap and stringent mapping settings (approximate minimum identity = 0.95). 10% of the mapped reads were selected at random and re-assembled using SPAdes 3.50 (Bankevich et al, 2012) with mismatch corrector enabled (-careful). The re-assembly was further refined by removing short and low-coverage contigs (length < 500, average coverage < 10-fold). The quality of the re-assembled genome was assessed using CheckM 1.05 (Parks et al, 2015) running the lineage-specific workflow and genome annotation was performed using Prokka 1.12 (Seemann, 2014a) in metagenomic mode (-metagenome) and the RAST online annotation server (Aziz et al, 2008). The annotation of key metabolic pathways was manually inspected and refined.

The Whole Genome Shotgun project of "*Ca. Methylomirabilis limnetica*" has been deposited at DDBJ/ENA/GenBank under the accession NVQC00000000 and BioProject PRJNA401219. The version described in this paper is version NVQC01000000.

For microbial community analysis from metagenomic Illumina reads, trimmed paired-end reads matching the 16S rRNA gene sequence were identified using SortMeRNA 2.1 (Kopylova et al, 2012) and supplied archaeal and bacterial 16S rRNA databases (silva-arc-16S-id95, silva-bac-16S-id90). Paired-end rRNA gene sequences

were then merged using BBmerge (Bushnell, 2016) with a minimum overlap of 20 bases. The merged reads (~8,700 – 11,400 sequences for each metagenome) were submitted to the SILVAngs web service (Quast et al, 2013) for taxonomic classification.

Pairwise average nucleotide identity (ANI) values between the genomes of “*Ca. M. limnetica*” and “*Ca. M. oxyfera*” were calculated using BLAST (ANlB) and the JSpeciesWS online service (Richter et al, 2015). Relative genome sequence coverage of “*Ca. M. oxyfera*” (Supplementary Figure 2) was calculated by mapping trimmed metagenomic sequences from Lake Zug (160 m) to the genome of “*Ca. M. oxyfera*” (retrieved from GenBank; accession FP565575) using BBmap 35.43 (Bushnell, 2016) and standard settings. Average genome coverage (500 bp interval) was calculated and visualized using BLAST Ring Image Generator (Alikhan et al, 2011). Gene coordinates of selected genes were imported from GenBank and Refs. (Luesken et al, 2012; Wu et al, 2011a). Homologs shared between “*Ca. M. limnetica*” and “*Ca. M. oxyfera*” were identified by using BLASTP (Camacho et al, 2009) with protein-coding CDS of “*Ca. M. limnetica*” as queries and all protein-coding CDS of “*Ca. M. limnetica*” as subject database. The homologs reported in Tables 2 and 3 represent the top BLASTP hit (by *e*-value and % sequence identity) and were manually inspected to assure that the alignment coverage was sufficient (typically > 90%)

Multiple sequence alignment of amino-acid sequences of nitric oxide reductase was done following the previous alignment by (Ettwig et al, 2012). Sequences were retrieved from GenBank, imported into JalView 2.10.1 (Waterhouse et al, 2009) and aligned using ClustalOmega 1.0.2 (Sievers et al, 2011) web service implemented in JalView.

Metatranscriptome data analysis

Illumina reads were trimmed using Trimmomatic 0.32 (Bolger et al, 2014) performing removal of Illumina adapters (ILLUMINACLIP:TruSeq3-SE.fa:2:30:10), adaptive trimming (MAXINFO:100:0.2) and retaining reads with a minimum length of 75 bp (MINLEN:75). Ribosomal RNA (rRNA) reads were removed from the trimmed reads using SortMeRNA 2.1 (Kopylova et al, 2012) and the prepackaged 8 rRNA databases (silva-bac-16s-id90, silva-arc-id95, silva-euk-18s-id95, silva-bac-23s-id98, silva-arc-23s-id98, silva-euk-28s-id98, rfam-5s-id98, rfam-5.8s-id98). The non-rRNA reads were mapped to the genome of “*Ca. M. limnetica*” using Bowtie2 2.1.0 (Langmead & Salzberg,

2012) and standard parameters. Indexed BAM files were generated using samtools 0.1.19 (Li et al, 2009) and the count of alignment to genomic features (based on the indexed BAM file as well as GFF file generated by Prokka) was performed using bedtools 2.23.0 multicov tool (Quinlan & Hall, 2010). Normalized gene transcription was quantified as “reads per kilobase and million” (RPKM) (Mortazavi et al, 2008) which was calculated by counting the number of mapping reads per gene divided by gene length (in kilobases) and sum of reads mapping to all genes (in millions).

Phylogenetic analyses

Full length 16S rRNA gene sequence was retrieved from the genome of “*Ca. M. limnetica*” using RNAmmer 1.2 (Lagesen et al, 2007), aligned using the SILVA incremental aligner (SINA) (Pruesse et al, 2012) and imported to the SILVA SSU NR99 database (release 123; (Quast et al, 2013)) using ARB 6.1 (Ludwig et al, 2004). Additional NC10 16S rRNA gene sequences originating from Lake Constance (Deutzmann & Schink, 2011), Brunssummerheide (Zhu et al, 2012) and the Eastern Tropical North Pacific (Padilla et al, 2016) were also added to this dataset. Maximum likelihood phylogenetic trees of 16S rRNA gene sequences were calculated using RAxML 7.7.2 (Stamatakis, 2006) integrated in ARB with the GAMMA model of rate heterogeneity and the GTR substitution model with 500 bootstraps.

NC10 PmoA amino-acid sequences were identified and retrieved from NCBI GenBank using blastp against the NCBI non-redundant protein database with the PmoA amino-acid sequence of “*Ca. M. limnetica*” as query. As an outgroup, methane and ammonium monooxygenase subunit A sequences of *Methylobacterium japonense* (PmoA, BAE86885.1), *Methylocystis* sp. SC2 (PmoA, CCJ08278.1), *Methylacidiphilum fumariolicum* SolV (PmoA1, CCG92750.1) and *Nitrosomonas cryotolerans* (AmoA, AAG60667.1) were added to the dataset. Maximum likelihood phylogenetic trees were calculated using RAxML 8.2.6 (Stamatakis, 2014) using the GAMMA model of rate heterogeneity and the substitution matrix and base frequency of the WAG model with 100 bootstraps (parameters -f a -k -N -m PROTGAMMAWAG). Phylogenetic trees were visualized using the Interactive Tree of life (iTOL v3) webservice (Letunic & Bork, 2016).

Etymology

"Candidatus Methylomirabilis limnetica" [lim.ne'ti.ca. N.L. fem. adj. *limnetica* pertaining to lakes]

Acknowledgements

We are grateful to the Swiss Federal Institute of Aquatic Science and Technology for the use of its boat, housing and research facilities. We thank Wessam Neweshy and Gabriele Klockgether for technical support, Soeren Ahmerkamp for help with flux calculations and Boran Kartal for helpful discussions. This study was financially supported by the Max Planck Society and the Deutsche Forschungsgemeinschaft (through the MARUM Center for Marine Environmental Sciences).

References

- Alikhan N-F, Petty NK, Zakour NLB, Beatson SA (2011) BLAST Ring Image Generator (BRIG): simple prokaryote genome comparisons. *BMC genomics* **12**: 402
- Aziz RK, Bartels D, Best AA, DeJongh M, Disz T, Edwards RA, Formsma K, Gerdes S, Glass EM, Kubal M (2008) The RAST Server: rapid annotations using subsystems technology. *BMC genomics* **9**: 75
- Bankevich A, Nurk S, Antipov D, Gurevich AA, Dvorkin M, Kulikov AS, Lesin VM, Nikolenko SI, Pham S, Pribelski AD (2012) SPAdes: a new genome assembly algorithm and its applications to single-cell sequencing. *Journal of Computational Biology* **19**: 455-477
- Bastviken D, Cole J, Pace M, Tranvik L (2004) Methane emissions from lakes: Dependence of lake characteristics, two regional assessments, and a global estimate. *Global Biogeochemical Cycles* **18**
- Bergmann DJ, Zahn JA, Hooper AB, DiSpirito AA (1998) Cytochrome P460 Genes from the Methanotroph *Methylococcus capsulatus* Bath. *Journal of Bacteriology* **180**: 6440-6445
- Berthold DA, Stenmark P (2003) Membrane-bound diiron carboxylate proteins. *Annual review of plant biology* **54**: 497-517
- Bhattacharjee AS, Motlagh AM, Jetten MS, Goel R (2016) Methane dependent denitrification-from ecosystem to laboratory-scale enrichment for engineering applications. *Water Res* **99**: 244-252
- Blees J, Niemann H, Wenk CB, Zopfi J, Schubert CJ, Kirf MK, Veronesi ML, Hitz C, Lehmann MF (2014) Micro-aerobic bacterial methane oxidation in the chemocline and anoxic water column of deep south-Alpine Lake Lugano (Switzerland). *Limnology and Oceanography* **59**: 311-324
- Blower TR, Salmond GP, Luisi BF (2011) Balancing at survival's edge: the structure and adaptive benefits of prokaryotic toxin-antitoxin partners. *Current opinion in structural biology* **21**: 109-118
- Bolger AM, Lohse M, Usadel B (2014) Trimmomatic: a flexible trimmer for Illumina sequence data. *Bioinformatics*: btu170
- Bowman JP (2014) The family Methylococcaceae. In *The Prokaryotes*, pp 411-440. Springer
- Braman RS, Hendrix SA (1989) Nanogram nitrite and nitrate determination in environmental and biological materials by vanadium (III) reduction with chemiluminescence detection. *Analytical Chemistry* **61**: 2715-2718

Buchfink B, Xie C, Huson DH (2015) Fast and sensitive protein alignment using DIAMOND. *Nature methods* **12**: 59-60

Bushnell B. (2016) BBMap short read aligner (<http://sourceforge.net/projects/bbmap>). <http://sourceforge.net/projects/bbmap>.

Buts L, Lah J, Dao-Thi M-H, Wyns L, Loris R (2005) Toxin–antitoxin modules as bacterial metabolic stress managers. *Trends in biochemical sciences* **30**: 672-679

Camacho C, Coulouris G, Avagyan V, Ma N, Papadopoulos J, Bealer K, Madden TL (2009) BLAST+: architecture and applications. *BMC bioinformatics* **10**: 1

Campbell MA, Nyerges G, Kozlowski JA, Poret-Peterson AT, Stein LY, Klotz MG (2011) Model of the molecular basis for hydroxylamine oxidation and nitrous oxide production in methanotrophic bacteria. *Fems Microbiology Letters* **322**: 82

Deutzmann JS, Schink B (2011) Anaerobic oxidation of methane in sediments of Lake Constance, an oligotrophic freshwater lake. *Applied and environmental microbiology* **77**: 4429-4436

Deutzmann JS, Stief P, Brandes J, Schink B (2014) Anaerobic methane oxidation coupled to denitrification is the dominant methane sink in a deep lake. *Proceedings of the National Academy of Sciences* **111**: 18273-18278

Dibrova DV, Cherepanov DA, Galperin MY, Skulachev VP, Mulkidjanian AY (2013) Evolution of cytochrome bc complexes: from membrane-anchored dehydrogenases of ancient bacteria to triggers of apoptosis in vertebrates. *Biochimica et Biophysica Acta (BBA)-Bioenergetics* **1827**: 1407-1427

Dibrova DV, Shalaeva DN, Galperin MY, Mulkidjanian AY (2017) Emergence of cytochrome bc complexes in the context of photosynthesis. *Physiologia Plantarum*

Dupont CL, Rusch DB, Yooseph S, Lombardo M-J, Richter RA, Valas R, Novotny M, Yee-Greenbaum J, Selengut JD, Haft DH (2012) Genomic insights to SAR86, an abundant and uncultivated marine bacterial lineage. *The ISME journal* **6**: 1186-1199

Ettwig KF, Butler MK, Le Paslier D, Pelletier E, Mangenot S, Kuypers MM, Schreiber F, Dutilh BE, Zedelius J, De Beer D (2010a) Nitrite-driven anaerobic methane oxidation by oxygenic bacteria. *Nature* **464**: 543-548

Ettwig KF, Butler MK, Le Paslier D, Pelletier E, Mangenot S, Kuypers MMM, Schreiber F, Dutilh BE, Zedelius J, de Beer D, Gloerich J, Wessels HJCT, van Alen T, Luesken F, Wu ML, van de Pas-Schoonen KT, Op den Camp HJM, Janssen-Megens EM, Francoijs K-J, Stunnenberg H, Weissenbach J, Jetten MSM, Strous M (2010b) Nitrite-driven anaerobic methane oxidation by oxygenic bacteria. *Nature* **464**: 543-548

Ettwig KF, Speth DR, Reimann J, Wu ML, Jetten MS, Keltjens JT (2012) Bacterial oxygen production in the dark. *Frontiers in microbiology* **3**: 273

- Ettwig KF, Zhu B, Speth D, Keltjens JT, Jetten MS, Kartal B (2016) Archaea catalyze iron-dependent anaerobic oxidation of methane. *Proceedings of the National Academy of Sciences* **113**: 12792-12796
- Goris J, Konstantinidis KT, Klappenbach JA, Coenye T, Vandamme P, Tiedje JM (2007) DNA–DNA hybridization values and their relationship to whole-genome sequence similarities. *International journal of systematic and evolutionary microbiology* **57**: 81-91
- Haroon MF, Hu S, Shi Y, Imelfort M, Keller J, Hugenholtz P, Yuan Z, Tyson GW (2013) Anaerobic oxidation of methane coupled to nitrate reduction in a novel archaeal lineage. *Nature* **500**: 567-570
- Hayes CS, Low DA (2009) Signals of growth regulation in bacteria. *Current opinion in microbiology* **12**: 667-673
- He Z, Cai C, Wang J, Xu X, Zheng P, Jetten MS, Hu B (2016) A novel denitrifying methanotroph of the NC10 phylum and its microcolony. *Scientific reports* **6**: 32241
- Holmes RM, Aminot A, K erouel R, Hooker BA, Peterson BJ (1999) A simple and precise method for measuring ammonium in marine and freshwater ecosystems. *Canadian Journal of Fisheries and Aquatic Sciences* **56**: 1801-1808
- H ugler M, Sievert SM (2010) Beyond the Calvin cycle: autotrophic carbon fixation in the ocean.
- Hyatt D, Chen G-L, LoCascio PF, Land ML, Larimer FW, Hauser LJ (2010) Prodigal: prokaryotic gene recognition and translation initiation site identification. *BMC bioinformatics* **11**: 1
- Kalyuzhnaya MG, Yang S, Rozova O, Smalley N, Clubb J, Lamb A, Gowda GN, Raftery D, Fu Y, Bringel F (2013) Highly efficient methane biocatalysis revealed in a methanotrophic bacterium. *Nature communications* **4**
- Karst SM, Kirkegaard RH, Albertsen M (2016) mmgenome: a toolbox for reproducible genome extraction from metagenomes. *bioRxiv*: 059121
- Kirf MK, Dinkel C, Schubert CJ, Wehrli B (2014) Submicromolar oxygen profiles at the oxic–anoxic boundary of temperate lakes. *Aquatic Geochemistry* **20**: 39-57
- Kits KD, Campbell DJ, Rosana AR, Stein LY (2015a) Diverse electron sources support denitrification under hypoxia in the obligate methanotroph *Methylobacterium album* strain BG8. *Frontiers in Microbiology* **6**
- Kits KD, Klotz MG, Stein LY (2015b) Methane oxidation coupled to nitrate reduction under hypoxia by the Gammaproteobacterium *Methylomonas denitrificans*, sp. nov. type strain FJG1. *Environmental microbiology* **17**: 3219-3232

Knittel K, Boetius A (2009) Anaerobic oxidation of methane: progress with an unknown process. *Annual review of microbiology* **63**: 311-334

Kojima H, Tokizawa R, Kogure K, Kobayashi Y, Itoh M, Shiah F-K, Okuda N, Fukui M (2014) Community structure of planktonic methane-oxidizing bacteria in a subtropical reservoir characterized by dominance of phylotype closely related to nitrite reducer. *Scientific reports* **4**: 5728

Kojima H, Tsutsumi M, Ishikawa K, Iwata T, Mußmann M, Fukui M (2012) Distribution of putative denitrifying methane oxidizing bacteria in sediment of a freshwater lake, Lake Biwa. *Systematic and Applied Microbiology* **35**: 233-238

Konstantinidis KT, Rossello-Mora R, Amann R (2017) Uncultivated microbes in need of their own taxonomy. *Isme Journal*

Kopylova E, Noé L, Touzet H (2012) SortMeRNA: fast and accurate filtering of ribosomal RNAs in metatranscriptomic data. *Bioinformatics* **28**: 3211-3217

Lagesen K, Hallin P, Rødland EA, Stærfeldt H-H, Rognes T, Ussery DW (2007) RNAmmer: consistent and rapid annotation of ribosomal RNA genes. *Nucleic Acids Research* **35**: 3100-3108

Langmead B, Salzberg SL (2012) Fast gapped-read alignment with Bowtie 2. *Nature methods* **9**: 357-359

Laslett D, Canback B (2004) ARAGORN, a program to detect tRNA genes and tmRNA genes in nucleotide sequences. *Nucleic Acids Research* **32**: 11-16

Letunic I, Bork P (2016) Interactive tree of life (iTOL) v3: an online tool for the display and annotation of phylogenetic and other trees. *Nucleic Acids Research* **44**: W242-W245

Li H, Handsaker B, Wysoker A, Fennell T, Ruan J, Homer N, Marth G, Abecasis G, Durbin R (2009) The sequence alignment/map format and SAMtools. *Bioinformatics* **25**: 2078-2079

López-Archilla AI, Moreira D, Velasco S, López-García P (2007) Archaeal and bacterial community composition of a pristine coastal aquifer in Donana National Park, Spain. *Aquat Microb Ecol* **47**: 123-139

Ludwig W, Strunk O, Westram R, Richter L, Meier H, Buchner A, Lai T, Steppi S, Jobb G, Förster W (2004) ARB: a software environment for sequence data. *Nucleic Acids Research* **32**: 1363-1371

Luesken FA, van Alen TA, van der Biezen E, Frijters C, Toonen G, Kampman C, Hendrickx TL, Zeeman G, Temmink H, Strous M (2011) Diversity and enrichment of nitrite-dependent anaerobic methane oxidizing bacteria from wastewater sludge. *Applied microbiology and biotechnology* **92**: 845

Luesken FA, Wu ML, Op den Camp HJ, Keltjens JT, Stunnenberg H, Francoijs KJ, Strous M, Jetten MS (2012) Effect of oxygen on the anaerobic methanotroph 'Candidatus Methyloirabilis oxyfera': kinetic and transcriptional analysis. *Environmental microbiology* **14**: 1024-1034

Milucka J, Kirf M, Lu L, Krupke A, Lam P, Littmann S, Kuypers MMM, Schubert CJ (2015) Methane oxidation coupled to oxygenic photosynthesis in anoxic waters. *ISME Journal* **9**: 1991-2002

Mortazavi A, Williams BA, McCue K, Schaeffer L, Wold B (2008) Mapping and quantifying mammalian transcriptomes by RNA-Seq. *Nature methods* **5**: 621-628

Müller B (1993) Sauerstoffentwicklung im Zugersee. Master's thesis. ETH Zürich,

Nurk S, Meleshko D, Korobeynikov A, Pevzner P (2016) metaSPAdes: a new versatile de novo metagenomics assembler. *arXiv preprint arXiv:160403071*

Nyerges G, Stein LY (2009) Ammonia cometabolism and product inhibition vary considerably among species of methanotrophic bacteria. *FEMS microbiology letters* **297**: 131-136

Op den Camp HJ, Islam T, Stott MB, Harhangi HR, Hynes A, Schouten S, Jetten MS, Birkeland NK, Pol A, Dunfield PF (2009) Environmental, genomic and taxonomic perspectives on methanotrophic Verrucomicrobia. *Environmental Microbiology Reports* **1**: 293-306

Oswald K, Graf JS, Littmann S, Tienken D, Brand A, Wehrli B, Albertsen M, Daims H, Wagner M, Kuypers MM (2017) Crenothrix are major methane consumers in stratified lakes. *The ISME journal*

Oswald K, Milucka J, Brand A, Hach P, Littmann S, Wehrli B, Kuypers MM, Schubert CJ (2016a) Aerobic gammaproteobacterial methanotrophs mitigate methane emissions from oxic and anoxic lake waters. *Limnology and Oceanography* **61**

Oswald K, Milucka J, Brand A, Hach P, Littmann S, Wehrli B, Kuypers MMM, Schubert CJ (2016b) Aerobic gammaproteobacterial methanotrophs mitigate methane emissions from oxic and anoxic lake waters. *Limnology and Oceanography*: n/a-n/a

Padilla CC, Bertagnolli AD, Bristow LA, Sarode N, Glass JB, Thamdrup B, Stewart FJ (2017) Metagenomic binning recovers a transcriptionally active Gammaproteobacterium linking methanotrophy to partial denitrification in an anoxic oxygen minimum zone. *Frontiers in Marine Science* **4**: 23

Padilla CC, Bristow LA, Sarode N, Garcia-Robledo E, Ramírez EG, Benson CR, Bourbonnais A, Altabet MA, Girguis PR, Thamdrup B (2016) NC10 bacteria in marine oxygen minimum zones. *The ISME journal* **10**: 2067-2071

Parks DH, Imelfort M, Skennerton CT, Hugenholtz P, Tyson GW (2015) CheckM: assessing the quality of microbial genomes recovered from isolates, single cells, and metagenomes. *Genome research* **25**: 1043-1055

Pereira MM, Santana M, Teixeira M (2001) A novel scenario for the evolution of haem-copper oxygen reductases. *Biochimica et Biophysica Acta (BBA)-Bioenergetics* **1505**: 185-208

Pernthaler A, Pernthaler J, Amann R (2002) Fluorescence in situ hybridization and catalyzed reporter deposition for the identification of marine bacteria. *Applied and environmental microbiology* **68**: 3094-3101

Pruesse E, Peplies J, Glöckner FO (2012) SINA: accurate high-throughput multiple sequence alignment of ribosomal RNA genes. *Bioinformatics* **28**: 1823-1829

Quast C, Pruesse E, Yilmaz P, Gerken J, Schweer T, Yarza P, Peplies J, Glöckner FO (2013) The SILVA ribosomal RNA gene database project: improved data processing and web-based tools. *Nucleic Acids Research* **41**: D590-D596

Quinlan AR, Hall IM (2010) BEDTools: a flexible suite of utilities for comparing genomic features. *Bioinformatics* **26**: 841-842

Raghoebarsing AA, Pol A, Van de Pas-Schoonen KT, Smolders AJ, Ettwig KF, Rijpstra WIC, Schouten S, Damsté JSS, den Camp HJO, Jetten MS (2006) A microbial consortium couples anaerobic methane oxidation to denitrification. *Nature* **440**: 918-921

Rasigraf O, Kool DM, Jetten MS, Damsté JSS, Ettwig KF (2014) Autotrophic carbon dioxide fixation via the Calvin-Benson-Bassham cycle by the denitrifying methanotroph "Candidatus Methyloirabilis oxyfera". *Applied and environmental microbiology* **80**: 2451-2460

Reeburgh WS (2003) Global methane biogeochemistry. *Treatise on geochemistry* **4**: 347

Richter M, Rosselló-Móra R (2009) Shifting the genomic gold standard for the prokaryotic species definition. *Proceedings of the National Academy of Sciences* **106**: 19126-19131

Richter M, Rosselló-Móra R, Glöckner FO, Peplies J (2015) JSpeciesWS: a web server for prokaryotic species circumscription based on pairwise genome comparison. *Bioinformatics*: btv681

Schubert CJ, Vazquez F, Lösekann-Behrens T, Knittel K, Tonolla M, Boetius A (2011) Evidence for anaerobic oxidation of methane in sediments of a freshwater system (Lago di Cadagno). *FEMS Microbiology Ecology* **76**: 26-38

Seemann T (2014a) Prokka: rapid prokaryotic genome annotation. *Bioinformatics*: btu153

Seemann T (2014b) Prokka: rapid prokaryotic genome annotation. *Bioinformatics* **30**: 2068-2069

Shen L-d, Hu B-l, Liu S, Chai X-p, He Z-f, Ren H-x, Liu Y, Geng S, Wang W, Tang J-l (2016) Anaerobic methane oxidation coupled to nitrite reduction can be a potential methane sink in coastal environments. *Applied microbiology and biotechnology* **100**: 7171-7180

Sievers F, Wilm A, Dineen D, Gibson TJ, Karplus K, Li W, Lopez R, McWilliam H, Remmert M, Söding J (2011) Fast, scalable generation of high-quality protein multiple sequence alignments using Clustal Omega. *Molecular systems biology* **7**: 539

Stamatakis A (2006) RAxML-VI-HPC: maximum likelihood-based phylogenetic analyses with thousands of taxa and mixed models. *Bioinformatics* **22**: 2688-2690

Stamatakis A (2014) RAxML version 8: a tool for phylogenetic analysis and post-analysis of large phylogenies. *Bioinformatics*: btu033

Waterhouse AM, Procter JB, Martin DM, Clamp M, Barton GJ (2009) Jalview Version 2—a multiple sequence alignment editor and analysis workbench. *Bioinformatics* **25**: 1189-1191

Weber HS, Habicht KS, Thamdrup B (2017) Anaerobic methanotrophic archaea of the ANME-2d cluster are active in a low-sulfate, iron-rich freshwater sediment. *Frontiers in microbiology* **8**

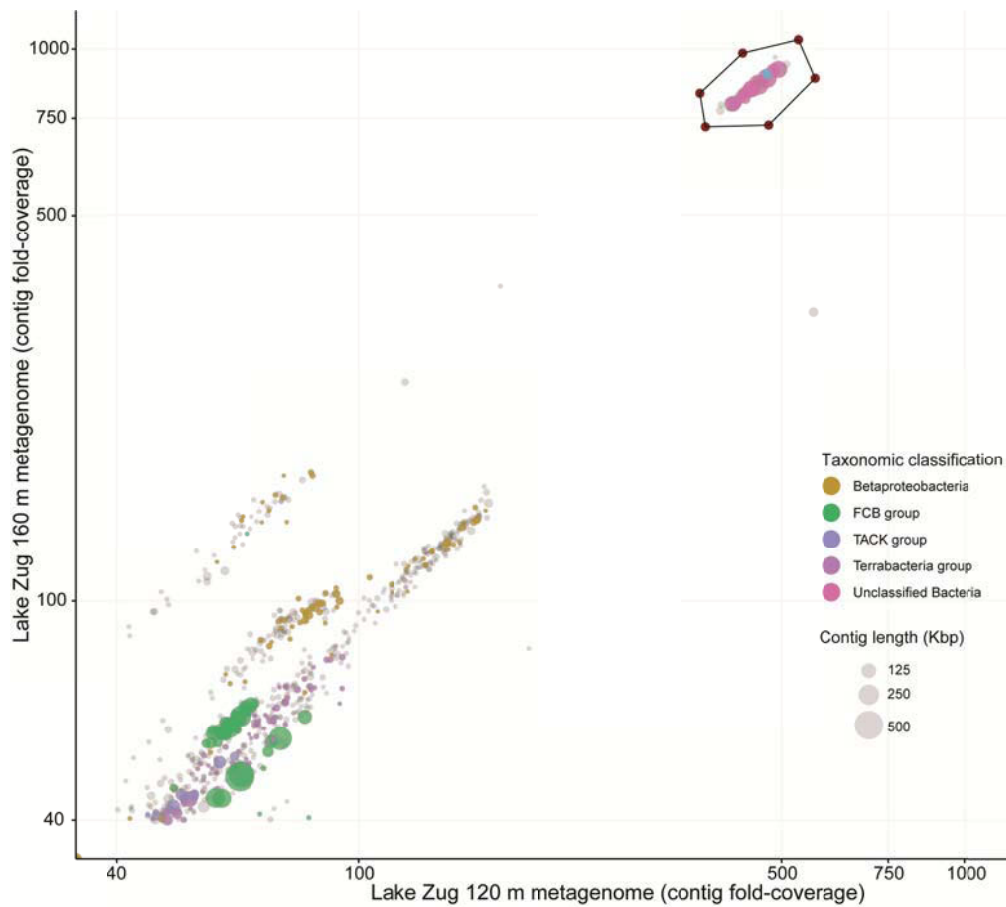
Wiesenburg DA, Guinasso Jr NL (1979) Equilibrium solubilities of methane, carbon monoxide, and hydrogen in water and sea water. *Journal of Chemical and Engineering Data* **24**: 356-360

Wu ML, de Vries S, van Alen TA, Butler MK, den Camp HJO, Keltjens JT, Jetten MS, Strous M (2011a) Physiological role of the respiratory quinol oxidase in the anaerobic nitrite-reducing methanotroph 'Candidatus Methyloirabilis oxyfera'. *Microbiology* **157**: 890-898

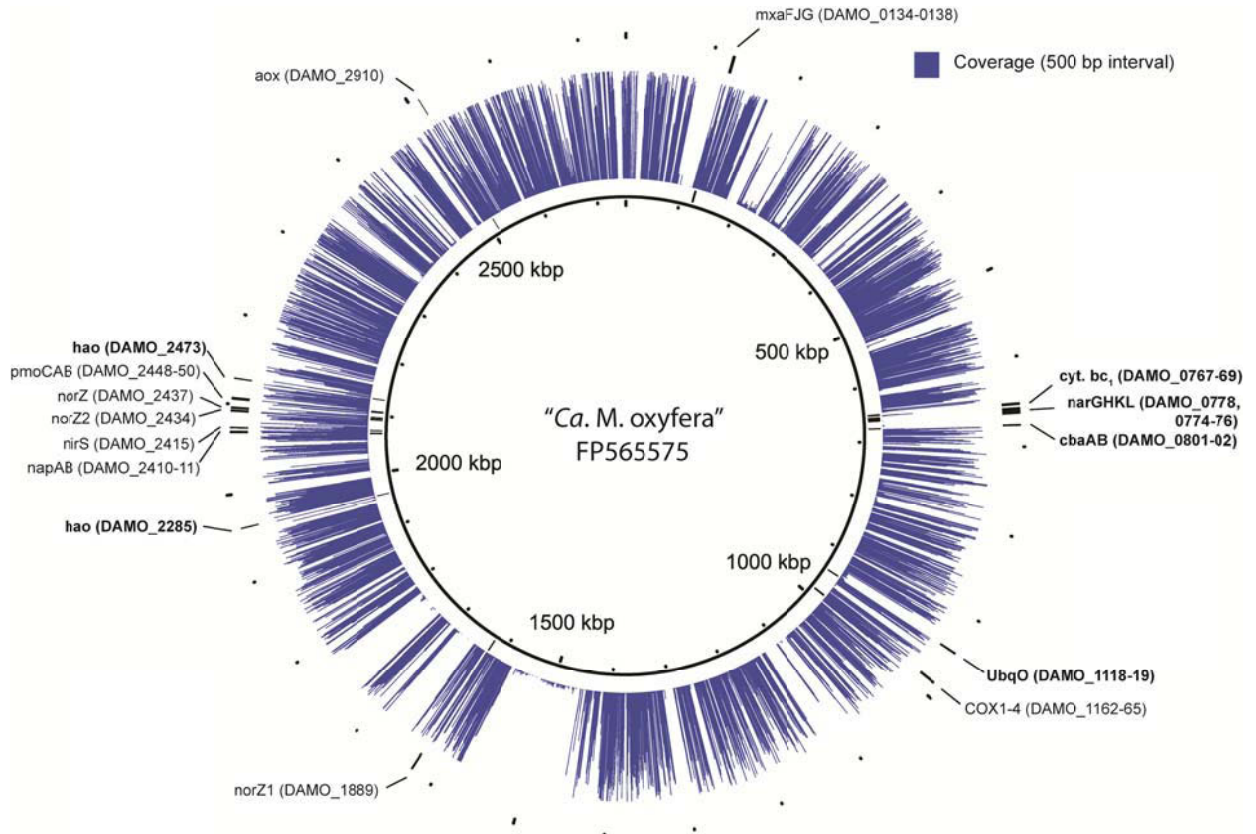
Wu ML, Ettwig KF, Jetten MS, Strous M, Keltjens JT, van Niftrik L. (2011b) A new intra-aerobic metabolism in the nitrite-dependent anaerobic methane-oxidizing bacterium Candidatus 'Methyloirabilis oxyfera'. Portland Press Limited.

Yarza P, Yilmaz P, Pruesse E, Glöckner FO, Ludwig W, Schleifer K-H, Whitman WB, Euzéby J, Amann R, Rosselló-Móra R (2014) Uniting the classification of cultured and uncultured bacteria and archaea using 16S rRNA gene sequences. *Nature Reviews Microbiology* **12**: 635-645

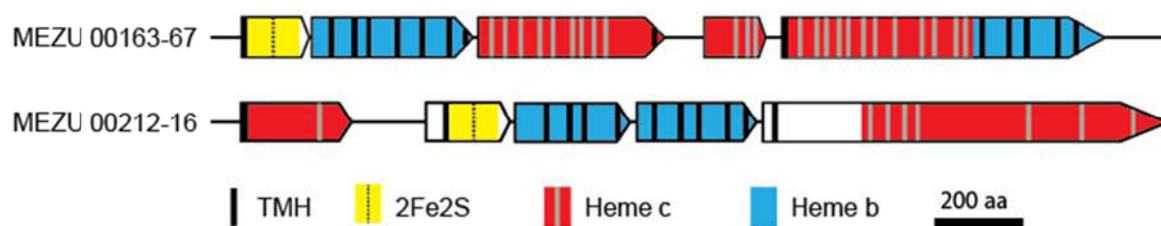
Zhu B, van Dijk G, Fritz C, Smolders AJ, Pol A, Jetten MS, Ettwig KF (2012) Anaerobic oxidization of methane in a minerotrophic peatland: enrichment of nitrite-dependent methane-oxidizing bacteria. *Applied and environmental microbiology* **78**: 8657-8665

Supplementary Material

Supplementary Figure 1. Differential coverage plot of the co-assembled metagenomes from Lake Zug. “*Ca. M. limnetica*” genomic bin (outlined) was extracted from the metagenomic contigs of the Lake Zug co-assembly by exploiting differential coverage binning. Each contig is represented by a circle and the circle size reflects contig length (in Kbp). Colored circles show taxonomic assignment of essential single copy genes; “*Ca. M. limnetica*” contigs were classified as unclassified bacteria.



Supplementary Figure 2. “*Ca. Methylomirabilis oxyfera*” genome coverage by metagenomic sequences of the Lake Zug 160 m metagenome. Shown is the circular genome of “*Ca. M. oxyfera*”; the middle ring shows average-fold genome coverage in blue (0 – 1000x, in 500bp intervals) by sequences of the metagenome from 160m depth. Genomic localization of selected functional genes of “*Ca. M. oxyfera*” involved in oxygen and nitrogen respiration as well as carbon metabolism are shown on the outer and inner ring as black intervals. Locus tags of the respective genes of are shown in brackets; gene names in bold typeface were not identified in the genome of “*Ca. M. limnetica*”.



Supplementary Figure 3. Organization of two gene clusters encoding for cytochromes *bc*-like complexes of “*Ca. M. limnetica*”. Position of domains/motifs and gene product length are drawn to scale (aa: amino acids) and motifs are specified in the Figure. Protein domains were identified using NCBI conserved domains database (Marchler-Bauer et al, 2016) or manually (for hemes c; using CxxCH motif); transmembrane helices were identified using the TMHMM Server 2.0 (<http://www.cbs.dtu.dk/services/TMHMM/>; (Krogh et al, 2001)) Abbreviations: TMH, transmembrane helix; 2Fe2S, Rieske 2Fe2S iron-sulfur cluster.

Supplementary Table S1. Overview of used oligonucleotide probes specific to NC10 bacteria. Listed are target group, 5'-3' sequence, % [v/v] formamide in the hybridization buffer and respective reference.

Probe	Target group	Probe sequence (5'-3')	% (v/v) Formamide	Mismatch (nt)*	Reference
DBACT-0193	NC10 bacteria	CGC TCG CCC CCT TTG GTC	50	1	(Raghoebarsing et al, 2006)
DBACT-0447		CGC CGC CAA GTC ATT CGT	50	5	
DBACT-1027		TCT CCA CGC TCC CTT GCG	40	0	

*Mismatch of respective probe to assembled “*Ca. M. limnetica*” 16S rRNA gene sequence.

Supplementary References

Krogh A, Larsson B, Von Heijne G, Sonnhammer EL (2001) Predicting transmembrane protein topology with a hidden Markov model: application to complete genomes. *Journal of molecular biology* **305**: 567-580

Marchler-Bauer A, Bo Y, Han L, He J, Lanczycki CJ, Lu S, Chitsaz F, Derbyshire MK, Geer RC, Gonzales NR (2016) CDD/SPARCLE: functional classification of proteins via subfamily domain architectures. *Nucleic Acids Research* **45**: D200-D203

Raghoebarsing AA, Pol A, Van de Pas-Schoonen KT, Smolders AJ, Ettwig KF, Rijpstra WIC, Schouten S, Damsté JSS, den Camp HJO, Jetten MS (2006) A microbial consortium couples anaerobic methane oxidation to denitrification. *Nature* **440**: 918-921

Chapter 4

Physiology of microorganisms mediating sulfate-dependent anaerobic oxidation of methane illuminated by functional metagenomics

Jon S. Graf¹, Boran Kartal¹, Jana Milucka¹, Timothy G. Ferdelman¹ and Marcel M.M. Kuypers¹

Potential co-authors who were involved in the presented work but have not yet read the manuscript:

Hans J. C. T. Wessels², Mike S.M. Jetten³, Daan R. Speth³, Theo van Alen³

¹Max Planck Institute for Marine Microbiology, Bremen, Germany; ²Radboud Proteomics Centre, Department of Laboratory Medicine, Radboud University Medical Center, Nijmegen, The Netherlands; ³Department of Microbiology, Institute for Water and Wetland Research, Radboud University, Nijmegen, The Netherlands.

Corresponding author: Jon Graf (jgraf@mpi-bremen.de)

Manuscript in preparation.

Author contributions

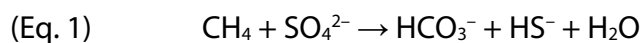
J.S.G., J.M., B.K., T.G.F. and M.M.M.K. designed research. J.S.G. performed research and analyzed bioinformatic data. H.J.C.T.W. performed proteomics and proteomic data analysis. D.R.S. and T.A. performed IonTorrent library construction and sequencing. M.M.M.K., J.M., B.K. and M.S.M.J. contributed material and analysis tools. J.S.G., B.K., J.M. and M.M.M.K. wrote the manuscript, with input from all co-authors

Summary

Sulfate-dependent anaerobic oxidation of methane (S-AOM) is mediated by a consortium of anaerobic methanotrophic archaea (ANME) and associated *Deltaproteobacteria*. This strictly anaerobic process is the dominant sink of methane in marine sediments and controls the flux of methane, a potent greenhouse gas, to the atmosphere. However, the absence of pure cultures of S-AOM microorganisms has hampered our understanding of their physiology and interactions. Here, we studied the metabolic potential and activity of S-AOM-associated microorganisms in a highly active S-AOM enrichment culture using a functional metagenomics approach, including metagenomic, metatranscriptomic and metaproteomic techniques. We reconstructed genomes of ANME-2c archaea and SEEP-SRB1 bacteria, which represent the first genomes of their respective genus or even family. We confirmed that ANME-2c archaea expressed a complete reverse methanogenesis pathway for methane oxidation and proposed several candidate genes, specifically two sulfite reductases, which might be involved in a previously proposed archaeal dissimilatory sulfate reduction pathway. Furthermore we raised the possibility of flavin-based electron bifurcation by soluble heterodisulfide reductase as an important but overlooked aspect in the electron transport chain of ANME. Our data also confirmed that SEEP-SRB1 expressed a complete sulfate reduction pathway and associated membrane-bound complexes, which arguably could also be involved in sulfur disproportionation. Moreover, we investigated the potential for electron transfer via multiheme cytochromes *c* and pili between ANME-2c and SEEP-SRB1.

Introduction

Marine sediments are hotspots of methane cycling. Methane, a potent greenhouse gas, is copious in anaerobic marine sediments where it originates predominantly from microbial degradation but also thermal breakdown of buried organic matter (Reeburgh, 2007). However, very little methane escapes the sediments mainly due to the activity of anaerobic methane-oxidizing microorganisms. These specialized microorganisms dine on methane in the complete absence of molecular oxygen but instead use sulfate, which is abundantly present in the marine environment, as electron acceptor for the anaerobic oxidation of methane (AOM). This biological process is termed sulfate-dependent anaerobic oxidation of methane (S-AOM, Eq. 1) and plays a pivotal role in regulating the flux of methane from marine sediments (Boetius & Wenzhöfer, 2013; Reeburgh, 2007).



The microorganisms that mediate S-AOM have puzzled researchers ever since the discovery of the S-AOM process in the mid-seventies (Barnes & Goldberg, 1976; Martens & Berner, 1974). The idea that S-AOM was the result of cooperation between two different microorganisms already emerged early on (Hoehler et al, 1994; Zehnder & Brock, 1979) and has been a central theme of S-AOM research ever since. Numerous studies have provided evidence that S-AOM is mediated by anaerobic methanotrophic archaea (ANME) and bacteria related to sulfate-reducing *Deltaproteobacteria* (Boetius et al, 2000; Hinrichs et al, 1999; Michaelis et al, 2002; Orphan et al, 2002). *In situ* but also *in vitro* studies have shown that ANME and the associated bacteria co-occur (or co-enrich) and often form tight aggregates further fueling the discussion about a commensalistic or even mutualistic relationship between the two microorganisms (Boetius et al, 2000; Knittel et al, 2005; Nauhaus et al, 2007; Nauhaus et al, 2002; Orphan et al, 2002).

Phylogenetically, methane-oxidizing ANME archaea form distinct groups related to methanogenic archaea within the phylum *Euryarchaeota* (Knittel & Boetius, 2009). The three main groups discovered thus far are related to the methanogenic orders of *Methanomicrobiales* (ANME-1) and *Methanosarcinales* (ANME-2 and -3) (Boetius et al, 2000; Hinrichs et al, 1999; Niemann et al, 2006). The ANME groups are separated by large phylogenetic distances and belong to different orders or families (Knittel &

Boetius, 2009; Knittel et al, 2005) – even the diversity within the ANME groups is considerable. For example, the polyphyletic ANME-2 group is subdivided into several subgroups (ANME-2a/b,c,d) (Martinez et al, 2006; Mills et al, 2005) that exhibit strikingly different physiology. Whereas ANME-2a/b and -2c appear to be associated with sulfate-dependent AOM (Knittel et al, 2005), “*Ca. Methanoperedens nitroreducens*” (ANME-2d) has not been observed in consortia and uses nitrate, iron or manganese instead of sulfate as electron acceptor (Arshad et al, 2015; Ettwig et al, 2016; Haroon et al, 2013a). The S-AOM associated *Deltaproteobacteria* are similarly diverse and are either related to the *Desulfosarcina/Desulfococcus* clade (DSS), *Desulfobulbus* (DBB) or “*Ca. Desulfofervidus*” (HotSeep1 cluster) (Holler et al, 2011; Krukenberg et al, 2016; Lösekann et al, 2007; Schreiber et al, 2010). DSS- and DBB-related members are further divided into four SEEP-SRB clades (Kleindienst et al, 2012). Thus far, all ANME groups have been shown to live in consortia – ANME-2 archaea are mostly associated with DSS and ANME-3 with DBB (Knittel & Boetius, 2009). However, ANME also have been consistently found without a partner (in particular ANME-1) or a partner unrelated to SEEP-SRB (Knittel et al, 2005; Lösekann et al, 2007; Orphan et al, 2002; Pernthaler et al, 2008; Schreiber et al, 2010).

The interplay between ANME and associated *Deltaproteobacteria* has been investigated in great detail but the mechanism is still not fully understood. Several lines of evidence have unambiguously established that all known groups of ANME archaea are capable of anaerobic oxidation of methane (Hallam et al, 2004; Hinrichs et al, 1999; Scheller et al, 2010). However, there still exists conflicting evidence about the role of the co-occurring and putatively sulfate-reducing bacteria associated with S-AOM. The phylogenetic association of DSS with other sulfate-reducing bacteria has led to the hypothesis of a syntrophic relationship between methane-oxidizing ANME and sulfate-reducing bacteria. Such a syntrophic relationship would however necessitate an electronic coupling between the partners for which several mechanisms have been proposed (see reviews by (Knittel & Boetius, 2009; Widdel et al, 2007)): I) direct interspecies electron transfer, II) diffusible redox-active mediators or III) reduced carbon compounds. Recent studies of ANME-1 and -2 have provided evidence in favor of direct interspecies electron transfer (McGlynn et al, 2015; Scheller et al, 2016; Skennerton et al, 2017; Wegener et al, 2015) whereas the latter mechanism involving transfer of reduced

carbon compounds but also H₂ has been extensively tested on different ANME groups but could not be confirmed (Nauhaus et al, 2005; Wegener et al, 2015; Wegener et al, 2008). Similarly, redox-active mediators such as humic acids, AQDS or phenazines did not appear to be suitable electron acceptors for methane oxidation by ANME-1 and -2 communities (Nauhaus et al, 2005). However, this observation was recently challenged by a study showing decoupling of archaeal methane oxidation by ANME-2 via diffusible electron acceptors (i.e. AQDS isomers) (Scheller et al, 2016). Yet a different S-AOM model has suggested that ANME-2 can couple methane oxidation to sulfate reduction independently of DSS, thus challenging the longstanding paradigm of a syntrophic relationship between S-AOM microorganisms (Milucka et al, 2012). According to the model, ANME-2 archaea perform both methane oxidation and sulfate reduction. Zero-valent sulfur formed by archaeal sulfate reduction could react abiotically under sulfidic conditions forming polysulfides which are subsequently disproportionated to sulfate and sulfide by the DSS.

Despite the surge of metagenomic studies, surprisingly few genomes of ANME and associated bacteria have been published. So far, genomes representing ANME subgroups ANME-1, -2a and -2d have been published (Arshad et al, 2015; Haroon et al, 2013a; Meyerdierks et al, 2010; Wang et al, 2014). Hence, our knowledge of the metabolic potential of the phylogenetically diverse ANME groups and subgroups is still incomplete. For example, no genome of ANME-2c group has been published yet, even though members of this subgroup are globally distributed and found in many marine sediments (Knittel & Boetius, 2009; Ruff et al, 2015). Likewise, we know very little about the metabolic potential of the S-AOM-associated bacteria for which only recently several genomes have become available (Krukenberg et al, 2016; Skennerton et al, 2017)

Here, we used a functional metagenomics approach to study the metabolic potential and activity of ANME-2c archaea and associated DSS bacteria present in an S-AOM enrichment culture. In particular we focused on metabolic pathways involved in methane and sulfur transformation. In addition, we evaluate different hypotheses surrounding the S-AOM mechanism using our genomic, transcriptomic and proteomic data.

Methods

Cultivation and maintenance of S-AOM enrichment culture

The S-AOM enrichment culture derived from a culture that has been enriched over 10 years from a sediment sample collected on a cruise of RV L'Atlante in September 2003 in the eastern Mediterranean Sea (Milucka et al, 2012). The ISIS culture was incubated in artificial SRB seawater medium (salts: 0.76 mmol l⁻¹ KBr, 8.05 mmol l⁻¹ KCl, 10 mmol l⁻¹ CaCl₂ * 2 H₂O, 27.9 mmol l⁻¹ MgCl₂ * 6 H₂O, 27.6 mmol l⁻¹ MgSO₄ * 7 H₂O, 451 mmol l⁻¹ NaCl, 4.67 mmol l⁻¹ NH₄Cl, 1.47 mmol l⁻¹ KH₂PO₄, 30 mmol l⁻¹ NaHCO₃; vitamins and trace elements: according to (Widdel & Bak, 1992); redox indicator: 1 mg l⁻¹ Resazurin; reducing agent: 0.5 mmol l⁻¹ H₂S pH 7.5) anaerobically in serum bottles sealed with butyl rubber stoppers. Serum bottles having a N₂:CO₂ (90:10) headspace were pressurized with methane (Air Liquide) to 3 bar overpressure and incubated on a shaker (40 rotations min⁻¹.) at room temperature. Medium was regularly exchanged with fresh artificial seawater medium when sulfide concentrations reached ~ 20 mmol l⁻¹ in an anaerobic glove box (Mecaplex) under N₂:CO₂ (90:10) atmosphere.

Sulfide was determined spectrophotometrically at 670nm using the methylene blue method (Cline, 1969). Prior to sulfide determination, samples were filtered (0.45 µm) and immediately fixed with 5% ZnCl₂ (0.5x sample volume). For sulfate determination, samples fixed with ZnCl₂ (same as sulfide samples), filtered through a syringe filter (0.45 µm) and analyzed on a 761 Compact ion chromatograph (Methrom) equipped with CO₂ suppressor module, Zn trap (Metrosep A Trap 1-100/4.0) and a Metrosep A SUPP5 column. Carbonate buffer (3.2 mmol l⁻¹ Na₂CO₃, 1 mmol l⁻¹ NaHCO₃) served as an eluent.

A sulfur amended S-AOM culture, which was sequenced and used for differential coverage binning, was obtained by transferring biomass of 15 ml S-AOM enrichment culture anaerobically to an equal amount of sulfate-free artificial SRB seawater medium (same as S-AOM enrichment culture, except: 55.5 mmol l⁻¹ MgCl₂ * 6 H₂O, 0.0 mmol l⁻¹ MgSO₄ * 7 H₂O, 423 mmol l⁻¹ NaCl; trace element solution did not contain FeSO₄ * 7 H₂O) in a 50 ml serum bottle which was subsequently pressurized with 1 bar N₂. To this culture, colloidal sulfur stock solution (~30 mmol S l⁻¹ suspended in sulfate-free artificial SRB seawater medium) was added to a final sulfur concentration of ~ 3.5 mmol l⁻¹. Colloidal sulfur was prepared as described by (Steudel et al, 1988) except that the sulfur

pellet was suspended in sulfate-free SRB medium instead of H₂O after 9 rounds of peptization. The sulfur amended S-AOM culture was maintained by exchanging the medium roughly every 2 month with fresh sulfate-free artificial SRB seawater medium amended with colloidal sulfur stock solution (final sulfur concentration of ~3.5 mmol l⁻¹).

Catalyzed reporter deposition fluorescence *in situ* hybridization (CARD-FISH)

Aliquots of the S-AOM enrichment culture were fixed in 2% formaldehyde in 50 mM phosphate buffer (pH 7.4) at room temperature for 1h and filtered onto polycarbonate GTTP filters (0.2 µm pore size; Millipore). CARD-FISH was performed on filter pieces according to (Pernthaler et al, 2002). In brief, cells were permeabilized with lysozyme solution (10 mg ml⁻¹ lysozyme in 0.1 M Tris buffer containing 0.05 M EDTA) for 1 h at 37°C followed by sodium dodecyl sulfate (0.5% [m/m]) for 10 min. at room temperature. Endogenous peroxidases were bleached with 0.01 M hydrochloric acid. Hybridization was performed using specific oligonucleotide probes linked to horse radish peroxidase (Biomers, Germany) for ANME (ANME2-538) and DSS (DSS-658). Hybridization was performed for 3 h at 46°C at 40% (ANME2-538) or 50% (DSS-658) formamide concentration. Amplification was performed using tyramide Alexa 488 (1 µl ml⁻¹; for DSS-658) or Alexa 594 (1 µl ml⁻¹; for ANME2-538) for 20 min. at room temperature. For double-labeled CARD-FISH, this process was repeated (without permeabilization) after additional peroxidase inactivation with 0.5% H₂O₂ followed by ethanol wash. Filter pieces were then stained with 4',6-diamidino-2-phenylindole (DAPI, 1 µg ml⁻¹) for 20 min. at room temperature, embedded in a mounting solution (4:1 v/v Citifluor:Vectashield), mounted on glass slides and visualized by epifluorescence microscopy (Axioskop 2, Zeiss)

Total RNA and DNA extraction

S-AOM biomass was harvested by centrifugation (5 min at 5000 x g) from ~10ml S-AOM enrichment culture. Total RNA and genomic DNA was extracted from the cell pellet using Powersoil Total RNA isolation kit followed by DNA Elution Accessory Kit (both MoBio Laboratories) as per manufacturer's instructions. Additionally, genomic DNA was isolated from the same S-AOM enrichment culture using DNeasy Blood & Tissue kit (Qiagen) according to manufacturer's instructions. DNA from 5 ml sulfur-

amended S-AOM culture was harvested after 5 month of incubation as described above using the Powersoil Total RNA isolation kit followed by DNA Elution Accessory Kit.

Whole metagenomic and metatranscriptomic shotgun sequencing

Genomic DNA extracted from the S-AOM enrichment culture ("Powersoil" and "Blood&Tissue" DNA extraction) was fragmented by sonication (600 - 700bp) using a Covaris S2 sonicator (Covaris, USA), libraries were prepared using NEBNext Ultra DNA Library Prep Kit for Illumina (New England Biolabs) and paired-end sequencing (2 x 250bp) was performed using the Illumina MiSeq platform with Illumina Chemistry v3 (Illumina). Library preparation and MiSeq sequencing was performed by the Max Planck-Genome-center Cologne, Germany (<http://mpgc.mpipz.mpg.de/home/>).

Genomic DNA obtained from the sulfur-amended S-AOM culture was sheared for 6 minutes using the Ion Xpress™ Plus Fragment Library Kit following the manufacturer's instructions. Further library preparation was performed using the Ion Plus Fragment Library Kit following manufacturer's instructions. Size selection of the library was performed using an E-gel 2% agarose gel. Emulsion PCR was performed using the Ion PGM™ Template OT2 400 kit and sequencing was performed on an IonTorrent PGM using the Ion PGM™ sequencing 400 kit and an Ion 318v2 chip. All kits used in this section were obtained from Life technologies.

Total RNA extracted from the S-AOM enrichment culture was enriched for messenger RNA by partial removal of ribosomal RNA using the MICROBExpress™ Bacterial mRNA Enrichment Kit (Ambion) following manufacturer's instructions. Further library preparation was performed using the Ion Total RNA-Seq Kit v2 following manufacturer's instructions, with 10 min fragmentation. Size selection of the library was performed using an E-gel 2% agarose gel. Emulsion PCR was performed using the Ion PGM™ Template OT2 200 kit and sequencing was performed on an IonTorrent PGM using the Ion PGM™ sequencing 200 kit and an Ion 318v2 chip, resulting in resulting 4.5 million reads with an average length of 116 bp. All kits used for metatranscriptomic shotgun sequencing were obtained from Life technologies.

Metagenome assembly and genome binning

Reads obtained from Illumina MiSeq sequencing were quality checked using FastQC (Andrews, 2010) and trimming as well as adapter removal was done using

Trimmomatic 0.32 (Bolger et al, 2014) and parameters MINLEN:20 ILLUMINACLIP:TruSeq3-PE.fa:2:30:10 LEADING:3 TRAILING:3 SLIDINGWINDOW:4:15 MINLEN:50.

To remove low abundance reads and facilitate de-novo assembly, trimmed reads were binned by kmer depth using BBnorm of the BBmap package (Bushnell, 2016b) prior to assembly (S-AOM "Powersoil": 30 – 550 kmer depth; S-AOM "Blood&Tissue": 50 – 1000 kmer depth). The filtered reads of the two samples were then assembled separately using SPAdes v3.1.0 (Bankevich et al, 2012) with mismatch corrector option enabled (--careful) and k-mer sizes of 21, 33, 55, 77, 99 and 127.

Binning of metagenomic contigs was performed using a combination of differential coverage and tetranucleotide frequency binning implemented in the mmgenome 0.6.3 workflow (Albertsen et al, 2013; Karst et al, 2016). The ANME-2c genome was obtained from the "Blood&Tissue" assembly by differential coverage binning between "Blood&Tissue" and "Powersoil" datasets. The preliminary genomic bin of ANME-2c was further refined using tetranucleotide frequency (Supplementary Figure 3). Using the same principles, a preliminary genome of SEEP-SRB1 was obtained from the "Powersoil" assembly. The preliminary SEEP-SRB1 genomic bin was further refined by differential coverage using metagenomic reads of the sulfur-amended S-AOM culture and "Blood&Tissue" datasets (Supplementary Figure 4).

For binning of both genomes, only contigs longer than 500 bp were used and the average coverage of each contig was computed directly using BBmap 35.43 (Bushnell, 2016a) with default parameters. Prodigal 2.60 (Hyatt et al, 2010) in metagenomic mode was used to predict open reading frames which were subsequently searched using HMMER 3.1b (Sean R. Eddy, 2015) against a set of 107 hidden markov models of essential single copy genes using default settings and trusted cutoff (-cut_tc) enabled. Protein sequences coding for essential single copy genes were searched against NCBI non-redundant database using BLASTP (Camacho et al, 2009) and a maximum e-value cutoff of $1e^{-6}$. The taxonomy (class level) of each essential single copy gene was assigned using MEGAN5 (Huson et al, 2007) (with the previously generated BLASTP xml file as input) and the mmgenome script "hmm.majority.vote.pl".

For genome re-assembly, reads used for the initial assembly (ANME-2c: "Blood&Tissue", SEEP-SRB1: "Powersoil") were mapped to the binned contigs

representing the genomes ANME-2c and SEEP-SRB1 using BBmap (Bushnell, 2016b) and stringent settings (approximate minimum identity = 0.98). Mapped reads were reassembled using SPAdes 3.5.0 (Bankevich et al, 2012) with mismatch corrector enabled (--careful), read coverage cutoff (--cov-cutoff 10) and default parameters. Small and low coverage contigs (<500bp; <10x coverage) were removed and quality of the reassembled bins was assessed using CheckM 1.05 (Parks et al, 2015) running the lineage-specific workflow. The two obtained genomes were annotated using Prokka 1.11 in metagenomic mode (Seemann, 2014) and RAST annotation server (Aziz et al, 2008).

Phylogenetic analyses

Full length 16S rRNA gene sequences were retrieved from the ANME-2c and SEEP-SRB1 genomes using RNAmmer 1.2 (Lagesen et al, 2007), aligned using the SILVA incremental aligner (SINA) 1.2.11 (Pruesse et al, 2012) and imported to the SILVA SSU NR99_123 database (Quast et al, 2013) using ARB 6.1 (Ludwig et al, 2004). Maximum likelihood phylogenetic trees of 16S rRNA gene sequences were calculated using RAXML 7.7.2 integrated in ARB with the GAMMA model of rate heterogeneity and the GTR substitution model with 100 bootstraps.

For microbial community analysis from metagenomic Illumina reads (only Blood&Tissue DNA extraction), trimmed paired-end reads matching the 16S rRNA gene were identified using SortMeRNA 2.1 (Kopylova et al, 2012) and supplied archaeal and bacterial 16S rRNA databases (silva-arc-16S-id95, silva-bac-16S-id90). Paired-end rRNA gene sequences were then merged using BBmerge (Bushnell, 2016b) with a minimum overlap of 20 bases. Merged reads were submitted to the SILVAngs web service (Quast et al, 2013) for taxonomic classification.

Pairwise average amino acid identity (AAI) values were calculated using the web AAI calculator web service of the enveomics collection (<http://enveomics.ce.gatech.edu/aai/>, (Rodriguez-R & Konstantinidis, 2016)). Protein sequences of following reference genomes were retrieved: ANME-1, FP565147.1, (Meyerdierks et al, 2010); ANME-2a, IMG 2565956544, (Wang et al, 2014); "*Ca. M. nitroreducens*", IMG 2515154041, (Haroon et al, 2013a) and SEEP-SRB1 genomes of BioProject identifiers PRJNA326769 and PRJNA290197 (Skennerton et al, 2017).

Transcriptomic data analyses

Metatranscriptomic reads (4,386,143 sequences) were filtered by length (30bp cut-off), the surviving reads (4,1824,727) were processed using SortMeRNA 2.1 (Kopylova et al, 2012) and the prepackaged 8 rRNA databases (silva-bac-16s-id90, silva-arc-id95, silva-euk-18s-id95, silva-bac-23s-id98, silva-arc-23s-id98, silva-euk-28s-id98, rfam-5s-id98, rfam-5.8s-id98). The remaining non-rRNA reads (499,588) were mapped to the ANME-2c and SEEP-SRB1 genomes using Bowtie2 and standard parameters (Langmead & Salzberg, 2012). For each gene, normalized gene expression was quantified as “reads per kilobase and million” (RPKM) which is calculated by counting the number of mapping reads per gene divided by gene length (in kilobases) and total amount of mapped reads (in million). Mapped reads were quantified using bedtools multicov v2.23.0 (Quinlan & Hall, 2010) and normalized gene expression for each gene (in RPKM) was quantified using the Bioconductor package edgeR 3.6.8 (Robinson et al, 2010).

Metaproteomics

15 ml S-AOM enrichment culture was harvested by centrifugation (5 min. at 5000 x g) and the resulting biomass pellet was flash frozen in liquid nitrogen and stored at –80°C until further processing. The pellet was thawed and total protein was extracted and solubilized using RapiGest reagent (Waters). In-solution protein digested was performed as described previously (Wessels et al, 2010). Briefly, proteins were reduced by incubating the sample for 20 minutes in 10 mM DTT at room temperature. Subsequently, reduced cysteine residues were alkylated by incubating the sample with 50 mM chloroacetamide for 20 minutes at room temperature in the dark. Subsequently, proteins were pre-digested using 0.5ug LysC enzyme (cuts C-terminal to Lys) for 3 hours at 37 degrees Celsius. Next, the sample was diluted 3 times with 50 mM ammonium bicarbonate and Trypsin was added (0.5 µg) for overnight digestion at 37 degrees Celsius. The resulting peptide mixture was desalted and concentrated using C18 reversed phase solid phase extraction tips (Agilent Technologies C18 Omix tips).

Proteomic analysis using LC–MS/MS was performed as described previously (Wessels et al, 2010). Measurements were performed using a nano-Advance nanoflow liquid chromatography system (Bruker Daltonics) coupled via electron spray ionization

captive sprayer to a maXis Plus UHR Qq-ToF mass spectrometer. Chromatographic separation was performed using a Acclaim PepMap 100 trapping column (75 μ m x 2 cm packed with nanoViper, 3 μ m 100 \AA C18 particles; Thermo Scientific) and Acclaim PepMap RSLC analytical column (40 $^{\circ}$ C; 75 μ m x 15 cm, nanoViper, 2 μ m 100 \AA C18 particles; Thermo Scientific). 3 μ g tryptic digest peptide mixture was loaded on to the trapping column at 7 μ l/min and eluted during a 240 min linear gradient of 3 – 35% acetonitrile in 0.1% formic acid at a flow rate of 500 nl/min. The mass spectrometer was operated in positive ion mode (AutoMSn; data dependent MS/MS): 3 sec duty cycle, mass range 200-3200 m/z, 2Hz full MS spectra rate, precursor intensity scaled MS/MS acquisition rate (3Hz @ 2000 cts - 20Hz @ 100.000 cts), preferred charge state range z=2-4+, only precursors within range of 400-1400 m/z, exclude singly charged precursors, 0.5min dynamic exclusion enabled, reconsider precursor if current intensity/previous intensity >4, exclude after 1 spectrum). Fragmentation experiments were performed using collision induced dissociation.

Raw MS/MS data were processed using MaxQuant software v.1.5.0.0 (Cox & Mann, 2008). The following settings were used for peptide and protein identification: carbamidomethyl (Cys) as fixed modification, oxidation (Met), and deamidation (NQ) as variable modifications, predefined MS and MS/MS settings for Bruker Qq-TOF instruments, minimal peptide length six amino acids and a maximum allowed false discovery rate of 1% at both the peptide and protein level. Translated coding DNA sequences were obtained from the Prokka annotation and were used as protein sequence database for searches of the MS/MS data. Protein abundance values were calculated as intensity based absolute quantification (iBAQ) values (Schwanhäusser et al, 2011).

Results

Activity and CARD-FISH of S-AOM enrichment culture

In this study we used a highly enriched S-AOM culture obtained through continuous cultivation of batch cultures from sediments of the Mediterranean mud volcano Isis. The sediment was collected in September 2003 on a cruise of the R/V *L'Atalante* and has been maintained and sub-cultured on artificial seawater medium amended with methane ever since. The sediment-free enrichment culture was highly active – with methane as the sole electron donor, this culture reduced sulfate nearly stoichiometrically to sulfide at high rates ($\sim 0.5 \text{ mmol l}^{-1} \text{ d}^{-1}$) (Figure 1a). In the absence of methane, no significant sulfate reduction or sulfide production was observed. Using specific CARD-FISH probes for DSS (DSS-658) and ANME-2 (ANME-2-538) we found that the majority of DAPI-stained cells in the enrichment culture were stained by either DSS or ANME-2 probe (Figure 1b, 1c; for details on used probes, see Supplementary Table 2).

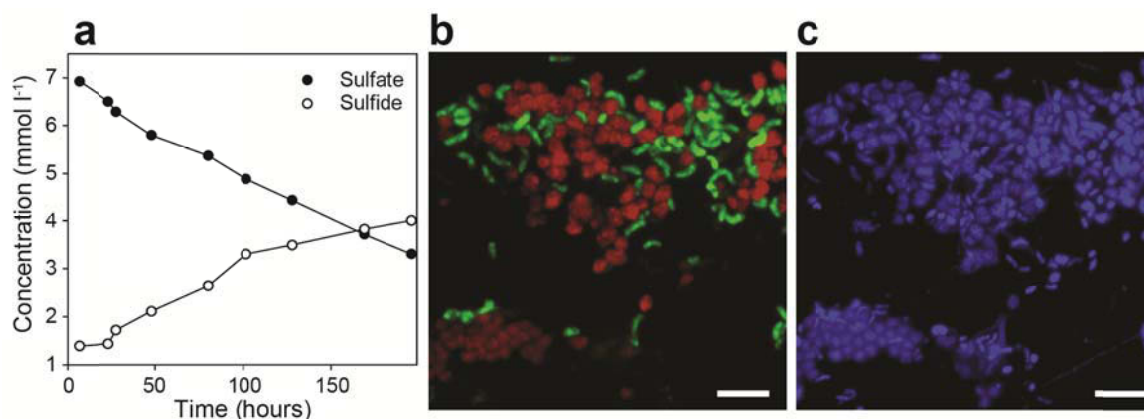


Figure 1. Microbial activity and CARD-FISH of the S-AOM enrichment culture. a, Sulfate consumption and sulfide production of S-AOM enrichment culture during 200 h incubation with methane as sole electron donor. b, Double hybridization CARD-FISH image of S-AOM aggregate labeled with probes DSS-658 (green, using Alexa488) and ANME-2-538 (red, using Alexa594). c, Same field of view as (b) stained with DAPI. Scale bar represents 5 μm .

Genome reconstruction and phylogenetic assignment of the dominant S-AOM-associated microorganisms

To obtain the genomic blueprint of the S-AOM-associated microorganisms in the S-AOM enrichment culture, DNA was extracted from the enrichment culture and subjected to next-generation sequencing. First, we retrieved and classified the 16S rRNA gene reads from the metagenomic dataset (Blood&Tissue DNA extraction) to acquire an initial overview of the microbial community. Based on this analysis we estimated that

ANME-2 or SEEP-SRB constituted the majority of the microbial population in the enrichment culture. 16S rRNA gene sequences phylogenetically assigned to ANME-2 or SEEP-SRB groups accounted together for approximately 57% of all classified sequences. 31% of all 16S rRNA gene sequences were classified as ANME-2 of which the majority was ANME-2c (~65% of ANME-2) and the rest ANME-2a/b (~35% of ANME-2). The S-AOM-associated SEEP-SRB1 and 2 clades constituted 19% and 7% of all sequences, respectively.

Next, the metagenomic reads were preprocessed, assembled and binned, resulting in two metagenomic bins that represented the genomic sequences of the two most abundant microbial populations (Supplementary Figure 3 and 4). The bins were preliminarily assigned to *Deltaproteobacteria* or *Euryarchaeota* based on taxonomic analysis of single copy genes. After reassembling, the genome quality was estimated with CheckM (Parks et al, 2015), which indicated that the genomes were almost complete (>95%) and contained little contamination (<6%). The analysis also revealed that both genomes exhibited significant strain heterogeneity (~50%; Table 1) and therefore likely represented population genomes of closely related strains. Using the same analysis, considerable strain heterogeneity was also observed for other published genomes of ANME-2a and ANME-1 (27% and 80%, respectively; (Meyerdierks et al, 2010; Wang et al, 2014)) but not for "*Ca. Methanoperedens nitroreducens*". The general features of the ANME-2c and SEEP-SRB1 genomes that were obtained in this study are summarized in Table 1.

Table 1. Overview of genome statistics of SEEP-SRB1 and ANME-2c. Coding sequences, rRNAs and coding sequences were predicted using Prodigal (Hyatt et al, 2010) and RNAmmer (Lagesen et al, 2007) implemented in Prokka (Seemann, 2014). Genome quality metrics were computed using CheckM (Parks et al, 2015) running the lineage specific workflow.

	SEEP-SRB1	ANME-2c
Contigs	250	206
Genome size (bases)	3,765,937	2,834,694
GC content (%)	41.6	49.9
Coding sequences	3,469	2,909
rRNAs	16S-23S-5S	23S/16S
Completeness / Contamination / Strain heterogeneity (%)	98.1 / 1.3 / 50.0 (marker sets: 156)	95.6 / 5.5 / 41.7 (marker sets:154)

The assembled full-length 16S rRNA gene sequence present in each genomic bin was then used for a more detailed taxonomic classification. We were able to assign the two genomes, which were putatively assigned to *Euryarchaeota* and *Deltaproteobacteria*, to the dominant ANME-2c and SEEP-SRB1 population present in the enrichment culture (Supplementary Figure 1 and 2). Closely related 16S rRNA gene sequences (>98% identity) of the ANME-2c and SEEP-SRB1 genome have been retrieved from methane-rich sediments, particularly methane seeps, from around the globe such as Mediterranean mud volcanoes Kazan and Amsterdam, Hydrate Ridge, Santa Monica Basin and also near the island Elba (Meyerdierks et al, 2005; Pachiadaki et al, 2010; Scheller et al, 2016; Wegener et al, 2016). Comparative 16S rRNA gene sequence and average amino acid identity (AAI) analysis with published genomes of ANME and SEEP-SRB suggested that two genomes described here are the first of their respective genus or even family. For both ANME-2c and SEEP-SRB1, AAI and 16S rRNA gene identity values to published genomes of the respective groups clearly exceeded the proposed category thresholds for new genera (<95% 16S rRNA gene identity; <65% AAI; (Konstantinidis et al, 2017)). We found that our ANME-2c genome was most closely related to a genome of ANME-2a (Wang et al, 2014) to which it shared 89.1% 16S rRNA gene identity and 54.9% AAI. For the SEEP-SRB1 genome we found that it shared 52.2–58.0% AAI with several recently published genomes assigned to SEEP-SRB1 (Skennerton et al, 2017).

Metatranscriptomic and metaproteomic data analysis

To quantify transcription of functional genes of SEEP-SRB1 and ANME-2c we extracted total RNA from the S-AOM enrichment culture incubated for one week in fresh medium. Total RNA was subjected to rRNA depletion followed by whole metatranscriptome shotgun sequencing and *in silico* removal of rRNA reads. The remaining non-rRNA reads (499,588) were then mapped to the SEEP-SRB1 and ANME-2c genomes. In total, 47.7% of all non-rRNA reads mapped to the two genomes (ANME-2c 34.2%; SEEP-SRB1 13.5%). Gene transcription was quantified for each coding sequence as RPKM (reads per Kb of gene per million of mapped reads, (Mortazavi et al, 2008)). For the metaproteome, whole-cell protein including cytosolic and membrane fraction were extracted from several mg biomass of the enrichment culture harvested after 1 week of incubation in fresh medium. 3µg protein was tryptically digested and analyzed by liquid

chromatography-mass spectrometry resulting in 43946 MS/MS spectra. Translated predicted coding sequences of SEEP-SRB1 and ANME-2c genomes were used as custom database for analysis in MaxQuant (Cox & Mann, 2008) to which 8.5% (3755) MS/MS spectra matched. In total 1763 peptides or 198 unique proteins (128 ANME proteins, 70 SEEP-SRB1 proteins) were identified using 1% false discovery rate as validation/assessment criteria. Protein abundance was estimated using the intensity based absolute quantification method (iBAQ, (Schwanhäusser et al, 2011)).

Methane oxidation pathway and electron transport chain of ANME-2c

Within the ANME-2c genome we identified all genes encoding for a full reverse methanogenesis pathway (Figure 2; Extended Data Table 1), including N₅,N₁₀-methylene-tetrahydromethanopterin reductase (*mer*), which previously wasn't detected in ANME-1 metagenomes (Hallam et al, 2004; Meyerdierks et al, 2010). Several genes encoding for subunits of enzymes of the reverse methanogenesis pathway such as tetrahydromethanopterin (H₄MPT) S-methyltransferase (*mtr*), N₅,N₁₀-methylene-H₄MPT reductase (*mer*), methenyl-H₄MPT cyclohydrolase (*mch*) and formylmethanofuran dehydrogenase (*fmd*) were present multiple times in the ANME-2c genome (Extended Data Table 1). The amino-acid sequence identity between duplicate sequences was 30–40% for Mtr and 43–48% in case of Mer and Mch. All genes encoding for the seven core enzymes of the reverse methanogenesis pathway were highly transcribed, in particular methyl-coenzyme M reductase (*mcrABG*; RPKM = 43,000–70,000). In case of duplicate genes we found that only one copy was predominantly transcribed (>10-fold higher RPKM). Gene transcription of reverse methanogenesis genes gradually decreased in oxidative direction throughout the pathway from approximately 70,000 RPKM (*mcr*) to <1,000 RPKM (*fmd*). Consistent with our transcriptomic results, we identified at least one or more subunits of all seven core enzymes involved reverse methanogenesis in the metaproteome thus confirming that ANME-2c expresses the full reverse methanogenesis pathway (Extended Data Table 1). Proteins of the reverse methanogenesis pathway (in particular Mcr and Mtd, iBAQ score 0.1–6.3 x 10⁶) were among the most abundant proteins of ANME-2c identified in the metaproteome (Supplementary Figure 5).

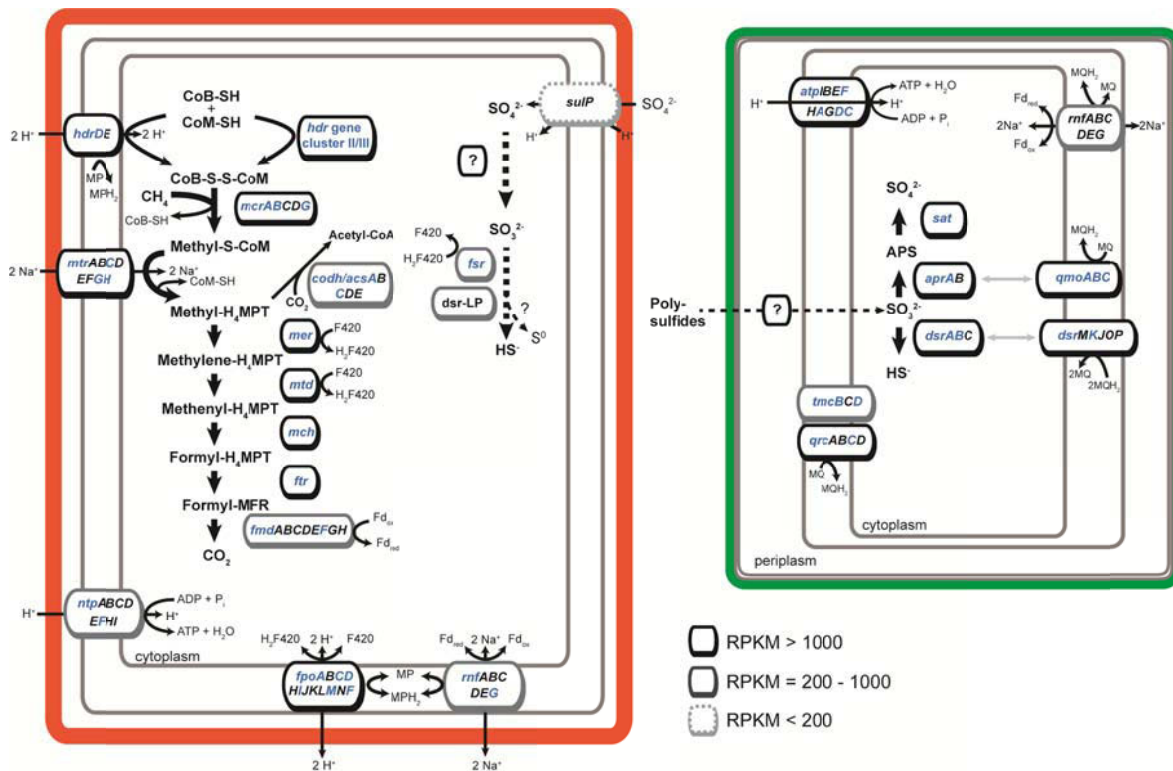


Figure 2. Metabolic scheme of ANME-2c and SEEP-SRB1 with emphasis on dissimilatory pathways and membrane-bound respiratory complexes. Predicted metabolic potential of ANME-2c (red outline) and SEEP-SRB1 (green outline) in respect to dissimilatory carbon and sulfur metabolism and associated respiratory and energy generating complexes. Key genes are shown in boxes and expression (in RPKM; if multiple subunits the average RPKM was used) is depicted by the respective outline. Expressed genes that were identified in the metaproteome are shown in blue. Abbreviations (unless noted in text): *codh/acs*, CO dehydrogenase/acetyl-CoA synthase; *ntp*, V-type ATP synthase; *fpo*, H_2F_{420} dehydrogenase; *rnf*, rhodobacter nitrogen fixation complex; *sulP*, sulfate permease; *atp*, ATP-synthase.

Next we searched for genes of the membrane-bound electron transport chain of ANME-2c that could potentially accept reducing equivalents originating from the reverse methanogenesis pathway. We identified well transcribed genes of a membrane-bound heterodisulfide reductase (*hdrDE*), H_2F_{420} dehydrogenase (*fpoABCDHIJKLMNF*) as well as Rnf complex (*rnfABCDEG*; Figure 2; Extended Data Table 1). The oxidation of coenzyme M and B coupled to the reduction of methanophenazine could proceed via transcribed HdrDE (RPKM = 1,444–2,187) of which HdrD was identified in the metaproteome (iBAQ = 17.5×10^3). Furthermore, oxidation of reduced coenzyme F420 and ferredoxin could be coupled to the reduction of membrane-soluble methanophenazine via membrane-bound H_2F_{420} dehydrogenase (Fpo, average RPKM = 1,685) and Rnf complex (average RPKM = 950), respectively. Within the metaproteome we were able to detect six subunits of Fpo (FpoACDIMF, iBAQ = $2.0\text{--}282.3 \times 10^3$) and one subunit of Rnf (RnfG, iBAQ = 62.2×10^3). In addition to membrane-bound Hdr, ANME-2c

encoded three gene clusters related to soluble heterodisulfide reductases that could be involved in electron transfer reactions (Supplementary Table 5). Hdr gene cluster I encoded for a poorly transcribed heterodisulfide reductase (*hdrABC*, RPKM = 21–44) that was not identified in the metaproteome. In contrast, Hdr cluster II (ANME_02102–06) encoded for a HdrD-like protein, HdrABC and δ -subunit of methylviologen-reducing hydrogenase (MvhD), which were comparably much higher transcribed (RPKM = 743–1,748). A third Hdr gene cluster (III), which was also well transcribed (RPKM = 855–1,365), was composed of genes encoding for HdrA, MvhD as well as two proteins with similarity to β -subunit of coenzyme F420 hydrogenase/dehydrogenase and α -subunit of formate dehydrogenase (FdhA), respectively. In contrast to Hdr cluster I, prominent expression of almost all genes of the well transcribed Hdr clusters II and III was confirmed by our metaproteomic analysis (iBAQ = 2.0×10^4 – 6.1×10^5 ; Supplementary Figure 5).

ANME-2c encodes several well transcribed multi-heme cytochromes *c*

Within the ANME-2c genome we identified eleven genes encoding for multi-heme cytochromes *c* (MHC; Supplementary Table 3), which encoded for proteins that contained two or more heme-binding motifs (>2 CxxCH). Of these 11 MHC genes, three genes (ANME_02168, 01594, 02604) were substantially transcribed (>1,000 RPKM) and encoded for MHCs with 13 and 11 heme-binding motifs. Distant homologs of these well transcribed MHCs were identified in “*Ca. Methanoperedens nitroreducens*” and *Geoalkalibacter subterraneus* annotated as hypothetical proteins (39% and 28% amino-acid sequence identity, respectively; Supplementary Table 3). Despite their high transcription, expression of these MHCs could not be detected. The only MHC of ANME-2c identified in the metaproteome (ANME_01820) contained 31 heme-binding motifs and was apparently low in abundance (iBAQ = 263) and weakly transcribed (RPKM = 48).

Two adjacent MHC genes of ANME-2c (ANME_02055–56) encoded for proteins with 16 and 17 heme binding motifs, respectively, one of which contained two putative S-layer domains (ANME_02055). Transcription of both genes was low (RPKM < 170) and the encoded proteins were not detected in the metaproteome. Combined together, these two genes were similar to a single gene encoding for a MHC/S-layer fusion protein of in ANME-2a, which has been previously described (IMG-MER identifier 2566125052, (McGlynn et al, 2015)). It appears that ANME_02055 represented the N-terminus

(residue 1–1395; 38% amino acid identity) and ANME_02056 the C-terminus (residue 1419–2108; 41% amino acid identity) of the S-layer MHC homolog of ANME-2a. Other genes encoding for MHCs with S-layer domains were not detected in the ANME-2c genome.

Genome-inferred metabolic capacity for dissimilatory sulfur metabolism of ANME-2c

No genes encoding for the canonical dissimilatory sulfate reduction pathway (Sat, Apr, Dsr) were detected in the ANME-2c genome, which is consistent with previous genomic and immunological labeling studies of S-AOM-associated ANME archaea (Hallam et al, 2004; Meyerdierks et al, 2010; Milucka et al, 2013; Wang et al, 2014). However, within the ANME-2c genome we identified a putative sulfate permease of the sulP family (ANME_02902, RPKM = 12) as well as three genes that could potentially be involved in dissimilatory sulfur metabolism. These three genes were located in close genomic proximity to each other and encoded for a F420-dependent sulfite reductase (Fsr, ANME_01246), a small siroheme sulfite reductase-like protein (Dsr-LP, ANME_01242) and an octaheme cytochrome *c* similar to tetrathionate reductase (OTR, ANME_01244). The latter protein sequence shared only low similarity with OTR of *Shewanella oneidensis* MR-1 (30% amino acid sequence identity; 83% coverage) but retained most of the conserved residues of the active site and substrate binding pocket found in OTR from *Shewanella oneidensis* MR-1 (Supplementary Figure 7, (Mowat et al, 2004)). We found that ANME-2c transcribed the genes encoding for Fsr, Dsr-LP as well as OTR-like protein (RPKM = 207–464) and expression of Fsr (iBAQ = 42.8×10^3) was confirmed by our metaproteomic data.

Dissimilatory sulfur metabolism, electron transport and type IV pili of SEEP-SRB1

Within the SEEP-SRB1 genome we identified all genes encoding for the canonical sulfate reduction pathway (Figure 2) including ATP sulfurylase (Sat), APS reductase (AprAB), dissimilatory sulfite reductase (DsrAB) and DsrC protein. All these genes were well transcribed (RPKM = 7,425 – 26,401) and expression was also confirmed by our metaproteomic data (Extended Data Table 2). Moreover, Sat, AprAB and DsrAB were among the most abundant SEEP-SRB1 proteins identified in the metaproteome (iBAQ 158.0 – 516.5×10^3 ; Supplementary Figure 5b). Well transcribed genes encoding for

soluble DsrC protein (RPKM = 14,340) as well as membrane-bound complexes DsrMKJOP and QmoABC (average RPKM = 1,685–2,049) were also encoded in the SEEP-SRB1 genome (Figure 2). With the exception of DsrC, at least one subunit of all these complexes was also detected in the metaproteome (iBAQ = 13.5–118.4 x 10³; Extended Data Table 2).

Next, we searched for membrane-bound complexes involved in electron transport such as quinone-reducing complex (Qrc) or tetraheme cytochrome membrane complex (Tmc), which are often present in bacteria that also contain enzymes for sulfate reduction (Grein et al, 2013; Rabus et al, 2015). Within the SEEP-SRB1 genome we identified well transcribed genes encoding for the membrane-bound respiratory quinone-reducing complex (QrcABCD, RPKM = 1068 – 2102) and partial tetraheme cytochrome membrane complex (TmcBCD, RPKM = 359 – 829). In agreement with the prominent transcription of both complexes, we could confirm expression of QrcC (iBAQ = 19.9 x 10³) and TmcBC (iBAQ = 28.0 – 187.0 x 10³ ; Extended Data Table 2). Periplasmic hydrogenases or formate dehydrogenases, which have been shown to donate electrons via tetraheme cytochromes *c* to Qrc and Tmc (Grein et al, 2013), were not encoded in the genome of SEEP-SRB1.

Cytochromes *c* and type IV pili of SEEP-SRB1

In the SEEP-SRB1 genome we identified total of 25 genes encoding for multi-heme cytochromes *c* with up to 26 heme-binding sites (Supplementary Table 4). The majority of these MHC genes were transcribed and encoded for proteins with 4–12 heme binding motifs. The highest transcription was observed for genes encoding for three tetraheme cytochromes *c* (RPKM = 938–20111; DSS_00053, DSS_2785 and DSS_03053) and genes associated with heme-containing, respiratory enzymes (i.e. QrcA and DsrJ; RPKM = 986–2,102). Despite the observed transcription of most MHC genes, we only identified a single MHC protein (DSS_03494, iBAQ = 8.8 x 10³) in the metaproteome, of which no transcripts were identified in the metatranscriptome.

The SEEP-SRB1 genome encoded several genes encoding for type IV pili (Extended Data Table 2) including genes encoding for the inner membrane alignment complex (*pilMNOP*), the outer membrane secretin pore (*pilQ*) and two pre-pilins (*pilA*). Transcription of these genes was comparatively low (RPKM = 44–144) except for one

pilA gene (RPKM = 402) and no pili-associated proteins could be detected in the metaproteome.

Discussion

Reverse methanogenesis pathway and electron transport chain of ANME-2c

To date, almost all genomes of ANME archaea have been found to encode a complete reverse methanogenesis pathway for methane oxidation (Arshad et al, 2015; Hallam et al, 2004; Haroon et al, 2013b; Meyerdierks et al, 2010; Meyerdierks et al, 2005; Wang et al, 2014). While most genomic studies focusing on ANME found a complete pathway, it was suggested that ANME-1 archaea might encode an incomplete reverse methanogenesis pathway that was missing Mer (Meyerdierks et al, 2010). Here we show that ANME-2c archaea in the S-AOM enrichment culture encode a “conventional” full reverse methanogenesis pathway. Furthermore, we were able to confirm that ANME-2c transcribed and, for the first time, expressed the full reverse methanogenesis pathway. Interestingly, the ANME-2c genome encoded for multiple, sequence-divergent copies of several genes of the reverse methanogenesis pathway of which only one copy was predominantly transcribed and expressed. Redundancy and sequence divergence of reverse methanogenesis genes in ANME-2 genomes appear to be not unusual and has also been observed for ANME-2a (Wang et al, 2014) and “*Ca. Methanoperedens nitroreducens*” (Haroon et al, 2013a).

From the methanogenesis pathway, which has been systematically studied in methanogenic archaea (for review see (Thauer, 1998; Thauer et al, 2008)), reducing equivalents for methanogenesis are supplied by three electron carriers: coenzyme M and B, coenzyme F420 (twice) and ferredoxin. Since the same pathway, albeit in reverse, catalyzes anaerobic oxidation of methane, it is reasonable to assume that these electron carriers serve as direct electron acceptors in the reverse methanogenesis pathway (Thauer, 2011). Oxidation of CoM-SH/CoB-SH in ANME-2c might proceed via soluble and membrane-bound Hdr. Membrane-bound Hdr could couple the oxidation of CoM-SH/CoB-SH to the reduction of membrane-integral methanophenazine but would likely have to be driven by scalar translocation of protons to the cytoplasm (Abken et al, 1998; Deppenmeier & Müller, 2007; Welte & Deppenmeier, 2011).

Since the ANME-2c did not encode catalytic subunits of hydrogenases, it is unlikely that CoM-SH/CoB-SH oxidation is coupled to H₂ production (with H⁺ as electron acceptor) via Hdr–hydrogenase complex known from hydrogenotrophic methanogens (Kaster et al, 2011).

Oxidation of reduced coenzyme F420 and ferredoxin could be coupled to the reduction of methanophenazine by F420 dehydrogenase and Rnf complex, respectively. Both complexes were encoded in the ANME-2c genome and have also been identified in ANME-2a (Wang et al, 2014). These two complexes are likely part of an energy conserving electron transport system known from methanogenic archaea (Bäumer et al, 2000; Deppenmeier, 2004; Kumagai et al, 1997; Li et al, 2006; Schlegel et al, 2012). We found that membrane-bound Hdr, F420 dehydrogenase and Rnf complex were well transcribed and expressed in ANME-2c; hence our data further corroborates a redox coupling of reverse methanogenesis with membrane-integral methanophenazine that has been previously proposed for ANME-2a (McGlynn et al, 2015). However, this redox coupling might be more complex and intertwined through interconversion of redox carriers by soluble Hdrs. Two well transcribed and expressed soluble Hdr gene clusters of ANME-2c (Supplementary Table 5), which are also present in other ANME-2 genomes (Figure 3), would be well suited to conduct such a mechanism.

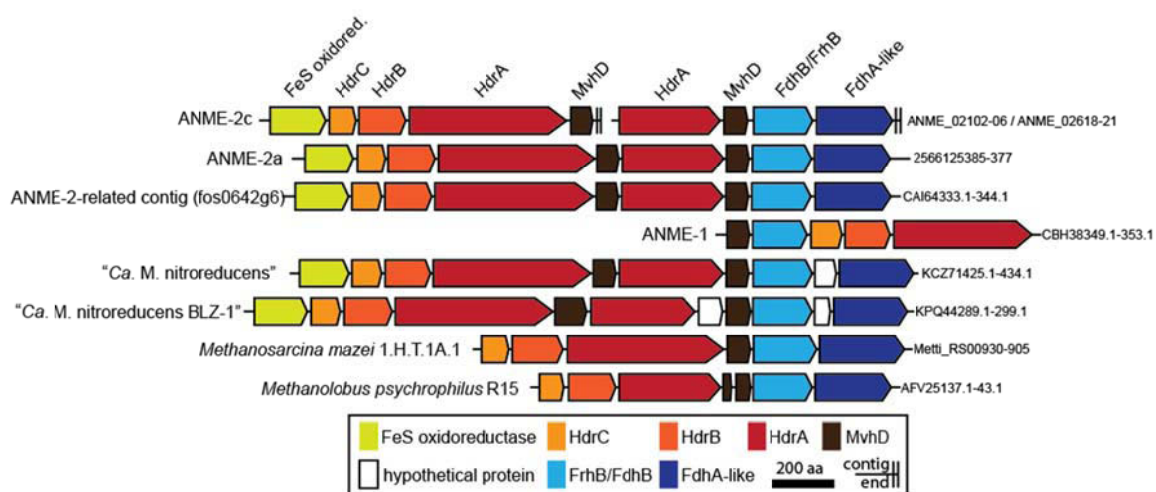


Figure 3. Genomic neighborhood of genes encoding for soluble heterodisulfide reductase of ANME and methanogenic archaea. Genomic neighborhood of ANME-2c heterodisulfide gene clusters II and III (top) in comparison to similarly arranged Hdr gene clusters found in other ANME genomes as well as methanogenic archaea (*Methanosarcina mazei*, *Methanlobus psychrophilus*). Genes are colored by their respective annotation (see legend) and the GenBank or IMG-ER accession numbers are shown to the right of each sequence. Abbreviations: HdrABC, heterodisulfide reductase subunits ABC; MvhD, methylviologen-reducing hydrogenase subunit

D; FrhB/FdhB, coenzyme F420-reducing hydrogenase/formate dehydrogenase subunit B; FdhA-like, formate dehydrogenase subunit A-like.

These Hdrs, which include the electron-bifurcating HdrA subunit, could in principle allow for flavin-based electron bifurcation-mediated interconversion of reducing equivalents between the redox carriers. Electron bifurcation by Hdr, which are widespread enzymes in anaerobic bacteria and archaea (Buckel & Thauer, 2013), might be an additional mechanism by ANME-2c to conserve energy. Similar to the reduction of ferredoxin in methanogens (Kaster et al, 2011), flavin-based electron bifurcation could also generate low redox potential electrons. These electrons could in principle enable ANME-2c to catalyze reduction reactions, such as sulfate to sulfite, with a very low redox potential.

Possible routes and sinks for electrons originating from the reverse methanogenesis pathway

Although ANME-2c encodes all enzymes necessary to couple methane oxidation to the reduction of the membrane-integral methanophenazine, it is unclear where the electrons go from there. Two routes have been proposed: I) archaeal sulfate reduction (Milucka et al, 2012) or II) transfer to an extracellular electron acceptor (either sulfate-reducing bacteria or metal ions) (McGlynn et al, 2015; Scheller et al, 2016; Wegener et al, 2015). For the latter route it was suggested that reducing equivalents from methanophenazine could be transferred via a membrane-bound cytochrome *b* and extracellular cytochromes *c* (possibly containing S-layer domains) to an extracellular electron acceptor (McGlynn et al, 2015). Although we identified a well transcribed and expressed membrane-bound cytochrome *b* (ANME_00241, RPKM = 1,246, iBAQ = 17.4 x 10³), the physiological function of this cytochrome *b* still needs to be clarified. Moreover, we found that transcription of the S-layer MHC gene by ANME-2c was low (RPKM = 65) and the corresponding protein could also not be detected in the metaproteome. Since very little is known about the function of MHCs in archaea (Kletzin et al, 2015), it remains unknown whether other well transcribed MHC of ANME-2c are indeed involved in electron transfer or fulfill a different physiological function.

Alternatively, archaeal sulfate reduction, which was previously proposed by (Milucka et al, 2012), might be supplied by reducing equivalents from the methanophenazine pool. Direct reduction of sulfate to sulfite with methanophenazine

as electron donor is thermodynamically problematic as the redox potential E° of methanophenazine/dihydromethanophenazine redox couple (-165 mV) is well above the redox potential of the $\text{SO}_4^{2-}/\text{HSO}_3^-$ couple (-512 mV) (Thauer et al, 2007; Tietze et al, 2003). It is currently unclear how sulfate reduction to sulfite in ANME-2c might proceed; however, it was previously speculated that sulfate reduction could be coupled (potentially via ferredoxin) to Formyl-MFR/ $\text{CO}_2 + \text{MFR}$ redox couple which operates at a sufficiently low potential (E° between -500 mV and -530 mV, (Thauer, 1998)) (Milucka et al, 2012; Thauer, 2011). Alternatively, we hypothesize that electrons with a sufficiently low redox potential could be generated via electron bifurcation by soluble heterodisulfide reductase of ANME-2c.

Sulfite, which might be an intermediate of archaeal sulfate reduction, could in principle be reduced directly to sulfide with methanophenazine. This reaction would be thermodynamically not a problem as the redox potential of $\text{HSO}_3^- / \text{HS}^-$ couple is sufficiently high (-120 mV; (Thauer et al, 2007)) to allow reduction by methanophenazine (-165 mV). Reducing equivalents from methanophenazine could be transferred for example via membrane-bound cytochrome *b* directly or indirectly (e.g. cytochrome *c*) to the small sulfite reductase-like protein (Dsr-LP) encoded within the genome of ANME-2c. Alternatively, sulfite reduction could also proceed in a presumably non-energy conserving manner via F420-dependent sulfite reductase using reduced coenzyme F420 as electron donor. In any case, intracellular sulfite levels would have to be tightly controlled since sulfite is an inhibitor of methanogenesis and is therefore also expected to inhibit reverse methanogenesis (Johnson & Mukhopadhyay, 2008b).

It is also possible that these sulfite reductases have physiological functions unrelated to dissimilatory S metabolism (such as sulfite detoxification, which was shown for Fsr (Johnson & Mukhopadhyay, 2005; Johnson & Mukhopadhyay, 2008a)); yet it is intriguing that the sulfite reductase genes, which were identified in other ANME genomes (Supplementary Figure 6), were transcribed and Fsr could even be detected in the metaproteome although sulfite was never added to the S-AOM enrichment culture.

Role of SEEP-SRB1 bacteria in S-AOM

In this study we showed that SEEP-SRB1 bacteria encoded all enzymes of the canonical sulfate reduction pathway (Sat, AprAB, DsrAB, DsrC) as well as membrane-bound QmoABC and DsrMKJOP complexes. Genes encoding for these proteins were

among the highest transcribed genes of SEEP-SRB1 and with the exception of DsrC, expression of all proteins was detected in the metaproteome. However, studies of sulfur disproportionating bacteria (i.e. *Desulfocapsa* or *Desulfobulbus*) also have shown that the same enzymes catalyze sulfur disproportionation (Finster, 2008; Finster et al, 2013; Frederiksen & Finster, 2003). It is therefore difficult to ascertain from our data and without physiological experiments whether SEEP-SRB1 perform sulfate reduction or sulfur disproportionation. However, considering that a physiological study by Milucka et al. (2012) has shown that DSS bacteria in the enrichment culture are capable of sulfur disproportionation, it is plausible that these well transcribed and expressed enzymes are involved in disproportionation. Sulfur disproportionation is still poorly understood process but it was suggested that sulfite is a central intermediate (Böttcher et al, 2005; Finster, 2008; Frederiksen & Finster, 2003). In particular it is unknown how polysulfides, which seem to be the disproportionated by DSS (Milucka et al, 2012), could be converted to sulfite. Conspicuous membrane-bound molybdopterin oxidoreductases or polysulfide reductases, which have been implicated in sulfur species interconversion in disproportionating bacteria (Finster et al, 2013; Mardanov et al, 2016), were not present in the SEEP-SRB1 genome.

Within the SEEP-SRB1 genome we identified well transcribed and expressed electron-accepting, membrane-bound complexes Qrc and Tmc. These complexes are commonly found in sulfate-reducing bacteria and have been shown to accept electrons, which are ultimately funneled into sulfate reduction, from periplasmic enzymes (e.g. hydrogenase, formate dehydrogenase) via periplasmic tetraheme cytochromes c_3 (Grein et al, 2013). The prominent transcription of Qrc, Tmc as well as of several genes encoding for tetraheme cytochrome c_3 (RPKM = 938 –20,112) leave little doubt that these enzymes are important modules in the electron transport chain of SEEP-SRB1. Intriguingly, periplasmic hydrogenases or formate dehydrogenases were absent from the SEEP-SRB1 genome, which suggests an alternative periplasmic source of reducing power. Skennerton et al. (2017) and Krukenberg et al. (2016) argued that, based on a syntrophic S-AOM model, electrons transferred from ANME archaea might be fed through tetraheme cytochromes c_3 into the electron transport chain of the sulfate-reducing bacterial partner. Alternatively we suggest that Qrc and Tmc might be electron-accepting complexes (via tetraheme cytochromes c_3) of a yet to be identified,

periplasmic enzyme involved sulfur disproportionation; for example, this putative enzyme could be involved in the initial interconversion of polysulfide to sulfite. In any case, further physiological experiments are needed to substantiate these hypotheses.

Experiments with syntrophic co-cultures of *Geobacter* have suggested that multi-heme cytochromes *c* and pili might be involved in direct exchange of electrons between microorganisms (Summers et al, 2010). Similarly it was suggested that direct interspecies transfer in thermophilic S-AOM might be facilitated through nanowire-like structures formed by type IV pili (Wegener et al, 2015), which however has been questioned recently (Walker et al, 2017). Although SEEP-SRB1 also encoded a complete set of genes for type IV pili, we did not observe high transcription of pili genes. In contrast to "*Ca. Desulfofervidus auxilii*", which transcribed *pilA* at similar levels to *dsrA* under syntrophic conditions (Wegener et al, 2015), we found that transcription by SEEP-SRB1 of *pilA* (RPKM = 402) was orders of magnitudes lower than *dsrA* (RPKM = 16,402). Furthermore, we could not detect expression of type IV pili proteins in the metaproteome. Nevertheless it might still be possible that SEEP-SRB1 utilizes pili to mediate cellular functions such as cell adhesion or microcolony formation (Craig et al, 2004).

Electron transfer mediated by multi-heme cytochromes *c* of the S-AOM-associated bacterial partner (and ANME) has been proposed as mode of electron transfer that might not necessarily rely on conductive pili but rather on a cytochrome *c*-mediated conductive extracellular matrix (McGlynn et al, 2015; Skennerton et al, 2017). We found that SEEP-SRB1 encoded and transcribed several multi-heme cytochromes *c* that could be indeed involved in electron transfer. With one exception, none of these sometimes well transcribed multi-heme cytochromes *c* were detected in the metaproteome. It is unclear if these proteins were not expressed or if they were not detected for unknown, technical reasons related to the metaproteomic analyses. In any case, several aspects of cytochrome-mediated electron transfer in S-AOM consortia are still unresolved (reviewed by (Lovley, 2016)) and the physiological function of the multi-heme cytochromes *c* has yet to be directly demonstrated.

Acknowledgments

We thank Kirsten Imhoff for support with sulfate measurements and Harald Gruber-Vodicka for general advice with bioinformatic analyses. This study was financially supported by the Max Planck Society and the Deutsche Forschungsgemeinschaft (through the MARUM Center for Marine Environmental Sciences).

References

- Abken H-J, Tietze M, Brodersen J, Bäumer S, Beifuss U, Deppenmeier U (1998) Isolation and characterization of methanophenazine and function of phenazines in membrane-bound electron transport of *Methanosarcina mazei* Gö1. *Journal of Bacteriology* **180**: 2027-2032
- Albertsen M, Hugenholtz P, Skarshewski A, Nielsen KL, Tyson GW, Nielsen PH (2013) Genome sequences of rare, uncultured bacteria obtained by differential coverage binning of multiple metagenomes. *Nature biotechnology* **31**: 533-538
- Andrews S (2010) FastQC: A quality control tool for high throughput sequence data. <http://www.bioinformatics.bbsrc.ac.uk/projects/fastqc>
- Arshad A, Speth DR, de Graaf RM, den Camp HJO, Jetten MS, Welte CU (2015) A metagenomics-based metabolic model of nitrate-dependent anaerobic oxidation of methane by *Methanoperedens*-like archaea. *Frontiers in microbiology* **6**
- Aziz RK, Bartels D, Best AA, DeJongh M, Disz T, Edwards RA, Formsma K, Gerdes S, Glass EM, Kubal M (2008) The RAST Server: rapid annotations using subsystems technology. *BMC genomics* **9**: 75
- Bankevich A, Nurk S, Antipov D, Gurevich AA, Dvorkin M, Kulikov AS, Lesin VM, Nikolenko SI, Pham S, Pribelski AD (2012) SPAdes: a new genome assembly algorithm and its applications to single-cell sequencing. *Journal of Computational Biology* **19**: 455-477
- Barnes R, Goldberg E (1976) Methane production and consumption in anoxic marine sediments. *Geology* **4**: 297-300
- Bäumer S, Ide T, Jacobi C, Johann A, Gottschalk G, Deppenmeier U (2000) The F420H₂ Dehydrogenase from *Methanosarcina mazei* Is a Redox-driven Proton Pump Closely Related to NADH Dehydrogenases. *Journal of Biological Chemistry* **275**: 17968-17973
- Boetius A, Ravensschlag K, Schubert CJ, Rickert D, Widdel F, Gieseke A, Amann R, Jørgensen BB, Witte U, Pfannkuche O (2000) A marine microbial consortium apparently mediating anaerobic oxidation of methane. *Nature* **407**: 623-626
- Boetius A, Wenzhöfer F (2013) Seafloor oxygen consumption fuelled by methane from cold seeps. *Nature Geoscience* **6**: 725-734
- Bolger AM, Lohse M, Usadel B (2014) Trimmomatic: a flexible trimmer for Illumina sequence data. *Bioinformatics*: btu170
- Böttcher ME, Thamdrup B, Gehre M, Theune A (2005) 34S/32S and 18O/16O fractionation during sulfur disproportionation by *Desulfobulbus propionicus*. *Geomicrobiology Journal* **22**: 219-226

Buckel W, Thauer RK (2013) Energy conservation via electron bifurcating ferredoxin reduction and proton/Na⁺ translocating ferredoxin oxidation. *Biochimica et Biophysica Acta (BBA)-Bioenergetics* **1827**: 94-113

Bushnell B. (2016b) BBMap short read aligner (<http://sourceforge.net/projects/bbmap>). <http://sourceforge.net/projects/bbmap>.

Camacho C, Coulouris G, Avagyan V, Ma N, Papadopoulos J, Bealer K, Madden TL (2009) BLAST+: architecture and applications. *BMC bioinformatics* **10**: 1

Cline JD (1969) Spectrophotometric determination of hydrogen sulfide in natural waters. *Limnology and Oceanography* **14**: 454-458

Cox J, Mann M (2008) MaxQuant enables high peptide identification rates, individualized ppb-range mass accuracies and proteome-wide protein quantification. *Nature biotechnology* **26**: 1367-1372

Craig L, Pique ME, Tainer JA (2004) Type IV pilus structure and bacterial pathogenicity. *Nature Reviews Microbiology* **2**: 363

Deppenmeier U (2004) The membrane-bound electron transport system of *Methanosarcina* species. *Journal of bioenergetics and biomembranes* **36**: 55-64

Deppenmeier U, Müller V (2007) Life close to the thermodynamic limit: how methanogenic archaea conserve energy. In *Bioenergetics*, pp 123-152. Springer

Ettwig KF, Zhu B, Speth D, Keltjens JT, Jetten MS, Kartal B (2016) Archaea catalyze iron-dependent anaerobic oxidation of methane. *Proceedings of the National Academy of Sciences* **113**: 12792-12796

Finster K (2008) Microbiological disproportionation of inorganic sulfur compounds. *Journal of Sulfur Chemistry* **29**: 281-292

Finster KW, Kjeldsen KU, Kube M, Reinhardt R, Mussmann M, Amann R, Schreiber L (2013) Complete genome sequence of *Desulfocapsa sulfexigens*, a marine deltaproteobacterium specialized in disproportionating inorganic sulfur compounds. *Standards in genomic sciences* **8**: 58

Frederiksen T-M, Finster K (2003) Sulfite-oxido-reductase is involved in the oxidation of sulfite in *Desulfocapsa sulfoexigens* during disproportionation of thiosulfate and elemental sulfur. *Biodegradation* **14**: 189-198

Grein F, Ramos AR, Venceslau SS, Pereira IA (2013) Unifying concepts in anaerobic respiration: insights from dissimilatory sulfur metabolism. *Biochimica et Biophysica Acta (BBA)-Bioenergetics* **1827**: 145-160

Hallam SJ, Putnam N, Preston CM, Detter JC, Rokhsar D, Richardson PM, DeLong EF (2004) Reverse methanogenesis: testing the hypothesis with environmental genomics. *Science* **305**: 1457-1462

Haroon MF, Hu S, Shi Y, Imelfort M, Keller J, Hugenholtz P, Yuan Z, Tyson GW (2013a) Anaerobic oxidation of methane coupled to nitrate reduction in a novel archaeal lineage. *Nature* **500**: 567-570

Haroon MF, Hu SH, Shi Y, Imelfort M, Keller J, Hugenholtz P, Yuan ZG, Tyson GW (2013b) Anaerobic oxidation of methane coupled to nitrate reduction in a novel archaeal lineage. *Nature* **500**: 567-570

Hinrichs K-U, Hayes JM, Sylva SP, Brewer PG, DeLong EF (1999) Methane-consuming archaeobacteria in marine sediments. *Nature* **398**: 802-805

Hoehler TM, Alperin MJ, Albert DB, Martens CS (1994) Field and laboratory studies of methane oxidation in an anoxic marine sediment: Evidence for a methanogen-sulfate reducer consortium. *Global Biogeochemical Cycles* **8**: 451-463

Holler T, Widdel F, Knittel K, Amann R, Kellermann MY, Hinrichs K-U, Teske A, Boetius A, Wegener G (2011) Thermophilic anaerobic oxidation of methane by marine microbial consortia. *The ISME journal* **5**: 1946-1956

Huson DH, Auch AF, Qi J, Schuster SC (2007) MEGAN analysis of metagenomic data. *Genome research* **17**: 377-386

Hyatt D, Chen G-L, LoCascio PF, Land ML, Larimer FW, Hauser LJ (2010) Prodigal: prokaryotic gene recognition and translation initiation site identification. *BMC bioinformatics* **11**: 1

Johnson EF, Mukhopadhyay B (2005) A new type of sulfite reductase, a novel coenzyme F420-dependent enzyme, from the methanarchaeon *Methanocaldococcus jannaschii*. *Journal of Biological Chemistry* **280**: 38776-38786

Johnson EF, Mukhopadhyay B (2008a) Coenzyme F420-dependent sulfite reductase-enabled sulfite detoxification and use of sulfite as a sole sulfur source by *Methanococcus maripaludis*. *Applied and environmental microbiology* **74**: 3591-3595

Johnson EF, Mukhopadhyay B (2008b) A novel coenzyme F420 dependent sulfite reductase and a small sulfite reductase in methanogenic archaea. *Microbial sulfur metabolism*: 202-216

Karst SM, Kirkegaard RH, Albertsen M (2016) mmgenome: a toolbox for reproducible genome extraction from metagenomes. *bioRxiv*: 059121

Kaster A-K, Moll J, Parey K, Thauer RK (2011) Coupling of ferredoxin and heterodisulfide reduction via electron bifurcation in hydrogenotrophic methanogenic archaea. *Proceedings of the National Academy of Sciences* **108**: 2981-2986

Kleindienst S, Ramette A, Amann R, Knittel K (2012) Distribution and in situ abundance of sulfate-reducing bacteria in diverse marine hydrocarbon seep sediments. *Environmental microbiology* **14**: 2689-2710

Kletzin A, Heimerl T, Flechsler J, van Niftrik L, Rachel R, Klingl A (2015) Cytochromes c in Archaea: distribution, maturation, cell architecture, and the special case of *Ignicoccus hospitalis*. *Frontiers in microbiology* **6**: 439

Knittel K, Boetius A (2009) Anaerobic oxidation of methane: progress with an unknown process. *Annual review of microbiology* **63**: 311-334

Knittel K, Lösekann T, Boetius A, Kort R, Amann R (2005) Diversity and distribution of methanotrophic archaea at cold seeps. *Applied and environmental microbiology* **71**: 467-479

Konstantinidis KT, Rossello-Mora R, Amann R (2017) Uncultivated microbes in need of their own taxonomy. *Isme Journal*

Kopylova E, Noé L, Touzet H (2012) SortMeRNA: fast and accurate filtering of ribosomal RNAs in metatranscriptomic data. *Bioinformatics* **28**: 3211-3217

Krukenberg V, Harding K, Richter M, Glöckner FO, Gruber-Vodicka HR, Adam B, Berg JS, Knittel K, Tegetmeyer HE, Boetius A (2016) *Candidatus Desulfofervidus auxilii*, a hydrogenotrophic sulfate-reducing bacterium involved in the thermophilic anaerobic oxidation of methane. *Environmental microbiology*

Kumagai H, Fujiwara T, Matsubara H, Saeki K (1997) Membrane localization, topology, and mutual stabilization of the rnfABC gene products in *Rhodobacter capsulatus* and implications for a new family of energy-coupling NADH oxidoreductases. *Biochemistry* **36**: 5509-5521

Lagesen K, Hallin P, Rødland EA, Stærfeldt H-H, Rognes T, Ussery DW (2007) RNAmmer: consistent and rapid annotation of ribosomal RNA genes. *Nucleic Acids Research* **35**: 3100-3108

Langmead B, Salzberg SL (2012) Fast gapped-read alignment with Bowtie 2. *Nature methods* **9**: 357-359

Li Q, Li L, Rejtar T, Lessner DJ, Karger BL, Ferry JG (2006) Electron transport in the pathway of acetate conversion to methane in the marine archaeon *Methanosarcina acetivorans*. *Journal of Bacteriology* **188**: 702-710

Lösekann T, Knittel K, Nadalig T, Fuchs B, Niemann H, Boetius A, Amann R (2007) Diversity and abundance of aerobic and anaerobic methane oxidizers at the Haakon Mosby Mud Volcano, Barents Sea. *Applied and environmental microbiology* **73**: 3348-3362

- Lovley DR (2016) Happy together: microbial communities that hook up to swap electrons. *The ISME journal*
- Ludwig W, Strunk O, Westram R, Richter L, Meier H, Buchner A, Lai T, Steppi S, Jobb G, Förster W (2004) ARB: a software environment for sequence data. *Nucleic Acids Research* **32**: 1363-1371
- Mardanov A, Beletsky A, Kadnikov V, Slobodkin A, Ravin N (2016) Genome analysis of *Thermosulfurimonas dismutans*, the first thermophilic sulfur-disproportionating bacterium of the phylum Thermodesulfobacteria. *Frontiers in microbiology* **7**: 950
- Martens CS, Berner RA (1974) Methane production in the interstitial waters of sulfate-depleted marine sediments. *Science* **185**: 1167-1169
- Martinez RJ, Mills HJ, Story S, Sobecky PA (2006) Prokaryotic diversity and metabolically active microbial populations in sediments from an active mud volcano in the Gulf of Mexico. *Environmental microbiology* **8**: 1783-1796
- McGlynn SE, Chadwick GL, Kempes CP, Orphan VJ (2015) Single cell activity reveals direct electron transfer in methanotrophic consortia. *Nature* **526**: 531-535
- Meyerdierks A, Kube M, Kostadinov I, Teeling H, Glöckner FO, Reinhardt R, Amann R (2010) Metagenome and mRNA expression analyses of anaerobic methanotrophic archaea of the ANME-1 group. *Environmental microbiology* **12**: 422-439
- Meyerdierks A, Kube M, Lombardot T, Knittel K, Bauer M, Glöckner FO, Reinhardt R, Amann R (2005) Insights into the genomes of archaea mediating the anaerobic oxidation of methane. *Environmental microbiology* **7**: 1937-1951
- Michaelis W, Seifert R, Nauhaus K, Treude T, Thiel V, Blumenberg M, Knittel K, Gieseke A, Peterknecht K, Pape T (2002) Microbial reefs in the Black Sea fueled by anaerobic oxidation of methane. *Science* **297**: 1013-1015
- Mills HJ, Martinez RJ, Story S, Sobecky PA (2005) Characterization of microbial community structure in Gulf of Mexico gas hydrates: comparative analysis of DNA-and RNA-derived clone libraries. *Applied and environmental microbiology* **71**: 3235-3247
- Milucka J, Ferdelman TG, Polerecky L, Franzke D, Wegener G, Schmid M, Lieberwirth I, Wagner M, Widdel F, Kuypers MM (2012) Zero-valent sulphur is a key intermediate in marine methane oxidation. *Nature*
- Milucka J, Widdel F, Shima S (2013) Immunological detection of enzymes for sulfate reduction in anaerobic methane-oxidizing consortia. *Environmental microbiology* **15**: 1561-1571
- Mortazavi A, Williams BA, McCue K, Schaeffer L, Wold B (2008) Mapping and quantifying mammalian transcriptomes by RNA-Seq. *Nature methods* **5**: 621-628

Mowat CG, Rothery E, Miles CS, McIver L, Doherty MK, Drewette K, Taylor P, Walkinshaw MD, Chapman SK, Reid GA (2004) Octaheme tetrathionate reductase is a respiratory enzyme with novel heme ligation. *Nature structural & molecular biology* **11**: 1023

Nauhaus K, Albrecht M, Elvert M, Boetius A, Widdel F (2007) In vitro cell growth of marine archaeal-bacterial consortia during anaerobic oxidation of methane with sulfate. *Environmental microbiology* **9**: 187-196

Nauhaus K, Boetius A, Krüger M, Widdel F (2002) In vitro demonstration of anaerobic oxidation of methane coupled to sulphate reduction in sediment from a marine gas hydrate area. *Environmental microbiology* **4**: 296-305

Nauhaus K, Treude T, Boetius A, Krüger M (2005) Environmental regulation of the anaerobic oxidation of methane: a comparison of ANME-I and ANME-II communities. *Environmental microbiology* **7**: 98-106

Niemann H, Lösekann T, De Beer D, Elvert M, Nadalig T, Knittel K, Amann R, Sauter EJ, Schlüter M, Klages M (2006) Novel microbial communities of the Haakon Mosby mud volcano and their role as a methane sink. *Nature* **443**: 854-858

Orphan VJ, House CH, Hinrichs K-U, McKeegan KD, DeLong EF (2002) Multiple archaeal groups mediate methane oxidation in anoxic cold seep sediments. *Proceedings of the National Academy of Sciences* **99**: 7663-7668

Pachiadaki MG, Lykousis V, Stefanou EG, Kormas KA (2010) Prokaryotic community structure and diversity in the sediments of an active submarine mud volcano (Kazan mud volcano, East Mediterranean Sea). *FEMS Microbiology Ecology* **72**: 429-444

Parks DH, Imelfort M, Skennerton CT, Hugenholtz P, Tyson GW (2015) CheckM: assessing the quality of microbial genomes recovered from isolates, single cells, and metagenomes. *Genome research* **25**: 1043-1055

Pernthaler A, Dekas AE, Brown CT, Goffredi SK, Embaye T, Orphan VJ (2008) Diverse syntrophic partnerships from deep-sea methane vents revealed by direct cell capture and metagenomics. *Proceedings of the National Academy of Sciences* **105**: 7052-7057

Pernthaler A, Pernthaler J, Amann R (2002) Fluorescence in situ hybridization and catalyzed reporter deposition for the identification of marine bacteria. *Applied and environmental microbiology* **68**: 3094-3101

Pruesse E, Peplies J, Glöckner FO (2012) SINA: accurate high-throughput multiple sequence alignment of ribosomal RNA genes. *Bioinformatics* **28**: 1823-1829

Quast C, Pruesse E, Yilmaz P, Gerken J, Schweer T, Yarza P, Peplies J, Glöckner FO (2013) The SILVA ribosomal RNA gene database project: improved data processing and web-based tools. *Nucleic Acids Research* **41**: D590-D596

Quinlan AR, Hall IM (2010) BEDTools: a flexible suite of utilities for comparing genomic features. *Bioinformatics* **26**: 841-842

Rabus R, Venceslau SS, Wöhlbrand L, Voordouw G, Wall JD, Pereira IA (2015) Chapter Two-A post-genomic view of the ecophysiology, catabolism and biotechnological relevance of sulphate-reducing prokaryotes. *Advances in microbial physiology* **66**: 55-321

Reeburgh WS (2007) Oceanic methane biogeochemistry. *Chemical reviews* **107**: 486-513

Robinson MD, McCarthy DJ, Smyth GK (2010) edgeR: a Bioconductor package for differential expression analysis of digital gene expression data. *Bioinformatics* **26**: 139-140

Rodriguez-R LM, Konstantinidis KT. (2016) The enveomics collection: a toolbox for specialized analyses of microbial genomes and metagenomes. PeerJ Preprints.

Ruff SE, Biddle JF, Teske AP, Knittel K, Boetius A, Ramette A (2015) Global dispersion and local diversification of the methane seep microbiome. *Proceedings of the National Academy of Sciences* **112**: 4015-4020

Scheller S, Goenrich M, Boecher R, Thauer RK, Jaun B (2010) The key nickel enzyme of methanogenesis catalyses the anaerobic oxidation of methane. *Nature* **465**: 606-608

Scheller S, Yu H, Chadwick GL, McGlynn SE, Orphan VJ (2016) Artificial electron acceptors decouple archaeal methane oxidation from sulfate reduction. *Science* **351**: 703-707

Schlegel K, Welte C, Deppenmeier U, Müller V (2012) Electron transport during acetoclastic methanogenesis by *Methanosarcina acetivorans* involves a sodium-translocating Rnf complex. *FEBS Journal* **279**: 4444-4452

Schreiber L, Holler T, Knittel K, Meyerdierks A, Amann R (2010) Identification of the dominant sulfate-reducing bacterial partner of anaerobic methanotrophs of the ANME-2 clade. *Environmental microbiology* **12**: 2327-2340

Schwanhäusser B, Busse D, Li N, Dittmar G, Schuchhardt J, Wolf J, Chen W, Selbach M (2011) Global quantification of mammalian gene expression control. *Nature* **473**: 337

Sean R. Eddy (2015) <http://hmmer.org/>.

Seemann T (2014) Prokka: rapid prokaryotic genome annotation. *Bioinformatics* **30**: 2068-2069

Skennerton CT, Chourey K, Iyer R, Hettich RL, Tyson GW, Orphan VJ (2017) Methane-Fueled Syntrophy through Extracellular Electron Transfer: Uncovering the Genomic Traits Conserved within Diverse Bacterial Partners of Anaerobic Methanotrophic Archaea. *mBio* **8**: e00530-00517

Steudel R, Göbel T, Holdt G (1988) The molecular composition of hydrophilic sulfur sols prepared by acid decomposition of thiosulfate [1]. *Zeitschrift für Naturforschung B* **43**: 203-218

Summers ZM, Fogarty HE, Leang C, Franks AE, Malvankar NS, Lovley DR (2010) Direct exchange of electrons within aggregates of an evolved syntrophic coculture of anaerobic bacteria. *Science* **330**: 1413-1415

Thauer RK (1998) Biochemistry of methanogenesis: a tribute to Marjory Stephenson: 1998 Marjory Stephenson Prize Lecture. *Microbiology* **144**: 2377-2406

Thauer RK (2011) Anaerobic oxidation of methane with sulfate: on the reversibility of the reactions that are catalyzed by enzymes also involved in methanogenesis from CO₂. *Current opinion in microbiology* **14**: 292-299

Thauer RK, Kaster A-K, Seedorf H, Buckel W, Hedderich R (2008) Methanogenic archaea: ecologically relevant differences in energy conservation. *Nature Reviews Microbiology* **6**: 579-591

Thauer RK, Stackebrandt E, Hamilton WA (2007) Energy metabolism and phylogenetic diversity of sulphate-reducing bacteria. *Sulphate-reducing bacteria: Environmental and engineered systems*: 1-37

Tietze M, Beuchle A, Lamla I, Orth N, Dehler M, Greiner G, Beifuss U (2003) Redox Potentials of Methanophenazine and CoB-S-S-CoM, Factors Involved in Electron Transport in Methanogenic Archaea. *Chembiochem* **4**: 333-335

Walker DJ, Adhikari RY, Holmes DE, Ward JE, Woodard TL, Nevin KP, Lovley DR (2017) Electrically Conductive Pili from Pilin Genes of Phylogenetically Diverse Microorganisms. *bioRxiv*: 118059

Wang F-P, Zhang Y, Chen Y, He Y, Qi J, Hinrichs K-U, Zhang X-X, Xiao X, Boon N (2014) Methanotrophic archaea possessing diverging methane-oxidizing and electron-transporting pathways. *The ISME journal* **8**: 1069-1078

Wegener G, Krukenberg V, Riedel D, Tegetmeyer HE, Boetius A (2015) Intercellular wiring enables electron transfer between methanotrophic archaea and bacteria. *Nature* **526**: 587-590

Wegener G, Krukenberg V, Ruff SE, Kellermann MY, Knittel K (2016) Metabolic capabilities of microorganisms involved in and associated with the anaerobic oxidation of methane. *Frontiers in microbiology* **7**

Wegener G, Niemann H, Elvert M, Hinrichs KU, Boetius A (2008) Assimilation of methane and inorganic carbon by microbial communities mediating the anaerobic oxidation of methane. *Environmental microbiology* **10**: 2287-2298

Welte C, Deppenmeier U (2011) Membrane-bound electron transport in *Methanosaeta thermophila*. *Journal of Bacteriology* **193**: 2868-2870

Wessels H, Gloerich J, van der Biezen E, Jetten M, Kartal B (2010) Liquid chromatography-mass spectrometry-based proteomics of *Nitrosomonas*. *Methods in enzymology* **486**: 465-482

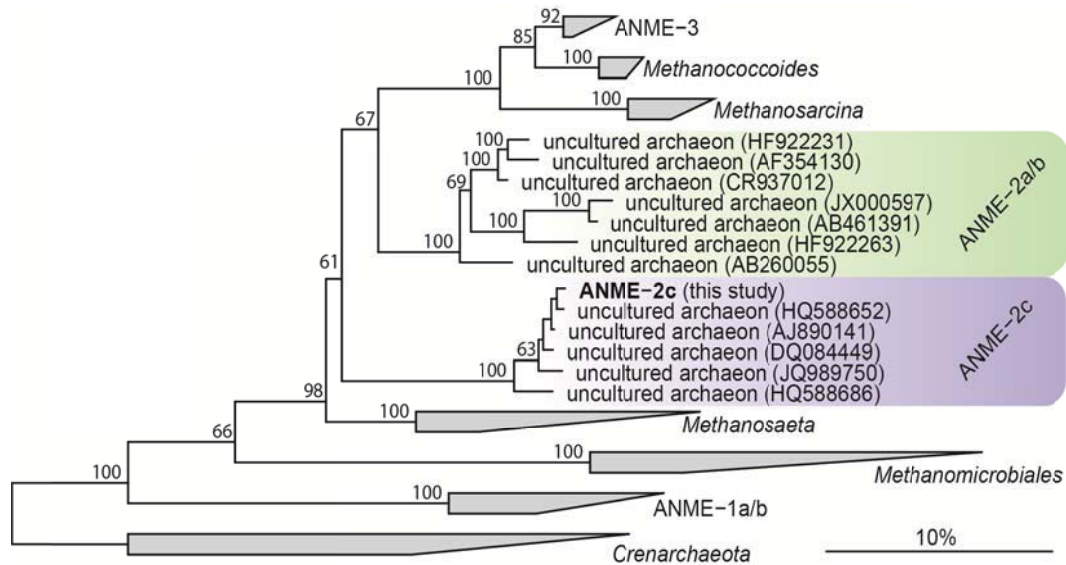
Widdel F, Bak F (1992) Gram-negative mesophilic sulfate-reducing bacteria. In *The prokaryotes*, pp 3352-3378. Springer

Widdel F, Musat F, Knittel K, Galushko A (2007) *Anaerobic degradation of hydrocarbons with sulphate as electron acceptor*: Cambridge, UK: Cambridge University Press.

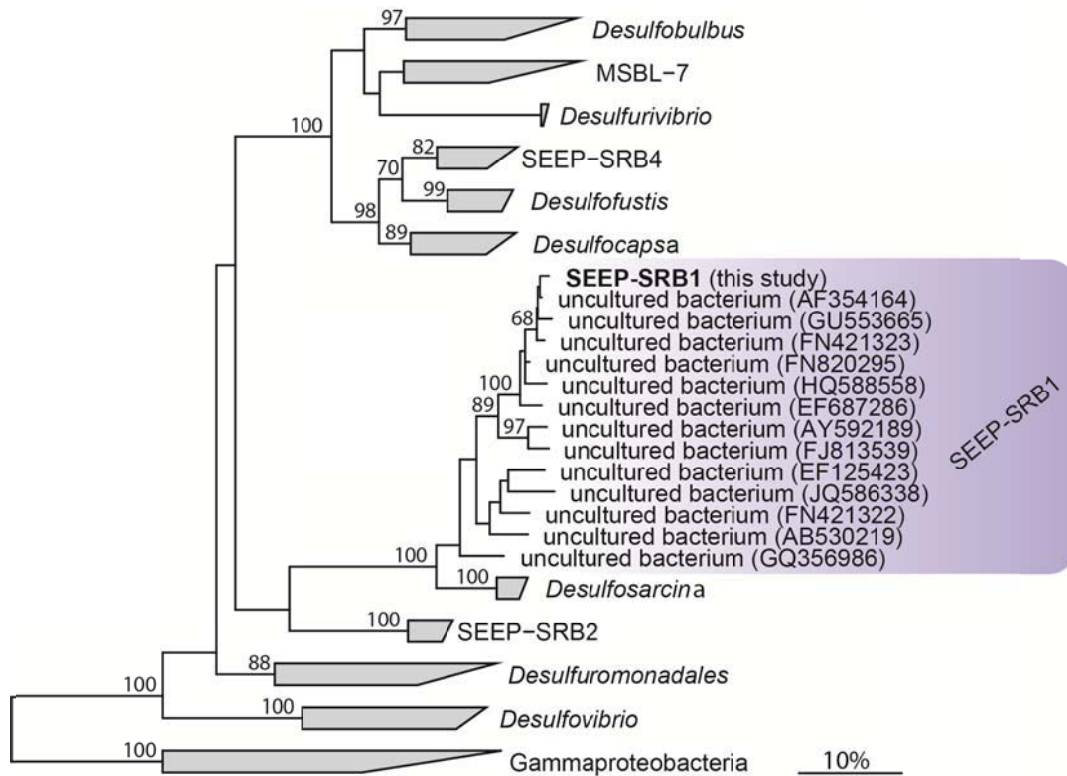
Zehnder A, Brock T (1979) Methane formation and methane oxidation by methanogenic bacteria. *Journal of Bacteriology* **137**: 420-432

Supplementary Information & Extended Data Tables

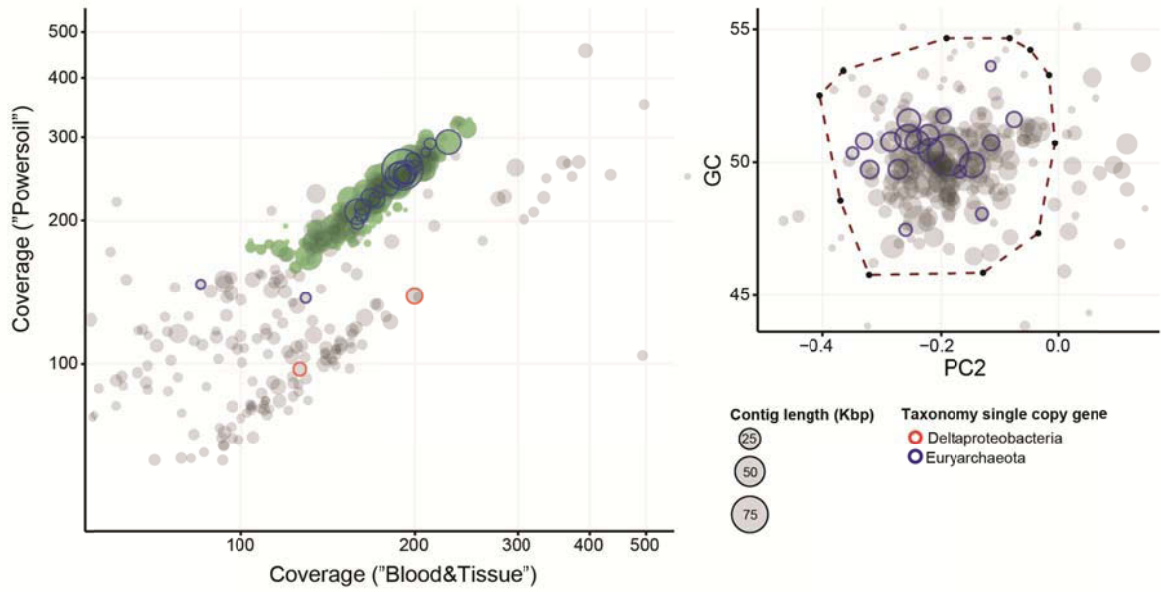
Supplementary Figures



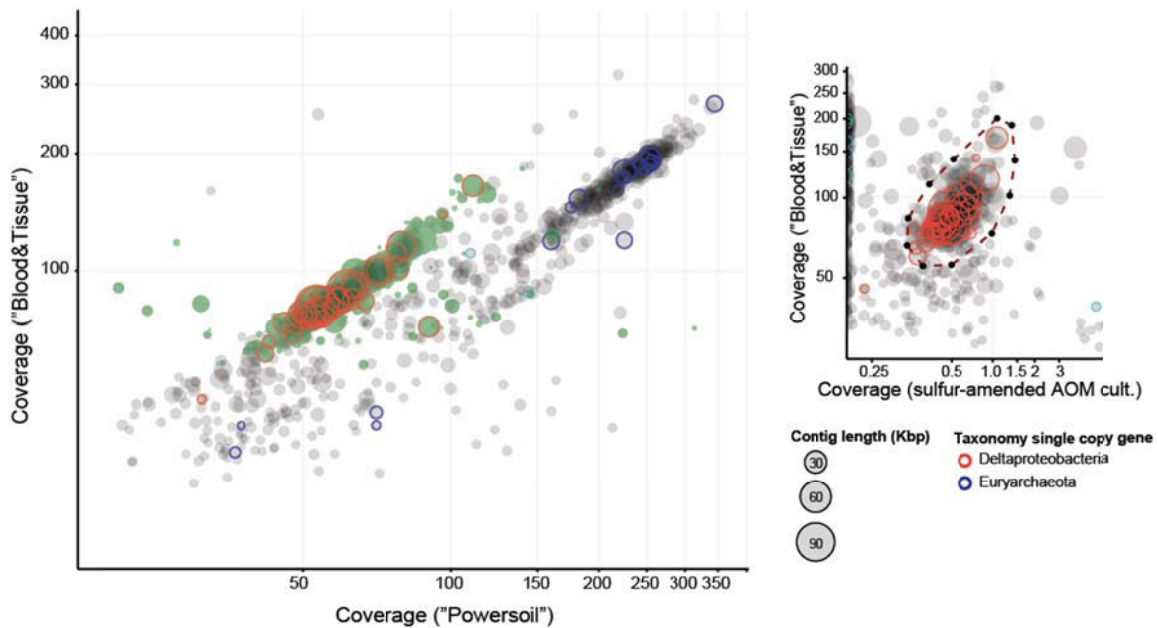
Supplementary Figure 1. Maximum likelihood phylogenetic tree (60 taxa) showing the phylogenetic affiliation of 16S rRNA gene retrieved from the ANME-2c genome. Tree calculation was performed using RAxML8 implemented in the ARB software package without constraining the alignment with a filter or weighting mask. Bootstrap values > 60 (out of 100) are shown in front of each node. The taxonomic affiliations indicated by the grouped taxa are based on the SILVA SSU reference database (release 123, (Pruesse et al, 2007)). 6 type strains diversely spread among *Crenarchaeota* were used as outgroup. Nucleotide accession numbers are listed in brackets. The bar depicts an estimated nucleotide sequence divergence of 10%.



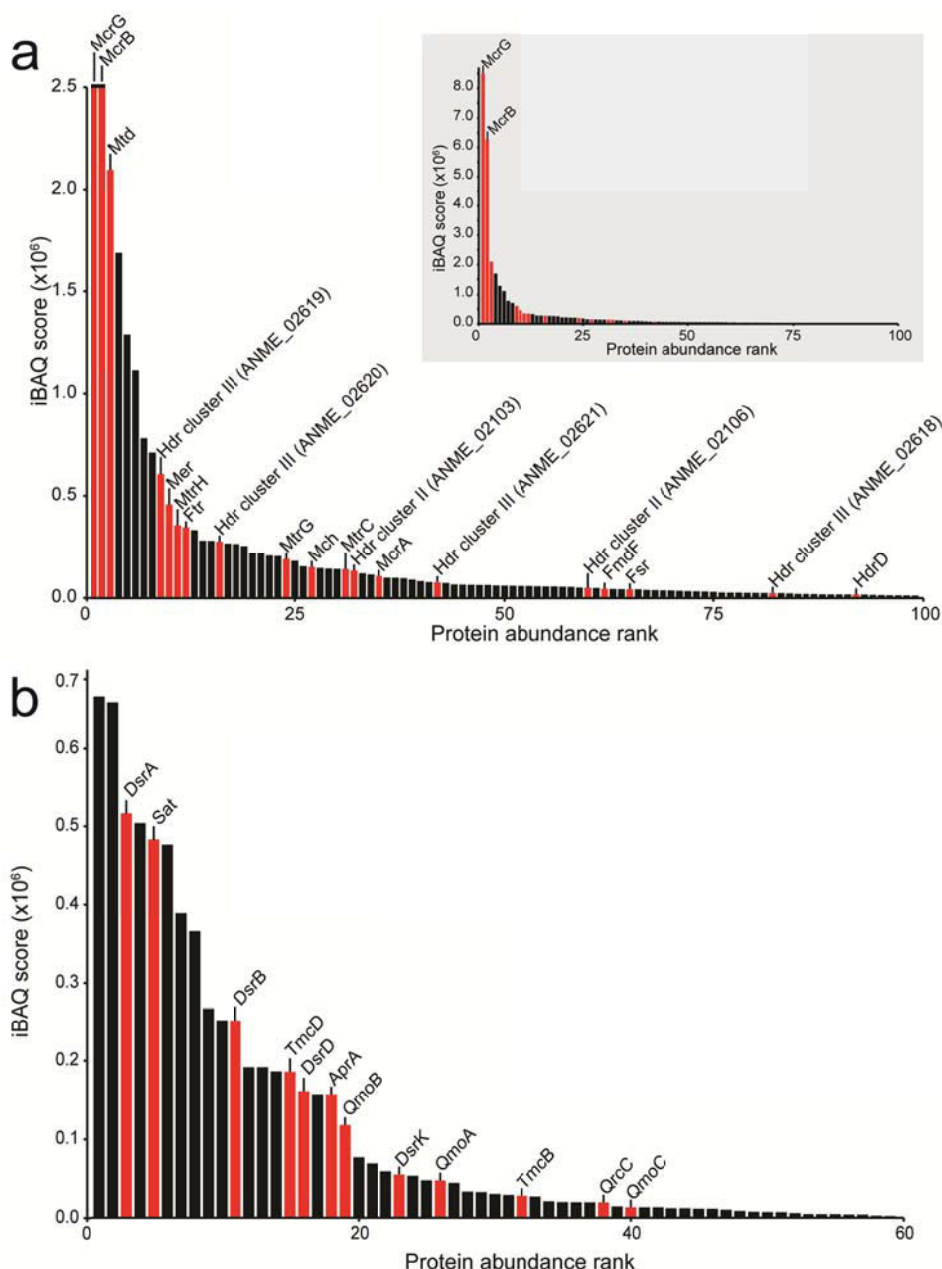
Supplementary Figure 2. Maximum likelihood phylogenetic tree (66 taxa) showing the phylogenetic affiliation of 16S rRNA gene retrieved from the SEEP-SRB1 genome. Tree calculation was performed using RAXML8 implemented in the ARB software package without constraining the alignment with a filter or weighting mask. Bootstrap values > 60 (out of 100) are shown in front of each node. The taxonomic affiliations indicated by the grouped taxa are based on the SILVA SSU reference database (release 123, (Pruesse et al, 2007)). Nine type strains diversely spread among *Gammaproteobacteria* were used as outgroup. Nucleotide accession numbers are listed in brackets. The bar depicts an estimated nucleotide sequence divergence of 10%.



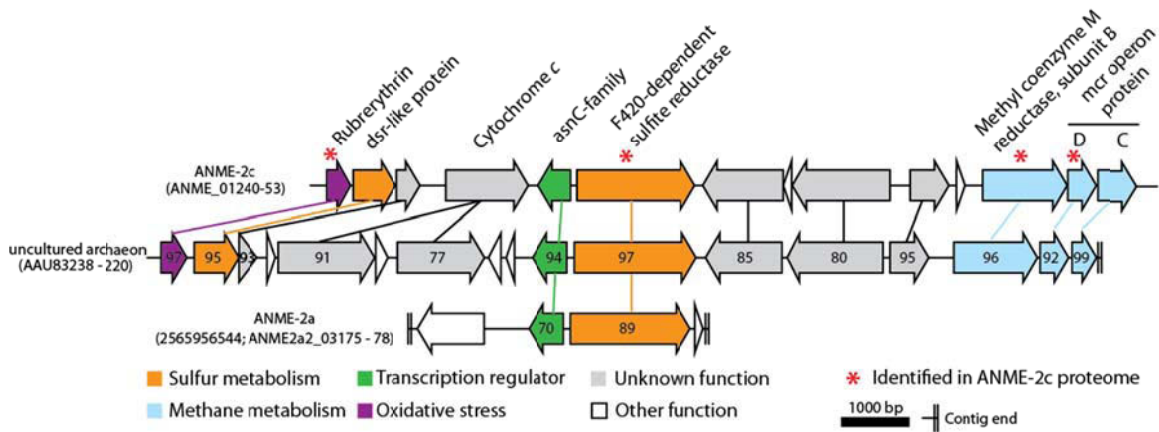
Supplementary Figure 3. Metagenomic binning of ANME-2c genome. Metagenomic contigs obtained from the “Powersoil” assembly were binned in a first step using differential coverage between sequencing datasets “Powersoil” and “Blood&Tissue”. This preliminary bin was refined based on tetranucleotide frequency and GC content (small plot). In total 198 contigs were extracted (filled green circles). Each circle represents a contig with size proportional to contig length and color indicates taxonomic contig classification (based on single copy genes).



Supplementary Figure 4. Metagenomic binning of SEEP-SRB1 genome. Metagenomic contigs of the “Blood&Tissue” assembly were binned based on differential coverage in sequencing datasets “Powersoil” and “Blood&Tissue”. The preliminary bin was refined using contig coverage from metagenomic reads obtained from a sulfur-amended S-AOM culture and the “Blood&Tissue” dataset (small plot). In total 246 contigs were extracted (filled green circles). Each circle represents a contig with size proportional to contig length and color indicates taxonomic contig classification (based on single copy genes).



Supplementary Figure 5. Metaproteome-inferred protein abundance levels (by iBAQ score) of ANME-2c and SEEP-SRB1. a, Displayed are the 100 most abundant proteins of ANME-2c inferred from their intensity based absolute quantification (iBAQ) values identified in the metaproteome. Indicated in red are proteins involved in reverse methanogenesis and proteins found in Hdr-associated gene clusters (see Supplementary Table 5). Inline figure shows the same data with full-scale y-axis. b, 60 most abundant proteins of SEEP-SRB1 identified in the metaproteome. In red, proteins involved in dissimilatory sulfur metabolism and associated electron donating complexes are shown.



Supplementary Figure 6. Comparison of the gene neighborhood surrounding sulfite reductases genes of ANME-2c and other ANME. Depicted are the genomic neighborhoods surrounding two sulfite reductases and octaheme cytochrome *c* of ANME-2c as well as homologous regions identified in other ANME (ANME-2a genome (Wang et al, 2014) and fragment of an uncultured archaeon assigned to ANME (GZfos27A8; (Hallam et al, 2004)). Arrows represent predicted genes (with gene annotation on top); connecting lines depict amino-acid sequence to respective genes of ANME-2c (in %, shown within gene arrows). Expressed genes of ANME-2c are indicated by a red star.

OTR <i>Shewanella oneidensis</i> (1SP3)	1 ANPHKDV LKGPFTTGSEVTTQCLTCHEEQATDMMKTS HWTW - - ELEQKLPDR 50
ANME OTR-like protein (ANME_01244)	31 AASAAEGTHAGIAEYKGAET-CLACHQEEGEGFVTSIHNTWMGEATHVVGKE 81
OTR <i>Shewanella oneidensis</i> (1SP3)	51 TVVRGK KNS I NNFVAISSNEPRCTSC H AGYGWKDN-TFDF - - KDKT - - - - K 95
ANME OTR-like protein (ANME_01244)	82 GNMTGKVVGVNEF CVGAKSNEAF CGKCHAGSGTCCNCTCDCAAKKMICPIEK 133
OTR <i>Shewanella oneidensis</i> (1SP3)	96 VDCLICHDTTGTYYKDPAGAGEPMAKLDLAKIAQNVGAPVRDNCGSCHFYGG 147
ANME OTR-like protein (ANME_01244)	134 IDCLICH - - APNYKK - TATG - PDPS IDATAAARAVGLPTREMCLRCHGTAG 180
OTR <i>Shewanella oneidensis</i> (1SP3)	148 GGD AVKHGDLDSMAYPDKATDVHMDS DGNNFQCQNCHTTEKHQISGNAMGV 199
ANME OTR-like protein (ANME_01244)	181 GGDNNKRGDIELAMGADAVSRDL DVHMSA - GMTQDCHVFIDHHVSGRGM DL 231
OTR <i>Shewanella oneidensis</i> (1SP3)	200 SPGGIDH-IGCE - - NCHDSAPHSNKKL - NHTATVACQTCHIPFFAKNEPTK 247
ANME OTR-like protein (ANME_01244)	232 RIDDTDFLVTCDKKNCHGSEPHYEGSMY NQHTDRIYCTACHVTAYGKVVQTV E 283
OTR <i>Shewanella oneidensis</i> (1SP3)	248 MQWDWSTAGDDKPE TVDQY GKHTYQKKGNFVWEKMKVPQYAWYNGTANAY - 298
ANME OTR-like protein (ANME_01244)	284 MSRDW - - GY - RPPN - DNNALRMTMYTP - YIVRESNPAPIHVWWRWSEILD 329
OTR <i>Shewanella oneidensis</i> (1SP3)	299 MAGDKM - DSNVVTKLTYPMGDINDAKAKIYPFKVHTGKQIYDKLKNIFITPK 349
ANME OTR-like protein (ANME_01244)	330 LADPAVPDS DGFVMAKPVGGIDNPASKIYSARLHLGRQPWD - - - - - 371
OTR <i>Shewanella oneidensis</i> (1SP3)	350 TYGKGGYWSEFDWNLAAKLGMEANPTMLEKGIKYSGEYDFAATEMWWRI NHM 401
ANME OTR-like protein (ANME_01244)	372 - - - GAHMLPFK - TMTVLMSDNMTQALFESTGKIYDPIQYVDAKRYMGLFHG 418
OTR <i>Shewanella oneidensis</i> (1SP3)	402 VSPKEQALNCNDCHNKGTRL DWQALGYQGDP MNKQGP KHKQ 443
ANME OTR-like protein (ANME_01244)	419 VSPKDDALTCQDCHEDHV - IDFEALGY - - DVEK DASGNLISA 457

Supplementary Figure 7. Pairwise alignment of octaheme tetrathionate reductase (OTR) of *Shewanella oneidensis* MR-1 and OTR-like protein of ANME-2c. Amino-acid sequences of *Shewanella oneidensis* MR-1 OTR (PDB accession 1SP3) and OTR-like protein of ANME-2c (ANME_01244) were pairwise aligned using JalView (Waterhouse et al, 2009). Heme-binding motifs are indicated with roman numerals (I-VIII) and residues of the active site of *Shewanella* OTR (according to (Mowat et al, 2004)) are shown in blue.

Supplementary Tables

Supplementary Table 1. Summary of sequencing datasets used in this study.

Sequencing dataset	Sequencing technology	No. of (paired-end) reads
AOM Powersoil	MiSeq, 2x250 bp	7,594,147
AOM Blood&Tissue	MiSeq, 2x250 bp	5,895,760
AOM, sulfur-amended	IonTorrent PGM, 318v2 chip	5,300,000
AOM transcriptome	IonTorrent PGM, 318v2 chip	4,386,143

Supplementary Table 2. Overview of used oligonucleotide probes. Listed are target groups, probe sequence, formamide concentration in the hybridization buffer and references.

Probe	Target group	Probe sequence (5'- 3')	Formamide % [v/v]	Reference
DSS-658	<i>Desulfosarcina/</i> <i>Desulfococcus</i> group	TCC ACT TCC CTC TCC CAT	50	(Manz et al, 1998)
ANME-2-538	ANME-2	GGC TAC CAC TCG GGC CGC	50	(Treude et al, 2005)

Supplementary Table 3. Multiheme cytochromes c encoded in the ANME-2c genome (11 total). Overview of number of heme binding motifs (identified by CxxCH motif), PfamA domain prediction (highest scoring hit by bit score), best blastp hit against NCBI Refseq database (by e-value, cutoff 1e-6), normalized gene transcription (in RPKM) and intensity based absolute quantification (iBAQ) values (ND: not detected).

ORF	# of CxxCH motifs	Pfam domain prediction (accession) ¹	Best blastp hit against NCBI Refseq			RPKM	iBAQ score
			% Ident. / % Query cov.	Expected (E)-value	Subject description (accession)		
ANME_01820	31	NosD (PF05048.12)	26 / 45	7e-24	hypothetical protein [Ferroglobus placidus] (WP_012965185.1)	48	263
ANME_02055	17	Cytochrome_C7 (PF14522.5)	34 / 57	5e-108	hypothetical protein [Ca. Methanoperedens nitroreducens] (WP_081810296.1)	65	ND
ANME_02056	16	Cytochrome_C7 (PF14522.5)	37 / 89	1e-165	hypothetical protein [Ca. Methanoperedens nitroreducens] (WP_048088239.1)	171	ND
ANME_02168	16	Cytochrom_c3_2 (PF14537.5)	32 / 96	1e-28	hypothetical protein [Malonomonas rubra] (WP_072904729.1)	117	ND
ANME_02775	13	Cytochrome_C7 (PF14522.5)	28 / 91	7e-17	hypothetical protein [Geoalkalibacter subterraneus] (WP_052464494.1)	3249	ND
ANME_01594	11	Cytochrom_c3_2 (PF14537.5)	39 / 94	7e-56	hypothetical protein [Ca. Methanoperedens nitroreducens] (WP_048089353.1)	3,322	ND
ANME_02604	11	Cytochrom_c3_2 (PF14537.5)	39 / 96	4e-61	hypothetical protein [Ca. Methanoperedens nitroreducens] (WP_048089353.1)	1124	ND
ANME_00931	8	Multi-haem_cyto (PF13447.5)	49 / 91	3e-145	cytochrome c [Geoglobus ahangari] (WP_048094836.1)	39	ND
ANME_01244	7	Cytochrome_cB (PF11783.7)	34 / 78	3e-71	hypothetical protein [Carboxydotherrnus islandicus] (WP_075864688.1)	277	ND
ANME_02229	3	Cytochrome_C7 (PF14522.5)	24 / 93	1e-11	hypothetical protein [Archaeoglobus veneficus] (WP_013683060.1)	274	ND
ANME_02742	3	NA	30 / 99	3e-24	hypothetical protein [Candidatus Methanoperedens nitroreducens] (WP_048092729.1)	61	ND

¹Using hmmscan (Eddy et al, 2013) against PfamA with e-value cutoff 1e-6; only best hit is shown

Supplementary Table 4. Multiheme cytochromes c encoded in the SEEP-SRB1 genome (25 total). Overview of number of heme binding motifs (identified by CxxCH motif), PfamA domain prediction (highest scoring hit by bit score), best blastp hit against NCBI Refseq database (by e-value, cutoff 1e-6), normalized gene transcription (in RPKM) and intensity based absolute quantification (iBAQ) values (ND: not detected).

ORF	# of CxxCH motifs	PfamA domain prediction (accession) ¹	Best blastp hit against NCBI Refseq			RPKM	iBAQ score
			% Identity / % Query coverage	Expected (E)-value	Subject description (accession)		
DSS_03491	26	Paired_CXXCH_1 (PF09699.9)	42 / 98	0.0	hypothetical protein [Candidatus Desulfofervidus auxilii] (WP_066060701.1)	51	ND
DSS_02216	20	Cytochrome_C7 (PF14522.5)	42 / 99	4e-119	hypothetical protein [Desulfoformonas acetoxidans] (WP_006002535.1)	160	ND
DSS_03490	16	Paired_CXXCH_1 (PF09699.9)	38 / 96	9e-89	hypothetical protein [Candidatus Desulfofervidus auxilii] (WP_066060703.1)	40	ND
DSS_02214	12	Cytochrom_c3_2 (PF14537.5)	41 / 96	4e-71	hypothetical protein [Candidatus Desulfofervidus auxilii] (WP_066060678.1)	651	ND
DSS_02217	12	Cytochrom_c3_2 (PF14537.5)	52 / 70	2e-74	hypothetical protein [Desulfoformonas acetoxidans] (WP_006002534.1)	475	ND
DSS_03476	12	Paired_CXXCH_1 (PF09699.9)	51 / 88	1e-82	hypothetical protein [Desulfoformonas acetoxidans] (WP_005999026.1)	767	ND
DSS_03488	12	Paired_CXXCH_1 (PF09699.9)	49 / 79	1e-77	hypothetical protein [Thermosulfidbacter takaii] (WP_068548847.1)	112	ND
DSS_03475	11	Cytochrom_c3_2 (PF14537.5)	50 / 97	1e-84	hypothetical protein [Candidatus Desulfofervidus auxilii] (WP_066060676.1)	642	ND
DSS_00313	8	Cytochrom_c3_2 (PF14537.5)	72 / 99	0.0	hypothetical protein [Desulfofobacter postgatei] (WP_004072403.1)	236	ND
DSS_01102	8	Multi-haem_cyto (PF13447.5)	34 / 94	4e-62	cytochrome c [Geobacter sp. M18] (WP_041248644.1)	0	ND
DSS_03191	8	Multi-haem_cyto (PF13447.5)	98 / 80	0.0	cytochrome c [Desulfosarcina sp. Bu55] (WP_027353404.1)	280	ND
DSS_02872	7	Paired_CXXCH_1 (PF09699.9)	42 / 97	8e-85	hypothetical protein [Desulfoformonas acetoxidans] (WP_005999017.1)	126	ND
DSS_02125	6	Cytochrom_NNT (PF03264.13)	62 / 53	5e-59	beta-ketoacyl-ACP synthase [Desulfovibrio frigidus] (WP_034602861.1)	51	ND
DSS_02871	6	Paired_CXXCH_1 (PF09699.9)	45 / 99	1e-86	hypothetical protein [Thermodesulfator atlanticus] (WP_022853152.1)	555	ND
DSS_03485	6	Cytochrom_c3_2 (PF14537.5)	47 / 97	3e-101	hypothetical protein [Thermodesulfator autotrophicus] (WP_068541895.1)	646	ND
DSS_01051	5	Cytochrome_C7 (PF14522.5)	63 / 97	9e-110	cytochrome c [Spirochaeta odontotermitis] (WP_037561289.1)	2,102	ND
DSS_01938	5	Cytochrome_C554 (PF13435.5)	70 / 99	0.0	hypothetical protein [Candidatus Desulfofervidus auxilii] (WP_066060300.1)	0	ND
DSS_03484	5	Paired_CXXCH_1 (PF09699.9)	34 / 97	8e-47	hypothetical protein [Thermosulfidbacter takaii] (WP_068548872.1)	896	ND
DSS_03494	5	NA (NA)	26 / 91	4e-30	hypothetical protein [Geothalibacter subterraneus] (WP_040201254.1)	0	8782
DSS_00053	4	Cytochrom_CIII (PF02085.15)	46 / 98	2e-26	acidic cytochrome c3 [Desulfovibrio bizeriensis] (WP_078685818.1)	938	ND
DSS_02785	4	Cytochrom_CIII (PF02085.15)	74 / 100	2e-54	cytochrome c [Desulfosarcina sp. Bu55] (WP_027353763.1)	1,063	ND
DSS_03053	4	Cytochrom_CIII (PF02085.15)	55 / 93	9e-50	hypothetical protein [Desulfatirhabdium butyrivorans] (WP_051328492.1)	20,112	ND
DSS_03375	4	Cytochrom_c3_2 (PF14537.5)	53 / 87	1e-54	cytochrome C [Thermodesulfobacterium aggregans] (WP_059176285.1)	206	ND
DSS_03204	3	Cytochrome_C554 (PF13435.5)	72 / 96	1e-67	hypothetical protein [Desulfosarcina sp. Bu55] (WP_027354831.1)	986	ND
DSS_03477	3	Paired_CXXCH_1 (PF09699.9)	46 / 99	1e-63	hypothetical protein [Thermodesulfator atlanticus] (WP_022853152.1)	1,251	ND

¹ Using hmmscan against PfamA with e-value cutoff 1e-6; only best hit is shown

Supplementary Table 5. Comparison of heterodisulfide reductase related gene clusters encoded in the ANME-2c genome. Shown are the ANME-2c ORF identifier, the respective gene annotation, Hdr gene cluster identifier, best blastp hit (by e-value or bit-score) against NCBI non-redundant database, normalized gene transcription (in RPKM) and intensity based absolute quantification (iBAQ) values (ND: not detected).

ORF	Annotation	Hdr gene cluster identifier	Best blast hit against NCBI non-redundant protein database			RPKM	iBAQ score
			% Identity / % Query coverage	Expected (E)-value	Subject description (accession)		
ANME_01561	hdrA	I	66 / 99	0.0	hypothetical protein [Ca. Methanoperedens nitroreducens] (WP_052368903.1)	21	ND
ANME_01562	hdrB	I	71 / 94	7e-161	heterodisulfide reductase subunit HDRB [Methanosarcina mazei Go1] (AAM30676.1)	43	ND
ANME_01563	hdrC	I	63 / 93	4e-69	CoB--CoM heterodisulfide reductase subunit C [Methanosarcina sp. Ant1] (OEU41064.1)	14	ND
ANME_02102	hdrD	II	60 / 96	2e-150	iron-sulfur binding reductase [uncultured archaeon] (CAI64333.1)	826	ND
ANME_02103	hdrC	II	71 / 99	3e-88	probable heterodisulfide reductase chain C [uncultured archaeon] (CAI64334.1)	743	134,980
ANME_02104	hdrB	II	72 / 99	1e-161	heterodisulfide reductase subunit B [uncultured archaeon] (CAI64335.1)	895	ND
ANME_02105	hdrA	II	71 / 97	0.0	heterodisulfide reductase like protein, subunit A [uncultured archaeon] (CAI64336.1)	1,183	10,238
ANME_02106	mvhD	II	72 / 100	9e-75	methyl viologen-reducing hydrogenase delta chain [uncultured archaeon] (CAI64337.1)	1,748	51,224
ANME_02618	hdrA	III	69 / 99	0.0	disulfide reductase [Ca. Methanoperedens nitroreducens] (WP_081810234.1)	854	24,461
ANME_02619	mvhD	III	74 / 93	3e-78	methyl-viologen-reducing hydrogenase subunit delta [Ca. Methanoperedens nitroreducens] (WP_048091371.1)	1,005	610,470
ANME_02620	-	III	62 / 99	0.0	formate dehydrogenase, beta subunit [Candidatus Methanoperedens sp. BLZ1] (KPQ42894.1)	874	278,500
ANME_02621	-	III	51 / 98	2e-159	formate dehydrogenase like protein alpha chain [uncultured archaeon] (CAI64341.1)	1,365	77,228
ANME_02238	hdrD	-	56 / 99	4e-179	disulfide reductase [Methermicrococcus shengliensis] (WP_042686138.1)	2,187	17,449
ANME_02239	hdrE	-	46 / 98	5e-70	disulfide reductase [Methanosarcina sp. Ant1] (OEU43375.1)	1,444	ND

Extended Data Tables

Extended Data Table 1. Gene transcription (in RPKM) and expression (iBAQ score values) of selected ANME-2c genes.

Locus Tag	Product	Gene	RPKM	(iBAQ score)
Reverse methanogenesis				
ANME_01255	Methyl-coenzyme M reductase subunit alpha	mcrA	69751	108730
ANME_01254	Methyl-coenzyme M reductase subunit gamma	mcrG	62611	8498500
ANME_01252	Methyl-coenzyme M reductase II operon protein D	mcrD	57482	0
ANME_01253	Methyl-coenzyme M reductase I operon protein C	mcrC	47278	-
ANME_01251	Methyl-coenzyme M reductase subunit beta	mcrB	43094	6279000
ANME_00191	Tetrahydromethanopterin S-methyltransferase subunit A 1	mtrA1_1	5356	-
ANME_02416	Tetrahydromethanopterin S-methyltransferase subunit A 1	mtrA1_2	82	-
ANME_00192	Tetrahydromethanopterin S-methyltransferase subunit B	mtrB_1	4541	-
ANME_02415	Tetrahydromethanopterin S-methyltransferase subunit B	mtrB_2	116	-
ANME_00193	Tetrahydromethanopterin S-methyltransferase subunit C	mtrC_1	4496	142920
ANME_02414	Tetrahydromethanopterin S-methyltransferase subunit C	mtrC_2	85	-
ANME_00194	Tetrahydromethanopterin S-methyltransferase subunit D	mtrD_1	3789	-
ANME_02413	Tetrahydromethanopterin S-methyltransferase subunit D	mtrD_2	76	-
ANME_00195	Tetrahydromethanopterin S-methyltransferase subunit E	mtrE_1	3494	-
ANME_02412	Tetrahydromethanopterin S-methyltransferase subunit E	mtrE_2	82	-
ANME_00190	Tetrahydromethanopterin S-methyltransferase subunit F	mtrF_1	3460	-
ANME_02417	Tetrahydromethanopterin S-methyltransferase subunit F	mtrF_2	263	-
ANME_00189	Tetrahydromethanopterin S-methyltransferase subunit G	mtrG_1	5554	192810
ANME_02418	Tetrahydromethanopterin S-methyltransferase subunit G	mtrG_2	42	-
ANME_00188	Tetrahydromethanopterin S-methyltransferase subunit H	mtrH_1	4404	358820
ANME_02419	Tetrahydromethanopterin S-methyltransferase subunit H	mtrH_2	123	-
ANME_01600	5,10-methylenetetrahydromethanopterin reductase	mer_1	7815	461460
ANME_02420	5,10-methylenetetrahydromethanopterin reductase	mer_2	78	-
ANME_02010	F420-dependent methylenetetrahydromethanopterin dehydrogenase	Mtd	2687	2097600
ANME_00995	Methenyltetrahydromethanopterin cyclohydrolase	mch_2	1922	152900
ANME_00210	Methenyltetrahydromethanopterin cyclohydrolase	mch_1	243	-
ANME_00875	Formylmethanofuran--tetrahydromethanopterin formyltransferase	frt	1459	348430
ANME_00035	Molybdenum dependent formylmethanofuran dehydrogenase F	FmdF	2070	45492
ANME_00036	Molybdenum dependent formylmethanofuran dehydrogenase E	FmdE	648	-
ANME_00038	Molybdenum dependent formylmethanofuran dehydrogenase D	FmdD	74	-
ANME_00039	Molybdenum dependent formylmethanofuran dehydrogenase B	FmdB	137	-
ANME_00040	Molybdenum dependent formylmethanofuran dehydrogenase A	FmdA	65	-
ANME_00041	Tungsten dependent formylmethanofuran dehydrogenase C	FwdC	110	-
ANME_02722	Formylmethanofuran dehydrogenase operon gene G	FmdG	112	-
ANME_02723	Formylmethanofuran dehydrogenase B	FmdB	105	-
ANME_02724	Formylmethanofuran dehydrogenase D	FmdD	50	-

Locus Tag	Product	Gene	RPKM	(iBAQ score)
F420:H2 dehydrogenase				
ANME_01599	F(420)H(2) dehydrogenase subunit F	FpoF	2236	57780
ANME_01773	F(420)H(2) dehydrogenase subunit L	FpoL_1	22	-
ANME_01775	F(420)H(2) dehydrogenase subunit L	FpoL_2	23	-
ANME_01776	F(420)H(2) dehydrogenase subunit N	FpoN_1	23	-
ANME_02463	F(420)H(2) dehydrogenase subunit A	FpoA	580	20160
ANME_02464	F(420)H(2) dehydrogenase subunit B	FpoB	1514	-
ANME_02465	F(420)H(2) dehydrogenase subunit C	FpoC	2176	282960
ANME_02466	F(420)H(2) dehydrogenase subunit D	FpoD	1991	209950
ANME_02467	F(420)H(2) dehydrogenase subunit H	FpoH	803	-
ANME_02468	F(420)H(2) dehydrogenase subunit I	FpoI	2395	266070
ANME_02469	F(420)H(2) dehydrogenase subunit J	FpoJ_1	753	-
ANME_02470	F(420)H(2) dehydrogenase subunit J	FpoJ_2	1502	-
ANME_02471	F(420)H(2) dehydrogenase subunit K	FpoK	1874	-
ANME_02472	F(420)H(2) dehydrogenase subunit L	FpoL_3	1503	-
ANME_02473	F(420)H(2) dehydrogenase subunit M	FpoM	1660	91267
ANME_02474	F(420)H(2) dehydrogenase subunit N	FpoN_2	1998	-
V-type ATP synthase				
ANME_01521	V-type ATP synthase alpha chain	ntpA	631	-
ANME_01522	V-type ATP synthase beta chain	ntpB	559	-
ANME_00655	V-type ATP synthase subunit C	ntpC	254	-
ANME_00478	V-type ATP synthase subunit D	ntpD	125	-
ANME_02026	V-type ATP synthase subunit E	ntpE	652	0
ANME_01520	V-type ATP synthase subunit F	ntpF	212	55864
ANME_02029	V-type ATP synthase subunit H	ntpH	305	-
ANME_02028	V-type ATP synthase subunit I	ntpI	362	-
ANME_02027	V-type ATP synthase subunit K	ntpK	457	-
Electron transport complex Rnf				
ANME_02108	Electron transport complex protein RnfB	RnfB	2415	-
ANME_02109	Electron transport complex protein RnfA	RnfA	805	-
ANME_02110	Electron transport complex protein RnfE	RnfE	554	-
ANME_02111	Electron transport complex protein RnfG	RnfG	813	62234
ANME_02112	Electron transport complex protein RnfD	RnfD	229	-
ANME_02113	Electron transport complex protein RnfC	RnfC	882	-
Heterodisulfide reductase				
ANME_01561	CoB--CoM heterodisulfide reductase iron-sulfur subunit A	hdrA	21	-
ANME_01562	CoB--CoM heterodisulfide reductase subunit B	hdrB	43	-
ANME_01563	CoB--CoM heterodisulfide reductase iron-sulfur subunit C	hdrC	13	-
ANME_02102	CoB--CoM heterodisulfide reductase iron-sulfur subunit D	hdrD	826	-
ANME_02103	CoB--CoM heterodisulfide reductase iron-sulfur subunit C	hdrC	743	134980
ANME_02104	CoB--CoM heterodisulfide reductase subunit B	hdrB	895	-
ANME_02105	CoB--CoM heterodisulfide reductase iron-sulfur subunit A	hdrA	1183	10238
ANME_02106	F420-non-reducing hydrogenase iron-sulfur subunit D	mvhD	1748	51224

Locus Tag	Product	Gene	RPKM	(iBAQ score)
ANME_02618	CoB--CoM heterodisulfide reductase iron-sulfur subunit A	hdrA	854	24461
ANME_02619	F420-non-reducing hydrogenase mvh iron-sulfur subunit D	mvhD	1005	6410470
ANME_02620	Formate dehydrogenase subunit beta	fdhB	874	278500
ANME_02621	Formate dehydrogenase subunit alpha like protein	fdhA	1365	77228
ANME_02238	CoB--CoM heterodisulfide reductase iron-sulfur subunit D	hdrD	2187	17449
ANME_02239	CoB--CoM heterodisulfide reductase subunit E	hdrE	1444	-
ANME_01629	CoB--CoM heterodisulfide reductase iron-sulfur subunit A	hdrA	81	-
ANME_01884	CoB--CoM heterodisulfide reductase iron-sulfur subunit C	hdrC	28	-
Sulfite reductase				
ANME_01242	Sulfite reductase, dissimilatory-type subunit alpha	dsr-LP	207	-
ANME_01246	Coenzyme F420 sulfite reductase	fsr	465	42845
CO dehydrogenase/acetyl-CoA synthase				
ANME_01530	CO dehydrogenase/acetyl-CoA synthase subunit alpha	codh/acsA	368	7758
ANME_01195	CO dehydrogenase/acetyl-CoA synthase subunit beta	codh/acsC	538	14867
ANME_00895	CO dehydrogenase/acetyl-CoA synthase subunit delta	codh/acsD	430	-
ANME_01529	Co dehydrogenase/acetyl-CoA synthase subunit epsilon	codh/acsB	206	-
ANME_00917	CO dehydrogenase/acetyl-CoA synthase subunit gamma	codh/acsE	432	-
Acetyl-CoA synthase				
ANME_01542	Acetyl-CoA synthetase	acs	31	-
ANME_01678	Acetyl-CoA synthetase	acs	44	-
Multiheme cytochromes c				
ANME_01820	Doubled CXXCH motif (Paired_CXXCH_1)	-	48	263
ANME_02055	Immune inhibitor A peptidase M6	-	65	-
ANME_02056	Doubled CXXCH motif (Paired_CXXCH_1)	-	172	-
ANME_02168	hypothetical protein	-	117	-
ANME_02775	hypothetical protein	-	3249	-
ANME_01594	Class III cytochrome C family protein	-	3323	-
ANME_02604	hypothetical protein	-	1124	-
ANME_00931	Doubled CXXCH motif (Paired_CXXCH_1)	-	39	-
ANME_01244	Cytochrome c	-	277	-
ANME_02229	hypothetical protein	-	274	-
ANME_02742	hypothetical protein	-	61	-
ANME_02743	hypothetical protein	-	32	-

Extended Data Table 2. Gene transcription (in RPKM) and expression (iBAQ score values) of selected SEEP-SRB1 genes.

Locus Tag	Product	Gene	RPKM	iBAQ score
Sulfate reduction				
DSS_01055	Sulfate adenylyltransferase	sat	9431	483820
DSS_01059	Adenylylsulfate reductase subunit alpha	aprA	16402	158030
DSS_01060	Adenylylsulfate reductase subunit beta	aprB	11025	-
DSS_03055	Dissimilatory sulfite reductase, subunit D	dsrD	3217	161890
DSS_03056	Dissimilatory sulfite reductase, subunit B	dsrB	8401	252000
DSS_03057	Dissimilatory sulfite reductase, subunit A	dsrA	7425	516530
DSS_02004	Dissimilatory sulfite reductase, subunit C	dsrC	14340	-
Membrane-bound respiratory complexes				
DSS_01056	Quinone-interacting membrane-bound oxidoreductase subunit C	QmoC	1613	13492
DSS_01057	Quinone-interacting membrane-bound oxidoreductase subunit B	QmoB	2360	118360
DSS_01058	Quinone-interacting membrane-bound oxidoreductase subunit A	QmoA	2175	47615
DSS_03202	Sulfite reduction-associated complex DsrMKJOP protein DsrP	DsrP	1800	-
DSS_03203	Sulfite reduction-associated complex DsrMKJOP protein DsrO	DsrO	2697	-
DSS_03204	Sulfite reduction-associated complex DsrMKJOP protein DsrJ	DsrJ	986	-
DSS_03205	Sulfite reduction-associated complex DsrMKJOP protein DsrK	DsrK	1890	55069
DSS_03206	Sulfite reduction-associated complex DsrMKJOP protein DsrM	DsrM	1669	-
DSS_00347	Transmembrane complex subunit B	TmcB	829	28078
DSS_00348	Transmembrane complex subunit C	TmcC	391	-
DSS_00349	Transmembrane complex subunit D	TmcD	359	187050
ATP synthase				
DSS_03414	ATP synthase F0 sector subunit b`	-	833	-
DSS_03415	ATP synthase F0 sector subunit b	atpF	3310	30352
DSS_03416	ATP synthase subunit delta	atpH	5140	-
DSS_03417	ATP synthase subunit alpha	atpA	2804	158070
DSS_03418	ATP synthase gamma chain	atpG	1020	-
DSS_03419	ATP synthase subunit beta	atpD	3399	187420
DSS_03420	ATP synthase epsilon chain	atpC	4860	21110
DSS_00164	ATP synthase protein I	atpI	1111	-
DSS_00165	ATP synthase protein I2	atpI2	786	-
DSS_00166	ATP synthase F0 sector subunit a	atpB	1028	-
DSS_00167	ATP synthase F0 sector subunit c	atpE	37122	-
CO dehydrogenase/acetyl-CoA synthase				
DSS_00568	CO dehydrogenase/acetyl-CoA synthase subunit alpha	codh/acsA	258	-
DSS_00577	CO dehydrogenase/acetyl-CoA synthase subunit delta	codh/acsD	429	-
DSS_00578	CO dehydrogenase/acetyl-CoA synthase subunit beta	codh/acsB	529	-
DSS_00579	CO dehydrogenase/acetyl-CoA synthase subunit gamma	codh/acsC	225	5855
DSS_00580	CO dehydrogenase/acetyl-CoA synthase subunit epsilon	codh/acsE	744	-
Acetyl-CoA synthetase				
DSS_01221	Acetyl-coenzyme A synthetase	acs	363	-
DSS_02306	Acetyl-coenzyme A synthetase	acs	157	-

Locus Tag	Product	Gene	RPKM	iBAQ score
Cytochromes c				
DSS_03053	Class III cytochrome C family protein	-	20112	-
DSS_02785	Acidic cytochrome c3 precursor	-	1064	-
DSS_00053	Acidic cytochrome c3 precursor	-	938	-
DSS_03485	Doubled CXXCH motif (Paired_CXXCH_1)	-	646	-
DSS_02871	Doubled CXXCH motif (Paired_CXXCH_1)	-	555	-
Type IV pili				
DSS_01738	Type IV pilus biogenesis protein pilQ	pilQ	45	-
DSS_01739	Type IV pilus biogenesis protein pilP	pilP	77	-
DSS_01740	Type IV pilus biogenesis protein pilO	pilO	81	-
DSS_01741	Type IV pilus biogenesis protein pilN	pilN	88	-
DSS_01742	Type IV pilus biogenesis protein pilM	pilM	144	-
DSS_03230	type IV pilus assembly protein pilY	pilY	318	-
DSS_03234	type IV pilus modification protein PilV	pilV	134	-
DSS_02280	type IV pilin pilA	pilA	124	-
DSS_00514	type IV pilin pilA	pilA_2	402	-
Heterodisulfide reductase				
DSS_00569	heterodisulfide reductase, subunit A	hdrA	251	-
DSS_00570	heterodisulfide reductase, subunit B	hdrB	127	-
DSS_00571	heterodisulfide reductase, subunit C	hdrC	354	-
DSS_00038	Heterodisulfide reductase subunit A	HdrA	100	-
DSS_00039	Heterodisulfide reductase subunit F1'	HdrF1'	293	-
DSS_00040	Heterodisulfide reductase subunit F1	HdrF1	86	-
DSS_03353	CoB--CoM heterodisulfide reductase subunit C	hdrC	0	-

Supplementary References

Eddy S (2013) HMMER 3.1b1. <http://hmmer.org>.

Hallam SJ, Putnam N, Preston CM, Detter JC, Rokhsar D, Richardson PM, DeLong EF (2004) Reverse methanogenesis: testing the hypothesis with environmental genomics. *Science* **305**: 1457-1462

Manz W, Eisenbrecher M, Neu TR, Szewzyk U (1998) Abundance and spatial organization of Gram-negative sulfate-reducing bacteria in activated sludge investigated by in situ probing with specific 16S rRNA targeted oligonucleotides. *FEMS Microbiology Ecology* **25**: 43-61

Mowat CG, Rothery E, Miles CS, Mclver L, Doherty MK, Drewette K, Taylor P, Walkinshaw MD, Chapman SK, Reid GA (2004) Octaheme tetrathionate reductase is a respiratory enzyme with novel heme ligation. *Nature structural & molecular biology* **11**: 1023-1024

Pruesse E, Quast C, Knittel K, Fuchs BM, Ludwig WG, Peplies J, Glockner FO (2007) SILVA: a comprehensive online resource for quality checked and aligned ribosomal RNA sequence data compatible with ARB. *Nucleic Acids Research* **35**: 7188-7196

Treude T, Knittel K, Blumenberg M, Seifert R, Boetius A (2005) Subsurface microbial methanotrophic mats in the Black Sea. *Applied and environmental microbiology* **71**: 6375-6378

Wang F-P, Zhang Y, Chen Y, He Y, Qi J, Hinrichs K-U, Zhang X-X, Xiao X, Boon N (2014) Methanotrophic archaea possessing diverging methane-oxidizing and electron-transporting pathways. *The ISME journal* **8**: 1069-1078

Waterhouse AM, Procter JB, Martin D, Clamp M, Barton GJ (2009) Jalview Version 2—a multiple sequence alignment editor and analysis workbench. *Bioinformatics* **25**: 1189-1191

Chapter 5

Cycling of phosphate associated with microorganisms involved in the sulfate-dependent anaerobic oxidation of methane

Jon S. Graf^{1,2}, Timothy G. Ferdelman¹, Jana Milucka¹, Sten Littmann¹ and Marcel M.M. Kuypers¹

¹Department of Biogeochemistry, Max Planck Institute for Marine Microbiology, Bremen, Germany; ²MARUM – Center for Marine Environmental Sciences, University of Bremen, Bremen, Germany

Corresponding author: Jon Graf (jgraf@mpi-bremen.de)

Manuscript in preparation.

Author contributions

J.S.G. and T.G.F. designed research. J.S.G. performed radiotracer incubation experiments and data analysis. J.S.G. and S. L. performed electron microscopy, energy dispersive x-ray measurements and data analysis. M.M.M.K and J.M. contributed material and analysis tools. J.S.G. and T.G.F. wrote and edited the manuscript with contributions from all co-authors.

Summary

Studies suggest that microbes associated with the sulfate-dependent anaerobic oxidation of methane (S-AOM) may directly influence sedimentary P cycling. Unusual authigenesis of iron (Fe) and phosphorus (P)-bearing minerals within S-AOM dominated sediment horizons have been observed (Jilbert & Slomp, 2013) and Fe- and P-rich particles have been found within S-AOM-associated microbes (Milucka et al, 2012). To investigate inorganic phosphorus (P_i) cycling associated with S-AOM, we performed trace radioactive $^{33}P_i$ experiments on an S-AOM enrichment culture incubated under low ($\sim 4 \mu\text{mol l}^{-1}$) and high ($\sim 0.5 \text{ mmol l}^{-1}$) phosphate concentrations. S-AOM biomass cultivated at high phosphate contained 9.1 dry-wt% HCl-extractable phosphate, which was Mg-bound, while the biomass cultivated at low phosphate concentration contained <0.1 dry-wt% phosphate. The particulate phosphate phase was likely located extracellularly. Phosphorus-rich inclusions in the enrichment culture biomass were not detected by scanning transmission electron microscopy (STEM) coupled with energy dispersive X-ray analysis (EDX). In the radiotracer experiments, $^{33}P_i$ was removed from the aqueous phase and into a P_i -bearing particulate phase located in the S-AOM biomass flocs only under S- S-AOM conditions. In the absence of methane, and S-AOM, $^{33}P_i$ uptake from solution ceased. Bulk dissolved P_i concentrations, however, remained constant under both S-AOM and control conditions. These results suggest that organisms within the enrichment culture induce P_i exchange processes when active (i.e. in the presence of methane). Exchange rates inferred from the radiotracer were substantial since the turnover time of soluble phosphate was estimated in the range of 3 – 9 days in the cultures. Epicellular phosphate may help to ameliorate eventual carbonate encrustation e.g. through the complexation of Ca^{2+} and Mg^{2+} ions or by creation of P_i -rich microenvironments surrounding the S-AOM aggregates.

Introduction

Sulfate-dependent anaerobic oxidation of methane (S-AOM) has a major role in coupling biogeochemical cycles of sulfur and carbon in sediments. S-AOM was discovered nearly 35 years ago from sediment porewater profiles showing concurrent disappearance of both methane and sulfate at the so-called sulfate-methane transition zones (SMTZ), where upward diffusing methane was consumed by downward diffusing sulfate (Barnes & Goldberg, 1976; Martens & Berner, 1974; Reeburgh, 1976).

Subsequent studies demonstrated that sulfate-coupled AOM is mediated by anaerobic methanotrophic archaea (ANME) and sulfate-reducing bacteria belonging to the *Desulfosarcina/Desulfococcus* clade (DSS) (Boetius et al, 2000; Hinrichs et al, 2000; Hoehler et al, 1994; Nauhaus et al, 2002). Despite the low free energy change associated with sulfate-dependent AOM, estimates indicate that S-AOM consumes > 90 % of methane produced in marine sediments. Therefore, S-AOM plays an important part in regulating greenhouse gas emission from the ocean seafloor (Reeburgh, 2007).

The influence of S-AOM on biogeochemical cycles extends beyond the cycling of carbon and sulfur to phosphorus (P) and iron (Fe). The sedimentary Fe and P cycles are tightly linked due to the efficient scavenging of dissolved inorganic phosphate (P_i) by particulate Fe(III) oxo-hydroxides. Once deposited, P_i can be released within deeper, sulfidic sediment layers by reductive dissolution of the Fe(III) oxo-hydroxides. This mechanism, along with organic matter degradation, is a major cause for elevated P_i concentrations characteristically found in sulfidic sediment horizons such as the SMTZ (e.g. (McManus et al, 1997; Sundby et al, 1992)). Therefore, the SMTZ can act as a source of P_i that either diffuses upwards and downwards where it can further react to form authigenic P-bearing phase, e.g. carbonate fluoroapatite (Ruttenberg & Berner, 1993,) both above and below the SMTZ (März et al, 2008).

Authigenic Fe(II) phosphates (e.g. vivianite) have been identified as the main P burial phase in Fe-rich large river fan sediments and brackish marginal-sea sediments, where authigenesis of Fe(II) phosphates below the SMTZ is most likely driven by high free Fe(II) concentrations (Burns, 1997; März et al, 2008; Slomp et al, 2013). In sediments of the Baltic and the Black Sea, authigenesis of Fe(II) phosphate was also observed to occur within sulfidic, S-AOM-associated sediment layers (Dijkstra et al, 2014; Egger et al, 2015; Jilbert & Slomp, 2013). The formation of vivianite in these latter cases did not

appear to be driven by supersaturation of the pore water with respect to vivianite. The authors of these studies suggest that the Fe(II) phosphates forming in these sulfidic environments may be strongly influenced by the S-AOM process itself.

Intriguingly, distinct Fe- and P-rich inclusions have been identified within the cytoplasm of DSS cells associated with S-AOM mats found in the sulfidic zone of the Black Sea (Milucka et al, 2012). Furthermore, in the same study bacterial DSS cells could be distinguished from the ANME cells by their relatively greater P:C contents. These observations are consistent with the hypothesis that S-AOM associated cells may be directly involved in the inorganic P enrichment or P mineral authigenesis, but the hypothesis has not been directly tested.

Therefore, we investigated the influence of S-AOM activity on P distributions and cycling in a similar enrichment culture. Here we report on the elemental composition and geochemistry of the of the S-AOM biomass in the enrichment culture – both at the bulk and on the single-cell level. We then use ^{33}P radiotracer at low and high phosphate concentrations to investigate the microbial control of P uptake associated with S-AOM.

Methods

Culture origin and cultivation

The S-AOM enrichment culture derived from a culture that has been enriched over 10 years from a sediment sample collected on a cruise of RV L'Atlante in September 2003 in the eastern Mediterranean Sea (Milucka et al, 2012). The ISIS culture was incubated in artificial SRB seawater medium (salts: 0.76 mmol l⁻¹ KBr, 8.05 mmol l⁻¹ KCl, 10 mmol l⁻¹ CaCl₂ * 2 H₂O, 27.9 mmol l⁻¹ MgCl₂ * 6 H₂O, 27.6 mmol l⁻¹ MgSO₄ * 7 H₂O, 451 mmol l⁻¹ NaCl, 4.67 mmol l⁻¹ NH₄Cl, 1.47 mmol l⁻¹ KH₂PO₄, 30 mmol l⁻¹ NaHCO₃; vitamins and trace elements: according to (Widdel & Bak, 1992); redox indicator: 1 mg l⁻¹ Resazurin; reducing agent: 0.5 mmol l⁻¹ H₂S pH 7.5) anaerobically in serum bottles sealed with butyl rubber stoppers. Serum bottles having a N₂:CO₂ (90:10) headspace were pressurized with methane (Air Liquide, Germany) to 3 bar overpressure and incubated on a shaker (40 rotations min⁻¹.) at room temperature. Medium was regularly exchanged with fresh artificial seawater medium when sulfide concentrations reached ~ 20 mmol l⁻¹ in an anaerobic glove box (Mecaplex, Switzerland) under N₂:CO₂ (90:10) atmosphere. Growth (doubling times) are estimated to be several month (Milucka et al, 2012). The low phosphate enrichment culture was derived from the high phosphate culture by incubation for 2 months (with occasional medium exchanges) in medium containing 10 μmol l⁻¹ phosphate. After each medium exchange, free P_i concentration gradually increased over several days. The medium exchanges were repeated until no increase of P_i concentration could be observed.

Chemical analysis

Total dissolved sulfide was determined spectrophotometrically at 670nm using the methylene blue method (Cline, 1969) and was adapted for small volumes. Prior to sulfide determination, samples were filtered through a 0.45 μm syringe filter and immediately fixed with 5% ZnCl₂ (0.5x sample volume).

Sulfate was determined on samples filtered through a 0.45 μm syringe filter, immediately fixed with ZnCl₂ (same as sulfide samples), and centrifuged at 12000 relative centrifugal force (RCF, in g) for 5 min. Sulfate in the supernatant was determined on a 761 Compact ion chromatograph (Methrom AG, Switzerland) equipped with CO₂

suppressor module, Zn trap (Metrosep A Trap 1-100/4.0) and a Metrosep A SUPP5 column. Carbonate buffer (3.2 mmol l⁻¹ Na₂CO₃, 1 mmol l⁻¹ NaHCO₃) served as an eluent.

Inorganic phosphate was determined spectrophotometrically by molybdenum blue method at 820nm (Murphy & Riley, 1958). Prior to the analysis, samples were filtered through a 0.45 µm syringe filter and stored for several days at 4°C until interfering sulfide was oxidized by oxygen.

STEM-EDX

Biomass was fixed with 4% formaldehyde (FA) in 0.1M 3-(N-morpholino)propanesulfonic acid (MOPS) buffer (pH 7.4). To 1ml biomass in medium an equal volume of fixative was added and the cells were incubated with head-over-head rotation for 15 min. at 21°C. Biomass was pelleted by centrifugation for 2 min. at 800 RCF (21°C), supernatant was decanted and replaced with fresh fixative, followed by 2h fixation with head-over-head rotation at 21°C. Subsequently cells were washed 5x with 0.1 M MOPS buffer (pH7.4) by pelleting the biomass at 800 RCF (1 min., 21°C) decanting the supernatant and replacing it with fresh buffer. After the last wash, buffer was replaced for 12% gelatin in 0.1 M PHEM (60 mM piperazine-N,N'-bis(2-ethanesulfonic acid), 25 mM 4-(2-hydroxyethyl)-1-piperazineethanesulfonic acid, 10 mM ethylene glycol tetraacetic acid, 2 mM MgCl₂, pH 6.9) at 37°C and the fixed biomass was incubated for 5 min. at 37°C with intermitted resuspension. Next the biomass was pelleted at 1600 RCF for 3 min. at 37°C and the sample was solidified on ice for 15 min. Samples were removed from the microtubes, excess gelatin was trimmed off using a razorblade and the pellet was diced in blocks of 1-2 mm³. Sample blocks were infiltrated overnight at 4°C with 2.3 M sucrose in PHEM buffer and the next day mounted on specimen pins and frozen in liquid nitrogen. Samples were cryosectioned (75 nm sections) using a cryo-ultramicrotome UC7/FC7 (Leica Microsystems, Austria). Cryosections were picked up with a drop of 1% methyl cellulose and 1.15 M sucrose in PHEM buffer and transferred to formvar-carbon-coated copper hexagonal 100 mesh grids.

STEM imaging was performed on a Quanta FEG 250 (FEI, Netherlands) equipped with and Everhart-Thornley detector for transmission electron imaging (14 regions) under high vacuum mode at 20 kV. EDX was done using a dual detector system XFlash

6|30 (energy resolution Mn K_α < 123 eV, detector area = 30 mm²; BrukerNano, Germany) at a working distance of 10 mm.

Elemental analysis by ICP-OES

Biomass was filtered onto weighed 0.22 μm GTTP filters (dried in desiccator for 24h; Millipore, Germany) and washed very briefly with 0.5M NaCl solution followed by MQ water. Filters were dried at 80°C overnight and dry mass was determined (~1 mg) before incubation in 1M HCl for 1h at 55°C. The filter and loose biomass was collected by centrifugation (12000 RCF, 10 min.) and washed twice with 1M HCl. The washings and the extract were combined and Ca, Mg, Fe, P, S, Ni and Co were determined by inductively coupled plasma-optical emission spectrometer (ICP-OES) that was equipped with an ultrasonic nebulizer (PerkinElmer Optima 3300 R).

³³P radiotracer incubation experiments

15 ml aliquots of the S-AOM enrichment culture were transferred into 30 ml serum bottles sealed with butyl rubber stoppers. The medium was exchanged twice (incubation time: 6h) with modified SRB seawater medium (modifications: 10 mmol l⁻¹ MgSO₄ * 7 H₂O, 45.5 mmol l⁻¹ MgCl₂ * 6 H₂O, 0.5 or 0.005 mmol l⁻¹ KH₂PO₄, 15 mmol l⁻¹ NaHCO) before carrier-free ³³P-phosphate radiotracer (Hartmann Analytics, Germany) and 1.5 mmol l⁻¹ NaH¹³CO₃ (Sigma-Aldrich, USA) was added. Serum bottles were pressurized with 2 bar methane or N₂:CO₂ (90:10). Samples were taken regularly for liquid scintillation counting, sulfate, sulfide and phosphate determination. Samples for scintillation counting were filtered through a 0.22 μm GTTP filter (Millipore, Germany). The filter was briefly washed once with modified SRB medium and twice with 1M HCl. ³³P activity in the filtrate (medium) and on the filter was determined by liquid scintillation counting (liquid scintillation counter: 2900TR LSA, Packard, USA; scintillation fluid: IrgaSafe, PerkinElmer, USA).

Results

Ultrastructure as well as single-cell and bulk elemental characterization of S-AOM biomass

Scanning transmission electron microscopy (STEM) of thin sections of the S-AOM biomass showed a well-mixed community of ANME and DSS that formed defined, big clusters several hundred micrometers in diameter. ANME and DSS cells were distinguished based on morphology and presence or absence of the double membrane that enclosed the gram-negative DSS cells.

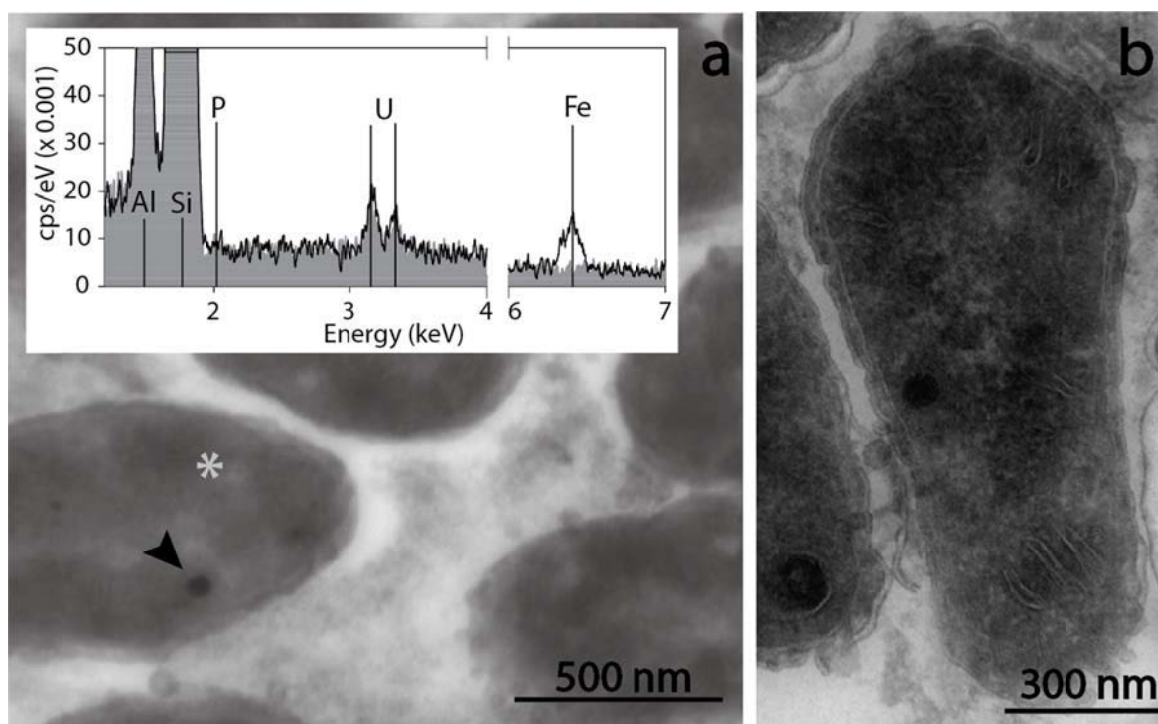


Figure 1. Ultrastructure and intracellular particles of DSS bacteria. a, Brightfield STEM picture of the high phosphate culture featuring DSS cell containing intracellular particle (black arrow). Spectra show EDX spot measurements of intracellular particle (black EDX spectrum) and cellular background indicated by a gray star (grey EDX spectrum). Vertical lines depict K_{α} lines of the respective elements (for U, M_{α} and M_{β} line is shown). Al, Si and U signals originate from the STEM detector or staining. Spectra were smoothed using simple moving average (window size = 0.01 keV). b, Brightfield STEM picture of a DSS cell of the high phosphate culture. Visible is the double membrane including invaginations and intracellular particle.

We observed particles within the cytoplasm of a small fraction of the DSS population in both low and high phosphate cultures (Fig. 1b). The intracellular particles exhibited high angle electron scattering, were 20 – 100 nm in diameter and rarely more than one per DSS cell was observed. Subsequent EDX analysis of several of these particles ($n=9$) revealed Fe enrichment relative to cellular background in almost all cases ($n=7$); however, no other major elements could be detected by EDX in the particles (Fig.

1a). Peaks of uranium (U), copper (Cu), aluminum (Al) and silicon (Si) are system peaks originating from staining (U), copper mounting grid (Cu) or detector (Al and Si).

The S-AOM flocs formed in the enrichment culture differed in appearance and geochemical characteristics depending on the ambient phosphate concentration. Elemental analysis by ICP-OES of HCl extracts highlighted major differences in the elemental composition of low and high P_i biomass flocs. We found 9.1 dry-wt% HCl-extractable P_i in the high and only small amounts (< 0.1 dry-wt %) in low phosphate biomass flocs (Table 1). P_i and Mg were present in approximately equimolar amounts in the HCl extracts of low and high phosphate biomass. Calcium content was only 1.6% for the high phosphate enrichments, but 22.4 %wt for the low phosphate treatments. In the latter case, the Ca was most likely bound as calcium carbonate, which was visible by eye as a white precipitate encrusting the black biomass flocs, and distinct needle-shaped carbonate crystals observed under higher magnification (see Supplementary Fig. S3). Other elements determined in the acidic extracts such as Fe, Mn, Ni and Co constituted < 1 %wt of the dry mass of both cultures (Table 1 and Supplementary Table S2).

Table 1. Elemental composition of biomass determined by ICP-OES in HCl extracts of low and high phosphate incubations.

Incubation	Ca	Mg	Fe	PO_4^{3-}
	%wt dry mass mmol (g dry mass) ⁻¹	%wt dry mass μ mol (g dry mass) ⁻¹	%wt dry mass μ mol (g dry mass) ⁻¹	%wt dry mass μ mol (g dry mass) ⁻¹
Low phosphate	22.35 5.577	0.01 4	0.04 7	0.05 5
High phosphate	1.62 0.404	3.35 1370	0.42 75	9.08 956

³³P radiotracer incubations

Phosphate cycling in low and high phosphate S-AOM enrichment cultures was investigated using ³³P radiotracer. Rates are summarized in Table 2. In the presence of methane, sustained sulfate reduction took place as indicated by the linearly increasing sulfide and decreasing sulfate concentrations (Fig. 2a and b). The sulfate reduction rate (SRR) calculated from the sulfate concentrations was 16.2 and 53.8 μ mol l⁻¹ h⁻¹ in low and high P_i incubations, respectively. In both low and high P_i incubations, the SRR was typically 1.6-times greater than the sulfide production rate. When methane was

omitted, sulfate reduction ceased as indicated by the constant sulfate and sulfide concentrations over time.

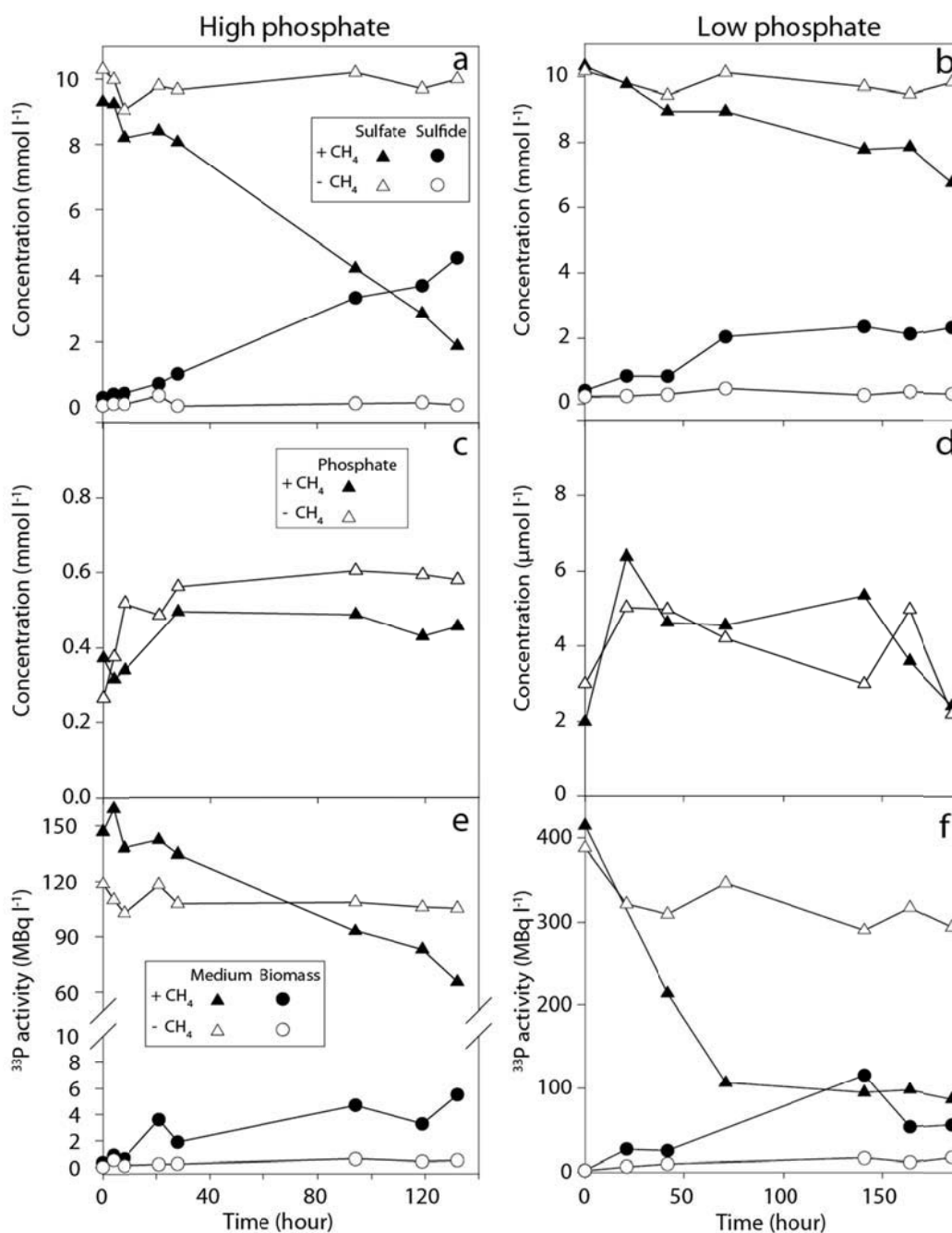


Figure 2. ^{33}P radiotracer experiments of high and low phosphate incubations. Sulfate and sulfide concentration (a and b), phosphate concentration (c and d) and ^{33}P activity in the medium and washed biomass flocs (e and f) are shown for high phosphate (left panels; a,c,e) and low phosphate radiotracer incubations (right panels; b,d,f). Filled glyphs represent experiments amended with methane, open glyphs were control experiments not amended with methane.

In the high P_i incubation phosphate concentration increased within the first 24h from 0.15 mmol l^{-1} to 0.5 (with methane) and 0.6 mmol l^{-1} (without methane) and remained approximately constant thereafter (Fig. 2c). Such an increase was not

observed in the low P_i incubations; there the P_i concentration fluctuated without significant trend between 2 and 6 $\mu\text{mol l}^{-1}$ in both the control and methane amended incubations (Fig. 2d). In contrast to the bulk P_i concentrations, ^{33}P activity in the medium ($^{33}\text{P}_m$) exhibited a decrease in all incubations where S-AOM was occurring, i.e., where methane was present and sulfate was being consumed. For the high P_i incubation, the $^{33}\text{P}_m$ decrease was approximately linear throughout the experiment from 146 to 65 MBq ($-0.62 \text{ MBq l}^{-1} \text{ h}^{-1}$; Fig. 2e). $^{33}\text{P}_m$ of the low P_i incubation decreased initially over the first 70 hours from 414 to 106 MBq l^{-1} ($-4.4 \text{ MBq l}^{-1} \text{ h}^{-1}$; 0 – 70h; Fig. 2f) and then remained approximately constant thereafter (70–185h). In the absence of methane, and therefore no AOM activity, $^{33}\text{P}_m$ activity remained constant in the high P_i incubation or decreased only slightly in the presence of low concentrations of P_i (Fig. 2e and f).

Table 2. Sulfate reduction rate and rates of ^{33}P change obtained from radiotracer experiments of low and high phosphate experiment amended with methane.

	Low phosphate experiment	High phosphate experiment
Sulfate reduction rate ($\mu\text{mol l}^{-1} \text{ h}^{-1}$)	16.2 ($r^2=0.93$)	53.8 ($r^2=0.98$)
Average phosphate concentration ($\mu\text{mol l}^{-1}$)	4.1	414.7
$\Delta^{33}\text{P}$ activity in medium ($\text{MBq l}^{-1} \text{ h}^{-1}$)	4.37 ($r^2=0.99$; 0 – 70h)	0.62 ($r^2=0.97$)
^{33}P derived P cycling rate ($\mu\text{mol l}^{-1} \text{ h}^{-1}$)	0.053 (0 – 70h)	1.86
$\Delta^{33}\text{P}$ activity washed biomass ($\text{MBq l}^{-1} \text{ h}^{-1}$)	0.561 ($r^2=0.72$; 0 – 42h) 0.355 ($r^2=0.52$; 0 – 185h)	0.030 ($r^2=0.72$)

S-AOM enrichment culture flocs washed with 1M HCl of both high P_i and low P_i S-AOM active incubations were distinctly more enriched in radiotracer when compared to the control incubations without methane (Fig. 2e and f). The recovered ^{33}P activity in the washed biomass at the end of the methane amended incubation was ~ 6 and 17 % of $^{33}\text{P}_m$ lost from the medium for high and low P_i incubation, respectively. ^{33}P activity in the wash fraction was confirmed by scintillation counting but was not systematically quantified.

To test whether the P_i cycling is an indirect effect caused by of chemical changes occurring within the medium during S-AOM (e.g. co-precipitation due to increased alkalinity), we performed a control experiment where the changes were replicated in the absence of methane (Fig. 3). In brief, we incubated radiotracer-free S-AOM

enrichment culture for ~2 weeks with methane, exchanged the medium with fresh medium containing radiotracer and added the old medium stepwise in the absence of methane. The old medium contained 8.7 mmol l⁻¹ sulfide, 2.4 mmol l⁻¹ sulfate and at least 23 mmol l⁻¹ DIC (based on the sum of the added DIC and methane derived DIC). The addition of old medium increased sulfide concentration from 0.3 to 7.5 mmol l⁻¹ and lowered sulfate concentration from 11 to 5 mmol l⁻¹ in our control experiment. The DIC concentration was estimated to have increased from 15 mmol l⁻¹ to ~ 26 mmol l⁻¹. These changing conditions had very little effect on the dilution-corrected ³³P activity which remained approximately constant. Small changes at the time points of amendment were attributed to the propagation of dilution effects resulting from sampling and the addition of old medium.

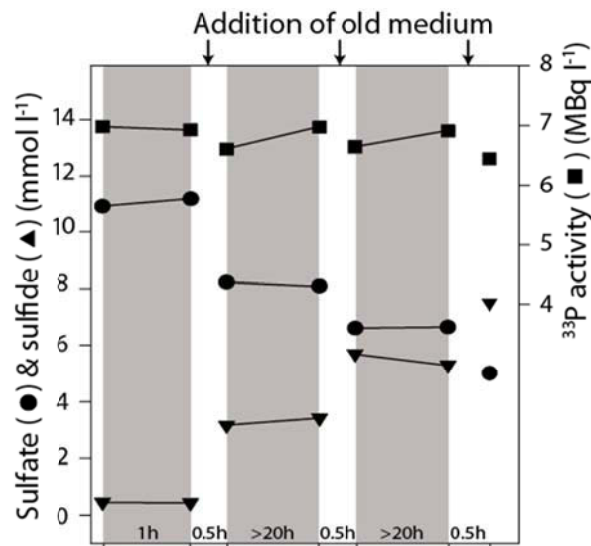


Figure 3. Abiotic control experiment without methane to which old medium was added.

Samples were taken just before and after each of the three old medium additions (indicated by arrows). After each addition the system was left to equilibrate (gray shaded areas) for > 20h. On x-axis, the time between sampling timepoints is denoted. ³³P activity was corrected for the dilution effect introduced by the addition of old medium.

Discussion

P_i cycling under S-AOM conditions

The experiments with ³³P demonstrate that there is indeed a link between the activity of S-AOM microorganisms and inorganic phosphate cycling. ³³P was removed from solution when methane was present in both the low and high phosphate experiments (Fig. 2a and b). Without methane, ³³P_m activity remained unchanged (high P_i incubation) or slowly decreased (low P_i incubation). Because bulk net distributions of P_i did not change over time in the experiments, the decrease in ³³P activity indicates that P exchanges between the solution and solid, biomass-containing phases. This exchange occurs only when S-AOM occurs.

One possibility is that the ³³P_m removal from solution simply reflects a side-effect cause by the changing medium chemistry during the course of the experiment. P_i adsorption and co-precipitation with carbonate minerals has been previously reported (de Kanel & Morse, 1978; Otsuki & Wetzel, 1972) and might indirectly influence P cycling in our culture due to the increased carbonate alkalinity generated by the S-AOM process. Nevertheless, our experiments with adding old medium to replicate changes in the extent of the S-AOM reaction, i.e., decreasing sulfate, and corresponding increases in sulfide and carbonate alkalinity, had no effect on total dissolved ³³P activity (Fig. 4). Moreover, the decline in ³³P_m during the methane amended conditions was immediate, when changes in the medium chemistry associated with would be minimal. In the absence of methane and S-AOM, we could not induce ³³P_m uptake; therefore we propose an active and direct involvement of the S-AOM-associated microbes in this process.

One possibility is that S-AOM microorganisms store excess P. Microbial P_i uptake for biomass formation or storage, however, is unlikely the main driving mechanism behind the observed radiotracer behavior in our cultures. In case of uptake or storage, one would expect that the radiotracer and P_i show similar behavior. Our results did not exhibit such behavior since the ³³P_m activity substantially decreased even while P_i concentration remained approximately constant. Furthermore, apparent rates of P_i removal (based on the change of ³³P activity and the mean phosphate concentration) of 1.86 (high P_i exp.) and 0.053 μmol l⁻¹ h⁻¹ (low P_i exp.) are substantial; they yield turnover times for dissolved P_i of 9 days (high P_i exp.) and 3 days (low P_i exp.) respectively. The

rates are nearly two orders of magnitude larger than the estimated assimilatory P_i uptake rates (few $\text{nmols l}^{-1} \text{h}^{-1}$; Supplementary Table S1). Furthermore, only a small fraction of ^{33}P lost from the medium was retained in the biomass after brief washing with 1M HCl. Extraction of organic P or a common P storage product, e.g. polyphosphate, has been reported to require prolonged exposure (hours) to 1M HCl and high temperatures (Eixler et al, 2005; Ruttenberg, 1992), but exposure to 1M HCl in our experiments was brief (minutes).

Rather than uptake and storage within the biomass, exchange of free P_i with a particulate P_i pool appears to be a more likely mechanism. To provide some level of insight into the nature of the solid phase P_i pool, we determined bulk elemental composition in acidic HCl extracts (analyzed by ICP-OES) of biomass flocs. When switching the medium of the high phosphate culture to lower phosphate concentrations we observed a gradual increase of free phosphate (visible in Fig. 2f), independent of S-AOM activity, and indicating dissolution of a P mineral. This was confirmed by our bulk elemental analysis where we found 9.1 dry-wt% HCl-extractable P_i in the high and only small amounts (< 0.1 dry-wt %) in low phosphate biomass flocs. Our results indicated almost equimolar concentrations of Mg and P_i in high ($1.44 \text{ mol Mg (mol } P_i)^{-1}$) and low P_i biomass ($0.78 \text{ mol Mg (mol } P_i)^{-1}$). Therefore P_i seems to be bound in an Mg containing P mineral, which is consistent with reports of P_i precipitating as Mg-Ca phosphate under similar abiotic conditions (Golubev et al, 1999).

The bulk P_i extraction method also does not distinguish between extra- and intracellular P_i , but the application of STEM-EDX revealed intracellular particles only within the DSS cells of both low and high phosphate cultures. Similar Fe-rich particles have been found in DSS from S-AOM-active bacterial mats from the Black Sea that were also enriched in P (Milucka et al, 2012) or S (Reitner et al, 2005b; Reitner et al, 2005a). While EDX analysis of several of our particles ($n=9$) also showed almost always Fe enrichment in contrast to cellular background, neither P, Mg nor S could be detected. As a result we suggest that the Mg-bearing phosphate mineral involved in P_i cycling is located extracellularly. In our experiments we found no evidence of significant authigenesis of Fe-bearing phosphate minerals that was recently reported to occur within the SMTZ (Dijkstra et al, 2014; Jilbert & Slomp, 2013), but free ferrous iron

concentrations are not expected to be significant in our cultures (e.g. Fe is added only as a trace element).

Interestingly, throughout both the high and low P_i experiments, bulk P_i concentrations remained constant. These apparently contradictory results are readily resolved if we consider that the bulk P_i rapidly achieves a steady-state concentration between the solid phase (including biomass) and the solution phase, whereas, the $^{33}P_i$ added to the solution phase is initially not in steady-state. During P cycling, free P_i and radiotracer transition into a particulate P_i pool at the same rate as P_i (and subsequently ^{33}P) is released again. Over time, $^{33}P_m$ activity will decrease and radiotracer will accumulate in the particulate pool. The system eventually settles in a steady state in respect to ^{33}P after which ^{33}P activity in both pools will remain constant despite ongoing P_i exchange. We hypothesize that steady state was reached in the low phosphate radiotracer incubation visible by constant $^{33}P_m$ activity from 70h onwards despite ongoing S-AOM activity (inferred by sulfate and sulfide concentrations). Thus, a biologically induced exchange process between P_i and extracellular, inorganic P minerals is the most likely explanation for the observed ^{33}P radiotracer behavior.

Possible mechanism and function of P_i exchange

In marine environments, microbe P-mineral interactions are well studied. For example, microbes have been identified as important players due to their ability to release P_i from organic matter (Baturin & Bezrukov, 1979) and their involvement in deposition of P-bearing minerals (Diaz et al, 2008; Schulz & Schulz, 2005). Nonetheless, we could not find reports in the literature which have specifically implicated microbes in the exchange of free P_i with P-minerals as described in our study. This might be related to the fact that the P cycling described in this study is a cryptic process (no net-change of P_i concentration) that reveals itself through the application of P isotopes. So far very few studies have used P radioisotopes to investigate sedimentary P cycling processes and therefore microbe P-mineral exchange might be an overlooked aspect. It remains to be shown if our observations also hold true for in-situ conditions and that they are a unique feature of S-AOM-associated microbes.

It is unclear how P cycling could benefit S-AOM-associated microbes. We note that the S-AOM enrichment culture, which was kept for several months at low phosphate concentrations ($< 10 \mu\text{mol l}^{-1}$) showed gradually decreasing S-AOM rates

(inferred by sulfide production; data not shown) and simultaneous, creeping carbonatization of the biomass. Carbonate mineral formation was likely facilitated by low phosphate concentrations since phosphate has been shown to inhibit calcite and aragonite precipitation (Berner et al, 1978; Plant & House, 2002). Carbonate encrusting the biomass could have had a disruptive effect on the S-AOM microbes through e.g. diffusive barrier formation or mechanical stress that led to decreased S-AOM rates. We hypothesize that by continuously liberating P_i from e.g. a slow forming P_i -bearing mineral phase, S-AOM microbes could potentially increase local P_i concentration to protect themselves from carbonatization. Such a microbial driven process could have interesting implications for sedimentary processes through creation of P_i -rich microenvironments.

Conclusions

Our results show that S-AOM-associated microbes cycle P_i between soluble P_i and particulate P_i , latter is likely located extracellularly and Mg-bound. Cycling appears to be actively performed by the microbes and was only observed when cultures were “energized” by methane. P_i cycling rates were significant since the time of turnover of free P_i was estimated to be 3 – 9 days (depending on P_i concentration). We speculate that P_i cycling act as a protection mechanism against excessive carbonatization of the biomass.

Acknowledgments

We thank Chao Peng and Tobias Goldhammer for assistance with the ICP-OES measurement, Rob Mesman for preparation of thin sections as well as assistance with STEM-EDX measurements and Kirsten Imhoff for assistance with sulfate measurements. This work was financially supported by the Max Planck Society and the MARUM Center for Marine Environmental Sciences.

References

- Barnes R, Goldberg E (1976) Methane production and consumption in anoxic marine sediments. *Geology* **4**: 297-300
- Baturin G, Bezrukov P (1979) Phosphorites on the sea floor and their origin. *Marine Geology* **31**: 317-332
- Berner RA, Westrich JT, Graber R, Smith J, Martens CS (1978) Inhibition of aragonite precipitation from supersaturated seawater; a laboratory and field study. *American Journal of Science* **278**: 816-837
- Boetius A, Ravensschlag K, Schubert CJ, Rickert D, Widdel F, Gieseke A, Amann R, Jorgensen BB, Witte U, Pfannkuche O (2000) A marine microbial consortium apparently mediating anaerobic oxidation of methane. *Nature* **407**: 623-626
- Burns S (1997) Early diagenesis in Amazon Fan sediments. In *Proceedings of the ocean drilling program. Scientific results*, Vol. 155, pp 497-504.
- Cline JD (1969) Spectrophotometric Determination of Hydrogen Sulfide in Natural Waters. *Limnol Oceanogr* **14**: 454-458
- de Kanel J, Morse JW (1978) The chemistry of orthophosphate uptake from seawater on to calcite and aragonite. *Geochimica et Cosmochimica Acta* **42**: 1335-1340
- Diaz J, Ingall E, Benitez-Nelson C, Paterson D, de Jonge MD, McNulty I, Brandes JA (2008) Marine polyphosphate: a key player in geologic phosphorus sequestration. *Science* **320**: 652-655
- Dijkstra N, Kraal P, Kuypers MM, Schmetzer B, Slomp CP (2014) Are iron-phosphate minerals a sink for phosphorus in anoxic black sea sediments?
- Egger M, Jilbert T, Behrends T, Rivard C, Slomp CP (2015) Vivianite is a major sink for phosphorus in methanogenic coastal surface sediments. *Geochimica et Cosmochimica Acta* **169**: 217-235
- Eixler S, Selig U, Karsten U (2005) Extraction and detection methods for polyphosphate storage in autotrophic planktonic organisms. *Hydrobiologia* **533**: 135-143
- Golubev SV, Pokrovsky OS, Savenko VS (1999) Unseeded precipitation of calcium and magnesium phosphates from modified seawater solutions. *Journal of crystal growth* **205**: 354-360
- Hinrichs K-U, Summons RE, Orphan V, Sylva SP, Hayes JM (2000) Molecular and isotopic analysis of anaerobic methane-oxidizing communities in marine sediments. *Organic Geochemistry* **31**: 1685-1701

Hoehler TM, Alperin MJ, Albert DB, Martens CS (1994) Field and Laboratory Studies of Methane Oxidation in an Anoxic Marine Sediment - Evidence for a Methanogen-Sulfate Reducer Consortium. *Global Biogeochem Cy* **8**: 451-463

Jilbert T, Slomp CP (2013) Iron and manganese shuttles control the formation of authigenic phosphorus minerals in the euxinic basins of the Baltic Sea. *Geochimica et Cosmochimica Acta* **107**: 155-169

Martens CS, Berner RA (1974) Methane production in the interstitial waters of sulfate-depleted marine sediments. *Science* **185**: 1167-1169

März C, Hoffmann J, Bleil U, De Lange G, Kasten S (2008) Diagenetic changes of magnetic and geochemical signals by anaerobic methane oxidation in sediments of the Zambezi deep-sea fan (SW Indian Ocean). *Marine Geology* **255**: 118-130

McManus J, Berelson WM, Coale KH, Johnson KS, Kilgore TE (1997) Phosphorus regeneration in continental margin sediments. *Geochimica et Cosmochimica Acta* **61**: 2891-2907

Milucka J, Ferdeman TG, Polerecky L, Franzke D, Wegener G, Schmid M, Lieberwirth I, Wagner M, Widdel F, Kuypers MMM (2012) Zero-valent sulphur is a key intermediate in marine methane oxidation. *Nature* **491**: 541-546

Murphy J, Riley J (1958) A single-solution method for the determination of soluble phosphate in sea water. *Journal of the Marine Biological Association of the United Kingdom* **37**: 9-14

Nauhaus K, Boetius A, Krüger M, Widdel F (2002) In vitro demonstration of anaerobic oxidation of methane coupled to sulphate reduction in sediment from a marine gas hydrate area. *Environmental Microbiology* **4**: 296-305

Otsuki A, Wetzel RG (1972) Coprecipitation of phosphate with carbonates in a marl lake. *Limnology and Oceanography* **17**: 763-767

Plant L, House W (2002) Precipitation of calcite in the presence of inorganic phosphate. *Colloids and Surfaces A: Physicochemical and Engineering Aspects* **203**: 143-153

Reeburgh WS (1976) Methane consumption in Cariaco Trench waters and sediments. *Earth and Planetary Science Letters* **28**: 337-344

Reeburgh WS (2007) Oceanic Methane Biogeochemistry. *Chemical Reviews* **107**: 486-513

Reitner J, Peckmann J, Blumenberg M, Michaelis W, Reimer A, Thiel V (2005b) Concretionary methane-seep carbonates and associated microbial communities in Black Sea sediments. *Palaeogeography, Palaeoclimatology, Palaeoecology* **227**: 18-30

Reitner J, Peckmann J, Reimer A, Schumann G, Thiel V (2005a) Methane-derived carbonate build-ups and associated microbial communities at cold seeps on the lower Crimean shelf (Black Sea). *Facies* **51**: 66-79

Ruttenberg KC (1992) Development of a Sequential Extraction Method for Different Forms of Phosphorus in Marine Sediments. *Limnology and Oceanography* **37**: 1460-1482

Ruttenberg KC, Berner RA (1993) Authigenic apatite formation and burial in sediments from non-upwelling, continental margin environments. *Geochimica et Cosmochimica Acta* **57**: 991-1007

Schulz HN, Schulz HD (2005) Large sulfur bacteria and the formation of phosphorite. *Science* **307**: 416-418

Slomp CP, Mort HP, Jilbert T, Reed DC, Gustafsson BG, Wolthers M (2013) Coupled dynamics of iron and phosphorus in sediments of an oligotrophic coastal basin and the impact of anaerobic oxidation of methane. *PLoS ONE* **8**: e62386

Sundby Br, Gobeil C, Silverberg N, Alfonso M (1992) The phosphorus cycle in coastal marine sediments. *Limnology and Oceanography* **37**: 1129-1145

Widdel F, Bak F (1992) Gram-negative mesophilic sulfate-reducing bacteria. In *The prokaryotes*, pp 3352-3378. Springer

Supplementary Information

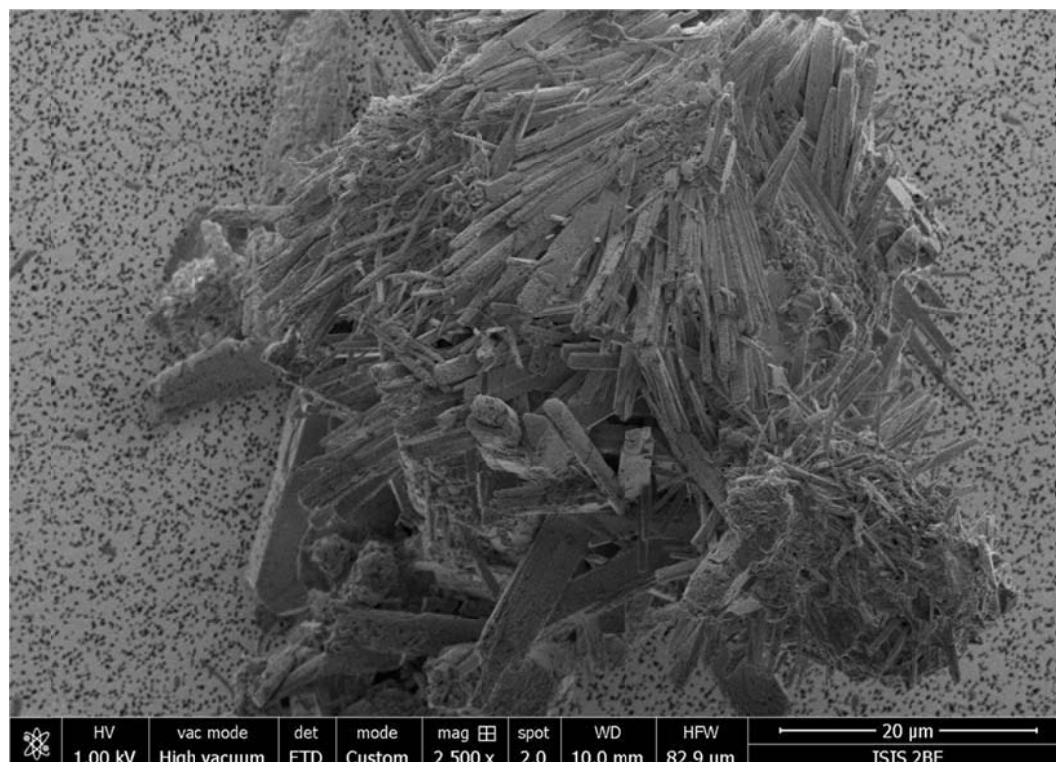
Supplementary Tables and Figures

Supplementary Table S1. Estimation of assimilatory phosphate uptake rates. Sulfate reduction rate (SRR) was calculated by linear regression of the sulfate concentration. DIC uptake was estimated from the SRR assuming 1% uptake efficiency related to SRR for a similar S-AOM enrichment culture (personal communication G. Wegener). DIC uptake rate was converted into DIP uptake rate using Redfield ratio 106C:1P.

Experiment	Sulfate reduction rate (SRR) ($\mu\text{mol l}^{-1} \text{h}^{-1}$)	DIC uptake assuming 1% efficiency ($\mu\text{mol l}^{-1} \text{h}^{-1}$)	DIP uptake assuming Redfield ratio ($\text{nmol l}^{-1} \text{h}^{-1}$)
Low phosphate	16.2	0.16	1.5
High phosphate	53.8	0.54	5.1

Supplementary Table S2. Elemental analysis of major trace elements by ICP-OES of low and high phosphate S-AOM biomass extracted by 1M HCl [in mg (g dry mass)⁻¹].

	Ca	Mg	Fe	P	S	Mn	Ni	Co
Low phosphate	22.35	0.16	0.45	0.16	1.38	0.16	0.07	0.08
High phosphate	16.22	33.53	4.24	29.29	4.81	1.69	0.51	0.62



Supplementary Figure S3. Crystalline mineral of low phosphate S-AOM incubation. Shown is a scanning electron microscope image (2500x magnification, 1.00 kV) of crystalline structures, presumably a carbonate-mineral, present in the low phosphate incubation.

Chapter 6

Conclusions and Outlook

This thesis provides a deeper understanding on microbial methane oxidation in freshwater and marine systems by studying several groups of microorganisms that drive this process in the environment. The study of these microorganisms is important because they play a key role in controlling emissions of the greenhouse gas methane to the atmosphere. The novel insights gained into the metabolic potential and activity of these microorganisms allows us to better understand their role and contribution towards the biogeochemical cycling of methane and other intersecting element cycles.

Methane oxidation in lakes - physiology and ecology of two contrasting microbial groups

The majority of methane oxidation occurring in freshwater lakes is commonly thought to be performed by aerobic methanotrophs, yet little is known about the importance and physiology of individual groups that mediate this process. In this thesis we investigated the methane-oxidizing community in Swiss temperate lakes, which are typical examples of eutrophic stratified lakes found in many temperate regions. We looked into the ecology, activity and physiology of two contrasting methane-oxidizing groups with hitherto poorly characterized environmental relevance: the filamentous *Crenothrix* bacteria (Chapter 2) and the wondrous NC10 bacteria (Chapter 3).

Thus far, *Crenothrix* bacteria were infamous for infesting and clogging drinking water supplies but little was known about their physiology and role in the environment besides their methanotrophic lifestyle (Stoecker et al, 2006b). In Chapter 2 we show that *Crenothrix* bacteria are important players in the methane cycle of freshwater lakes. At first, this finding was unexpected since *Crenothrix* bacteria only constituted a minor fraction of the indigenous methane-oxidizing microbial community, which was mainly composed of gamma-proteobacterial methane oxidizing bacteria (gamma-MOB). By measuring the activity of single *Crenothrix* filaments using nanometer-scale secondary ion mass spectrometry (nanoSIMS), we showed that the large *Crenothrix* bacteria overall oxidized as much methane as the more abundant but smaller gamma-MOB. This highlights that comparatively rare microorganisms can have a large ecological impact

on their environment and that abundance is not always a good indicator for importance.

Using next-generation sequencing and genome binning techniques, we then reconstructed three *Crenothrix* genomes (from Lake Zug and a water treatment plant) to gain a better insight into the metabolic potential of these uncultivated methanotrophs. Phylogenetic analyses of these genomes showed that the genus *Crenothrix* appears to be polyphyletic, harboring several species, and might be more diverse and therefore more widely distributed than previously assumed. Furthermore we show that *Crenothrix* do not possess an “unusual” particulate methane monooxygenase (pMMO, (Stoecker et al, 2006a)) but rather possess a “classical” gamma-proteobacterial pMMO. This is important since “unusual” PmoA previously assigned to *Crenothrix*, which has been shown to be an ammonium monooxygenase of *Nitrospira* bacteria (Daims et al, 2015; van Kessel et al, 2015), serves as an important marker for the detection of these physiologically different microorganisms in the environment. Additionally, we found that PmoA of *Crenothrix* might be affected by lateral gene transfer, which should be considered in studies that rely on PmoA as marker for *Crenothrix*.

Although methane oxidation and abundance of gamma-MOB was generally highest at the oxycline, our study demonstrated that *Crenothrix* bacteria, which we also identified in anoxic waters of Lake Zug and Rotsee, were apparently also capable of methane oxidation under both oxic as well as anoxic and denitrifying conditions. Genomic analysis further supported that *Crenothrix* appear to be well adapted to oxygen-limited conditions as the genome encoded a partial respiratory denitrification pathway and genes for mixed acid fermentation. Both systems are emerging features of “aerobic” methanotrophs that might allow these microorganisms to thrive even under oxygen-limiting conditions (Chistoserdova, 2015; Kalyuzhnaya et al, 2013; Kits et al, 2015; Knief, 2015). However, the role and contribution of denitrifying aerobic methanotrophs towards N cycling in these systems, which are often eutrophied and receive high inputs of N, is still poorly understood. Although further studies are needed to assess and quantify methane-dependent growth of *Crenothrix* (and other gamma-MOB) under nitrate-reducing conditions, our data suggests these microorganisms might be important links between the biogeochemical cycles of methane and nitrogen in freshwater lakes. Furthermore, it is also important to consider the end-product of

denitrification as ours and other genomic studies have shown that gamma-MOB consistently lack nitrous oxide reductase (Dam et al, 2013; Stein & Klotz, 2011), which might suggest N₂O (and possibly other nitrogen oxides) as an end product. N₂O has a substantially higher global warming potential than methane, therefore the role *Crenothrix* and other denitrifying gamma-MOB should also be considered in the environmental control of climate-relevant greenhouse gases other than methane.

In Chapter 3, we returned to Lake Zug in September 2016 to investigate the methanotrophic community, which was in the previous years mainly composed of gamma-MOB (Chapter 2, (Oswald et al, 2016a)). To our surprise we found that planktonic NC10 bacteria, which we did not detect in the previous years, dominated the microbial community in the deep, anoxic hypolimnion of Lake Zug where NC10 constituted up to 27% of the total microbial community. This was only the second report of abundant planktonic NC10 in the environment (Kojima et al, 2014). Previously, NC10 bacteria have been known to be widespread but rare members of the microbial community and their contribution to methane and nitrogen cycling in freshwater lakes remained poorly characterized.

The reconstructed genome of the dominant NC10 population represented a novel species of the genus "*Candidatus Methylomirabilis*", which we named "*Ca. Methylomirabilis limnetica*". This name was chosen to emphasize its lacustrine affiliation since closely related 16S rRNA gene sequences of "*Ca. M. limnetica*" have been retrieved from several freshwater lakes and reservoirs across the globe. The genome of "*Ca. M. limnetica*" contained all necessary genes for complete methane oxidation (via pMMO) and incomplete denitrification, including two non-canonical NO reductases that presumably function as O₂-producing nitric oxide dismutases. In comparison to "*Ca. Methylomirabilis oxyfera*", which was isolated from a Dutch ditch sediment (Raghoebarsing et al, 2006), we found that the genome of "*Ca. M. limnetica*" showed evidence possibly related to genome streamlining and adaptation to its planktonic habitat. A major difference was that "*Ca. M. limnetica*" encoded genes for gas vesicle formation as well as less homologs or variants of enzymes with apparently redundant function (i.e. heme-copper oxidases, cytochrome *bc*₁ complexes, methanol dehydrogenases), which might contribute to a more specialized and possibly opportunistic lifestyle of "*Ca. M. limnetica*". Our transcriptomic data provided further

evidence that "*Ca. M. limnetica*" was transcriptionally highly active *in situ* since up to a third of all mRNA transcripts from the metatranscriptome of the deeper depths could be assigned to "*Ca. M. limnetica*". Furthermore we found that genes involved in transcription and translation were well expressed by "*Ca. M. limnetica*", which suggested that the apparent bloom of "*Ca. M. limnetica*" was still ongoing. Transcription of functional genes related to methane oxidation and denitrification was in accord with the proposed lifestyle of NC10 bacteria; in particular our transcriptomic data confirmed that the presumably O₂-producing NO dismutase, which was highly transcribed *in situ*, appears to play a key role in the metabolism of by "*Ca. M. limnetica*".

Our findings highlight yet another unrecognized major player in methane cycling of freshwater lakes. In contrast to *Crenothrix*, which was identified in successive years, NC10 appears to favor certain but yet unknown conditions that may trigger a bloom. We speculate that non-steady-state conditions in September 2016 could have opened a niche for NC10, in particular we noticed that the oxycline was located at about 106 m depth, which was well above the usual depth (140-150 m) that was measured in previous years (Chapter 2, (Oswald et al, 2016b)). Although the high abundance and transcriptional activity of "*Ca. M. limnetica*" suggests that this microorganism could be a major player in methane and nitrogen cycling, further studies are needed to confirm and quantify its denitrifying and methane-oxidizing activity *in situ*. In this context it would also be important to elucidate the factors that trigger a bloom, which would aid to predict, measure and quantify their role in the environment. It might very well be that NC10 bacteria, which produce N₂ gas (Ettwig et al, 2010; Raghoebarsing et al, 2006), could temporarily become the main contributors of N-loss and methane oxidation in aquatic systems.

Marine S-AOM: Unraveling intertwined microorganisms

In Chapters 4 and 5 we continued on the topic of microbial methane oxidation with a focus on marine anaerobic oxidation of methane coupled to sulfate reduction (S-AOM). This microbially mediated process is widespread in marine sediments and is a major factor controlling the flux of methane from sediments to the ocean and eventually to the atmosphere.

In Chapter 4, the metabolic potential and activity of anaerobic methanotrophic archaea (ANME) and associated *Deltaproteobacteria* that mediate S-AOM was

investigated using a highly active S-AOM enrichment culture. A major goal was to untangle the physiology and metabolic activity of the individual microorganisms and use the generated metabolic model as a basis for the discussion an S-AOM mechanism previously proposed by Milucka et al. (2012). We focused on this particular model because the same S-AOM enrichment culture was used in both studies. This was an important aspect of our study since it is unknown if a single S-AOM mechanism is applicable to all ANME and DSS groups that mediate S-AOM.

First, we successfully reconstructed two genomes of ANME-2c and SEEP-SRB1, which to our knowledge represent the first genomes of their respective genus or even family. Our data confirmed that ANME-2c oxidize methane through a full reverse methanogenesis pathway. We also showed that ANME-2c encode and express a membrane-bound electron transport chain likely coupled to the methanogenesis pathway, as proposed previously (McGlynn et al, 2015). However, the role of soluble heterodisulfide reductases (Hdr) should be considered in this context. Although soluble Hdr of ANME have been discussed before (Arshad et al, 2015; Hallam et al, 2004; Meyerdierks et al, 2010; Meyerdierks et al, 2005), our study highlights that soluble Hdr, which were well transcribed and also expressed, are likely important puzzle pieces of the electron flow in ANME archaea and might be a key to understanding the mechanism of S-AOM. In particular, the possibility of flavin-based electron bifurcation is an intriguing aspect of soluble Hdr that thus far has been largely excluded from metabolic models of ANME. In any case, further biochemical studies are needed to confirm physiological role and activity of soluble Hdr in ANME-2c.

Another open question is the role of sulfur metabolism-associated genes – two sulfite reductases in particular – of ANME-2c. An assimilatory or detoxifying role, which has been described for the F420-dependent sulfite reductase in methanogens (Johnson & Mukhopadhyay, 2005) (Johnson & Mukhopadhyay, 2008), does not appear directly obvious. Like methanogens, ANME-2c likely directly assimilate sulfide as source of sulfur. Furthermore, formation of substantial amounts of sulfite, which was not added to the enrichment culture, seems unlikely. Hence we speculate that these sulfite reductases, which were transcribed, might be involved in a putative archaeal sulfate reduction pathway of ANME-2 that was proposed previously (Milucka et al, 2012). However, several open questions still remain: What could the end product of this putative

archaeal sulfate reduction pathway be? In relation to this, would these sulfite reductases be directly involved in dissimilatory reduction or would they fulfill auxiliary roles (e.g. removal of by-products)? And, finally, how and by what enzyme is sulfate reduced in the first place? Here, we speculate that electrons with sufficiently low redox potential could in principle be generated via flavin-based electron bifurcation. Although our functional genomics approach laid a solid foundation for future investigations, many of the aforementioned questions are difficult to answer without additional confirmation by physiological experiments.

Another aspect we investigated through our functional genomics study was the metabolic potential and activity S-AOM-associated SEEP-SRB1 bacteria. A major finding was that SEEP-SRB1 encoded, transcribed and expressed all genes of the canonical sulfate reduction pathway in addition to associated, membrane-bound complexes. However, this finding by itself was not necessarily indicative that SEEP-SRB1 have a sulfate-reducing, syntrophic life style. The same enzymes have also been suggested to mediate sulfur disproportionation and even sulfide oxidation in other *Deltaproteobacteria* (Finster, 2008; Frederiksen & Finster, 2003; Thorup et al, 2017); furthermore, physiological experiments by Milucka et al. (2012) have shown that DSS are capable of polysulfide (mostly likely disulfide) disproportionation. Although this suggests that SEEP-SRB1 use these enzymes for disproportionation, sulfate reduction by SEEP-SRB1 cannot be excluded based on our data. Also, it is still unclear how polysulfide would be initially converted to sulfite, which has been shown to be a crucial intermediate in other disproportionating bacteria (Finster, 2008). A key protein in this process could be the highly transcribed sulfur carrier protein DsrC, which has been shown to form a trisulfide bridge that includes a zero-valent sulfur atom bound to two cysteine residues and has been shown to be a key intermediate in reduction of sulfite to sulfide (Santos et al, 2015). In this respect it would be interesting to investigate the possibility of an interaction of DsrC (and the associated DsrMKJOP complex) with polysulfides, which might represent an entry mechanism of zero-valent sulfur during sulfur disproportionation (Thorup et al, 2017).

In the recent years, several studies have suggested direct interspecies electron transfer (DIET) as an alternative S-AOM mechanism to the one proposed by Milucka et al. (2012). Although electron transfer via conductive pili has been suggested to occur in

thermophilic S-AOM consortia (Wegener et al, 2015), our functional genomics data did not support transcription and expression of pili genes by SEEP-SRB1. Conversely, multi-heme cytochromes *c* (MHC) of ANME-2c and SEEP-SRB1, some of which we found to be well transcribed, might be more suitable candidates and have been previously proposed to mediate electron transfer in S-AOM consortia (McGlynn et al, 2015; Skennerton et al, 2017). However, a major challenge regarding the involvement of MHCs in electron transfer is that they are a diverse group of proteins and are often functionally poorly characterized (Kletzin et al, 2015). Therefore, presence of MHC genes in our and other S-AOM-associated microorganisms might serve as indirect evidence for DIET, but further studies are needed to directly prove conductance of electrons. This could be tested for example by directly measuring the conductance of individual S-AOM aggregates or by establishing an artificial consortia that mediate electron transfer solely via MHCs, which then could be modified and tested in various ways (e.g. differential gene transcription or heterologous gene expression).

Another important puzzle piece to understand the physiology and possible interaction between the two partners could be the membrane-bound complexes Qrc and Tmc of SEEP-SRB1. Those complexes, which were well transcribed and expressed, have been shown to serve as entry points for electrons derived from periplasmic reactions (classically periplasmic hydrogenases or formate dehydrogenases, (Grein et al, 2013)) and would therefore be candidates to accept exogenous electrons (possibly transferred via DIET from ANME). However, an involvement in polysulfide disproportionation might also be possible (as discussed in Chapter 4) and further studies are needed to clarify the source of electrons accepted by these complexes. An approach to further test and verify different hypotheses surrounding the S-AOM mechanism could involve analysis of differentially transcribed genes of both microorganisms in incubations grown under standard S-AOM and under disproportionating conditions without methane. Also, obtaining an ANME-free culture of SEEP-SRB1 (e.g. through incubation with polysulfide and without methane) would be immensely useful for further physiological and biochemical characterization. The opposite (i.e. enriching for ANME) might also be possible by using an artificial electron acceptors, which has been shown to decouple methane oxidation from sulfate

reduction in S-AOM microcosm experiments (Scheller et al, 2016), although it first has to be tested if this is also possible in our S-AOM enrichment culture.

In Chapter 5 we investigated a direct involvement of S-AOM-mediating microorganisms in the sedimentary phosphorus (P) cycle, which was hinted towards in two studies: Milucka et al. (2012) reported Fe- and P-rich particles in DSS bacteria of an S-AOM enrichment culture and ii) the discovery of unusual authigenesis of iron (Fe) and P-bearing minerals within S-AOM dominated sediment horizons (Jilbert & Slomp, 2013). Prompted by these findings we investigated whether S-AOM-mediating microorganisms may directly influence the P cycle in an S-AOM enrichment culture by combining ^{33}P radioactive tracer incubations, single cell imaging and elemental analysis of the S-AOM biomass. Interestingly, we found that the S-AOM-associated microorganisms actively shuffled P_i between a soluble and a particulate pool, which was likely an epicellular magnesium-bound phosphate mineral. In incubations at lower P_i concentrations, we observed the same effect but additionally observed substantial carbonatization of the S-AOM biomass, which coincided with decreased S-AOM activity. These findings demonstrate that S-AOM-associated microorganisms appear to utilize P_i beyond assimilatory uptake, however, further experiments are needed to show if the enigmatic shuffling of soluble and particulate P_i pools also occurs in the environment and how it might affect the sedimentary P cycle. To further test this and to expand preliminary work with sediment from the Black Sea, S-AOM-active sediments could be incubated under *in situ* conditions with ^{33}P radiotracer and the partitioning of the radiotracer into different sedimentary P reservoirs could be traced by sequential extraction using the SEDEX procedure (Ruttenberg, 1992). Additionally, this could be combined with microautoradiography-fluorescence *in situ* hybridization (Lee et al, 1999) to link uptake and storage of P, possibly as intracellular P-bearing mineral, to individual cells with known phylogenetic identity.

In conclusion, this thesis provides an intimate look into the inner workings of several methane-oxidizing microorganisms that inhabit marine as well as lacustrine systems. The use of functional metagenomics allowed us to not only study their metabolic potential, but also to predict their metabolic activity that underlies their ecophysiology. In combination with other techniques, we put the spotlight on two unrecognized freshwater methanotrophs and elucidate their metabolism and role in

the environment. Furthermore, we provide first insights into the genomic blueprint and metabolic activity of marine microorganisms that mediate the sulfate-dependent anaerobic oxidation of methane. Although many open questions remain, the results and data presented in this thesis further serve as foundation for future studies to hypothesize, test and provide answers to remaining as well as yet unasked questions pertaining to these small but mighty beasts.

Directions for future research

This thesis has illuminated the metabolic potential and activity of several methane-oxidizing microorganisms. It goes without saying that there remains much to be discovered and the more one begins to understand, the more questions suddenly surface. Hereinafter, some directions for future research are suggested and sketched out.

1. Anaerobic “aerobic” methanotrophs and the lacustrine nitrogen cycle

In Chapter 2, we highlighted that *Crenothrix* bacteria might also oxidize methane and thrive under oxygen-limited conditions by respiratory denitrification. Although this feature is an emerging topic in methanotroph research (Kits et al, 2015), still little is known how important and widespread denitrification coupled to methane oxidation by “aerobic” methanotrophs is. Yet, gamma-proteobacterial methanotrophs are considered the most important methane-oxidizing group in freshwater lakes and these habitats have conditions that might favor denitrifiers due to high nitrogen loads. Understanding the contribution of these methanotrophs towards overall denitrification in these systems would provide valuable insights into the lacustrine N cycle, and, thus help to interpret the role of methanotrophs in controlling climate-relevant greenhouse gases (i.e. methane and nitrous oxide).

2. Role of NC10 in the environment

As discussed in Chapter 3, the contribution of NC10 towards environmental methane and nitrogen cycling still needs to be verified and quantified. To do this, we have to first understand the conditions and factors that lead to the bloom of NC10 and subsequently determine their activity and overall contribution. This might be best studied in a high resolution (both temporally and spatially) multi-year sampling

campaign on Lake Zug and other stratified methane-rich lakes. This might provide much needed answers to understand how frequently NC10 blooms occur, which greatly affects our view on the environmental relevance of NC10. Furthermore, our study also begs the question if NC10 bacteria, which have been identified at low abundance in marine systems (Padilla et al, 2016), might show similar blooming behavior in marine environments similar to Lake Zug (i.e. the Black Sea).

3. Functional microbial communities surrounding freshwater methanotrophs

Certain methylotrophs and other microbial taxa (e.g. *Flavobacterium*) are often found to co-occur with methanotrophs in freshwater environments (Beck et al, 2013; Chistoserdova, 2015), which was also observed in our study of Lake Zug and Rotsee but was not elaborated on in this thesis. Although it is tempting to speculate that these so-called satellite communities feed off of by-products produced by methanotrophs (e.g. methanol), there is little direct evidence for such a cross-feeding. Furthermore, it is not known if the interaction is solely based on C1 compound(s) or if other substances potentially produced by methanotrophs (e.g. nitrogen oxides) also might play a role. By investigating the interaction of methanotrophs and the associated functional communities we might gain a more holistic view on the process of methane oxidation and the associated microorganisms in freshwater systems.

4. The mechanism of S-AOM in light of phylogenetic diversity

Despite the large phylogenetic differences between different groups of ANME archaea and associated DSS bacteria, it is in many cases still assumed that the same mechanism underlies S-AOM in all groups. However, studies of "*Ca. Methanoperedens nitroreducens*", which belongs to a subgroup of ANME-2, have shown that these archaea are functionally diverse and can couple methane oxidation to both iron as well as nitrate reduction (Ettwig et al, 2016; Haroon et al, 2013). Considering that for example ANME-2c are more closely related to "*Ca. M. nitroreducens*" than to ANME-1, it might just be that different groups of S-AOM-associated microorganisms have evolved separate mechanisms for apparently the same process. By expanding our functional genomics approach combined with standardized physiological experiments to yet

poorly characterized S-AOM-associated groups, it might be possible to illuminate and finally resolve this age-old question.

References

- Arshad A, Speth DR, de Graaf RM, den Camp HJO, Jetten MS, Welte CU (2015) A metagenomics-based metabolic model of nitrate-dependent anaerobic oxidation of methane by Methanoperedens-like archaea. *Frontiers in microbiology* **6**
- Beck DAC, Kalyuzhnaya MG, Malfatti S, Tringe SG, del Rio TG, Ivanova N, Lidstrom ME, Chistoserdova L (2013) A metagenomic insight into freshwater methane-utilizing communities and evidence for cooperation between the Methylococcaceae and the Methylophilaceae. *Peerj* **1**
- Chistoserdova L (2015) Methylootrophs in natural habitats: current insights through metagenomics. *Applied Microbiology and Biotechnology* **99**: 5763-5779
- Daims H, Lebedeva EV, Pjevac P, Han P, Herbold C, Albertsen M, Jehmlich N, Palatinszky M, Vierheilig J, Bulaev A, Kirkegaard RH, von Bergen M, Rattei T, Bendinger B, Nielsen PH, Wagner M (2015) Complete nitrification by Nitrospira bacteria. *Nature* **528**: 504-+
- Dam B, Dam S, Blom J, Liesack W (2013) Genome analysis coupled with physiological studies reveals a diverse nitrogen metabolism in Methylocystis sp. strain SC2. *PLoS one* **8**: e74767
- Ettwig KF, Butler MK, Le Paslier D, Pelletier E, Mangenot S, Kuypers MM, Schreiber F, Dutilh BE, Zedelius J, De Beer D (2010) Nitrite-driven anaerobic methane oxidation by oxygenic bacteria. *Nature* **464**: 543-548
- Ettwig KF, Zhu B, Speth D, Keltjens JT, Jetten MS, Kartal B (2016) Archaea catalyze iron-dependent anaerobic oxidation of methane. *Proceedings of the National Academy of Sciences* **113**: 12792-12796
- Finster K (2008) Microbiological disproportionation of inorganic sulfur compounds. *Journal of Sulfur Chemistry* **29**: 281-292
- Frederiksen T-M, Finster K (2003) Sulfite-oxido-reductase is involved in the oxidation of sulfite in *Desulfocapsa sulfoexigens* during disproportionation of thiosulfate and elemental sulfur. *Biodegradation* **14**: 189-198
- Grein F, Ramos AR, Venceslau SS, Pereira IA (2013) Unifying concepts in anaerobic respiration: insights from dissimilatory sulfur metabolism. *Biochimica et Biophysica Acta (BBA)-Bioenergetics* **1827**: 145-160
- Hallam SJ, Putnam N, Preston CM, Detter JC, Rokhsar D, Richardson PM, DeLong EF (2004) Reverse methanogenesis: testing the hypothesis with environmental genomics. *Science* **305**: 1457-1462
- Haroon MF, Hu S, Shi Y, Imelfort M, Keller J, Hugenholtz P, Yuan Z, Tyson GW (2013) Anaerobic oxidation of methane coupled to nitrate reduction in a novel archaeal lineage. *Nature* **500**: 567-570

Jilbert T, Slomp CP (2013) Iron and manganese shuttles control the formation of authigenic phosphorus minerals in the euxinic basins of the Baltic Sea. *Geochimica et Cosmochimica Acta* **107**: 155-169

Johnson EF, Mukhopadhyay B (2005) A new type of sulfite reductase, a novel coenzyme F420-dependent enzyme, from the methanarchaeon *Methanocaldococcus jannaschii*. *Journal of Biological Chemistry* **280**: 38776-38786

Johnson EF, Mukhopadhyay B (2008) Coenzyme F420-dependent sulfite reductase-enabled sulfite detoxification and use of sulfite as a sole sulfur source by *Methanococcus maripaludis*. *Applied and environmental microbiology* **74**: 3591-3595

Kalyuzhnaya MG, Yang S, Rozova O, Smalley N, Clubb J, Lamb A, Gowda GN, Raftery D, Fu Y, Bringel F (2013) Highly efficient methane biocatalysis revealed in a methanotrophic bacterium. *Nature communications* **4**

Kits KD, Klotz MG, Stein LY (2015) Methane oxidation coupled to nitrate reduction under hypoxia by the Gammaproteobacterium *Methylomonas denitrificans*, sp. nov. type strain FJG1. *Environmental microbiology* **17**: 3219-3232

Kletzin A, Heimerl T, Flechsler J, van Niftrik L, Rachel R, Klingl A (2015) Cytochromes c in Archaea: distribution, maturation, cell architecture, and the special case of *Ignicoccus hospitalis*. *Frontiers in microbiology* **6**: 439

Knief C (2015) Diversity and habitat preferences of cultivated and uncultivated aerobic methanotrophic bacteria evaluated based on *pmoA* as molecular marker. *Frontiers in Microbiology* **6**

Kojima H, Tokizawa R, Kogure K, Kobayashi Y, Itoh M, Shiah F-K, Okuda N, Fukui M (2014) Community structure of planktonic methane-oxidizing bacteria in a subtropical reservoir characterized by dominance of phylotype closely related to nitrite reducer. *Scientific reports* **4**: 5728

Lee N, Nielsen PH, Andreasen KH, Juretschko S, Nielsen JL, Schleifer K-H, Wagner M (1999) Combination of fluorescent in situ hybridization and microautoradiography—a new tool for structure-function analyses in microbial ecology. *Applied and environmental microbiology* **65**: 1289-1297

McGlynn SE, Chadwick GL, Kempes CP, Orphan VJ (2015) Single cell activity reveals direct electron transfer in methanotrophic consortia. *Nature* **526**: 531-535

Meyerdierks A, Kube M, Kostadinov I, Teeling H, Glöckner FO, Reinhardt R, Amann R (2010) Metagenome and mRNA expression analyses of anaerobic methanotrophic archaea of the ANME-1 group. *Environmental microbiology* **12**: 422-439

Meyerdierks A, Kube M, Lombardot T, Knittel K, Bauer M, Glöckner FO, Reinhardt R, Amann R (2005) Insights into the genomes of archaea mediating the anaerobic oxidation of methane. *Environmental microbiology* **7**: 1937-1951

Milucka J, Ferdelman TG, Polerecky L, Franzke D, Wegener G, Schmid M, Lieberwirth I, Wagner M, Widdel F, Kuypers MM (2012) Zero-valent sulphur is a key intermediate in marine methane oxidation. *Nature*

Oswald K, Milucka J, Brand A, Hach P, Littmann S, Wehrli B, Kuypers MM, Schubert CJ (2016a) Aerobic gammaproteobacterial methanotrophs mitigate methane emissions from oxic and anoxic lake waters. *Limnology and Oceanography* **61**

Oswald K, Milucka J, Brand A, Hach P, Littmann S, Wehrli B, Kuypers MMM, Schubert CJ (2016b) Aerobic gammaproteobacterial methanotrophs mitigate methane emissions from oxic and anoxic lake waters. *Limnology and Oceanography*: n/a-n/a

Padilla CC, Bristow LA, Sarode N, Garcia-Robledo E, Ramírez EG, Benson CR, Bourbonnais A, Altabet MA, Girguis PR, Thamdrup B (2016) NC10 bacteria in marine oxygen minimum zones. *The ISME journal* **10**: 2067-2071

Raghoebarsing AA, Pol A, Van de Pas-Schoonen KT, Smolders AJ, Ettwig KF, Rijpstra WIC, Schouten S, Damsté JSS, den Camp HJO, Jetten MS (2006) A microbial consortium couples anaerobic methane oxidation to denitrification. *Nature* **440**: 918-921

Ruttenberg KC (1992) Development of a sequential extraction method for different forms of phosphorus in marine sediments. *Limnology and Oceanography* **37**: 1460-1482

Santos AA, Venceslau SS, Grein F, Leavitt WD, Dahl C, Johnston DT, Pereira IA (2015) A protein trisulfide couples dissimilatory sulfate reduction to energy conservation. *Science* **350**: 1541-1545

Scheller S, Yu H, Chadwick GL, McGlynn SE, Orphan VJ (2016) Artificial electron acceptors decouple archaeal methane oxidation from sulfate reduction. *Science* **351**: 703-707

Skenneron CT, Chourey K, Iyer R, Hettich RL, Tyson GW, Orphan VJ (2017) Methane-Fueled Syntrophy through Extracellular Electron Transfer: Uncovering the Genomic Traits Conserved within Diverse Bacterial Partners of Anaerobic Methanotrophic Archaea. *mBio* **8**: e00530-00517

Stein LY, Klotz MG. (2011) Nitrifying and denitrifying pathways of methanotrophic bacteria. Portland Press Limited.

Stoecker K, Bendinger B, Schoning B, Nielsen PH, Nielsen JL, Baranyi C, Toenshoff ER, Daims H, Wagner M (2006a) Cohn's Crenothrix is a filamentous methane oxidizer with an unusual methane monooxygenase. *Proceedings of the National Academy of Sciences of the United States of America* **103**: 2363-2367

Stoecker K, Bendinger B, Schöning B, Nielsen PH, Nielsen JL, Baranyi C, Toenshoff ER, Daims H, Wagner M (2006b) Cohn's *Crenothrix* is a filamentous methane oxidizer with an unusual methane monooxygenase. *Proceedings of the National Academy of Sciences of the United States of America* **103**: 2363-2367

Thorup C, Schramm A, Findlay AJ, Finster KW, Schreiber L (2017) Disguised as a Sulfate Reducer: Growth of the Deltaproteobacterium *Desulfurivibrio alkaliphilus* by Sulfide Oxidation with Nitrate. *mBio* **8**: e00671-00617

van Kessel MA, Speth DR, Albertsen M, Nielsen PH, den Camp HJO, Kartal B, Jetten MS, Lücker S (2015) Complete nitrification by a single microorganism. *Nature* **528**: 555-559

Wegener G, Krukenberg V, Riedel D, Tegetmeyer HE, Boetius A (2015) Intercellular wiring enables electron transfer between methanotrophic archaea and bacteria. *Nature* **526**: 587-590

Acknowledgements

This thesis would not have been possible without the help and support which I have received from my friends and colleagues. I would like to express my gratitude and appreciation in particular to:

- ... Prof. Marcel Kuypers for giving me the opportunity to work in his group and for being my Doktorvater. Thank you for your insightful advice, encouraging support, thoughtful guidance and patience that you have shown over the years. Your scientific enthusiasm was contagious and made science truly thrilling!
- ... Prof. Michael Wagner for agreeing to review my thesis, even on such short notice.
- ... Jana Milucka, thank you for your guidance, help and advice as well as for the stimulating discussions. Also, thank you for encouraging me and for remaining calm in times when I was not.
- ... Tim Ferdelman, for introducing me to biogeochemistry and for sharing your knowledge, expertise and enthusiasm about sulfur, phosphorus and many other things.
- ... Hannah Marchant, for explaining a whole bunch of N cycle to me and for your encouragement, advice and assistance during stressful times.
- ... Boran Kartal for his scientific help and advice in- and outside of thesis committee meetings. I would also like to thank him for organizing my research visits to Nijmegen and extend my gratitude to also Mike Jetten, Joachim Reimann, Daan Speth, Naomi de Almeida, Rob Mesman, Christina Ferousi and other members of the Microbiology Department in Nijmegen for their assistance, support and hospitality during my visits
- ... Harald Gruber-Vodicka and Sabine Kasten, for offering me much useful advice and contributed as members of my thesis committee.
- ... Hans Wessels for generating and analyzing the AOM proteome data. Thank you for your help and sharing your expertise with me!
- ... the technical and administrative support teams at the MPI and MarMic, specifically Christiane Glöckner, Anita Tingberg, Tina Peters, Bettina Lamers, Carsten John and Olaf Gundermann.

- ... all members of the Biogeochemistry group, for creating a such great and fun work environment. In particular I want to thank Kirsten Imhoff, Daniela Tienken, Gabriele Klockgether, Swantje Lilienthal and Sten Littmann for their technical help, support and the many nice times chatting. Furthermore I would also like to thank Ulrike Tietjen for her organizational help.
- ... the many great people at the MPI who helped me a lot and made working here a very pleasant experience: Caroline Buckner, my office buddies Clara Martinez Perez and Cameron Callbeck, Soeren Ahmerkamp, Nadine Lehnen, Katharina Kitzinger, Niels Schoffelen, Philipp Hach, Wiebke Mohr, Laura Bristow, Jasmine Berg and many more.
- ... mini vernachlässigtä Fründe ir Schwiiz won ih vill zweni bsuecht gha han: Benu, Michel, die drü Andreas (Tsaki, Mac und de Frü), Bagi, Laura und d'Denise.
- ... my godmother Maya and my godfather Markus, for nourishing my scientific curiosity since I was a child, and motivating me to pursue a career in science all these years.
- ... finally I would like to thank my parents, Annemarie and Daniel, and my Fiona - without your unending support, patience and love I would not be writing this. This is for you.

Appendix A

Contributions to other studies

Denitrifying community in coastal sediments performs aerobic and anaerobic respiration simultaneously

Hannah K. Marchant^{1,§}, Soeren Ahmerkamp¹, Gaute Lavik¹, Halina E. Tegetmeyer^{1,2,3}, Jon Graf¹, Judith M. Klatt^{1,4}, Moritz Holtappels^{1,3,5}, Eva Walpersdorf¹ and Marcel M. M. Kuypers¹

¹Department of Biogeochemistry, Max Planck Institute for Marine Microbiology, Bremen, Germany; ²Center for Biotechnology, Bielefeld University, Bielefeld, Germany; ³Alfred Wegener Institute, Helmholtz Center for Polar and Marine Research, Bremerhaven; ⁴Geomicrobiology Laboratory, Department of Earth & Environmental Sciences, University of Michigan, Ann Arbor MI, USA; ⁵Marum—Centre for Marine Environmental Science, Bremen, Germany

[§] Corresponding author: Hannah Marchant (hmarchan@mpi-bremen.de)

Published in *The ISME Journal*

doi: 10.1038/ismej.2017.51

Chemolithoheterotrophic bacteria play a key role in sulfide oxidation and denitrification in sulfidic shelf waters

Cameron M. Callbeck¹, Chris Pelzer^{1,2}, Gaute Lavik¹, Timothy G. Ferdelman^{1,§}, Harald Schunck⁴, Jon S. Graf¹, Sten Littmann¹, Bernhard Fuchs¹, Philipp F. Hach¹, Tim Kalvelage^{1,3}, Ruth A. Schmitz⁴, Marcel M. M. Kuypers¹

¹Department of Biogeochemistry, Max Planck Institute for Marine Microbiology, Bremen, Germany; ²Department of Microbiology, IWW, Radboud University Nijmegen, Nijmegen, The Netherlands; ³Institute of Biogeochemistry and Pollutant Dynamics, ETH Zürich, Switzerland; ⁴Institute for General Microbiology, University of Kiel, Kiel, Germany

[§] Corresponding author: Timothy Ferdelman (tferdelm@mpi-bremen.de)

For submission to *The ISME Journal*

Metabolic specialization of denitrifiers in permeable sediments leads to N₂O emissions

Hannah K. Marchant^{1*}, Halina E. Tegetmeyer^{2,3}, Soeren Ahmerkamp¹, Moritz Holtappels^{1,6}, Gaute Lavik¹, Jon S. Graf¹, Frank Schreiber^{1,3,4,5}, Marc Mussman^{1,7}, Marc Strous^{1,8}, Marcel M.M. Kuypers¹

¹Max Planck Institute for Marine Microbiology, Bremen; ²Center for Biotechnology, Bielefeld University; ³ETH Zurich, Swiss Federal Institute of Technology, Department of Environmental Systems Sciences, Zurich, Switzerland; ⁴Eawag, Swiss Federal Institute of Aquatic Science and Technology, Department of Environmental Microbiology, Switzerland; ⁵Federal Institute for Materials Research and Testing (BAM), Berlin; ⁶Current address: Alfred Wegener Institute, Helmholtz Center for Polar and Marine Research, Bremerhaven; ⁷Current address: Division of Microbial Ecology, University of Vienna, Vienna, Austria; ⁸Current address: University of Calgary, Calgary, Canada

[§] Corresponding author: Hannah Marchant (hmarchan@mpi-bremen.de)

For submission to *Environmental Microbiology*

Name / Name: Jon Graf Date / Date: 06.10.2017

Anschrift / Address: Reuterstrasse 54, 28217 Bremen

Erklärung / Affirmation

Ich versichere, dass / I affirm that

1. die Dissertation ohne unerlaubte fremde Hilfe angefertigt wurde /
I wrote the present thesis independently and without illicit assistance from third parties,

2. keine anderen als die von mir angegebenen Quellen und Hilfsmittel benutzt wurden und /
I used no sources other than those indicated nor aids other than those permissible,

3. die den benutzten Werken wörtlich oder inhaltlich entnommenen Stellen als solche kenntlich gemacht wurden. /
I appropriately referenced any text or content from other sources

Bremen _____, den / on this day 06.10.2017 _____

(Unterschrift / Signature)

